National Library of Canada
Acquisitions and Bibliographic Services Branch
395 Wellington Street
Ottawa, Ontario
K1A 0N4

Bibliothèque nationale du Canada
Direction des acquisitions et des services bibliographiques
395, rue Wellington
Ottawa (Ontario)
K1A 0N4

Your file Votre référence

Our file Notre référence

NOTICE

The quality of this microform is heavily dependent upon the quality of the original thesis submitted for microfilming. Every effort has been made to ensure the highest quality of reproduction possible.

If pages are missing, contact the university which granted the degree.

Some pages may have indistinct print especially if the original pages were typed with a poor typewriter ribbon or if the university sent us an inferior photocopy.

Reproduction in full or in part of this microform is governed by the Canadian Copyright Act, R.S.C. 1970, c. C-30, and subsequent amendments.

AVIS

La qualité de cette microforme dépend grandement de la qualité de la thèse soumise au microfilmage. Nous avons tout fait pour assurer une qualité supérieure de reproduction.

S'il manque des pages, veuillez communiquer avec l'université qui a conféré le grade.

La qualité d'impression de certaines pages peut laisser à désirer, surtout si les pages originales ont été dactylographiées à l'aide d'un ruban usé ou si l'université nous a fait parvenir une photocopie de qualité inférieure.

La reproduction, même partielle, de cette microforme est soumise à la Loi canadienne sur le droit d'auteur, SRC 1970, c. C-30, et ses amendements subséquents.

Canada

UNIVERSITY OF ALBERTA

THE GEOCHEMICAL AND HYDRAULIC EVOLUTION OF REACTION FRONTS IN SAND COLUMNS

BY

© ALAN ERNEST FRYAR

A THESIS

SUBMITTED TO THE FACULTY OF GRADUATE STUDIES AND RESEARCH

IN PARTIAL FULFILLMENT OF THE REQUIREMENTS FOR THE DEGREE

OF DOCTOR OF PHILOSOPHY

DEPARTMENT OF GEOLOGY

EDMONTON, ALBERTA

FALL 1992

National Library
of Canada

Acquisitions and
Bibliographic Services Branch

395 Wellington Street
Ottawa, Ontario
K1A 0N4

Bibliothèque nationale
du Canada

Direction des acquisitions et
des services bibliographiques

395, rue Wellington
Ottawa (Ontario)
K1A 0N4

Your file Votre référence

Our file Notre référence

The author has granted an irrevocable non-exclusive licence allowing the National Library of Canada to reproduce, loan, distribute or sell copies of his/her thesis by any means and in any form or format, making this thesis available to interested persons.

L'auteur a accordé une licence irrévocable et non exclusive permettant à la Bibliothèque nationale du Canada de reproduire, prêter, distribuer ou vendre des copies de sa thèse de quelque manière et sous quelque forme que ce soit pour mettre des exemplaires de cette thèse à la disposition des personnes intéressées.

The author retains ownership of the copyright in his/her thesis. Neither the thesis nor substantial extracts from it may be printed or otherwise reproduced without his/her permission.

L'auteur conserve la propriété du droit d'auteur qui protège sa thèse. Ni la thèse ni des extraits substantiels de celle-ci ne doivent être imprimés ou autrement reproduits sans son autorisation.

ISBN 0-315-77333-2

Canada

UNIVERSITY OF ALBERTA

RELEASE FORM

NAME OF AUTHOR: ALAN ERNEST FRYAR

TITLE OF THESIS: THE GEOCHEMICAL AND HYDRAULIC EVOLUTION OF REACTION ZONES IN SAND COLUMNS

DEGREE: DOCTOR OF PHILOSOPHY

YEAR THIS DEGREE GRANTED: FALL 1992

PERMISSION IS HEREBY GRANTED TO THE UNIVERSITY OF ALBERTA LIBRARY TO REPRODUCE SINGLE COPIES OF THIS THESIS AND TO LEND OR SELL SUCH COPIES FOR PRIVATE, SCHOLARLY OR SCIENTIFIC RESEARCH PURPOSES ONLY.

THE AUTHOR RESERVES ALL OTHER PUBLICATION AND OTHER RIGHTS IN ASSOCIATION WITH THE COPYRIGHT IN THE THESIS, AND EXCEPT AS HEREINBEFORE PROVIDED NEITHER THE THESIS NOR ANY SUBSTANTIAL PORTION THEREOF MAY BE PRINTED OR OTHERWISE REPRODUCED IN ANY MATERIAL FORM WHATEVER WITHOUT THE AUTHOR'S PRIOR WRITTEN PERMISSION.

.....Alan E. Fryar.....

Permanent address:

5230 Thunder Creek Road, #227

Austin, Texas 78759 U.S.A.

Date: Oct 6/1992

UNIVERSITY OF ALBERTA

FACULTY OF GRADUATE STUDIES AND RESEARCH

THE UNDERSIGNED CERTIFY THAT THEY HAVE READ, AND RECOMMEND TO THE FACULTY OF GRADUATE STUDIES AND RESEARCH FOR ACCEPTANCE, A THESIS ENTITLED *THE GEOCHEMICAL AND HYDRAULIC EVOLUTION OF REACTION FRONTS IN SAND COLUMNS* SUBMITTED BY *ALAN ERNEST FRYAR* IN PARTIAL FULFILLMENT OF THE REQUIREMENTS FOR THE DEGREE OF DOCTOR OF PHILOSOPHY.

Frank W. Schwartz
Dr. F.W. Schwartz (co-supervisor)

Dr. J. Tóth (co-supervisor)

Dr. B.E. Nesbitt

Dr. M.J. Dudas

Dr. W.D. Gunter

Dr. K. Muehlenbachs

ABSTRACT

Research into reaction front evolution associated with groundwater flow, particularly in contaminated systems, has been limited. To develop an improved understanding of the behavior of reaction fronts and the nature of coupling between fluid flow, solute transport, reaction, and hydraulic changes, experiments have been conducted in which dilute $Fe(ClO_4)_3$ solution was pumped through columns packed with a mixture of quartz sand and crushed calcite. The initial acidity of the solution promoted calcite dissolution; the resulting pH buffering promoted hydrolysis of dissolved iron and the precipitation of ferric oxyhydroxide. Variables included the initial percentage and grain-size distribution of calcite and the initial rate of fluid flow. At regular intervals during each experiment, the position of the visible precipitation front was traced, effluent chemistry was monitored, and hydraulic heads were measured in manometers along each column. At the end of each experiment, porewater and solid-phase samples were collected for chemical analyses.

Results indicate that the deposition of ferric oxyhydroxide peaks at, but is not restricted to, the visible front, where the neutralization of acidity generated by hydrolysis is completed. Even beyond the visible front, calcite dissolution and ferric oxyhydroxide precipitation continue gradually. Up-gradient from the front, where all calcite has been removed from the porous medium, ferric oxyhydroxide precipitation continues due to nucleation around older precipitate at a pH less than the influent pH. The deposition of ferric oxyhydroxide and entrapment of CO_2 (g) are together capable of reducing hydraulic conductivity by three orders of magnitude.

After initially propagating at the porewater velocity, the reaction front tends to decelerate toward a slower, relative uniform velocity. The frontal velocity, or the length of the reaction zone, is inversely proportional to the initial value of the Damkohler number, which relates the reaction rate to the fluid velocity at a given length scale. The

zonal length is related to the size of instabilities along the front, which is inversely related to the number of instabilities. However, the initial value of the Damkohler number cannot characterize the reduction of hydraulic conductivity in this system.

ACKNOWLEDGMENTS

During the course of this study, I have received assistance from many people, of whom I can name but a few. Frank Schwartz, my supervisor, has been unstinting in his guidance and support. Joe Tóth graciously agreed to step in as co-supervisor and has provided wise counsel. Marvin Dudas and Bruce Nesbitt, the remaining members of my supervisory committee, and Scott Bair and Sam Traina, who functioned as shadow committee members at Ohio State, provided the use of equipment and many valuable discussions. As external examiner, Don Siegel provided a thorough critique of the penultimate draft of this thesis. Nat Rutter and Alex Stelmach generously allowed me the use of their labs, as did the Department of Civil Engineering at the University of Alberta and the Byrd Polar Research Center at Ohio State. At the Alberta Research Council, George Sedgwick devoted time and resources to investigate the utility of computerized tomography scanning, while Steve Talman and Bill Gunter patiently answered my questions on reaction kinetics. Blake Onken and Lee Burris assisted with lab analyses at Ohio State. Gunter Faure and Liane Schlickenrieder translated Schulz (1988) for me. My classmates, particularly Rob and Jan Schincariol, Ben and Catherine Rostron, Joao and Angela Küpper, Abe Springer, and Allan Crowe, have helped and encouraged me in numerous ways. I appreciate everyone who provided reprints and technical advice. Finally, I am grateful to the Natural Sciences and Engineering Research Council, the Ohio Eminent Scholar Program, and the Department of Geology, University of Alberta, for financial assistance, and to the Bureau of Economic Geology, The University of Texas at Austin, for its patience in allowing me to bring this work to a successful conclusion.

This thesis is dedicated to my wife, Carol Ruthven, our son, and our parents, whose love and example have inspired and sustained me.

TABLE OF CONTENTS

1. INTRODUCTION 1

1.1. Overview 1

1.2. Criteria for Selecting the Chemical System 3

1.3. Reactions of Interest 5

1.3.1. Calcite dissolution 5

1.3.2. Precipitation of ferrihydrite 6

1.4. Dimensionless Groups and Frontal Behavior 10

2. MATERIALS AND METHODS 13

2.1. Column Design and Operation 13

2.2. Protocols for Monitoring and Sampling 17

2.3. Protocols for Sample Analyses and Parameter Calculations 20

2.3.1. Analyses of water and sediment samples 20

2.3.2. Calculating values of hydraulic conductivity 24

3. RESULTS 26

3.1. Characterizing Results in Terms of Initial Variables 26

3.2. Observations of Reaction Front Behavior 31

3.3. Geochemical Evolution of the System 42

3.3.1. Starting water composition 42

3.3.2. Effluent water composition 44

3.3.3. Porewater data 51

3.3.4. Solid-phase data 71

3.4. Hydraulic Evolution of the System 77

4. DISCUSSION 92

4.1. Mechanisms of Geochemical and Hydraulic Evolution 92

4.1.1. Initial geochemical evolution along the flowpath 92

4.1.2. Numerical modeling of geochemical speciation 98

4.1.3. Hydraulic changes 109

4.2. Behavior of the System under Different Initial Conditions 115

4.2.1. Trends in frontal or zonal length and velocity 115

4.2.2. Limitations of the Damkohler number 121

5. SUMMARY AND CONCLUSIONS 126

REFERENCES 129

APPENDICES

I. Grain Size and Calcite Surface Area Determinations 135

II. Supplementary Geochemical Data 142

III. Supplementary Hydraulic Data 159

LIST OF TABLES

Table 2.1.	Inside diameter and length of columns used in study.	14
Table 3.1.	Values of kinematic (breakthrough- and waterflood-derived) and volumetric porosity in study.	29
Table 3.2.	Initial values of physical and chemical parameters in study.	30
Table 3.3.	Frontal velocity values and goodness of fit for lines through Stage 3 of frontal advance plots.	38
Table 3.4.	Electrical conductivity values along flowpath for columns containing sieved calcite.	54
Table 3.5.	Electrical conductivity values along flowpath for columns 3 and 4 (containing unsieved calcite).	57
Table 3.6.	pH values along flowpath for columns containing sieved calcite.	58
Table 3.7.	TIC values along flowpath for columns containing sieved calcite.	60
Table 3.8.	Unfiltered Ca values along flowpath for columns containing sieved calcite.	63
Table 3.9.	Unfiltered Fe values along flowpath for columns containing sieved calcite.	67
Table 3.10.	Concentrations of ferrihydrite particles larger than 0.05 μm across (μg/g).	70
Table 3.11.	Solid-phase Ca values along flowpath for columns containing sieved calcite (μg/g (s)).	76
Table 3.12.	Solid-phase Fe values along flowpath for columns containing sieved calcite (μg/g (s)).	79
Table 3.13.	Background values of hydraulic conductivity and averages for experiments 1, 3, 4, and 5; C.V. refers to the coefficient of variation.	88
Table 4.1.	Values of saturation index with respect to calcite in porewater at the end of experiment 8.	101
Table 4.2.	Values of log P_{CO_2} in porewater at the end of experiment 7.	103
Table 4.3.	Values of saturation index with respect to ferric oxyhydroxide in porewater at the end of experiment 8; log K_{sp} = -37.1.	104
Table 4.4.	Values of saturation index with respect to ferric oxyhydroxide in porewater at the end of experiment 8; log K_{sp} = -38.3.	106

Table 4.5. Speciation of ferric monomers and simple polymers in influent solution and porewater at the end of experiment, column 8-1: (a) Fe^{3+}; (b) $Fe(OH)^{2+}$; (c) $Fe(OH)_2^{+}$; (d) $Fe(OH)_3^{o}$; (e) $Fe(OH)_4^{-}$; (f) $Fe_2(OH)_2^{4+}$; (g) $Fe_3(OH)_4^{5+}$. 107

Table 4.6. Values of saturation indices for calcite and ferric oxyhydroxide and values of log P_{CO_2} in porewater at the end of experiment, column 7-1. 110

Table 4.7. Values of frontal velocity v_f (determined by least-squares linear fits to observed post-plateau data) and of rear-boundary velocity v_l (calculated on the basis of a distribution coefficient as formulated by Lichtner (1988)). 118

Table I.1. Grain-size data for Ottawa sand replicates based on sieve analyses (sizes in mm, representing sieve sizes #16 - #120). 136

Table I.2. Grain-size data for crushed calcite replicates based on sieve and hydrometer analyses (sizes in mm). 137

Table I.3. Edge lengths of calcite particles which underwent sieve analyses. 139

Table I.4. Geometric surface area for sieve intervals (in m^2/g) (based on the harmonic mean edge length) and the corresponding surface area of those intervals (in m^2/m^3) based on the mass distribution of the crushed calcite replicates. 139

Table I.5. BET surface-area measurements on sets of triplicate calcite samples. 141

Table II.1. Reaction front position as a function of time for (a) experiment 1, (b) experiment 2, (c) experiment 3, (d) experiment 4. 143

Table II.2. Reaction front position as a function of time for (a) experiment 5, (b) experiment 6, (c) experiment 7, (d) experiment 8. 144

Table II.3. Electrical conductivity of influent solution for (a) experiment 5, (b) experiment 6, (c) experiment 7, (d) experiment 8. 146

Table II.4. pH of influent solution for (a) experiment 5, (b) experiment 6, (c) experiment 7, (d) experiment 8. 147

Table II.5. Fe concentration of influent solution for (a) experiment 5, (b) experiment 6, (c) experiment 7, (d) experiment 8. 148

Table II.6. Electrical conductivity of effluent for (a) experiment 1, (b) experiment 2, (c) experiment 3, (d) experiment 4. 149

Table II.7. Electrical conductivity of effluent for (a) experiment 5, (b) experiment 6, (c) experiment 7, (d) experiment 8. Values used for least-squares fitting of breakthrough curves marked by an asterisk. 151

Table II.8.	pH of effluent for (a) experiment 5, (b) experiment 6, (c) experiment 7, (d) experiment 8.	153
Table II.9.	TIC of effluent for (a) experiment 5, (b) experiment 6, (c) experiment 7, (d) experiment 8.	154
Table II.10.	Ca concentrations in effluent for (a) experiment 5, (b) experiment 6, (c) experiment 7, (d) experiment 8.	155
Table II.11.	Fe concentrations in effluent for (a) experiment 5, (b) experiment 6, (c) experiment 7, (d) experiment 8.	156
Table II.12.	Filtered Ca values for columns containing sieved calcite.	157
Table II.13.	Filtered Fe values for columns containing sieved calcite.	158
Table III.1.	Volumetric flow rates for (a) experiment 1, (b) experiment 2, (c) experiment 3, (d) experiment 4. Rates marked with an asterisk where adjusted to maintain flow.	160
Table III.2.	Volumetric flow rates for (a) experiment 5, (b) experiment 6, (c) experiment 7, (d) experiment 8.	161
Table III.3.	Hydraulic head values at distances x along columns (a) 1-1, (b) 1-2, (c) 1-3.	163
Table III.4.	Hydraulic head values at distances x along columns (a) 2-1, (b) 2-2, (c) 2-3.	165
Table III.5.	Hydraulic head values at distances x along columns (a) 3-1, (b) 3-2, (c) 3-3.	167
Table III.6.	Hydraulic head values at distances x along columns (a) 4-1, (b) 4-2, (c) 4-3.	169
Table III.7.	Hydraulic head values at distances x along columns (a) 5-1, (b) 5-2, (c) 5-3.	171
Table III.8.	Hydraulic head values at distances x along columns (a) 6-1, (b) 6-2, (c) 6-3.	174
Table III.9.	Hydraulic head values at distances x along columns (a) 7-1, (b) 7-2, (c) 7-3.	177
Table III.10.	Hydraulic head values at distances x along columns (a) 8-1, (b) 8-2, (c) 8-3.	179
Table III.11.	Hydraulic conductivity values, normalized with respect to the calculated mean initial value for experiment 1, for selected intervals along columns (a) 1-1, (b) 1-2.	181

Table III.12. Hydraulic conductivity values, normalized with respect to the calculated mean initial value for experiment 2, for selected intervals along columns (a) 2-1, (b) 2-2, (c) 2-3. 182

Table III.13. Hydraulic conductivity values, normalized with respect to the calculated mean initial value for experiment 3, for selected intervals along columns (a) 3-1, (b) 3-2, (c) 3-3. 183

Table III.14. Hydraulic conductivity values, normalized with respect to the calculated mean initial value for experiment 4, for selected intervals along columns (a) 4-1, (b) 4-2, (c) 4-3. 184

Table III.15. Hydraulic conductivity values, normalized with respect to the calculated mean initial value for experiment 5, for selected intervals along columns (a) 5-1, (b) 5-2, (c) 5-3. 185

Table III.16. Hydraulic conductivity values, normalized with respect to the calculated mean initial value for experiment 6, for selected intervals along columns (a) 6-1, (b) 6-2, (c) 6-3. 187

Table III.17. Hydraulic conductivity values, normalized with respect to the calculated mean initial value for experiment 7, for selected intervals along columns (a) 7-1, (b) 7-2, (c) 7-3. 189

Table III.18. Hydraulic conductivity values, normalized with respect to the calculated mean initial value for experiment 8, for selected intervals along columns (a) 8-1, (b) 8-2, (c) 8-3. 190

LIST OF FIGURES

Fig. 2.1. Triplicate columns for experiment 3, demonstrating representative set-up for experiments 1 to 8. The peristaltic pump in the background directs influent solution from a carboy above (not shown) to the inlet at the base, and thence up the column. Ports connected to manometers are spaced at 10-cm intervals within the medium; within the reaction zone, sample ports are spaced between manometer ports at 2.5-cm intervals. 15

Fig. 3.1. Experiment 2, column 2-3, showing gas front. (a) Top: t = 12 hr; maximum advance of gas front = 0.11 m, maximum advance of reaction front = 0.13 m. (b) Bottom: t =37 hr; gas front stationary; reaction front maximum at 0.18 m. 32

Fig. 3.2. Experiment P2, with reactive column (r) in foreground and control column (c) in background. (a) Top: t = 2 hr; maximum visible position of reaction front in P2r = 0.05 m. Note that dye front has surpassed position of reaction front in Stage 2. (b) Bottom: t = 24 hr (dye flushed from P2c). Note darkening of initial fingers and diversion of subsequent precipation. 34

Fig. 3.3. Maximum frontal advance as a function of time for (a) column 1-2 (Da_n = 26.4), (b) experiment 2 (Da_n = 11.2 (2-1), 5.89 (2.2), 1.92 (2-3)), (c) experiment 4 (Da_n = 12.1 (4-2)), (d) experiment 3 (Da_n = 5.04 to 5.43). 35

Fig. 3.4. Maximum frontal advance as a function of time for (a) experiment 6 (Da_n = 3.85 to 4.33), (b) experiment 5 (Da_n = 1.97 to 2.03), (c) experiment 7 (Da_n = 1.96 to 1.99), (d) experiment 8 (Da_n = 1.00 to 1.16). 36

Fig. 3.5. Differing inverse proportionalities between normalized Damkohler number and frontal velocity for experiments containing unsieved (1 to 3, 4 not shown) and sieved (5 to 8) calcite. 38

Fig. 3.6. Experiment 1, column 1-2, t = 480 hr; maximum advance of reaction front = 0.094 m. 40

Fig. 3.7. Experiment 2, column 2-2, t = 96 hr (column failed between 78 and 85 hr); maximum advance of reaction front = 0.086 m. 40

Fig. 3.8. Experiment 2, column 2-3, t = 168 hr; maximum advance of reaction front = 0.507 m. 41

Fig. 3.9. Electrical conductivity trends for effluent as a function of time, (a) column 1-3, (b) experiment 2, (c) experiment 4, (d) experiment 3. 45

Fig. 3.10. Electrical conductivity trends for effluent as a function of time, (a) experiment 6, (b) experiment 5, (c) experiment 7, (d) experiment 8. 46

Fig. 3.11. pH trends for effluent as a function of time, (a) experiment 6, (b) experiment 5, (c) experiment 7, (d) experiment 8. 48

Fig. 3.12. Total inorganic carbon trends for effluent as a function of time, (a) experiment 6, (b) experiment 5, (c) experiment 7, (d) experiment 8. 49

Fig. 3.13. Ca trends for effluent as a function of time, (a) experiment 6, (b) experiment 5, (c) experiment 7, (d) experiment 8. 50

Fig. 3.14. Fe trends for effluent as a function of time, (a) experiment 6, (b) experiment 5, (c) experiment 7, (d) experiment 8. 52

Fig. 3.15. Electrical conductivity trends along flowpath at the end of (a) experiment 6, (b) experiment 5, (c) experiment 7, (d) experiment 8. 55

Fig. 3.16. Electrical conductivity trends along flowpath at the end of (a) experiment 4, (b) experiment 3. 57

Fig. 3.17. pH trends along the flowpath at the end of (a) experiment 6, (b) experiment 5, (c) experiment 7, (d) experiment 8. 59

Fig. 3.18. Total inorganic carbon trends along the flowpath at the end of (a) experiment 6, (b) experiment 5, (c) experiment 7, (d) experiment 8. 61

Fig. 3.19. Ca trends in unfiltered porewater along the flowpath at the end of (a) experiment 6, (b) experiment 5, (c) experiment 7, (d) experiment 8. 64

Fig. 3.20. Trends in the Ca/TIC ratio along the flowpath at the end of (a) experiment 6, (b) experiment 5, (c) experiment 7, (d) experiment 8. 65

Fig. 3.21. Fe trends in unfiltered porewater at the end of (a) experiment 6, (b) experiment 5, (c) experiment 7, (d) experiment 8. 68

Fig. 3.22. Fe deposited between porewater sampling points at the end of (a) experiment 6, (b) experiment 5, (c) experiment 7, (d) experiment 8. 69

Fig. 3.23. Distributions of ferric oxyhydroxide particles >0.05 μm across (as μg Fe/g porewater) along flowpath at the end of (a) experiment 6, (b) experiment 5, (c) experiment 7, (d) experiment 8. 72

Fig. 3.24. Partly disaggregated sediment from lower endcap; column 1-2. 74

Fig. 3.25. Aggregate of several quartz grains indurated by ferrihydrite, (a) top, 100x, (b) bottom, 500x, scales as shown on photos. 75

Fig. 3.26. Solid-phase Ca, normalized against initial amount present, at the end of (a) experiment 6, (b) experiment 5, (c) experiment 7, (d) experiment 8. 78

Fig. 3.27. Solid-phase Fe at the end of (a) experiment 6, (b) experiment 5, (c) experiment 7, (d) experiment 8. 80

Fig. 3.28. Volumetric flow rate trends during (a) experiment 1, (b) experiment 2, (c) experiment 4, (d) experiment 3. 82

Fig. 3.29. Volumetric flow rate trends during (a) experiment 6, (b) experiment 5, (c) experiment 7, (d) experiment 8. 83

Fig. 3.30. Hydraulic head profiles at the inlet manometer during (a) experiment 1, (b) experiment 2, (c) experiment 4, (d) experiment 3. 85

Fig. 3.31. Hydraulic head profiles at the inlet manometer during (a) experiment 6, (b) experiment 5, (c) experiment 7, (d) experiment 8. 86

Fig. 3.32. Profiles of hydraulic conductivity, adjacent to the inlet, normalized against background values during (a) experiment 1, (b) experiment 2, (c) experiment 4, (d) experiment 3. 89

Fig. 3.33. Profiles of hydraulic conductivity, adjacent to the inlet, normalized against background values during (a) experiment 6, (b) experiment 5, (c) experiment 7, (d) experiment 8. 91

Fig. 4.1. Unfiltered porewater samples after collection from column 7-3. Distance from inlet at which sample was collected and concentrations are (left to right): 0.053 m, 330 μg/g; 0.104 m, 310 μg/g; 0.154 m, 230 μg/g; 0.205 m, 41 μg/g; 0.256 m, 3.8 μg/g. Note that reaction front fell between collection points for fourth and fifth samples. 94

Fig. 4.2. Possible mechanisms of ferric particle growth and deposition along flowpath in (a) zone of nucleation and (b) zone of proton attack on calcite. 96

Fig. 4.3. Conceptualization of reaction zonation along flowpath. 99

Fig. 4.4. Saturation index with respect to calcite along flowpath at the end of experiment 8. 101

Fig. 4.5. Calculated partial pressure (in atm) of CO_2 in porewater along flowpath at the end of experiment 7. 103

Fig. 4.6. Saturation index with respect to ferric oxyhydroxide along flowpath at the end of experiment 8; log K_{sp} = -37.1. 104

Fig. 4.7. Saturation index with respect to ferric oxyhydroxide along flowpath at the end of experiment 8; log K_{sp} = -38.3. 106

Fig. 4.8. Speciation of ferric monomers and simple polymers in influent solution and in porewater along flowpath at the end of experiment, column 8-1. 108

Fig. 4.9. Saturation indices of calcite and ferric oxyhydroxide and partial pressure of CO_2 along flowpath at the end of experiment, column 7-1; calculation based on concentrations of Fe and Ca in filtered porewater. 110

Fig. 4.10. Final normalized hydraulic conductivity values adjacent to inlet as a function of solid-phase Fe (μg/g) (s), experiments 5 to 8. 112

Fig. 4.11. Conceptualization of pore-throat constriction by ferric oxyhydroxide and occlusion by CO_2 (g). 114

Fig. 4.12. Normalized solid-phase Ca concentration profiles after experiments 5 and 7. 123

Fig. 4.13. Final solid-phase Fe concentrations (μg/g) (s) adjacent to inlet as a function of BET-equivalent surface area (m^2/m^3), experiments 5 to 8. 125

Fig. I.1. Cumulative grain-size curves for Ottawa sand based on sieve analyses. 136

Fig. I.2. Cumulative grain-size curves for crushed calcite based on sieve and hydrometer analyses. 137

1. INTRODUCTION

1.1. Overview

Many different geological phenomena have their origins in chemical mass transfer which often occurs between a fluid and a porous medium. Whether the problem is one of soil formation, sedimentary diagenesis, or mineral precipitation from contaminated groundwater, the interplay between flow and reaction is the same. As a solution in disequilibrium with solids moves into a porous medium, a front will form marking the boundary between reacted and unreacted zones. Commonly, changes in the solids due to dissolution and precipitation are most obvious. However, if changes in porosity and surface area result, the front may mark a hydraulic transition as well (Lund and Fogler, 1976). The morphology of the front and the velocity at which it moves result from the combined influence of reaction and mass transport. When the rate of reaction is much faster than the rate of fluid flow, the front propagates as an infinitesimally thin shock wave (Hekim and Fogler, 1980). In this case of local equilibrium, the front propagation is transport-controlled, because the progress of the reaction depends on the rate at which species in solution are being transported to and from the reaction sites. When the rate of precipitation or dissolution is slow relative to fluid flow, reaction progress is controlled by interactions at the mineral surface. Consequently, a zonation may develop so that moving boundaries separate unreacted from partially-reacted and partially-reacted from totally-reacted regions (Bahr, 1990). The transition between transport- and surface-controlled behavior is referred to as a mixed control regime. In systems containing several reactive minerals, multiple reaction fronts or zones may exist. The length and relative composition of each mineralic zone and the number of such zones vary with the flow and reaction rates (Dobrovolsky, 1987).

Both theoretical and experimental work indicates that instabilities may develop within the reaction front. An underlying cause of instabilities is the heterogeneous character of the porous medium. Flow preferentially seeks out local zones that are most permeable. In the simplest case, dissolution will be accelerated and permeability increased in these zones, thereby attracting more flow from adjacent zones along the reaction front. With sufficiently fast dissolution rates, the feedback can perturb a planar propagating front, creating fingers through which flow is accelerated and redirected (Ortoleva et al., 1987). In contrast, precipitation can repress the dissolution-transport loop by coating reaction sites or isolating larger regions through pore plugging and diversion of flow (Melkote and Jensen, 1989; Rege and Fogler, 1989).

The study of reaction fronts and their propagation is potentially important in the study of contaminant transport. Contaminants can ensue from industrial processes and mining so that waste streams contain hazardous concentrations of metals at low pH. These streams are prone to reacting with the porous medium, forcing dissolution until pH buffering occurs, then precipitating metallic salts. Cherry et al. (1984) have stated that, in predicting the movement of metals in such systems, "the critical task is the prediction of the advance of the front of the acidic zone." However, predictions are hampered by the difficulty of defining the types and rates of reactions controlling solute migration (Konikow and Papadopulos, 1988). When data on reaction kinetics do exist, simulating solute transport coupled to disequilibrium reactions requires considerable computational capacity, particularly if hydraulic evolution resulting from dissolution and precipitation is included. Only a few recent studies (e.g., Ortoleva et al., 1987; Hoefner and Fogler, 1988; Rege and Fogler, 1989; Steefel and Lasaga, 1990) have approached this problem, either through numerical modeling or laboratory experiments. There remains a need to examine the geochemical and hydraulic consequences of dissolution and precipitation in sediments while tracking the advance of the reaction front.

The goal of this thesis is to develop an improved understanding of the behavior of reaction fronts and the nature of coupling between fluid flow, solute transport, reaction, and hydraulic changes in groundwater settings. More specifically, I will use physical modeling to examine the mechanisms of and controls on reaction front propagation, perturbation, and zonation during the flow of oxidized iron solution through calcareous sands. The experimental approach involves tracking spatial and temporal trends of geochemical and hydraulic parameters as the reactive solution moves at different velocities through soil columns containing varying amounts of calcite.

Including this introduction, the thesis is organized in five chapters. The remainder of this chapter outlines how dimensionless groups can characterize reaction front behavior; provides the rationale for selecting the geochemical system; and reviews the pertinent reactions. Chapter 2 details the experimental set-up and analytical methods. The results of the experiments in terms of trends are given in Chapter 3. Mechanisms of geochemical evolution and hydraulic changes in the general system, and variations in frontal and zonal behavior as a function of flow rate and calcite percentage, are discussed in Chapter 4. Chapter 5 presents the summary and conclusions.

1.2. Criteria for Selecting the Chemical System

In modeling reaction and mass transport in the laboratory, it is desirable to select a chemical system which is both relatively simple and applicable to a variety of field settings. Applicability has sometimes been sacrificed in favor of simplicity, as in studies where fritted glass or sintered bronze have been acidized to simulate petroleum reservoir stimulation (Glover and Guin, 1973; Sinex et al., 1972). From a pragmatic perspective, the mixture of calcite and quartz sand that is used for all the experiments here is appealing because calcite is reactive, dissolving relatively rapidly at low pH, while quartz provides a relatively unreactive structural framework. In addition, the

composition of the sands can be easily varied, in contrast to natural limestones or sandstones. The introduction of Fe^{3+} solution is advantageous because its acidity induces calcite dissolution, which in turn causes the precipitation of a highly insoluble phase as pH is buffered. The hydrous character of this precipitate makes it potentially effective in reducing permeability. Its reddish color, in contrast to the relatively colorless quartz and calcite, facilitates visual tracking of the reaction front without the need for dyes.

From a field perspective, the ferric-calcareous system is relevant to both natural and anthropogenic topics. In the former case, hematitic terra rosa soils and goethitic rendzina soils both form on limestones in Mediterranean regions (Schwertmann and Taylor, 1989). Reardon et al. (1980) described a soil profile from southern Ontario in which, below the humus zone, secondary Fe oxyhydroxide coats sand grains and carbonates have been leached. At greater depth, there exists a leached/unleached contact, at which the coatings cease. A regional-scale geologic analog is active in southern Australia, where arid conditions promote subsurface drainage and highly weathered surficial strata possess limited acid neutralization capacity. The microbial reduction and dissolution of ferric oxyhydroxide coatings on aquifer sediments yields groundwaters with pH values as low as 2.8 and Fe concentrations as high as 0.004 molar (McArthur et al., 1991). The reoxidation of Fe in solution occurs via mixing with meteoric waters. At Fisherman Bay, South Australia, such groundwater discharges through marine carbonate sediments transgressing the quartzitic sand aquifer, so that a deposit of ferric oxyhydroxide is forming. Ferguson et al. (1983) have considered this as a possible mechanism for the formation of ore-grade ironstones.

The chemical system is relevant to various sorts of contaminant problems. For deep-well injection, Hower et al. (1972) and Scrivner et al. (1986) have provided case studies of the disposal of acidic, ferric waste into carbonate strata. As in the scenario for ore genesis, iron need not be externally introduced. The injection of acidic waste can

mobilize iron already present in aquifer sediments, with carbonate dissolution subsequently forcing the reprecipitation of iron oxides (Leenheer et al., 1976). Similar behavior can occur in acid-mine drainage (Wicks and Groves, 1991; Blowes et al., 1991).

1.3. Reactions of Interest

1.3.1. Calcite dissolution

The kinetics of calcite dissolution in aqueous systems have been studied by numerous workers, as reviewed by Plummer et al. (1979) and Dreybrodt (1988). Perhaps the most durable conceptual model is that formulated by Plummer et al. (1978). In this PWP (Plummer, Wigley, and Parkhurst) model, the mass flux R ($M/L^2/t$) is given by

$$(1.1)\ R = k_1[H^+] + k_2[H_2CO_3^*] + k_3[H_2O] - k_4[Ca^{2+}][HCO_3^-],$$

where k_n are rate constants (dimensions of L/t), [ ] indicates the activity of a species in the bulk solution (M/L^3), away from the calcite surface, and $H_2CO_3^* = H_2CO_3^o + CO_2$ (aq).

Each of the three forward (positive) rate terms in the PWP model predominates under different conditions of P_{CO2} and pH. At pH less than approximately 5.0, the first term, representing proton attack on the calcite surface, will be dominant. At pH greater than approximately 6.0 and P_{CO2} greater than approximately 0.1 atm, H_2CO_3 will facilitate dissolution, while at lower values of P_{CO2} in the same pH range calcite reaction with H_2O will predominate. These various regimes correspond to the surface reactions

(1.2) $CaCO_3 + H^+ = Ca^{2+} + HCO_3^-$

(1.3) $CaCO_3 + H_2CO_3^o = Ca^{2+} + 2HCO_3^-$

(1.4) $CaCO_3 + H_2O = Ca^{2+} + HCO_3^- + OH^-$.

At intermediate values of pH and P_{CO_2}, the influence of each forward term is comparable. The term containing k_4 includes forward and backward reactions close to equilibrium, thus accounting for precipitation. Talman (1991) and others have noted that the formulation of this last term is questionable and may need to include a dependence on $[CO_3^{2-}]$.

The control regime for calcite dissolution depends upon mass transport. Reactants and products are commonly thought of as diffusing across a boundary layer between the mineral surface and the bulk solution. The thickness of this layer, and thus the rate of diffusion, decreases as the bulk fluid velocity increases (Sjoberg and Rickard, 1984). For a sufficiently low velocity at acidic pH, calcite dissolution is controlled by the diffusion of H^+ to the surface and CO_2 away from the surface (Compton and Daly, 1984). With an increase in pH, the rate of attack is slower, so that dissolution becomes subject to mixed control. For a sufficiently high velocity at any pH, the rate of surface reaction becomes limiting (Sjoberg and Rickard, 1984). Compton et al. (1989) have shown that this transition can occur under laminar flow conditions at a pH below 4. However, Talman (1991) has noted that calcite dissolution is typically mixed-controlled.

1.3.2. Precipitation of ferric oxyhydroxide

When ferric salts are dissolved in water, the free ion Fe^{3+} begins to hydrolyze according to the reactions (Flynn, 1984)

(1.5) $Fe^{3+} + H_2O = Fe(OH)^{2+} + H^+$

(1.6) $Fe(OH)^{2+} + H_2O = Fe(OH)_2^+ + H^+$

(1.7) $Fe(OH)_2^+ + H_2O = Fe(OH)_3^o + H^+$

(1.8) $Fe(OH)_3^o + H_2O = Fe(OH)_4^- + H^+$

(1.9) $2Fe^{3+} + 2H_2O = Fe_2(OH)_2^{4+} + 2H^+$

(1.10) $3Fe^{3+} + 4H_2O = Fe_3(OH)_4^{5+} + 4H^+$

The species $Fe(OH)_n^{(3-n)}$ are referred to as monomers, while $Fe_2(OH)_2^{4+}$ (a dimer) and $Fe_3(OH)_4^{5+}$ (a trimer) are simple polymers, with the prefixes di- and tri- referring to the number of metal atoms in the polymers. By definition, the release of H^+ during hydrolysis lowers the pH of the solution. Fe^{3+} will continue to hydrolyze completely and relatively rapidly if the initial pH of the system after dissolution is greater than a critical value pH_B (Flynn, 1984). Otherwise, a waiting, or induction, period t_I ensues, after which hydrolysis goes to completion. The length of t_I increases with the initial concentration of Fe^{3+} because of decreased supersaturation with respect to ferric oxyhydroxide (Hsu, 1973). Stumm and Morgan (1970, p. 252) have noted that ferric solutions are only thermodynamically stable with respect to ferric oxyhydroxide for $Fe_T \geq 0.1$ M and pH < 2, and Fe(III) is ultimately maintained in solution only at $Fe_T < 10^{-10}$ M.

Polymerization occurs when hydrolyzed Fe species link up to form macromolecules made up of repeating structural units (Sisler et al., 1980, p. 834). One

possible mechanism of polymerization is the reaction (Hsu and Ragone, 1972; Melikhov et al., 1987; Grundl and Macalady, 1989)

$$(1.11)\quad nFe(OH)_3 = Fe_n(OH)_{3n}.$$

However, in reinterpreting the results of Hsu and Ragone (1972) and others, Flynn (1984) concluded that the polymer which forms the ferric oxyhydroxide macromolecule is cationic and continues to hydrolyze slowly. Each macromolecule is built from spheres 2 to 4 nm in diameter which contain approximately 100 Fe(III) ions in octahedral coordination with H_2O and OH^- (Flynn, 1984).

As polymerization progresses, the complete hydrolysis of monomeric species results. When the extra acidity thereby generated is buffered, as in calcareous systems, polymerization is accelerated. However, as pH increases, the number of spheres rises quickly at the expense of monomeric species, so that the growth of macromolecules through linkage of spheres is discouraged (Hsu and Ragone, 1972). Polymerization proceeds immediately if the initial pH is greater than pH_B. Polymerization and complete hydrolysis can also be induced, though, at t less than t_I and pH less than pH_B by seeding the solution with solution which has already begun to polymerize, thus promoting nucleation (Hsu, 1972). In each case, polymerization is followed by aggregation of particles and deposition (Flynn, 1984).

In strongly buffered systems, or with the rapid oxidation of Fe^{2+}, polymerization leads to the precipitation of a poorly crystalline ferric oxyhydroxide (Schwertmann and Taylor, 1989). This precipitate is commonly referred to as "amorphous hydrous iron(III) oxide" (Flynn, 1984) or "amorphous iron(III) hydroxide" (Hsu and Ragone, 1972). However, Schwertmann and Taylor (1989) state that the compound is ferrihydrite ($Fe_5HO_8 \cdot 4H_2O$), which exhibits short-range structural order

at the molecular level and therefore cannot strictly be considered amorphous. Reversing simplified dissolution reactions given by Flynn (1984), one obtains the precipitation reactions

(1.12) $Fe_2(OH)_5^+ = 2Fe(OH)_3$ ("amorphous") + H^+.

(1.13) $3Fe_2(OH)_5^+ = 5Fe(OH)_3$ ("amorphous") + H^+.

A continuum exists between dissolved, polymerized, and precipitated ferric species (Wang and Hsu, 1980) and between highly disordered and perfectly ordered structures (Schwertmann and Taylor, 1989). Therefore, it is possible the compound considered amorphous by Flynn (1984) and others is a neutralized polymer, from which ferrihydrite precipitates via a simplified dehydration reaction of the form

(1.14) $5Fe_n(OH)_{3n} = nFe_5HO_8 \cdot 4H_2O + 3nH_2O$.

Over a period of years, ferrihydrite may be transformed to hematite (α-Fe_2O_3) under hot, dry conditions, or to goethite (α-FeO(OH)) under cool, wet conditions (Schwertmann and Taylor, 1989).

The determination of a control regime when ferrihydrite precipitation accompanies calcite dissolution is more complicated than in the case of calcite dissolution alone. Via scanning electron microscopy, Loeppert and Hossner (1984) observed channels with stepped dislocations on calcite surfaces after reaction with $Fe(ClO_4)_3$ solution in stirred batch experiments. Such channels are indicative of surface-controlled dissolution. However, some rounding of edges and corners on calcite grains was evident, indicative of diffusion-controlled dissolution. The rate of

diffusion to reaction sites may have been slowed by a coating of ferrihydrite. Overall, mixed control of dissolution was probable.

1.4. Dimensionless Groups and Frontal Behavior

One can consider both dissolution and precipitation within the theoretical framework of heterogeneous reactions (those involving two phases). The PWP equation, for example, is of the general form (Plummer and Wigley, 1976)

$$(1.15)\quad j = (V/A)\, dC/dt,$$

where j is the mass flux ($M/L^2/t$), V is the solution volume (L^3), A is the reactive surface area (L^2), and C is the concentration of the reacting solute (M/L^3). For the sake of simplification, corrections for activity are being neglected and a heterogeneous, single-component reaction with linear rate is being assumed. The time rate of change of the concentration can be expressed as (Rickard and Sjoberg, 1983)

$$(1.16)\quad dC/dt = k\,(A/V)\,(C_{eq} - C_b),$$

where C_{eq} refers to the concentration of a dissolved salt in equilibrium with a solid and C_b the concentration of the salt in bulk solution. Redefining the reactive surface area with reference to the volume of the reactive solid (V_r) (L^3), one obtains (after White and Peterson, 1990)

$$(1.17)\quad A_r = (A/V) = n\,(A/V_r),$$

where A_r has dimensions of L^2/L^3 and n is the porosity (L^3/L^3), assumed for the purposes of this discussion to be constant. The reaction rate R can then be defined as

$$(1.18)\ dC/dt = R = A_r k\ (C_{eq} - C_b).$$

Equations 1.15 to 1.18 represent the temporal concentration gradient across the solution-solid interface in the absence of advective and diffusive/dispersive fluxes. If the solution volume is redefined as the volume of fluid in a representative elementary volume (REV) of porous medium, the temporal concentration gradient for the case of one-dimensional transport becomes

$$(1.19)\ \partial C/\partial t = D_h(\partial^2 C/\partial x^2) - v(\partial C/\partial x) + R/n$$

where v is the fluid velocity (L/t) and D_h is the coefficient of hydrodynamic dispersion ($M/L^2/t$) (after Domenico and Schwartz, 1990, p. 475).

Based on the generalized equation just developed, one can use dimensionless groups to characterize the dependence of front migration, geochemical zonation, and fingering on transport and reaction. Among these is the Peclet number,

$$(1.20)\ Pe = vl^*/D_h$$

where l^* is the length scale of the flow system (L) (Steefel and Lasaga, 1990). Pe pertains to transport-controlled systems, in which the competition to control the rate of reaction occurs between advective and dispersive (mixing-induced) transport. The second governing group is the Damkohler number (Steefel and Lasaga, 1990)

$$(1.21)\ Da = kA_r l^*/v.$$

The balance between v and the product kA_r represents the respective contributions of mass transport and the reaction rate to the progress of the front or zone, so that Da becomes dominant in surface-controlled systems. Local equilibrium, or transport control, is technically attained when kA_r goes to infinity (Lichtner, 1988).

The effect of velocity on front and zone behavior is complicated, because an increase in v has divergent impacts in transport- and surface-controlled cases (Steefel and Lasaga, 1990; Bahr, 1990). The length of the front decreases, and the growth of dissolution fingers is promoted, both as Pe increases in the transport-controlled case and as Da increases in the surface-controlled case. The length of fingers attains a maximum value in the intermediate case of mixed control, provided D_h is sufficiently high. The impact of precipitation upon dissolution fingering at different flow rates has been studied by Rege and Fogler (1989), who acidized limestone with $FeCl_3$ solution in flow-through cells. As transport-controlled dissolution at a constant, sufficiently low volumetric flow rate was followed by precipitation, each new finger was successively repressed until fluid traveled through the unblocked pores at a velocity too fast to permit plugging. Increasing the initial flow rate, or decreasing the initial value of Da, between experiments in such a system meant that the growth of fingers was less affected by plugging from the start.

2. MATERIALS AND METHODS

2.1. Column Design and Operation

Columns for flow and reaction studies used components which could be readily assembled "off-the-rack" and which were made of chemically resistant materials. Preliminary visual studies employed Kontes glass HPLC columns with Teflon end-fittings. Subsequent observations of reaction-front behavior, as well as geochemical and hydraulic data, were gathered in experiments using plastic columns constructed in the laboratory . Each plastic column consisted of clear PVC pipe, with fittings of PVC, ABS, and polyethylene; specifications are provided in Table 2.1. The diameter of these columns was intended to be large enough to minimize the percentage of flow which might occur preferentially along the wall, yet small enough that, at a 10:1 length-to-diameter ratio, the column would not be too heavy to safely stand upright when filled. At the base (inlet) of each column, a sintered stainless steel plate (Mott Metallurgical Corp., Farmington, Connecticut) containing tortuous pores 7 μm in diameter supported the medium and distributed flow. A disc of Teflon cloth at the top of the column held sand grains in place. Sample ports along one side of the plastic column contained manometers for measuring hydraulic head. In addition, one manometer, which was connected to the line or chamber below the plate, indicated head at the inlet.

Each column was packed with a mixture of washed and sieved Ottawa quartz sand (grade 2.6, U.S. Silica Co., Ottawa, Illinois) and crushed calcite (originally obtained as massively crystalline boulders from Earth Science Educator's Supply, Lee's Summit, Missouri). The experimental trials each consisted of three columns containing initially 1.02% to 10.0% calcite by volume (Figure 2.1). This mixture is representative of sandstones, which typically contain 0% to 30% calcite cement by volume (Blatt, 1982). Except for experiment 2, in which the initial amount of calcite was varied

Table 2.1.
Inside diameter and length of columns used in study. Difference in dimensions between preliminary experiments and remainder of experiments reflects glass (HPLC) columns versus plastic. Difference between experiments 1 to 4 and experiments 5 to 8 reflects slight difference in inside diameter of end fittings (columns in 1 to 4 could fit further into lower endcap). Lengths for experiments 1 to 5 accurate to within 0.01 m; exact lengths measured beginning with 6.

Experiment	Diam. (mm)	Length (m)
P1	50.8	0.610
P2	50.8	0.610
1-1	77.3	0.785
1-2	77.3	0.785
1-3	77.3	0.785
2-1	77.3	0.785
2-2	77.3	0.785
2-3	77.3	0.785
3-1	77.3	0.785
3-2	77.3	0.785
3-3	77.3	0.785
4-1	77.3	0.785
4-2	77.3	0.785
4-3	77.3	0.785
5-1	77.3	0.765
5-2	77.3	0.765
5-3	77.3	0.765
6-1	77.3	0.763
6-2	77.3	0.768
6-3	77.3	0.766
7-1	77.3	0.765
7-2	77.3	0.763
7-3	77.3	0.766
8-1	77.3	0.766
8-2	77.3	0.765
8-3	77.3	0.765

Figure 2.1.
Triplicate columns for experiment 3, demonstrating representative set-up for experiments 1 to 8. The peristaltic pump in the background directs influent solution from a carboy above (not shown) to the inlet at the base, and thence up the column. Ports connected to manometers are spaced at 10-cm intervals within the medium; within the reaction zone, sample ports are spaced between manometer ports at 2.5-cm intervals.

between columns, the three columns were replicates. In the studies with the glass columns and experiments 1 to 4 (performed at The Ohio State University), unsieved, unwashed calcite was used. Experiments 5 to 8 (performed at the University of Alberta), however, contained calcite which had been dry-sieved between #35 and #60 screens (500 - 250 μm), rinsed with deionized water, and air-dried. This size interval corresponded to the predominant size range of the Ottawa sand. Appendix I details grain-size analyses on samples of sand and crushed calcite, as well as surface-area measurements on calcite.

Packing columns in experiments 1 to 5 involved weighing out calcite to a mass equivalent to the desired volumetric percentage, then filling the remainder of the column with Ottawa sand. When, after repeated manual compaction, virtually no more sand could be added, the contents were homogenized in a cement mixer, then repacked and sealed. For experiments 6 to 8, both the percentage of calcite and the porosity were fixed. The mass of Ottawa sand necessary to fill each column in experiment 6 was weighed, then increased slightly to account for a longer period of compaction, before mixing. Computerized tomography (CT) scans of the lower third of each column in 6 indicated that, although quartz and calcite grains were slightly segregated adjacent to the wall, the final pack was relatively homogeneous (G. Sedgwick, Alberta Research Council, personal communication). For experiments 7 and 8, with known masses of both calcite and quartz, packing prior to mixing was eliminated.

Prior to initial saturation, each column was flooded with at least 10 pore volumes of CO_2 (g) in order to displace air (Sudicky et al., 1985; Schincariol, 1989). Subsequently, the gas was dissolved and displaced by upward-flowing deaired, deionized H_2O. The flow was directed upward to dampen any gravitational instabilities associated with subsequent solute transport. The dissolution of CO_2 (g) also created a weak H_2CO_3 (aq) acid preflush, thereby cleaning the surfaces of the quartz and calcite grains. Although small, scattered patches of gas were trapped against the walls of some

columns after waterflooding, CT scans of flooded columns prior to experiment 6 indicated that saturation was generally achieved. Flow was driven by gravity from a carboy at a level above that of the outlets, with rates being regulated by an Ismatec mv-ge peristaltic pump (Cole-Parmer Instrument Co., Chicago) at approximately 2.0 or 4.0 ml/min. The corresponding velocities, 1.9×10^{-5} to 4.1×10^{-5} m/s, were similar to the value of 4.0×10^{-5} m/s which Schulz (1988) considered as realistic for groundwater flow through surficial sands.

In the preliminary experiments, two different influent solutions were used. For P1, the influent solution to a control column contained 500 mg/l Rhodamine (WT) dye (Keystone Aniline Corp., Chicago). The second solution contained 500 mg/l dye and 3042 mg/l $NaClO_4$, giving a total solute mass equivalent to 0.01 moles of $Fe(ClO_4)_3$. In experiment P2, the dye-salt solution was used in the control column. In the reactive column, and in all subsequent experiments, a solution of approximately 0.01 moles $Fe(ClO_4)_3$ per kg was used (perchlorate salts obtained from GFS Chemicals, Columbus, Ohio). 0.01 moles $Fe(ClO_4)_3$ per kg was used by Hsu (1972) and Hsu and Ragone (1972) in their studies of polymerization, and by Loeppert and Hossner (1984) and Loeppert et al. (1984) in studies of calcite dissolution and ferrihydrite precipitation. The ClO_4^- salts were selected here because that ion only weakly complexes in solution (Schilt, 1979).

2.2. Protocols for Monitoring and Sampling

Physical measurements during each experiment included tracing the position of the visible ferric oxyhydroxide precipitation front; monitoring hydraulic heads in the manometers; and monitoring fluid flow rates at the outlet. Chemical measurements included monitoring pH and electrical conductivity of the fluid and collecting fluid samples for measuring inorganic carbon, Ca, and Fe. Sample handling and chemical

measurement techniques for experiments 1 to 4 were deemed afterward to have been inadequate, as discussed at the end of Section 2.3.1. Consequently, subsequent discussions of experimental protocols and chemical analyses are limited to experiments 5 to 8 except as noted otherwise. In order to maintain chemical sample integrity, labware was rinsed with deionized water, and almost always pre-rinsed with concentrated HCl, before reuse. Most labware, tubing, pipe, and fittings were soaked in a dilute solution of Micro detergent (Cole-Parmer) for at least 24 hours, then rinsed thoroughly with hot water and deionized water.

Following the introduction of $Fe(ClO_4)_3$ solution in each experiment, the electrical conductivity, hydraulic head, and flow rate were typically measured every one to two hours until a sharp rise in electrical conductivity indicated solute breakthrough at the downstream end of the column. The increase in electrical conductivity with breakthrough resulted from the first arrival at the outlet of the conservative species ClO_4^- and the products of calcite dissolution along the flowpath. The flow rate was monitored by collecting known quantities of effluent during a given interval of time. After experiment 1, only effluent samples were analyzed prior to the end of an experiment. The extraction of a porewater sample large enough for analysis during the experiment would bias subsequent reaction progress within a column. Apart from tracking breakthrough, all measurements were typically made at intervals of 3, 6, 12, 24, 36, and 48 hours, then every 24 hours thereafter until the conclusion of the experiment. Each effluent sample was split for pH, electrical conductivity, TIC, and dissolved cation measurements. Observations of the positions of the precipitation fronts, which were recorded both by photography and drawn traces on acetate overlays, were made according to this measurement schedule. Additionally, each time the $Fe(ClO_4)_3$ reservoir was replaced (usually every one to two days during a experiment), samples were taken to monitor pH, electrical conductivity, and Fe in the influent.

Beginning approximately 12 hr before the end of an experiment, porewater samples were collected from each column starting down the hydraulic gradient from the precipitation front and working progressively up-gradient. Commonly, two or three down-gradient ports and four or five up-gradient ports would be sampled, one at a time, per column, with all three columns being sampled simultaneously. As with the effluent samples, porewater was collected via dripping into 30-ml polyethylene sample vials, after a volume of fluid equal to or greater than the volume of the port and tubing had been evacuated. Flow through each port was controlled to minimize sample-related disturbances and to avoid induced flow from down-gradient. Moreover, sampling was conducted as expeditiously as possible to minimize sample contact with the atmosphere, and any headspace in the sample vial was kept to a minimum. For TIC measurement, atmospheric contact was minimized further by using disposable plastic syringes to extract separate samples in between flushing the lines and collecting drip samples. The drip samples of porewater were split for measuring pH, electrical conductivity, Ca, and Fe. All fluid samples were analyzed as quickly as possible, and were refrigerated if analyses could not be conducted within a few hours, at most 18.

At the end of an experiment, the reactions in the column were halted by freezing the porewater. Each column was clamped, transferred to a cold room with an ambient temperature of approximately -5° to -12°C, and placed upright atop dry ice as the column outlet was unclamped. A preferential freezing wave was thereby induced with minimal sample disturbance (A. Küpper, HBT-Agra, personal communication). The consolidated column was sawed into 0.025-m thick slices transverse to the long axis, then photographed to record the internal morphology of the precipitation zone, prior to subsampling.

2.3. Protocols for Sample Analyses and Parameter Calculations

2.3.1. Analyses of water and sediment samples

For pH measurement on water samples, a Radiometer model 26c pH meter was used with a Orion model 81-15 combination electrode, filled with 3 M $NaNO_3$ solution in order to avoid ClO_4^- interference. Whether because of heating associated with stirring, exchange of CO_2 (g) with the atmosphere, or some other factor, pH values had been observed to increase with time during previous measurements. The meter was therefore connected to a chart recorder (Houston Instrument model A-5113-5I). Traces recorded as corresponding to pH 2.00, 4.00, 7.00, and 10.00 buffers (Fisher Scientific) were observed to stabilize after approximately eight minutes. For every measurement, the chart reading was thus taken at room temperature eight minutes after the meter, stirrer, and recorder were started. The pH value for any sample was calculated from the line fit via least squares between the two nearest buffers. Samples for most of experiment 5 were measured without adjusting the calibration of the pH meter. However, for greater accuracy, the remaining porewater samples in 5 and all samples from subsequent experiments were measured with periodic recalibration of the meter. If more than 8 hr had elapsed since the meter was last calibrated, or if the pH between samples was sufficiently different, each of two buffers bounding the anticipated pH range was measured and the meter readings were adjusted for the correct temperature, after which new standard traces were recorded.

Electrical conductivity was measured at room temperature on unstirred samples using a Cole-Parmer conductivity/temperature meter with a dip cell and a microflow cell (experiments 1 to 4) and a Radiometer model 2f conductivity meter with a model CDC 104 electrode (experiments 5 to 8). In order to minimize the volume of fluid used, the CDC 104 electrode was inverted, then rinsed and refilled with the fluid to be measured.

Like pH, electrical conductivity changes with temperature, so readings were recorded as quickly as possible after filling. In experiments 5 to 8, the temperature in the laboratory, while ranging from 20 to 25°C, generally remained at 23 +/- 1 °C. The calibration of the Radiometer meter, which was not readily adjustable, was checked against a 0.1000 N KCl solution before each experiment, and was found to underestimate the standard reading by less than 4%. For experiments 1 to 4, the Cole-Parmer meter was occasionally recalibrated against a 0.005 N KCl standard solution, and readings were corrected by an automatic temperature compensator to 25°C.

Subsamples for TIC analysis, unlike cation samples, could not be acidified, so they were simply refrigerated until they could be analyzed after a experiment. TIC measurements were conducted on a Dohrmann carbon analyzer at the Oil Sands and Hydrocarbon Recovery (OSHR) Department, Alberta Research Council. The syringe containing each sample was uncapped and an appropriate volume of fluid was withdrawn and injected into the instrument using an HPLC syringe. The carbon analyzer was calibrated by the injection of varying volumes of 400 or 800 mg/l TIC standards prepared by OSHR staff. In order to account for a deviation from the original linear response of the instrument, a power fit was made to each standard curve using a transformed least-squares routine. TIC values for most experiment 5 samples were determined by fitting to a single curve, whereas subsequent results, for greater accuracy, were fit to a new standard curve for every 10 sample analyses.

Prior to cation analysis, all water samples were vacuum-filtered through a Nuclepore 0.05-µm polycarbonate filter mounted atop a Fisher Scientific Filtrator. Analyses by Byrne and Kester (1976) have shown 0.05 µm to be more reasonable than 0.45 µm (the pore size commonly used for filtration before atomic adsorption analysis) as a threshold between dissolved and colloidal Fe. Porewater samples for cation analysis were split, with a portion left unfiltered in order to determine total (suspended plus dissolved) Ca and Fe. For experiment 5, unfiltered samples were preserved only if

collected at or behind the reaction front. A quantity of solution containing 50000 mg/l La in 25% HCl was then added to each sample so that the resulting volume would contain 2000 mg/l La and 1% HCl (Dept. of Soil Science, Univ. of Alberta, 1987). The La was intended to damp interferences in the determination of Ca by atomic adsorption, while the acid served as a preservative. For greater accuracy, particularly in working with sample volumes less than 10 ml, virtually all solutions and dilutions in experiments 1 to 8 were prepared gravimetrically using an electronic balance readable to 0.01 g. Therefore, solution and suspension concentrations are reported in units of μg per g of fluid, and solid-phase concentrations in μg/g (s). After acidification, water samples were re-refrigerated prior to analysis.

Determinations of solid-phase Ca and Fe concentrations were begun by selecting sediment slices corresponding to the positions of the sample ports along the column and allowing those slices to thaw. In addition, the sediment within each endcap, below the first sample port, was thawed. Each sediment sample was then gently homogenized with a Scoopula for at least one minute, after which at least at least 5 g of the wet sediment was scooped into the glass Nuclepore filter holder. The remaining sediment was refrozen in case repeated analyses were necessary. Each subsample was then vacuum-filtered, rinsed with deionized water, and filtered again in order to remove residual porewater. Following oven-drying at approximately 105°C, the subsample was then weighed and 5 or 10 ml of concentrated HCl was added in order to dissolve calcite and ferric oxyhydroxide. The digestant was decanted into a 250-ml sample bottle and the sediment was rinsed several times with deionized water, with the rinse water being decanted into the bottle each time. Rinsing continued until the water was consistently colorless and the fluid mass approached 96% of its intended value (typically 50 g), whereupon the La/HCl solution was added to round out the mass. In order to remove any sand grains inadvertently added during decantation, the fluid was vacuum-filtered before analysis.

Atomic adsorption analyses on influent, effluent, porewater, and digested solid samples were run on a Perkin-Elmer model 503 spectrophotometer in the Department of Geology, University of Alberta, using different multi-element lamps for Ca and Fe. Readings were recorded in terms of adsorption units. Standard curves were generated after every 5 samples for experiment 5, and after every 10 samples for subsequent experiments, using 1.00, 3.00, and 5.00 μg/g (fluid) standards prepared from 1000 mg/l stock solutions (Ca from Fisher Scientific, Fe from BDH Chemicals), plus a deionized water blank. The blank and standards, like the samples, each contained 4% of the La/HCl solution by mass. Sample concentrations were calculated by fitting readings to the linear least-squares equation determined for the nearest set of standard measurements. Concentrations are reported to two significant figures except where readings were less than 0.010 absorption units, in which case readings are reported to a single significant figure. Serial dilutions were done as necessary; where readings taken at different dilutions for a single sample fell within the prescribed linear concentration range (up to 5.00 μg/g), their values were averaged. Reproducibility of analyses was good: the coefficient of variation for replicate values was no more than 1.1% for Ca and no more than 2.8% for Fe. After the analysis of water samples for experiment 6 and solid-phase samples for experiment 5 and column 6-1, it was noticed that absorption readings for Fe standards had begun to drift upward. Therefore, new standards were prepared for subsequent analyses, and concentration values for the samples in question were calculated by fitting to the last set of standard values deemed acceptable.

The chemical composition and texture of the precipitate were examined using X-ray diffraction and scanning electron microscopy, respectively. A sediment sample containing ferric oxyhydroxide was sonified and wet-sieved through a #200 (75-μm) screen, after which several drops of the resulting suspension were pipetted onto a glass slide and allowed to air-dry. A step-scan was run from 2.00° to 65.00° at 0.1° intervals using a Philips Electronics PW 1316/90 Wide Range Goniometer, XRG 3100 X-ray

Generator, and DMS-41 Data Measuring System in the Department of Agronomy at The Ohio State University. The diffractogram and a table listing the data points used to generate it were checked against cards listing the JCPDS (1984) standards for minerals which might have been present. Textural observations were made on sediment collected near the inlet of one of the columns from experiment 1. Micrographs of sediment subsamples were taken at magnifications of 35x to 1500x on a JEOL JSM-820 scanning electron microscope in the Department of Geological Sciences at The Ohio State University.

Several procedural shortcomings led to the decision to disregard most of the chemical data from experiments 1 to 4. Samples from experiments 1 and 2 were typically stored unacidified and with headspace in the vials for days at room temperature, so that a white precipitate formed (presumably $CaCO_3$ resulting from slow degassing of CO_2). These samples were then filtered prior to cation analyses, giving data unrepresentative of original Ca concentrations in solution. Porewater samples were not collected in experiment 2, and no unfiltered splits were analyzed in experiments 1 to 4; the pore size of the filters used was 0.45-μm, nine times larger than in experiments 5 to 8. As samples were serially diluted, the percentage of acid was not maintained at the original value of 4%, and no La was added to samples from experiment 1. No measurements of pH or of inorganic carbon concentrations were made for experiments 1 and 2. For experiments 3 and 4, the determination of stable pH values was problematic due to drift during measurement; this problem also affected alkalinity titrations, which were performed instead of TIC analyses.

2.3.2. Calculating values of hydraulic conductivity

Even though a peristaltic pump was used to regulate the flow in each column, the flow rate fluctuated to some extent. Values of hydraulic conductivity were thus

determined for different times during each experiment by extrapolating the nearest measurement of the flow rate to a set of hydraulic head measurements. Hydraulic conductivity (K, in dimensions L/t) was calculated from the one-dimensional form of Darcy's equation

$$(2.1)\ Q/A_{cs} = -K\ \Delta h/\Delta x$$

where Q is the flow rate (L^3/t), A_{cs} is the cross-sectional area (L^2), and $\Delta h/\Delta x$ is the hydraulic gradient between a given pair of manometers.

The hydraulic gradient between the inlet manometer, h_I, and the first manometer in the sand, h_1, incorporated the hydraulic conductivity of the porous metal plate (K_p). Its value, 0.0000448 m/s, is more than an order of magnitude less than the background hydraulic conductivity of the sand. The value of hydraulic conductivity, K(i-1), between the top of the plate and h_1 (a distance d(i-1)) was therefore determined from the equation for hydraulic conductivities in series

$$(2.2)\ K(i\text{-}1) = d(i\text{-}1)/((d_z/K_z) - (d_p/K_p)).$$

Here, K_z is the overall hydraulic conductivity, d_p is the thickness of the plate, and $d_z = d_p + d(i\text{-}1)$.

3. RESULTS

3.1. Characterizing Results in Terms of Initial Variables

It is of interest to examine the extent to which trends in geochemical and hydraulic parameters result from changes in the initial flow rate and/or the initial amount of calcite. Table 3.1 lists the values of flow rates, percentages of calcite, and related variables for the various experiments. Among the related variables, values of physical surface area (A_p) for calcite have been derived from replicate grain-size and surface-area analyses, as detailed in Appendix I. In the cases of both unsieved (experiments 1 to 4) and sieved (experiments 5 to 8) calcite, the physical surface area increases proportionally with the volumetric percentage of calcite.

As noted in equation 1.17 (Section 1.4), defining the reactive surface area involves the porosity n, values of which were specified for experiments 6 through 8. One can define the effective, or interconnected, porosity n_e which relates the volumetric flow rate to the porewater velocity (Domenico and Schwartz, 1990, p. 57):

$$(3.1)\quad n_e = Q/(vA_{cs}),\ \ n_e \leq n.$$

The effective porosity can be obtained from solute breakthrough curves, as given by the plots of electrical conductivity versus time in Section 3.3.2, using the equation

$$(3.2)\quad n_e = t_bQ/V_T,$$

where t_b is the length of time between the start of the experiment and breakthrough (as defined by $C/C_0 = 0.5$ (Freeze and Cherry, 1979, p. 390)) and V_T is the total volume of the porous medium. However, because of the likelihood that the velocity of porewater

with salt concentrations > 1000 μg/g was retarded by density contrasts (Schincariol, 1989), the calculated value of n_e is likely to overestimate the actual value. It is therefore more appropriate to calculate n_e based on the initial waterflooding of the column, for which t_b in equation 3.2 becomes the time to water breakthrough. Prior to experiment 6, though, columns were saturated by gravity-driven flow without using the pump, so Q was not constant during waterflooding.

By means of several assumptions, values of porosity and effective porosity have been calculated for experiments 1 to 5. For the final four experiments, measurements of electrical conductivity in effluent were sufficiently numerous to delineate the solute breakthrough curves, so times to breakthrough were calculated by least-squares linear fitting to the ascending part of each curve. The resulting average linear equations for experiments 5 and 6 were applied to the ascending parts of solute breakthrough curves for experiments 2 and 3, respectively, where data were sparse but initial values of velocity and of calcite content were similar to those in 5 and 6. Values of n_e based on solute breakthrough times were then calculated for experiments 2, 3 (except column 3-2, for which insufficient data were available), 5, 6, 7, and 8. For the last three experiments, the resulting values of n_e were plotted against the values calculated from waterflooding, the point (0,0) was added, and a relation was calculated by least-squares linear fitting. From this relation, values of n_e equivalent to waterflood-derived values were calculated for experiments 2, 3 (except 3-2), and 5. The values thus obtained were assumed to apply to experiments for which breakthrough data were lacking but initial calcite contents were similar: n_e for 2-1 to experiment 1; n_e for 2-2 to experiment 4; and the average n_e from 2-3, 3-1, and 3-3 to column 3-2. This final assumption is acceptable because the packing technique was relatively uniform for a specified amount of calcite, as indicated by a coefficient of variation of 12.9% in the n_e values for columns 2-3, 3-1, and 3-3. In the absence of data on n for experiments 1 to 5, n was assumed to be equal to n_e. Conversely, for experiment 7, values of n_e calculated from

waterflooding slightly overestimated the set value of n (a theoretical impossibility), so n_e was assumed equal to n. The various values of n and n_e are tabulated in Table 3.1. For experiments 6 to 8, where values of n_e could be independently calculated from waterflooding and from solute breakthrough, the former values were smaller, as expected.

Porewater velocities (Table 3.2) did not vary exactly by a factor of two between high- and low-flow experiments. The discrepancy results not only from differences in the effective porosity, but also from variations in the flow rate. These variations are due to the necessity of calibrating pump tubing individually for each column, as well as to the occurrence of occasional, small leaks. Initial values of velocity have not been calculated where the corresponding values of the flow rate were considered to be unrepresentative of the set flow rate. This occurred for column 1-3, where the first measured flow rate (1.31 ml/min) was markedly less than the set value (approximately 2 ml/min); 4-1, with a decline in the flow rate from 3.21 to 2.27 ml/min over the first 12 hr; and 4-3, with a decline in the flow rate from 2.05 to 1.39 ml/min over the first 37 hr.

Previous studies have observed that calcite dissolution (Talman, 1991) and associated ferrihydrite precipitation (Loeppert and Hossner, 1984) are subject to mixed control, in which the rates of reaction and transport compete to control reaction progress. For this reason, it is useful to examine the behavior of reaction fronts and zones in terms of varying the initial value of the Damkohler number ($kA_r l^*/v$) between experiments. In contrast to Rege and Fogler (1989), this was achieved by varying the initial surface area (of calcite) for some experiments and the initial velocity for others.

Formulating the initial value of the Damkohler number is problematic in that both dissolution and precipitation reactions are involved, which begs the question of which reaction rate constant to use. As noted in Section 1.3.2, the formulation is further complicated by the absence of a value of the reaction rate constant k for ferric oxyhydroxide precipitation. However, this conundrum can be avoided if one is merely

Table 3.1. Values of kinematic (breakthrough- and waterflood-derived) and volumetric porosity in study.

Column #	n break. (%)	n flood (%)	n eff. (%)	n vol. (%)
1-1		34.4	34.4	34.4
1-2		34.4	34.4	34.4
1-3		34.4	34.4	34.4
2-1	37.6	34.4	34.4	34.4
2-2	37.3	34.2	34.2	34.2
2-3	33.8	31.0	31.0	31.0
3-1	30.4	27.9	27.9	27.9
3-2		27.6	27.6	27.6
3-3	26.1	24.0	24.0	24.0
4-1		34.2	34.2	34.2
4-2		34.2	34.2	34.2
4-3		34.2	34.2	34.2
5-1	40.0	36.6	36.6	36.6
5-2	39.0	35.7	35.7	35.7
5-3	40.5	37.1	37.1	37.1
6-1	37.5	35.1	35.1	36.2
6-2	34.8	32.6	32.6	36.6
6-3	36.0	34.5	34.5	36.4
7-1	42.2	36.4	36.3	36.3
7-2	38.2	36.7	36.3	36.3
7-3	38.9	36.9	36.3	36.3
8-1	38.8	32.8	32.8	36.3
8-2	33.3	29.2	29.2	36.3
8-3	38.0	35.3	35.3	36.3

Table 3.2. Initial values of physical and chemical parameters in study.
* Q and v values taken before or just after start of run; Q values considered unrepresentative for 1-3 and unstable for 4-1 and 4-3, so no values of v were calculated in those cases.
**Time to failure for 1-1, 1-3, 2-1, and 2-2; time estimated for 2-1 and 2-2.

Column #	Vol. % calcite	A (m2/m3)	Q (ml/min)*	v (m/hr)*	run t (hr)**	normalized Da
1-1	10.0	61800	1.82	0.0676	211.25	25.1
1-2	10.0	61800	1.80	0.0669	536.98	25.4
1-3	10.0	61800	1.31		97.15	
2-1	10.0	61800	4.21	0.156	106.25	10.8
2-2	5.00	30800	4.03	0.151	84.92	5.59
2-3	2.00	11700	4.79	0.198	178.58	1.63
3-1	2.00	11200	1.89	0.0868	195.02	3.55
3-2	2.00	11200	1.81	0.0839	194.68	3.66
3-3	2.00	10700	1.75	0.0934	194.85	3.13
4-1	5.00	30800	3.21		168.78	
4-2	5.00	30800	1.84	0.0689	168.57	12.3
4-3	5.00	30800	2.05		168.42	
5-1	2.04	11200	4.03	0.141	171.40	2.12
5-2	2.04	11000	3.90	0.140	171.40	2.11
5-3	2.04	11300	3.99	0.138	171.40	2.18
6-1	2.04	11100	2.00	0.0730	167.87	4.06
6-2	2.03	11100	1.84	0.0721	167.87	4.14
6-3	2.04	11100	1.81	0.0672	167.87	4.44
7-1	1.02	5560	1.98	0.0698	169.52	2.13
7-2	1.02	5560	1.94	0.0684	169.50	2.17
7-3	1.02	5560	1.95	0.0687	169.48	2.17
8-1	1.02	5560	3.82	0.149	165.27	1.00
8-2	1.02	5560	3.36	0.147	165.27	1.01
8-3	1.02	5560	3.90	0.141	165.25	1.05

varying the initial Da, because the initial reactions of interest do not vary between experiments, and any rate constant selected should, by definition, be invariant. Lichtner (1988) defined the length scale l^* as the position of the boundary between partly-reacted and totally-reacted zones in the medium, which changes with time, while other authors, including Hoefner and Fogler (1988) and Steefel and Lasaga (1990), have considered l^* to be time-invariant. Following Steefel and Lasaga (1990), l^* is arbitrarily taken here as the length of the porous medium.

One can thus establish a basis for comparison between different experiments by defining for each column a normalized value of the initial Damkohler number:

$$(3.3)\quad Da_n = (kA_r l^*/v)/(kA_r l^*/v)_{min},$$

where values of l^*, v, and A_p are known. Because k is invariant, if A_p can be assumed to be linearly proportional to A_r (as discussed in Appendix I), it is not necessary to quantify k and A_r in order to identify the column with the smallest initial value of Da, $(kA_r l^*/v)_{min}$. Instead, k and the constant of proportionality between A_p and A_r cancel in the numerator and in the denominator of equation 3.3, and Da_n can be calculated by dividing the ratio $A_p l^*/v$ for each column by the smallest measured value, that of column 8-1. Values of Da_n (Table 3.2) range from 1.00 (column 8-1) to 25.4 (column 1-2).

3.2. Observations of Reaction Front Behavior

For this study, the reaction front is defined as the visible limit of precipitation. This definition will be evaluated later in light of concentration data along the column. However, gas commonly appeared ahead of the reaction front. For each column in experiment 2, regardless of the amount of calcite, a band of gas materialized approximately 0.15 m down-gradient from the inlet within 12 hr of introducing the

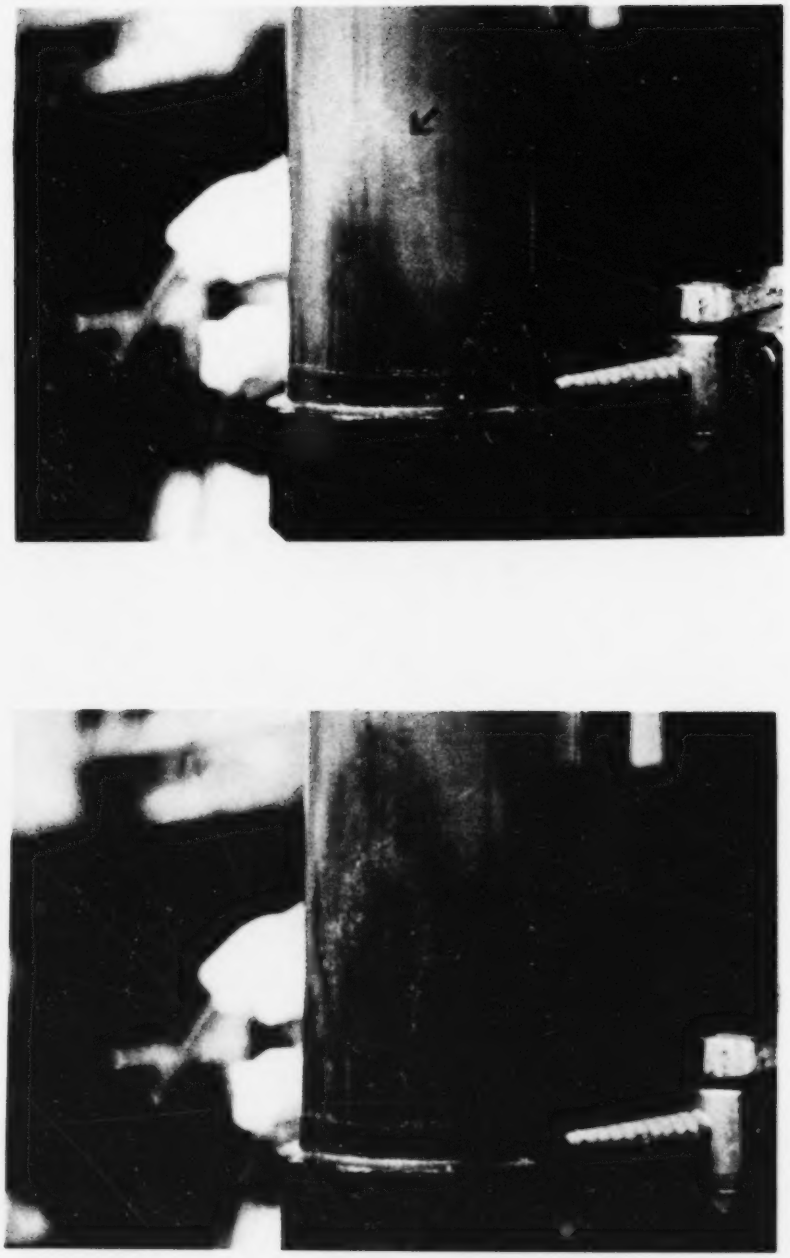

Figure 3.1.
Experiment 2, column 2-3, showing gas front.
(a) Top: t = 12 hr; maximum advance of gas front = 0.11 m, maximum advance of reaction front = 0.13 m.
(b) Bottom: t =37 hr; gas front stationary; reaction front maximum at 0.18m.

influent. This gas front (indicated by an arrow for Figure 3.1a, column 2-3) mimicked the shape of the reaction front, but, unlike the reaction front, it remained stationary after materializing (Figure 3.1b). In other experiments, gas entrapment was more patchy and diffuse, with occasional, vertical stringers of bubbles.

The propagation of the reaction front is illustrated for experiment P2 in Figures 3.2a - b. Infiltration of $Fe(ClO_4)_3$ solution and fingering were visible in the reactive column to a distance of approximately 0.05 m down-gradient within the first 30 minutes. After this time, the front virtually halted and the region which had been infiltrated began to darken, especially along the front (Figure 3.2a). The initial fingers did not lengthen further, but adjacent instabilities appeared. The front as a whole resumed propagation down-gradient at a reduced rate approximately 12 hr after starting (Figure 3.2b).

The $NaClO_4$-dye solution in the control column, with density approximating that of the influent, initially advanced in parallel with the reaction front, but continued to propagate after 30 minutes. Dye breakthrough at the outlet corresponded closely (+/- 10 minutes; elapsed time 3.5 hr) with the solute breakthrough in the reactive column, as indicated by a sharp rise in electrical conductivity. In experiment P1, the same dense dye solution had migrated more slowly than the corresponding dye solution without salt. This behavior suggests that the influent solution initially propagates at the porewater velocity limited by density contrasts.

The plots of maximum frontal advance, or the farthest down-gradient position of the reaction front, versus time are shown in Figures 3.3a-d for experiments 1 to 4 and Figures 3.4a-d for experiments 5 to 8. Experiment 8 (Figure 3.4d) concurred with P2 in displaying an initial, relatively rapid penetration of the reaction front, followed by a plateau of a few hours, then by sustained frontal advance at a rate slower than that of the first stage. The reaction front in column 2-3 decelerated to a final, relatively constant velocity, but the plot of frontal advance does not show a discernible plateau (Figure

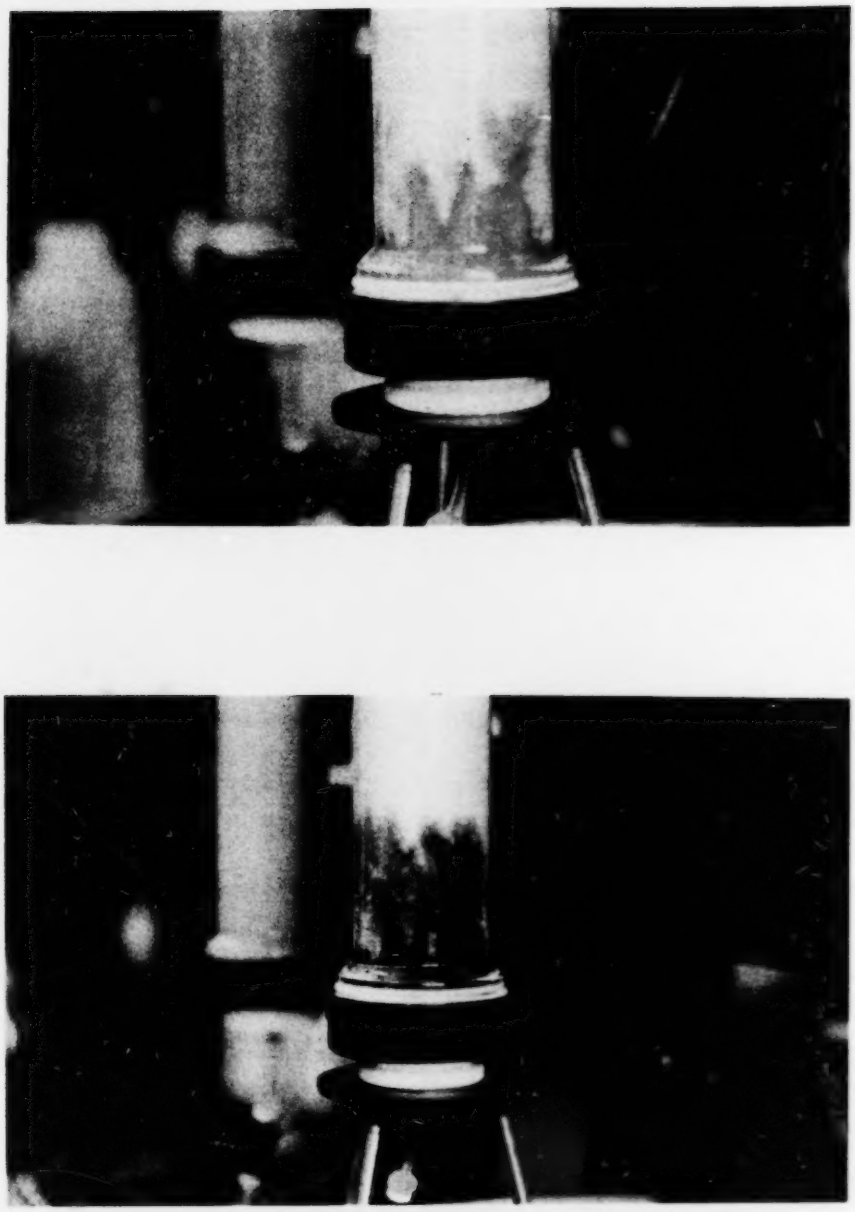

Figure 3.2.
Experiment P2, with reactive column (r) in foreground and control column (c) in background.
(a) Top: t = 2 hr; maximum visible position of reaction front in P2r = 0.05m. Note that dye front has surpassed position of reaction front in Stage 2.
(b) Bottom: t = 24 hr (dye flushed from P2c). Note darkening of initial fingers and diversion of subsequent precipation.

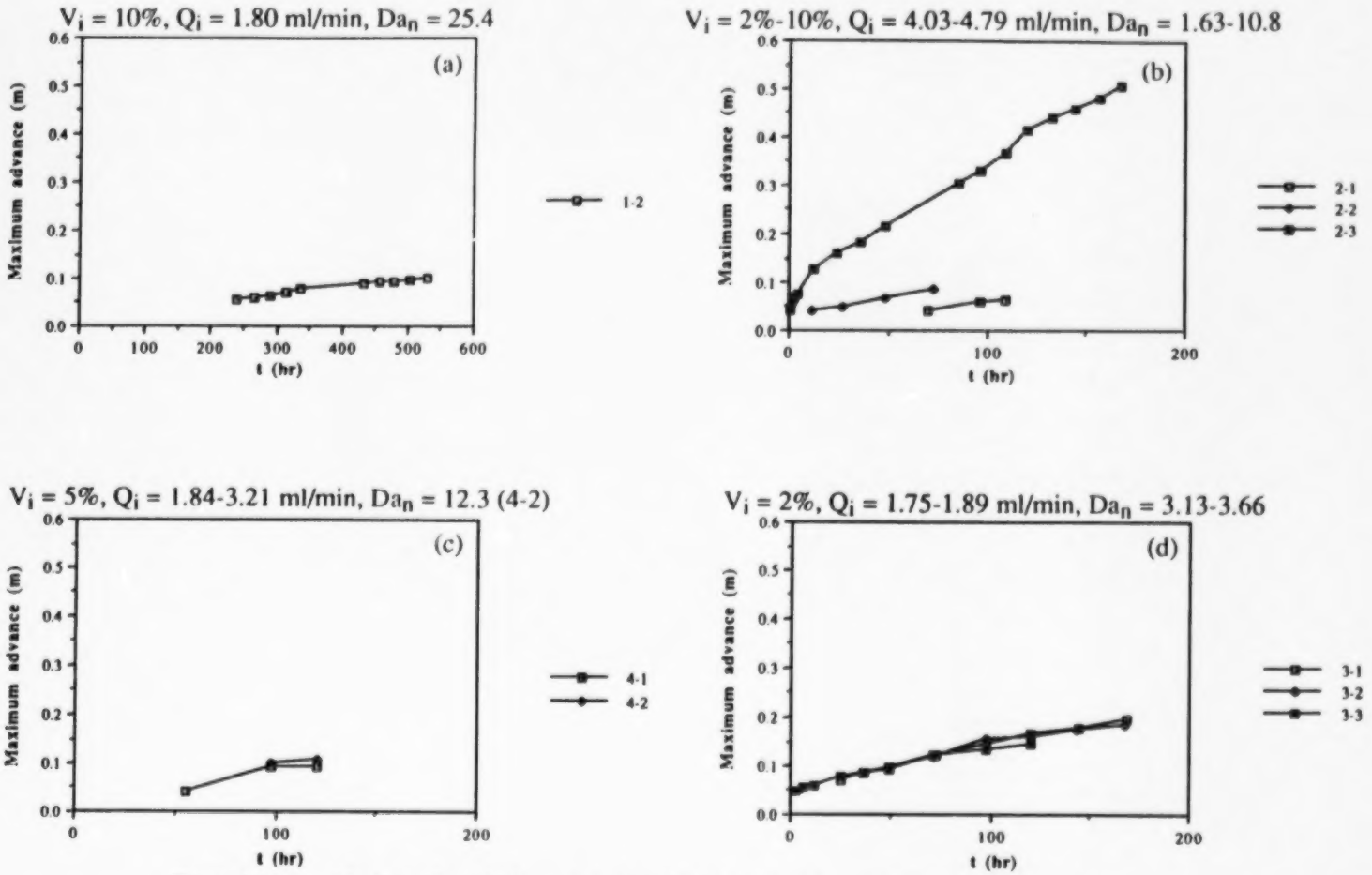

Figure 3.3. Maximum frontal advance as a function of time for (a) column 1-2, (b) experiment 2, (c) experiment 4, (d) experiment 3.

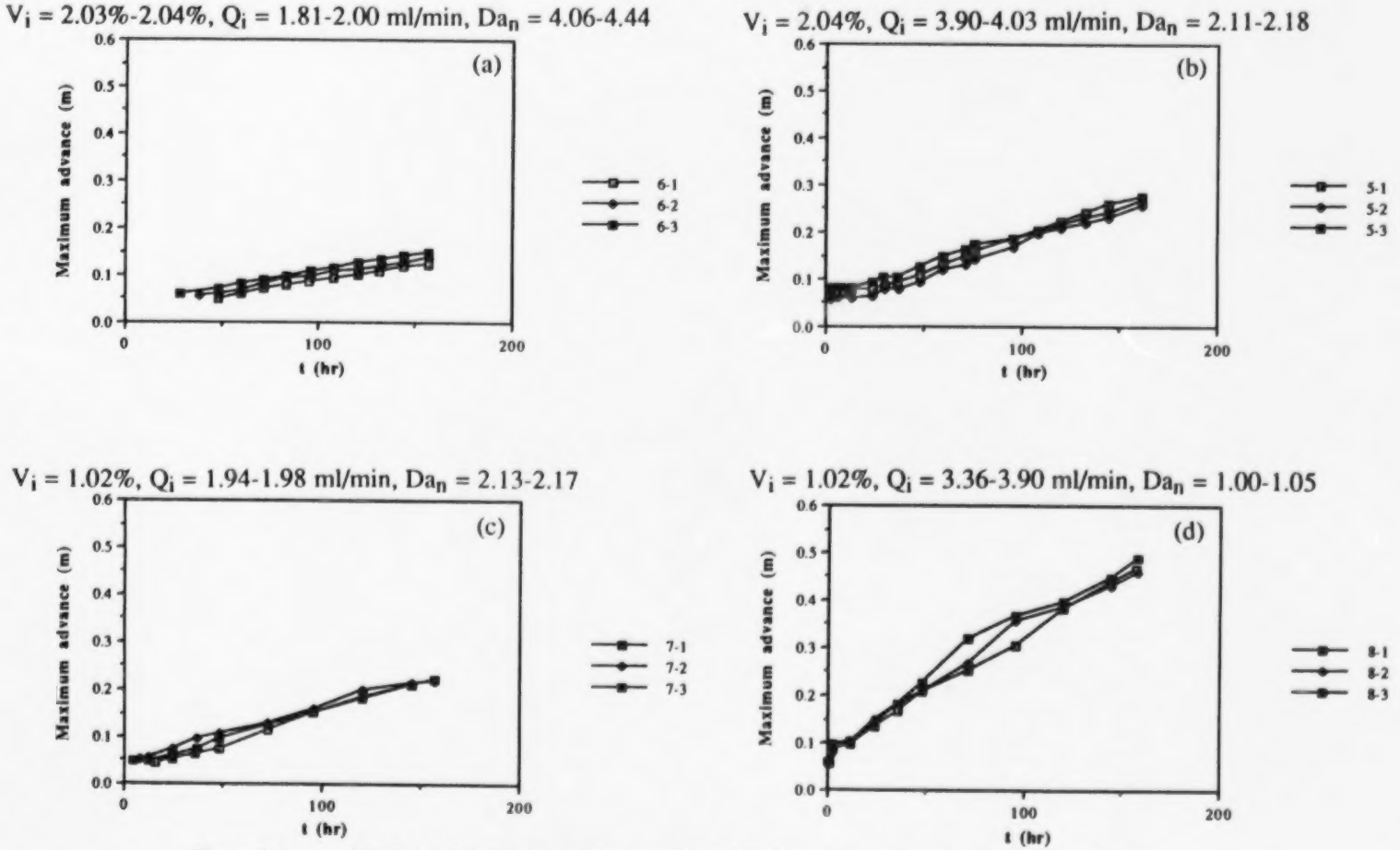

Figure 3.4. Maximum frontal advance as a function of time for (a) experiment 6, (b) experiment 5, (c) experiment 7, (d) experiment 8.

3.3d). As Da_n increased, the extent of the first stage of propagation presumably decreased, for reasons of hydraulics discussed in Sections 4.1.3 and 4.2.2. However, the opaque endcap in 1 to 8 blocked viewing of the lowest 0.04 m of each porous medium, in contrast to the glass column in P2. Thus, for experiments 5 and 7, the plots were relatively flat for the first several hours after the front became visible (Figures 3.4b, c), then steepened. For the high-Da_n cases of experiments 1, 4, and 6 and columns 2-1 and 2-2, the reaction front only became visible after 12 hr (2-1) to 187 hr (1-1), and the plots showed relatively linear upward trends. However, even where the initial penetration of the front was not visible, linear extrapolation of the frontal advance plots back to the y-axis tends to result in a non-zero value of frontal position at $t = 0$, indicating that the front probably decelerated within a period of several hours after the start of an experiment.

Values of frontal velocity (v_f) have been calculated from the final, relatively linear portions of the maximum advance plots (Table 3.3). The correlation coefficient (r^2) for the least-squares fit to each of these segments is at least 0.97. Thus, though the fronts may fluctuate, they tend not to decelerate after the first few hours of the experiments, except as noted below. It is clear that, for either sieved or unsieved calcite, the plots generally become steeper as Da_n decreases, so that v_f is inversely proportional to Da_n (Figure 3.5). The curves for the two sets of experiments (unsieved, 1 to 3, and sieved, 4 to 8) overlap; a combined plot of $1/v_f$ versus Da_n can be fit by a linear least-squares equation with a correlation coefficient of 0.99.

The frontal observations in experiments 1 to 4 are limited because the peristaltic pump created sufficiently high pressures in the inlets to rupture seals or retard the rate of flow. Frontal advance plots have not been generated for columns 1-1, 1-3, and 4-3. In 1-1, the front emerged at 187 hr, but the column failed between 194 and 211 hr. 1-3 failed at 97 hr, before the front became visible. The front did not emerge in 4-3 because the flow rate steadily declined from the initial value. Values of v_f have not been

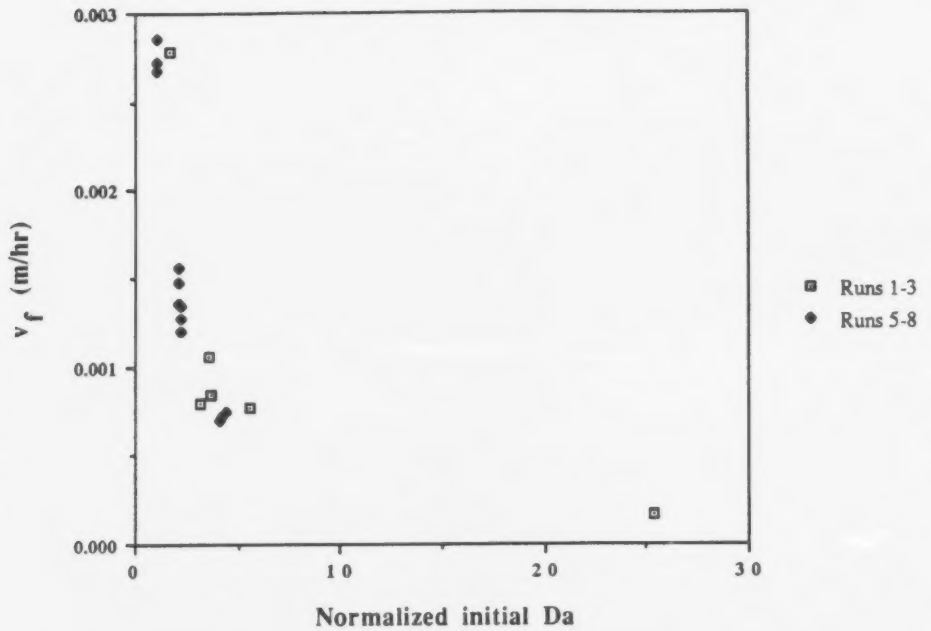

Figure 3.5.
Relationship between Da_n and frontal velocity for experiments containing unsieved (1 to 3, 4 not shown) and sieved (5 to 8) calcite.

Table 3.3.
Frontal velocity values and goodness of fit for lines through Stage 3 of frontal advance plots.

Column #	vf (m/hr)	r2
1-2	0.00016	0.98
2-2	0.00076	1.0
2-3	0.0028	1.0
3-1	0.0011	1.0
3-2	0.00084	0.97
3-3	0.00079	0.97
5-1	0.0016	1.0
5-2	0.0015	0.99
5-3	0.0013	0.99
6-1	0.00070	0.99
6-2	0.00072	0.99
6-3	0.00074	1.0
7-1	0.0014	0.99
7-2	0.0012	0.99
7-3	0.0013	1.0
8-1	0.0027	1.0
8-2	0.0027	0.99
8-3	0.0029	0.98

determined for columns 2-1, 4-1, and 4-2. The front only became visible in 2-1 after 70 hr and was tracked only until 106 hr, when the column failed, so that the frontal advance plot did not contain enough points for a reliable determination of v_f. Because of a control problem, the flow rate for 4-1 fluctuated for the first 12 hr. Of the remaining columns containing unsieved calcite, all except 1-2 eventually experienced a decline in flow rates or failed. However, prior to deceleration or failure, the final stage of frontal propagation was sufficiently linear to allow the determination of v_f in those columns.

The sizes and numbers of instabilities have not been quantified in these experiments, but one can examine qualitative trends in the development of instabilities (or fingering) along the reaction front, as Hoefner and Fogler (1988) did in acidizing limestone cores at varying flow rates. At the highest value of Da_n (column 1-2), the reaction front was relatively planar, but decorated with many small, dendritic instabilities (Figure 3.6). In the intermediate case of column 2-2, the size of the fingers increased and their number decreased with the decrease in Da_n (Figure 3.7). For column 2-3, which had a low value of Da_n, one or two instabilities several tenths of a meter long resulted (Figure 3.8). As was shown in Figures 3.1a and b, the number of instabilities at low Da_n decreases over time because they tend to merge. This tendency makes it difficult to identify individual fingers or to measure their lengths. A comparison of Figures 3.1a, 3.6 and 3.7 illustrates that the differences in instability development were evident at similar distances at different times. Observations of slices of frozen columns (not shown) indicated that instabilities commonly developed within the interior of columns, so that fingering was not merely an artifact of preferential flow along the wall of the column. It is thus evident that the maximum advance of the reaction front during the time scale of the experiments was related to the size of instabilities, which was in turn inversely related to the number of instabilities.

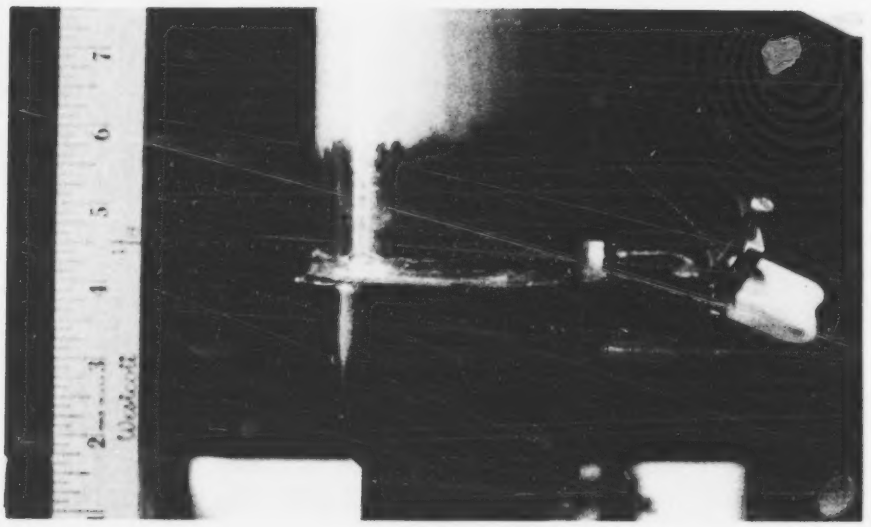

Figure 3.6.
Experiment 1, column 1-2, t = 480 hr; maximum advance of reaction front = 0.094 m.

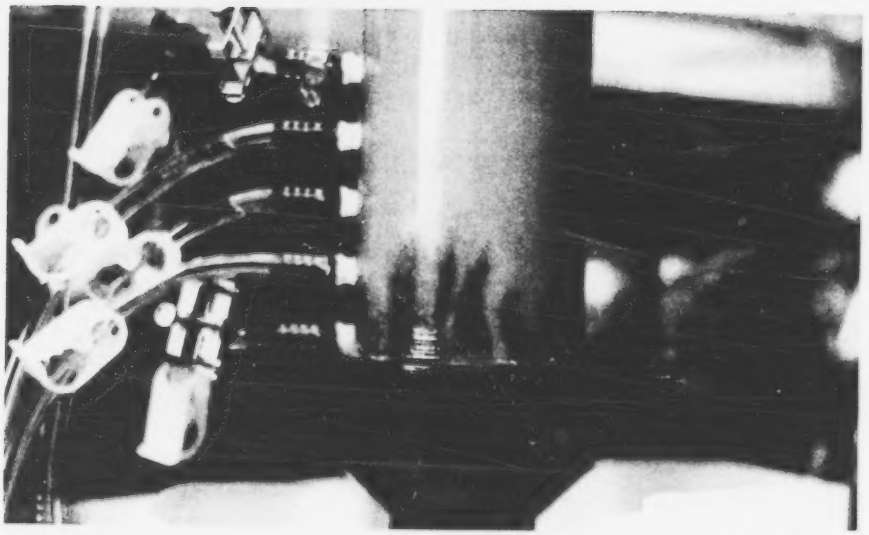

Figure 3.7.
Experiment 2, column 2-2, t = 96 hr (column failed between 78 and 85 hr); maximum advance of reaction front = 0.086 m.

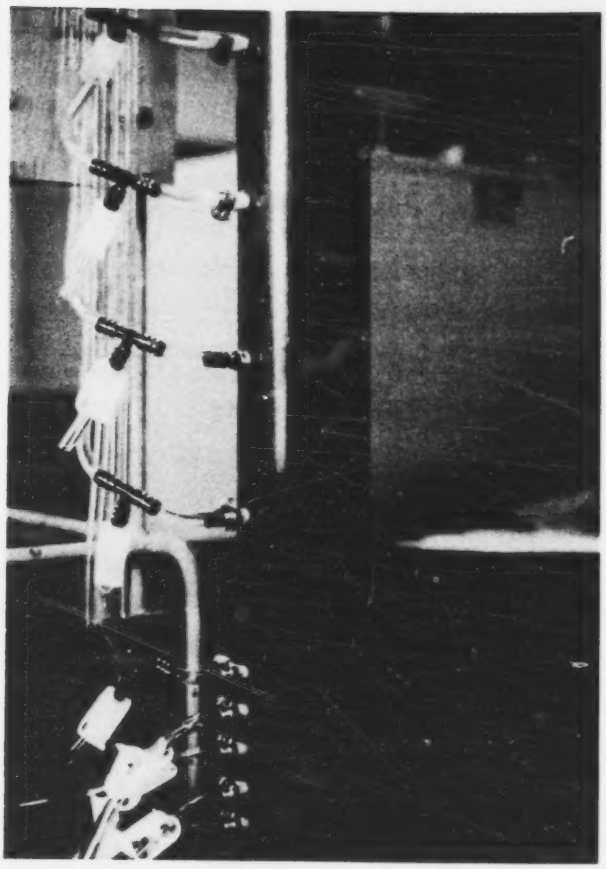

Figure 3.8.
Experiment 2, column 2-3, t = 168 hr; maximum advance of reaction front = 0.507 m.

3.3. Geochemical Evolution of the System

3.3.1. Starting water composition

As noted in Chapter 1, dilute $Fe(ClO_4)_3$ solutions can hydrolyze and polymerize. This behavior was of concern in this study because of the possibility of ferrihydrite precipitating prior to entering the porous medium. Therefore, batch-to-batch reproducibility in influent composition and the potential occurrence of auto-polymerization were evaluated by analyzing filtered and unfiltered samples of influent taken at various times during experiments 5 to 8. Results are tabulated in Appendix II.

Fluctuations in the electrical conductivity and pH of the influent solution were relatively minor. As a lack of discernible trends became apparent, electrical conductivity and pH measurements were performed only on unfiltered samples after experiment 5, and after 6, sampling only occurred for residual fluid as a carboy was replaced. For 5, early values of electrical conductivity (taken within several hr of preparation) for filtered influent averaged 3.30 dS/m, while late values (taken approximately 24 to 48 hr after preparation) averaged 3.33 dS/m. For 5 and 6 combined, early values for unfiltered influent averaged 3.41 dS/m, while late values (taken approximately 48 to 72 hr after preparation for 6) averaged 3.31 dS/m; late, unfiltered values for 7 and 8 averaged 3.40 dS/m. Values of pH on early and late filtered samples during experiment 5 averaged 2.44 and 2.42, respectively, whereas early and late pH measurements on unfiltered samples from 5 and 6 both averaged 2.43. Late, unfiltered pH values for 7 and 8 averaged 2.44. These results indicate negligible auto-polymerization.

Each batch of solution was assumed to have contained 0.01 mole $Fe(ClO_4)_3$ per kg H_2O, so that the influent concentration of Fe should have been 560 μg/g. However, mean concentrations from 5 and 6 combined were 390 μg/g for early unfiltered samples and 410 μg/g for early filtered samples. For experiments 5 to 8 combined, mean late

concentrations were reversed (410 μg/g for unfiltered samples, 390 μg/g for filtered samples). It was learned from GFS Chemicals, the manufacturer of the reagent, that synthesis of entirely anhydrous $Fe(ClO_4)_3$ was impossible and that the salt contained H_2O and possibly traces of $HClO_4$. The analyses on influent samples, though, show that the deviation from the ideal concentration was relatively consistent throughout the experiments.

The appearance of the solution is a final indicator of whether auto-polymerization is occurring. After the onset of auto-polymerization, Hsu and Ragone (1972) observed a pronounced increase in turbidity prior to a corresponding decrease in pH. During experiments 2, 4, and 5 to 8, the solution remained a clear, pale yellow throughout the lifetime of each batch, to as late as 72.6 hr (3.02 days) after preparation in experiments 5 to 8. However, due to differences in preparation and mixing, darkening and cloudiness were observed in the influent solution after approximately 175 hr of experiment 1, and during approximately the first 98 hr of experiment 3. The probable decreases in pH and dissolved Fe and increases in suspended Fe which resulted prior to infiltration complicate comparison of results from those experiments with results from others. Still, the consistency of reaction-front propagation trends within 1 to 4 prior to deceleration or failure and within 5 to 8 indicates that auto-polymerization of influent did not grossly affect 1 and 3.

Based on analyses from experiments 5 to 8, batch-to-batch reproducibility for the influent was excellent. Because the timing of sample collection and the filtration of samples did not appear to be influential, mean values of parameters were calculated from averaged values for all batches reported in 5 to 8. The overall electrical conductivity was 3.39 dS/m, the overall pH was 2.44, and the overall Fe concentration was 400 μg/g (0.0071 molal), with coefficients of variation of 2.48%, 1.22%, and 2.1%, respectively.

The pH value is supported by comparison with results from other studies. Following Hsu and Ragone (1972), who assumed equivalency of activity and concentration, the pH calculated from the rate law for the hydrolysis of Fe^{3+} (prior to polymerization) is 2.53. In comparison, the pH from the calculation of Hsu and Ragone (1973) for their own 0.01 molar $Fe(ClO_4)_3$ solution is 2.51, versus a measured pH of 2.27. No indication was given as to whether those workers, or Loeppert et al. (1984) and Loeppert and Hossner (1984), used the "anhydrous" salt. Hsu (1973) prepared $Fe(ClO_4)_3$ solutions from the hydrated salt ($Fe(ClO_4)_3 \cdot 10H_2O$) over a range of concentrations (0.0002 - 0.1 molar) to study variations in induction times for auto-polymerization. Based on a power curve fit to his Fe concentration versus initial pH data ($r^2 = 0.96$), the calculated pH of the solution for the current study, 2.32, is lower than measured. However, the corresponding power-fit induction time (2.6 days) is also less than observed.

3.3.2. Effluent water composition

Chemical analyses on effluent were useful for monitoring reaction progress prior to 144 hr, after which porewater "snapshots" were taken. Because of the relative ease of measurement, electrical conductivity data were the most numerous of all parameters monitored during the first 24 hr of each experiment. In general, the shapes of electrical conductivity curves appear to be similar, although data were sparse for experiments 1 to 4 (Figures 3.9a -d). The erratic behavior after breakthrough for column 1-3 (Figure 3.9a) cannot be readily explained. Profiles of the electrical conductivity of effluent (Figures 3.10a - d) appear to have overlapped for experiments 6 and 7 and for 5 and 8, with values slightly higher for the first pair than for the second. However, the maximum difference in final values of electrical conductivity was less than 8%, from a

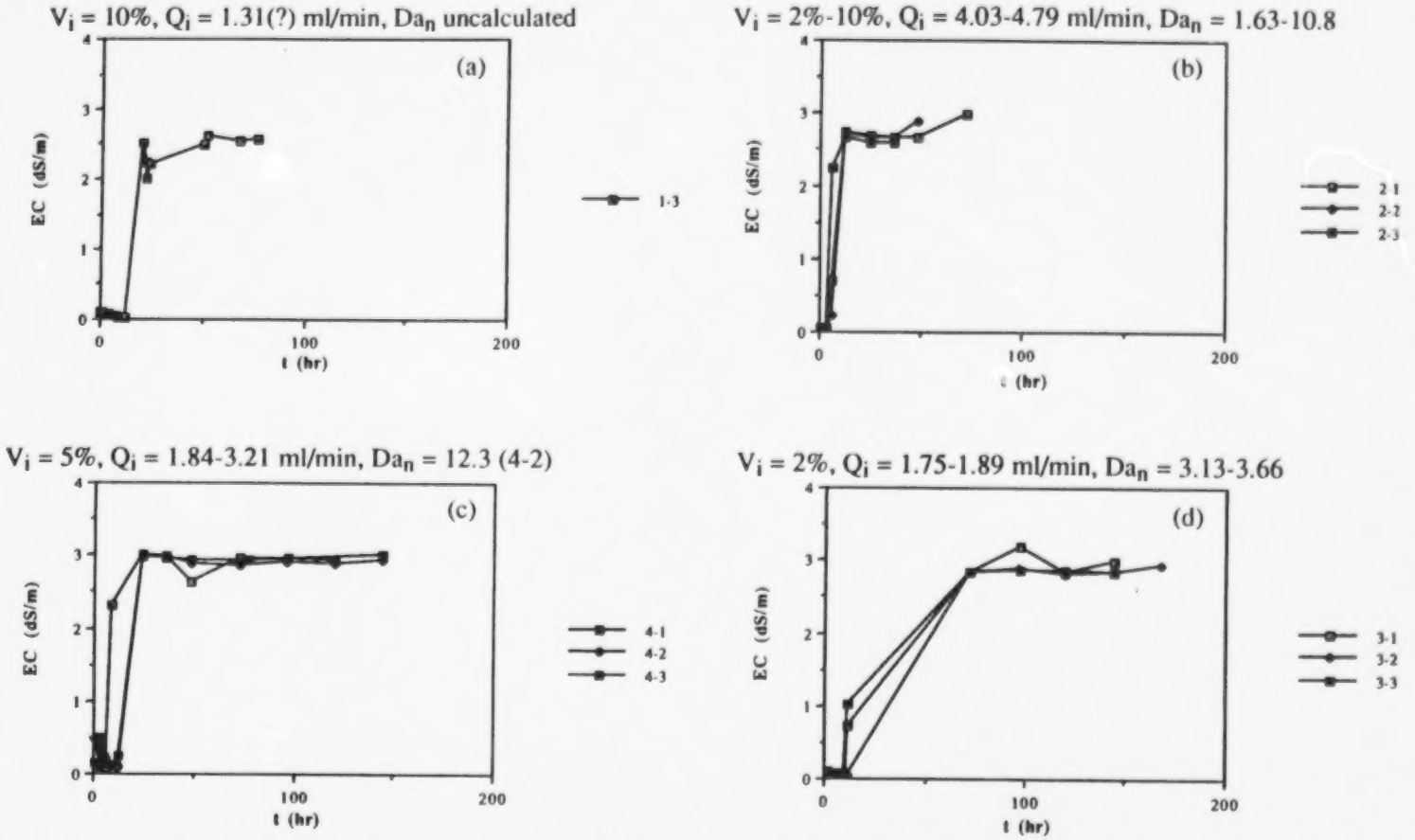

Figure 3.9. Electrical conductivity trends for effluent as a function of time, (a) column 1-3, (b) experiment 2, (c) experiment 4, (d) experiment 3.

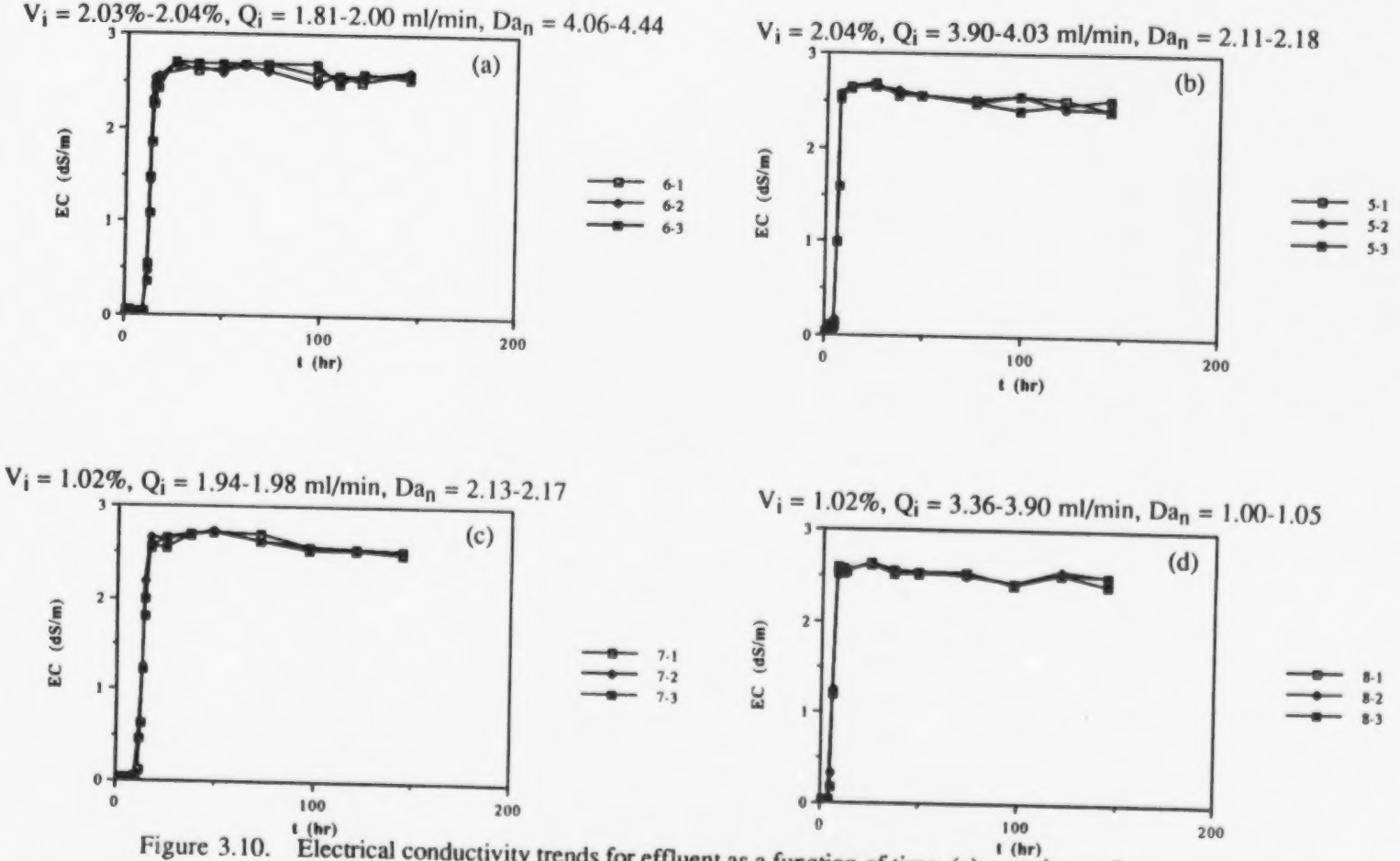

Figure 3.10. Electrical conductivity trends for effluent as a function of time, (a) experiment 6, (b) experiment 5, (c) experiment 7, (d) experiment 8.

low of 2.40 dS/m (experiment 5) to a high of 2.60 dS/m (experiment 6). The values of electrical conductivity and other parameters in effluent are tabulated in Appendix II.

Under the low flow conditions of experiments 6 and 7, pH attained maximum values at approximately 6 hr, prior to declining (Figures 3.11a, c). The pH profiles are similar for 6 and 7 after approximately 12 hr and for 5 and 8 (Figures 3.11b, d) after approximately 72 hr, with 5 and 8 being displaced downward relative to 6 and 7. Therefore, the trends in pH, like electrical conductivity, appear to reflect differences in initial flow rates between experiments but not differences in initial surface areas. However, final values of pH, while overlapping, generally declined with Da_n: the final pH ranges were 6.62 to 6.76 for 6, 6.53 to 6.70 for 5, 6.35 to 6.55 for 7, and 6.29 to 6.48 for 8.

The time variations in TIC and Ca concentrations were more complicated than those of other parameters. As Da_n decreased, TIC appeared to decline increasingly quickly, so that the shapes of the concentration versus time profiles became more concave upward. Values of TIC were generally highest for experiment 6 (Figure 3.12a), followed by experiments 7 (Figure 3.12c), 5 (Figure 3.12b), and 8 (Figure 3.12d). However, for reasons which are not clear, the profiles for 5 and 8 were similar until approximately 96 hr, when TIC values in 8 began to rebound. One would expect the profiles of 5 and 7 to overlap with a strict dependence on Da_n, or 6 and 7 to overlap with a dependence on flow rate alone, but neither appears to have been the case.

The time variation of Ca concentration in effluent (Figures 3.13a - d) was similar to those of electrical conductivity and pH. Concentration profiles appear to have varied with the flow rate but not the surface area, and values were slightly lower (by about 5%) for the high flow experiments. However, like the TIC profiles, the Ca values for experiment 5 fluctuated considerably after breakthrough (by as much as 18%). Some of the fluctuation in Ca was thought to have resulted from errors associated with filtration, so that a new filtration vessel was used in subsequent experiments. Because the

V_i = 2.03%-2.04%, Q_i = 1.81-2.00 ml/min, Da_n = 4.06-4.44

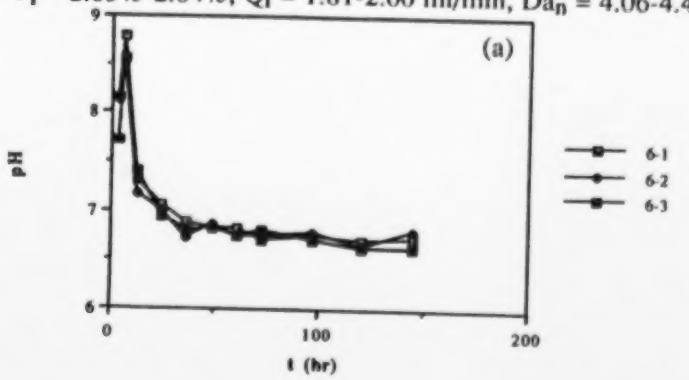

V_i = 2.04%, Q_i = 3.90-4.03 ml/min, Da_n = 2.11-2.18

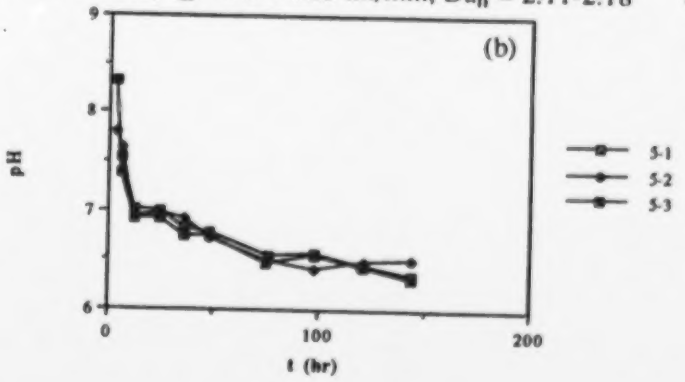

V_i = 1.02%, Q_i = 1.94-1.98 ml/min, Da_n = 2.13-2.17

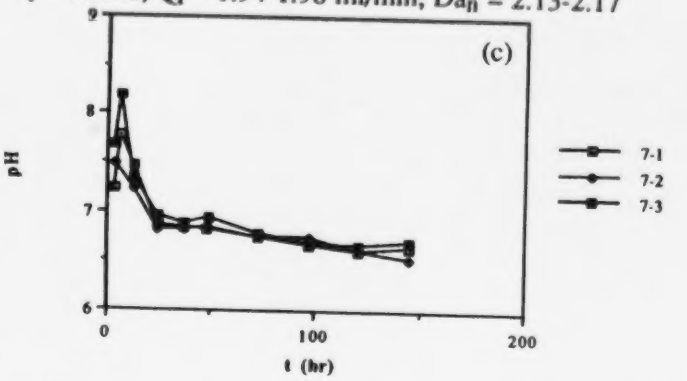

V_i = 1.02%, Q_i = 3.36-3.90 ml/min, Da_n = 1.00-1.05

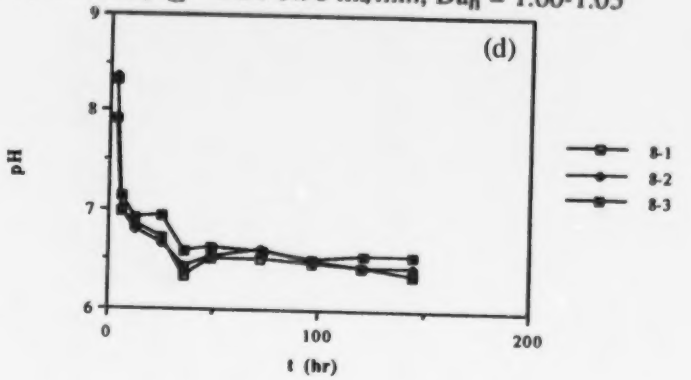

Figure 3.11 pH trends for effluent as a function of time, (a) experiment 6, (b) experiment 5, (c) experiment 7, (d) experiment 8.

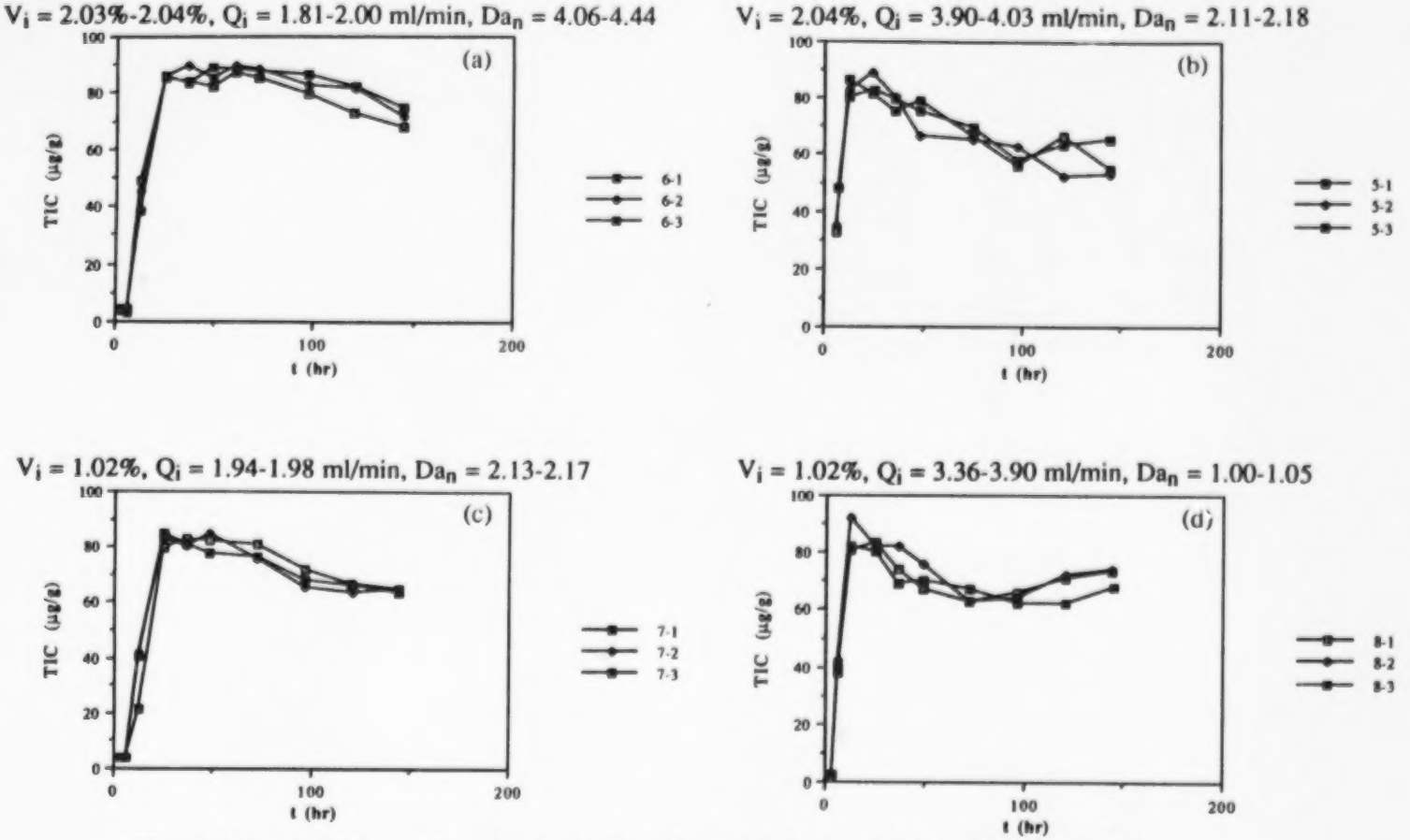

Figure 3.12. Total inorganic carbon trends for effluent as a function of time, (a) experiment 6, (b) experiment 5, (c) experiment 7, (d) experiment 8.

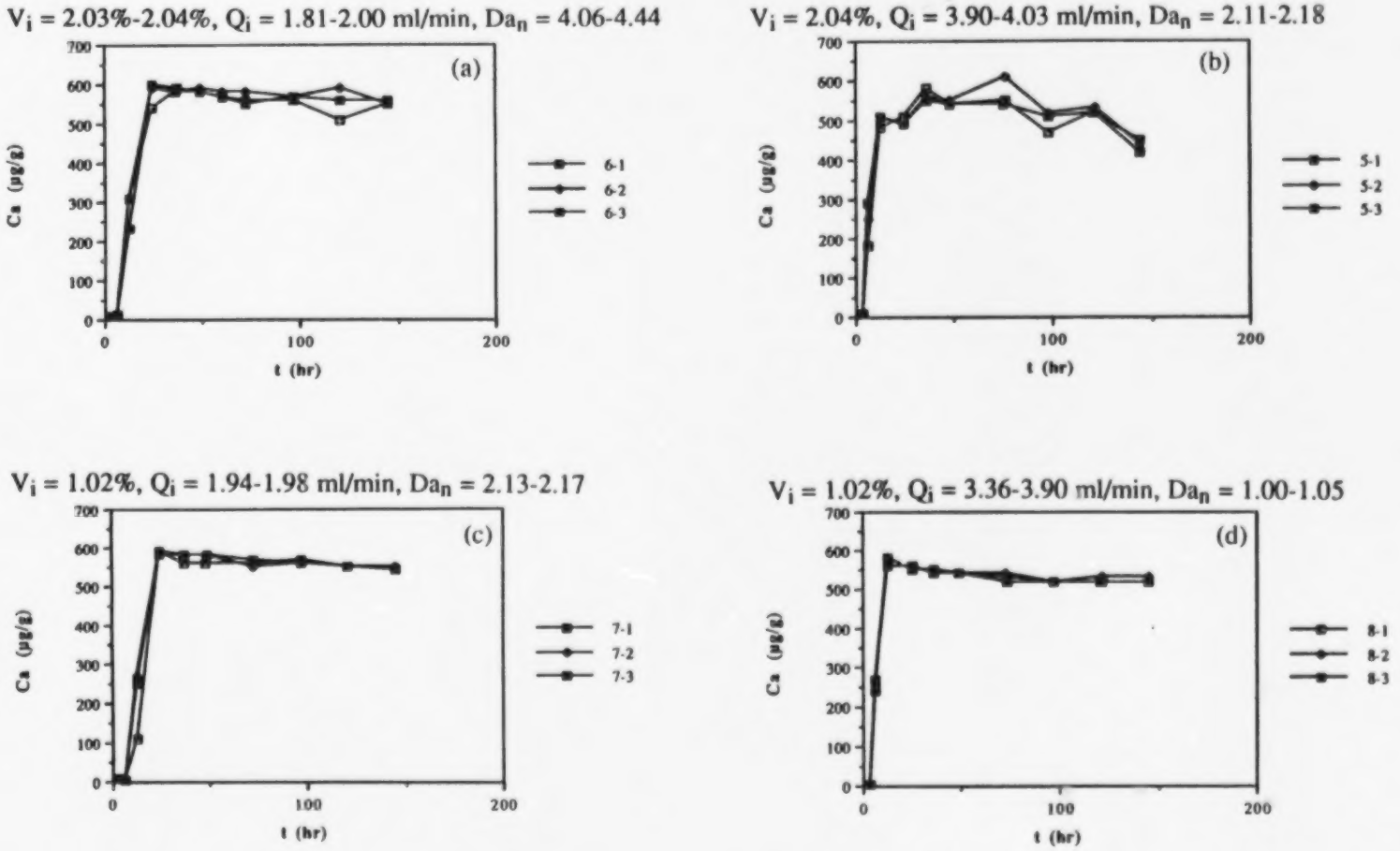

Figure 3.13. Ca trends for effluent as a function of time, (a) experiment 6, (b) experiment 5, (c) experiment 7, (d) experiment 8.

samples for TIC analysis were not filtered, though, another factor must have contributed to the fluctuations. One such factor could have been the patterns of fingering in 5, which appeared to be more irregular than in other experiments. The resulting heterogeneous character of frontal advance could have led to less smooth solute profiles in effluent.

In contrast to other parameters in effluent, the concentration of Fe tended to show a gradual, sustained increase above background values with increasing time for experiments 5, 7 and 8. In addition, the time at which Fe began to rise shortened, and the final concentration increased, with decreasing Da_n. For experiment 6 (Figure 3.14a), only column 6-1 seemed to increase above background (0.2 μg/g at 120 hr), and 6-1 decreased back to near-background Fe (0.08 μg/g) at 145 hr, so that breakthrough of Fe from influent may not have occurred. In columns 5-1 and 5-2, levels of Fe exceeded 1 μg/g before breakthrough. This behavior was probably due to incomplete flushing of the porous metal plates after they had been pre-rinsed with HCl, as indicated by decreases in concentration with subsequent measurements, so that the anomalous measurements have not been plotted. After 72 hr, Fe concentrations in effluent began increasing slightly beyond background levels (less than 0.09 μg/g), to 0.24 to 0.64 μg/g by 144 hr (Figure 3.14b). Fe began rising above background for columns 7-1 and 7-2 as of 120 hr (Figure 3.14c), to final concentrations of 0.31 μg/g for 7-1 and 0.28 μg/g for 7-2. In experiment 8, Fe emerged above background levels at 36 to 49 hr, and attained concentrations of 0.54 to 1.7 μg/g (Figure 3.14d).

3.3.3. Porewater data

Information on porewater chemistry serves to integrate influent and effluent data, solid-phase data, and observations of front migration. "Snapshots" of porewater chemistry were taken between 162 and 171 hr for experiment 5, 159 and 168 hr for 6,

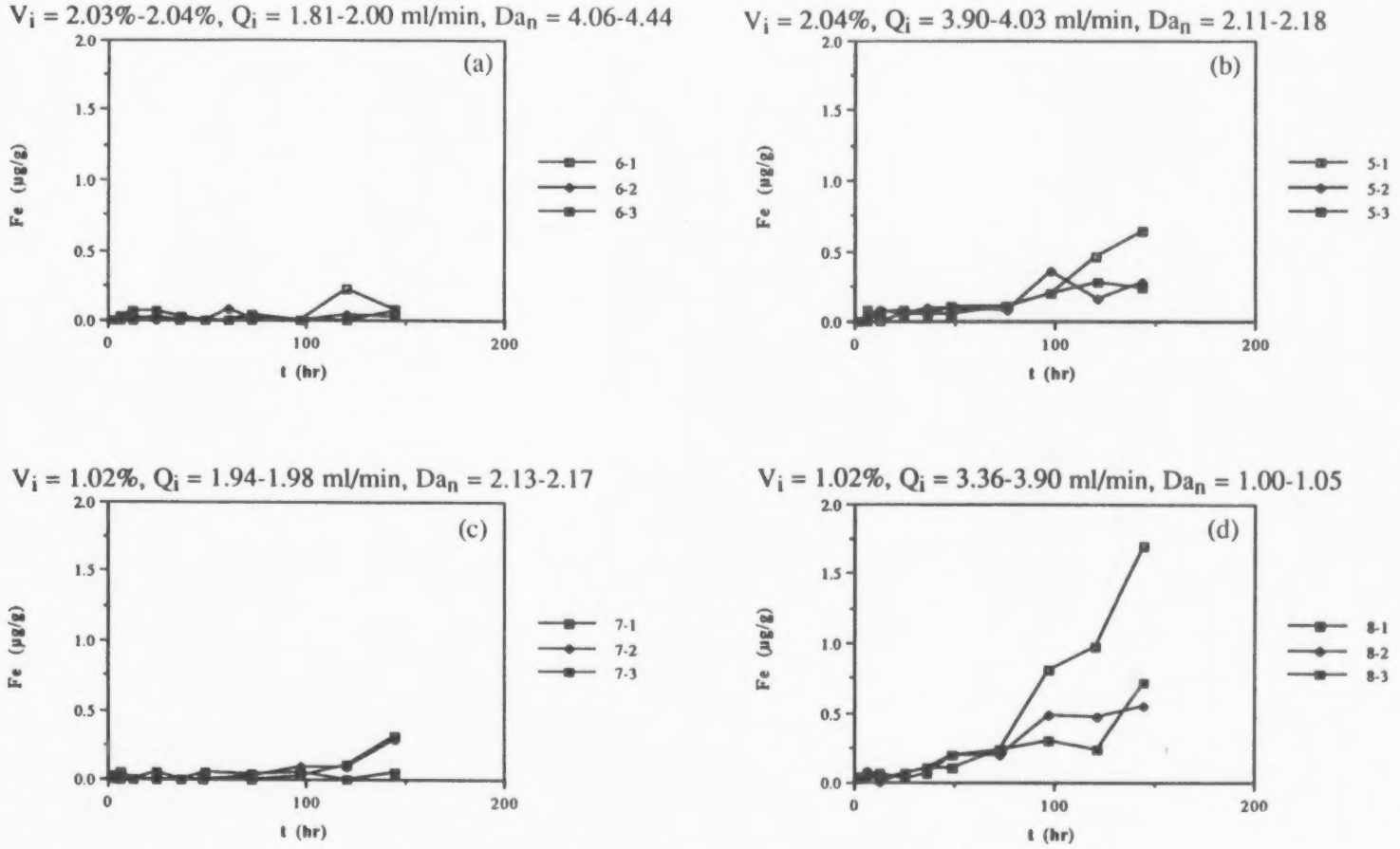

Figure 3.14. Fe trends for effluent as a function of time, (a) experiment 6, (b) experiment 5, (c) experiment 7, (d) experiment 8.

159 and 169 hr for 7, and 159 and 165 hr for 8. Sampling was concentrated within the reaction zone, which is defined here as extending from the inlet to the tip of the reaction front. Because of differences in the lengths of reaction zones, the locations of sampling points varied somewhat between experiments. However, for each column in experiments 5 to 8, port 1 was sampled (0.053 m from the inlet, at the top of the lower endcap). Like the outlet for effluent samples, port 1 constitutes a useful reference point for comparing chemical parameters at different values of Da_n. Chemical profiles in porewater are examined beginning at 0.053 m and progressing down-gradient. This orientation is opposite to that of temporal trends in effluent, because monitoring effluent chemistry as the reaction zone grows is analogous to moving up-gradient from the outlet through the medium.

Across experiments 5 to 8, porewater at 0.053 m exhibited electrical conductivity values greater than the mean influent value of 3.39 dS/m (Table 3.4). These values were the maximum observed except for experiment 8, in which electrical conductivity peaked at 0.129 m. The decline in values down-gradient appeared to become increasingly more gradual as the distance from the inlet to the reaction front increased between different experiments (Figures 3.15a - d). This trend toward less steep profiles corresponds to decreasing Da_n between experiments and is characteristic for all parameters in porewater and sediments. The complex, heterogeneous character of the reaction zones in experiment 5 led to variability in the profiles for electrical conductivity and other parameters along the columns (Figure 3.15b). The minimum value of electrical conductivity in experiments 5 to 8 occurred immediately ahead of the reaction front, beyond which values gradually increased down-gradient. The values of electrical conductivity for porewater sampled closest to the outlet in 5 to 8 overlapped the final effluent values.

Electrical conductivity profiles for experiments 3 and 4 became retarded by reductions in flow rates associated with pore plugging. The increase in electrical

Table 3.4. Electrical conductivity values along flowpath for columns containing sieved calcite.

x (m)	5-1 (dS/m)	5-2 (dS/m)	5-3 (dS/m)	6-1 (dS/m)	6-2 (dS/m)	6-3 (dS/m)
0.053	3.50	3.88	3.55	3.87	4.12	4.26
0.078				3.12	3.53	3.35
0.104	2.90	3.70	2.90	2.30	3.12	3.49
0.129				2.45	2.45	2.80
0.154	2.70	3.75	3.08	2.56	2.56	2.51
0.205	2.50	2.88	2.60			
0.230						
0.256	2.28	2.20	2.30			
0.307	2.40	2.20	2.20			
0.332						
0.434				2.56	2.56	2.52
0.535	2.52	2.30	2.40			
0.637						

x (m)	7-1 (dS/m)	7-2 (dS/m)	7-3 (dS/m)	8-1 (dS/m)	8-2 (dS/m)	8-3 (dS/m)
0.053	4.15	4.11	4.10	3.80	3.87	3.98
0.078						
0.104	4.11	3.99	3.98			
0.129				4.00	4.09	
0.154	3.32	3.11				
0.205	2.42	2.32	2.50			
0.230				3.75	3.41	3.44
0.256	2.41	2.43	2.41			
0.307						
0.332				3.28	3.19	
0.434	2.41	2.49	2.49	2.31	2.36	2.31
0.535				2.41	2.42	2.42
0.637	2.52	2.51	2.49	2.49	2.47	2.45

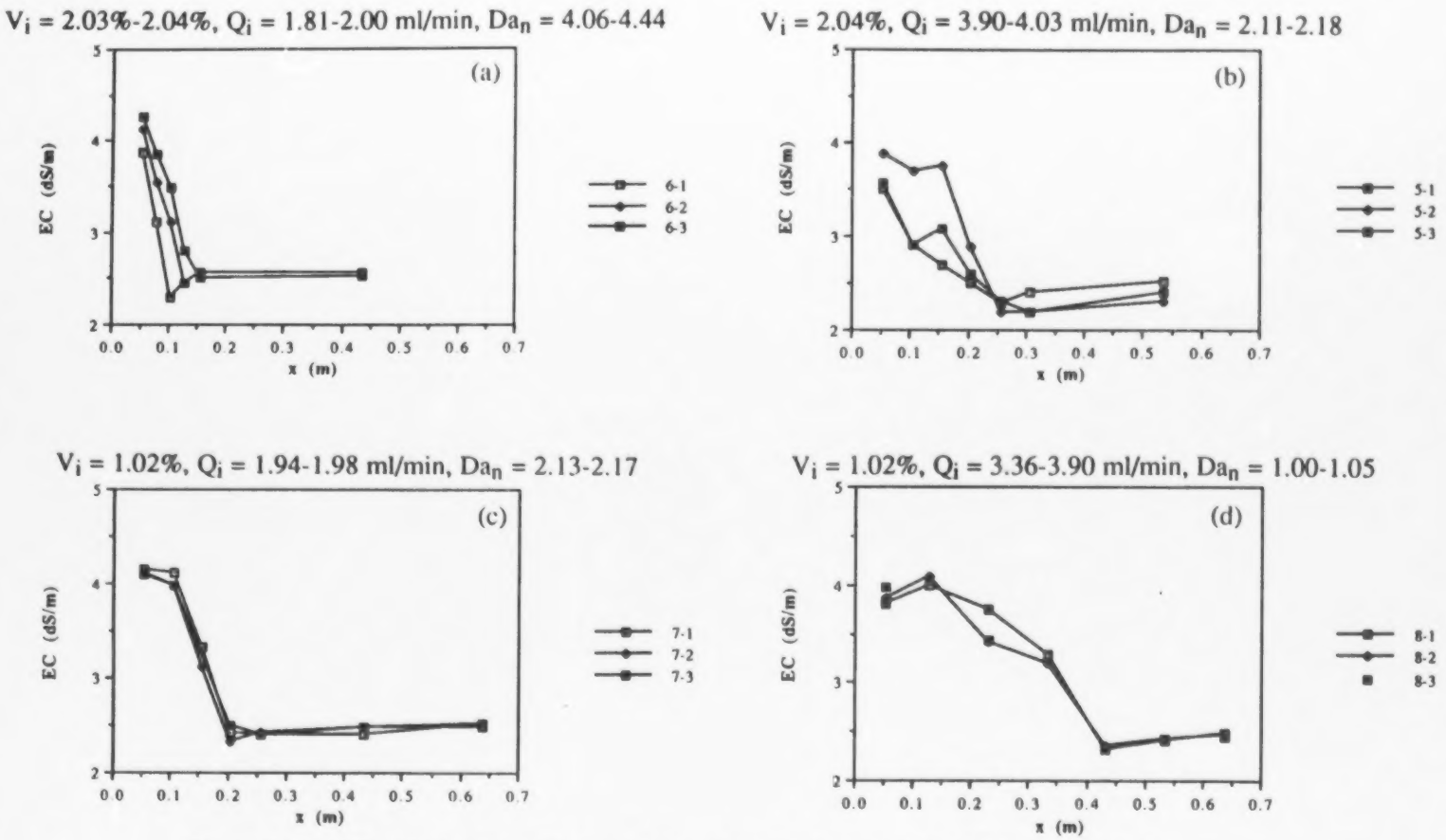

Figure 3.15. Electrical conductivity trends along flowpath at the end of (a) experiment 6, (b) experiment 5, (c) experiment 7, (d) experiment 8.

conductivity above influent values was not evident for experiment 4 (Table 3.5, Figure 3.16a), but the distance between the inlet and the reaction front was only approximately 0.1 m at the time of sampling, and values may have peaked between the inlet and the first sample point at 0.045 m. For experiment 3 (Table 3.5, Figure 3.16b), in which the distance to the front was greater, only column 3-3, which suffered the greatest reduction in flow rates, did not exhibit a value of electrical conductivity greater than the influent value.

In comparison with electrical conductivity, values of pH at 0.053 m were less than or (for column 5-3) equal to the mean pH of the influent in experiments 5 to 8 (Table 3.6). These represented pH minima except for column 5-2, in which the minimum occurred at 0.104 m, and experiment 8, with minima at 0.129 m. Although the profiles became less steep with decreasing Da_n, pH increased sharply across the reaction front in each case (Figures 3.17a - d). For 8, the tip of the reaction front arrived in each column during sampling at 0.434 m, so that the resulting pH values were slightly lower than those immediately across the front in previous experiments. The values closest to the outlet were less than the final pH values in effluent by several tenths of a unit.

TIC profiles in porewater, while more erratic than those of other parameters, generally corresponded well with pH profiles, as expected given their interdependency in carbonate equilibria. An average background value of 0.755 μg/g, attributable to uptake of atmospheric CO_2, was obtained from two samples of influent taken during experiment 5. The ranges in TIC at 0.053 m (Table 3.7), while overlapping, decreased with Da_n toward background levels. Like pH, TIC profiles jumped upward across the reaction front (Figures 3.18a - d). In experiments 5, 6, and 8, values of TIC tended to remain relatively steady or increase gradually farther down-gradient. However, perhaps due to heterogeneity in fingering, TIC peaked in run 7 at 0.434 m (Figure 3.18c), then

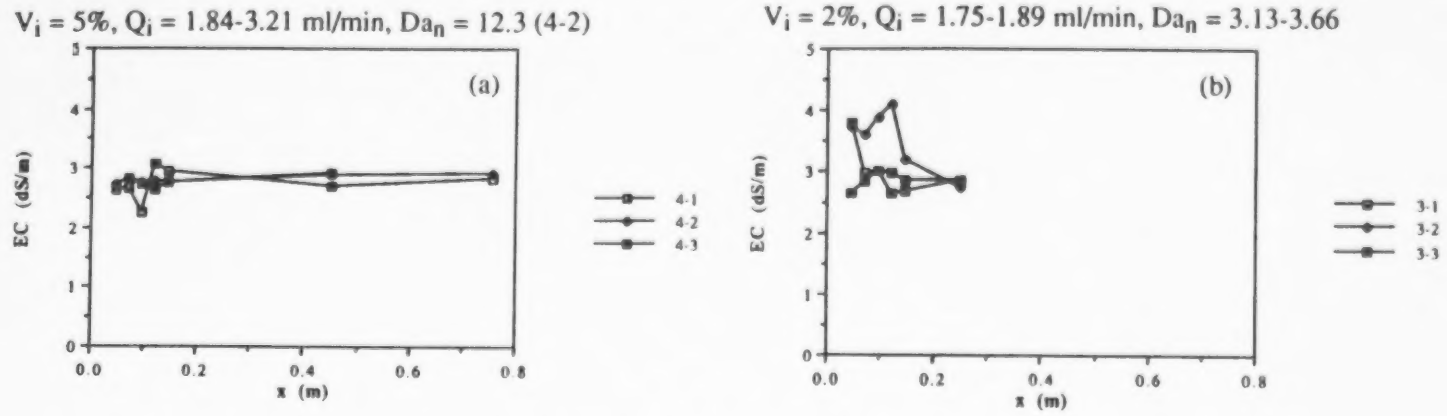

Figure 3.16. Electrical conductivity trends along flowpath at the end of (a) experiment 4, (b) experiment 3.

Table 3.5. Electrical conductivity values along flowpath for experiments 3 and 4 (containing unsieved calcite).

x (m)	EC 3-1 (dS/m)	EC 3-2 (dS/m)	EC 3-3 (dS/m)	EC 4-1 (dS/m)	EC 4-2 (dS/m)	EC 4-3 (dS/m)
0.045	3.78	3.72	2.64	2.62	2.72	
0.070	2.97	3.59	2.83	2.66	2.83	2.83
0.096	3.01	3.88	3.02	2.24	2.74	2.72
0.121	2.64	4.11	2.99	3.06	2.77	2.62
0.147	2.68	3.20	2.86	2.93	2.75	2.74
0.451				2.70	2.89	2.90
0.248	2.86	2.72	2.86			
0.756				2.82	2.91	

Table 3.6. pH values along flowpath for columns containing sieved calcite.

x (m)	pH 5-1	pH 5-2	pH 5-3	pH 6-1	pH 6-2	pH 6-3
0.053	2.35	2.28	2.43	2.30	2.25	2.22
0.078				2.53	2.39	2.30
0.104	2.63	2.23	2.45	5.91	2.56	2.41
0.129				6.17	6.18	2.73
0.154	2.66	2.35	2.55	6.13	6.06	6.15
0.205	3.08	2.60	2.85			
0.230						
0.256	6.03	5.89	6.15			
0.307	6.08	6.13	6.08			
0.332						
0.434				6.24	6.20	6.18
0.535	6.01	6.22	6.12			
0.637						

x (m)	pH 7-1	pH 7-2	pH 7-3	pH 8-1	pH 8-2	pH 8-3
0.053	2.25	2.25	2.25	2.34	2.33	2.31
0.078						
0.104	2.28	2.28	2.30			
0.129				2.30	2.28	2.28
0.154	2.48	2.59	2.48			
0.205	3.26	5.77	3.05			
0.230				2.30	2.44	2.44
0.256	6.05	6.13	6.08			
0.307						
0.332				2.48	2.51	2.51
0.434	6.15	6.17	6.15	5.62	5.80	5.55
0.535				6.14	6.14	6.14
0.637	6.18	6.18	6.22	6.07	6.21	6.16

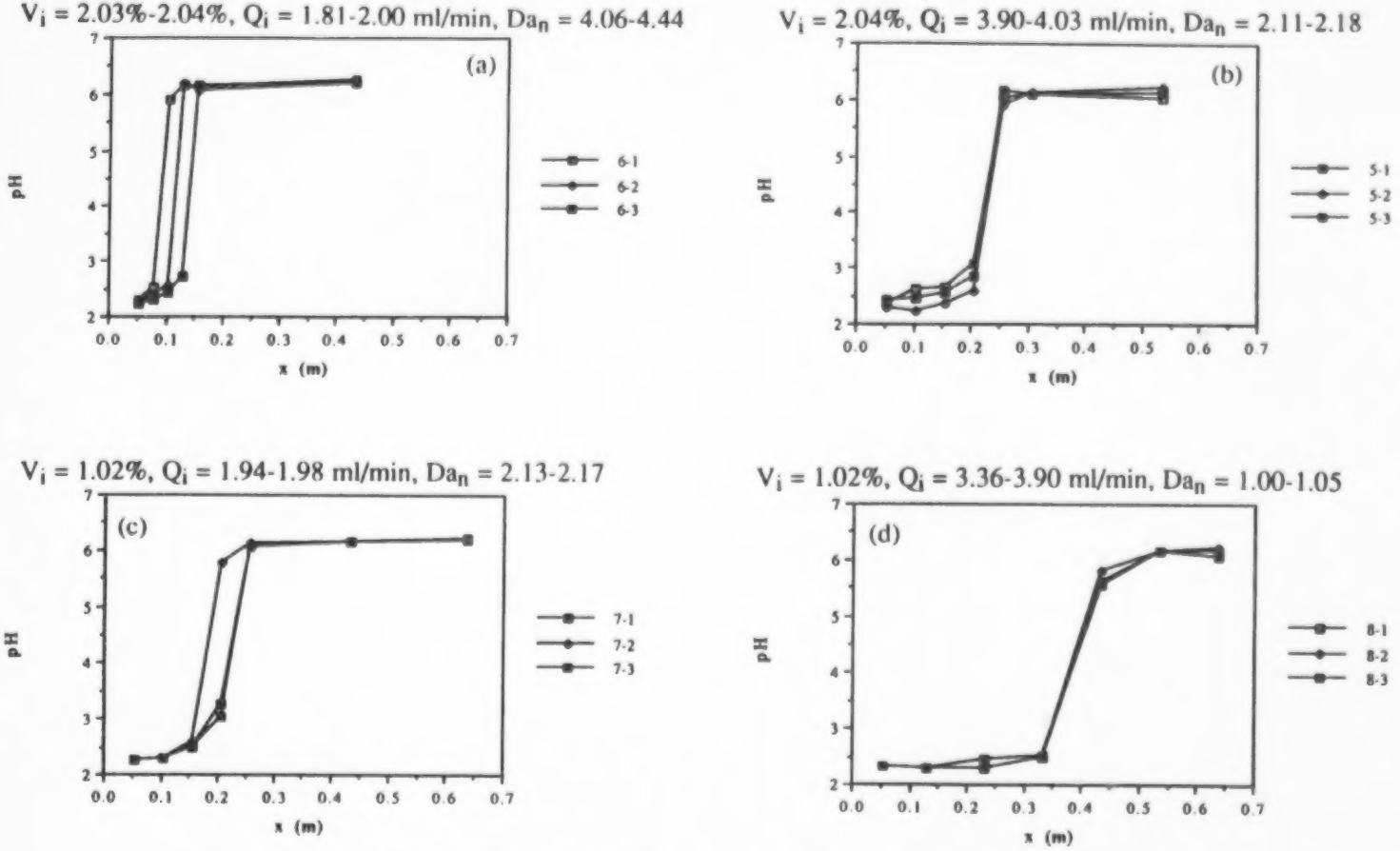

Figure 3.17. pH trends along the flowpath at the end of (a) experiment 6, (b) experiment 5, (c) experiment 7, (d) experiment 8.

Table 3.7. TIC values along flowpath for columns containing sieved calcite.

x (m)	TIC 5-1 (µg/g)	TIC 5-2 (µg/g)	TIC 5-3 (µg/g)	TIC 6-1 (µg/g)	TIC 6-2 (µg/g)	TIC 6-3 (µg/g)
0.053	10.5	0.719	12.3	17.6	4.77	0.937
0.078				37.9	14.5	5.09
0.104	8.52	3.14	27.8	88.0	48.1	13.2
0.129				105	81.2	49.7
0.154	17.3	9.39	20.7	107	101	104
0.205	23.1	35.1	54.1			
0.230						
0.256	91.3	74.8	84.0			
0.307	89.9	73.9	95.5			
0.332						
0.434				108	98.5	115
0.535	84.2	106	97.3			
0.637						

x (m)	TIC 7-1 (µg/g)	TIC 7-2 (µg/g)	TIC 7-3 (µg/g)	TIC 8-1 (µg/g)	TIC 8-2 (µg/g)	TIC 8-3 (µg/g)
0.053	0.58	1.59	1.07	0.39	0.46	0.53
0.078						
0.104	6.64	9.44	6.88			
0.129				3.4	1.7	2.2
0.154	43.0	69.8	30.9			
0.205	84.8	101	90.2			
0.230				17	51	25
0.256	94.6	95.0	93.2			
0.307						
0.332				44	60	55
0.434	115	108	114	110	110	110
0.535				110	120	110
0.637	108	94.8	104	120	120	120

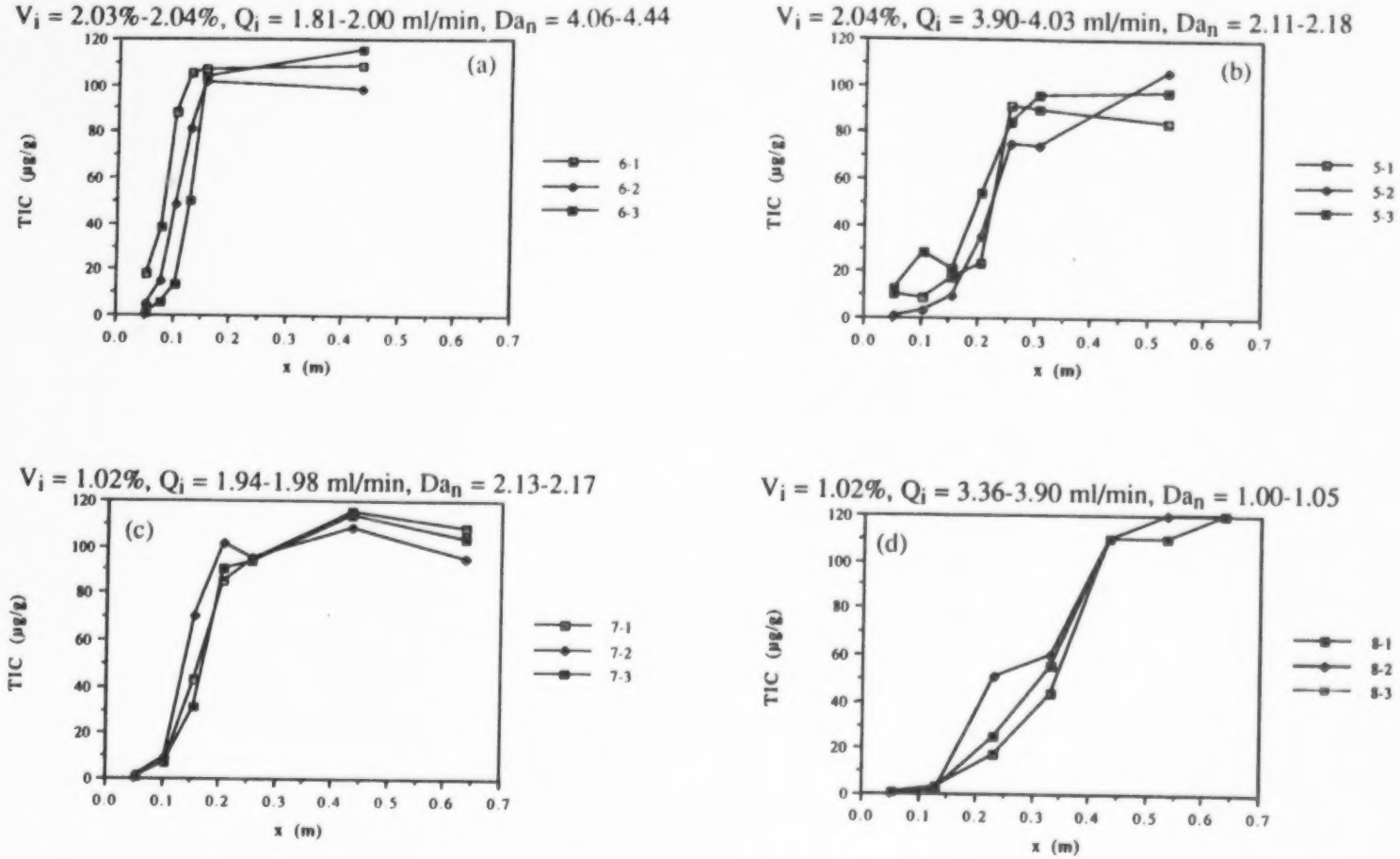

Figure 3.18. Total inorganic carbon trends along the flowpath at the end of (a) experiment 6, (b) experiment 5, (c) experiment 7, (d) experiment 8.

declined. Values of TIC in porewater nearest the outlet were 30 to 50 μg/g greater than final values in effluent.

Both filtered and unfiltered porewater splits were analyzed for Ca in order to evaluate the possible precipitation of calcite with degassing during sampling in experiments 5 to 8. Filtered values of Ca (tabulated in Appendix II) were within 10% of unfiltered values, except for a few instances close to the inlet where both sets of values were within analytical uncertainty, and two instances in experiment 5 where the difference was less than 15%. However, to be rigorous, only unfiltered values are plotted here. The ranges of those Ca values, like TIC, overlapped but tended to decrease with Da_n at 0.053 m (Table 3.8). The shapes of the Ca profiles are similar to those for pH and TIC (Figures 3.19a - d). However, as noted in Section 2.3.2, unfiltered samples were not collected for cation analysis beyond the reaction front in experiment 5. Relative to final values in effluent, Ca values in porewater nearest the outlet were lower in 6 and 7, equal in 8, and (for possible reasons detailed previously) higher in 5.

The presence of CO_2 within columns, while evident from observations of bubbles, can be examined in quantitative terms on the basis of mass balance constraints. During the congruent dissolution of calcite, one mole of C should be released for every mole of Ca, or, adjusting for differences in molecular weights, 1.00 g C for every 3.34 g Ca. The ratio of unfiltered Ca to TIC was plotted at each sampling point along each column in experiments 5 to 8 (Figures 3.20a - d). The values of Ca/TIC less than 3.34, as seen adjacent to the inlet in experiments 7 and 8, may reflect contributions of C from atmospheric CO_2 after the removal of calcite. In general, the Ca/TIC profiles were greater than 3.34, which indicates preferential enrichment of Ca due to exsolution of CO_2 (g).

Like Ca, Fe analyses were performed on filtered and unfiltered porewater splits in experiments 5 to 8. However, as Wang and Hsu (1980) have noted, a continuum

Table 3.8. Unfiltered Ca values along flowpath for columns containing sieved calcite.

x (m)	Ca 5-1 (µg/g)	Ca 5-2 (µg/g)	Ca 5-3 (µg/g)	Ca 6-1 (µg/g)	Ca 6-2 (µg/g)	Ca 6-3 (µg/g)
0.053	38	0.65	51	72	30	8.50
0.078				240	86	28
0.104	160	16	150	480	290	120
0.129				520	510	40.0
0.154	290		190	530	530	530
0.205	410	230	400			
0.230						
0.256						
0.307						
0.332						
0.434				540	540	540
0.535						
0.637						

x (m)	Ca 7-1 (µg/g)	Ca 7-2 (µg/g)	Ca 7-3 (µg/g)	Ca 8-1 (µg/g)	Ca 8-2 (µg/g)	Ca 8-3 (µg/g)
0.053	0.31	4.8	2.2	0.33	0.26	0.50
0.078						
0.104	39	54	41			
0.129				10	3.2	4.5
0.154	190	350	170			
0.205	450	500	440			
0.230				67	120	120
0.256	530	530	530			
0.307						
0.332				190	250	250
0.434	540	530	530	470	490	480
0.535				520	530	520
0.637	550	520	530	530	530	530

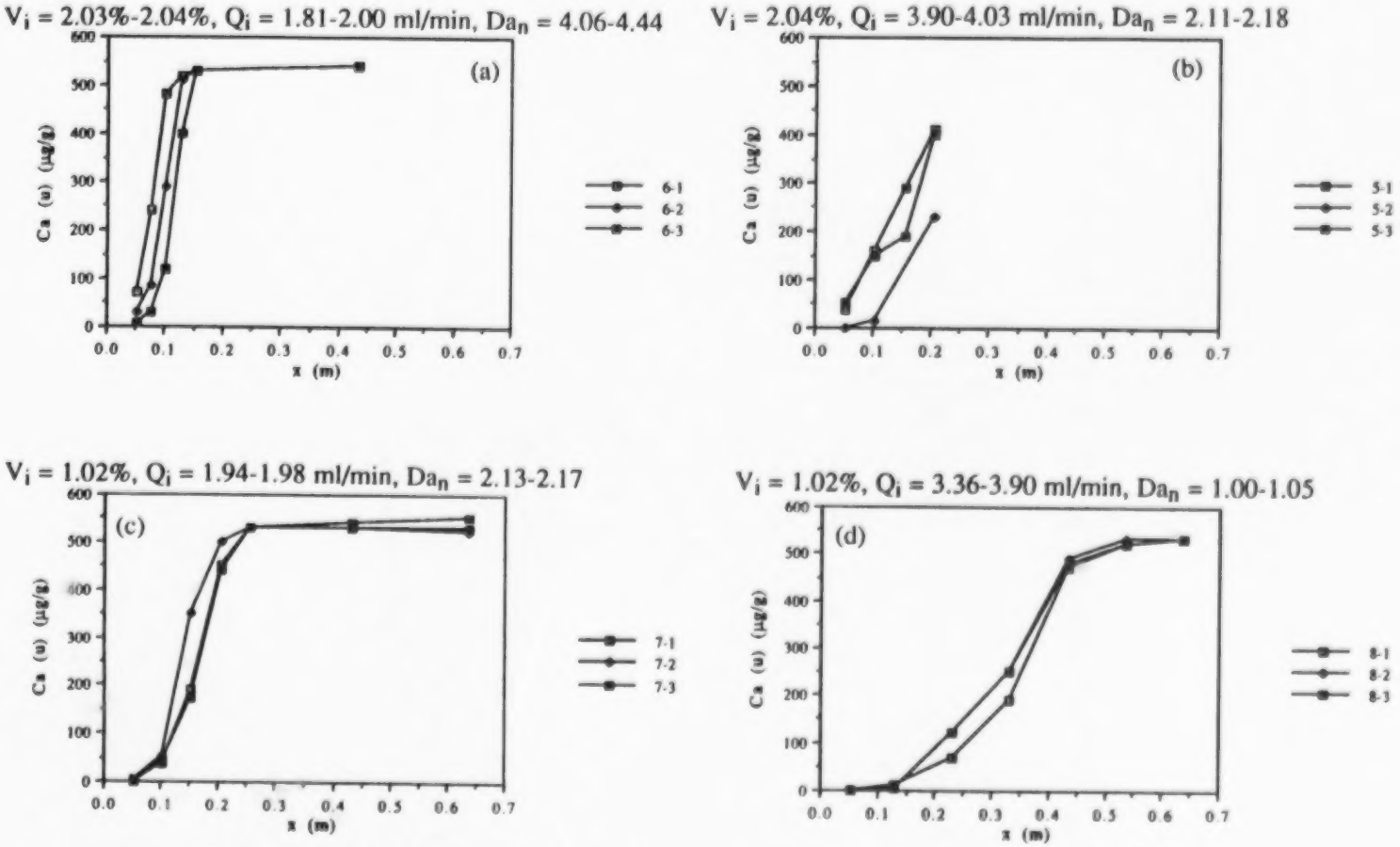

Figure 3.19. Ca trends in unfiltered porewater along the flowpath at the end of (a) experiment 6, (b) experiment 5, (c) experiment 7, (d) experiment 8.

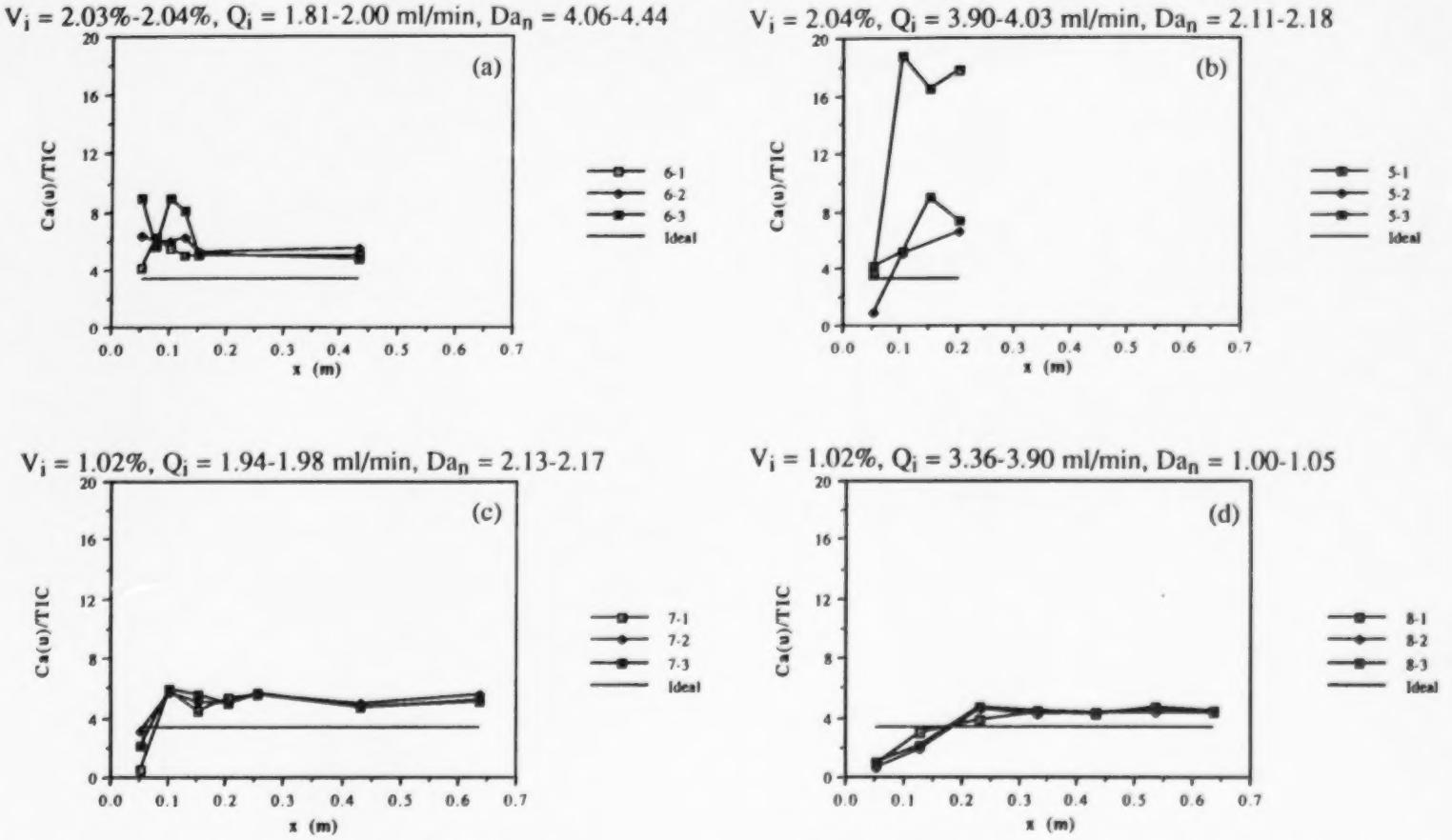

Figure 3.20. Trends in the Ca/TIC ratio along the flowpath at the end of (a) experiment 6, (b) experiment 5, (c) experiment 7, (d) experiment 8.

exists between dissolved and suspended Fe species because of the tendency for polymerization. Because the size of individual ferrihydrite particles is 2 to 5 nm (Schwertmann and Taylor, 1989), the 0.05-μm (50-nm) filter should have retained only larger aggregates of particles. Therefore, except as noted below, unfiltered Fe values are used, representing total (dissolved plus suspended) concentrations in porewater; filtered values are tabulated in Appendix II. The trend at x = 0.053 m was opposite to Ca and TIC: though ranges overlapped, Fe values increased as Da_n decreased (Table 3.9). In general, Fe concentrations decreased as Ca and TIC concentrations and pH increased (Figures 3.21a - d). Like previous parameters, values of Fe changed sharply across the reaction front. Although not discernible at the scale of Figure 3.19, Fe continued to decrease gradually farther down-gradient toward values in effluent.

The Fe concentration data can be examined in detail to see where Fe was being deposited in relation to the position of the reaction front around 165 hr (Figures 3.22a - d). Data points have been plotted based on linear interpolation between the nearest sampling points up- and down-gradient, with the amount lost taken as the difference between unfiltered concentrations at those nearest points. The first data point was plotted midway between the basal plate and 0.053 m, the concentration difference being between influent and the value at sample port 1. From values of 50 μg/g or more deposited adjacent to the inlet, all profiles, except those for columns 5-2 and 6-1, declined to secondary minima, with values ranging from 0 to 40 μg/g. The amount deposited then rebounded, peaking at values of 120 to 210 μg/g shortly behind the reaction front, before declining farther down-gradient.

The concentration distributions of suspended Fe aggregates larger than 50 nm across have been estimated by taking the difference between unfiltered and filtered Fe values (Table 3.10). Hsu (1972) has noted that filtration can be useful for determining the relative magnitude of particle-size distributions, but that it is not sufficiently accurate for quantitative interpretation. Therefore, only the trends in the > 50 nm profiles

Table 3.9. Unfiltered Fe values along flowpath for columns containing sieved calcite.

x (m)	Fe 5-1 (µg/g)	Fe 5-2 (µg/g)	Fe 5-3 (µg/g)	Fe 6-1 (µg/g)	Fe 6-2 (µg/g)	Fe 6-3 (µg/g)
0.053	350	340	320	300	310	330
0.078				190	310	320
0.104	250	340	280	2.3	150	270
0.129				1.1	1.6	77
0.154	130		230	1.1	1.3	1.3
0.205	55	200	82			
0.230						
0.256						
0.307						
0.332						
0.434				0.44	0.62	0.46
0.535						
0.637						

x (m)	Fe 7-1 (µg/g)	Fe 7-2 (µg/g)	Fe 7-3 (µg/g)	Fe 8-1 (µg/g)	Fe 8-2 (µg/g)	Fe 8-3 (µg/g)
0.053	330	350	330	350	350	350
0.078						
0.104	310	310	320			
0.129				340	330	330
0.154	230	120	250			
0.205	41	4.9	50			
0.230				300	280	280
0.256	3.8	2.8	2.9			
0.307						
0.332				230	200	190
0.434	2.5	2.2	1.9	13	6.6	13
0.535				3.1	2.9	3.0
0.637	1.5	1.4	1.1	2.7	2.3	2.2

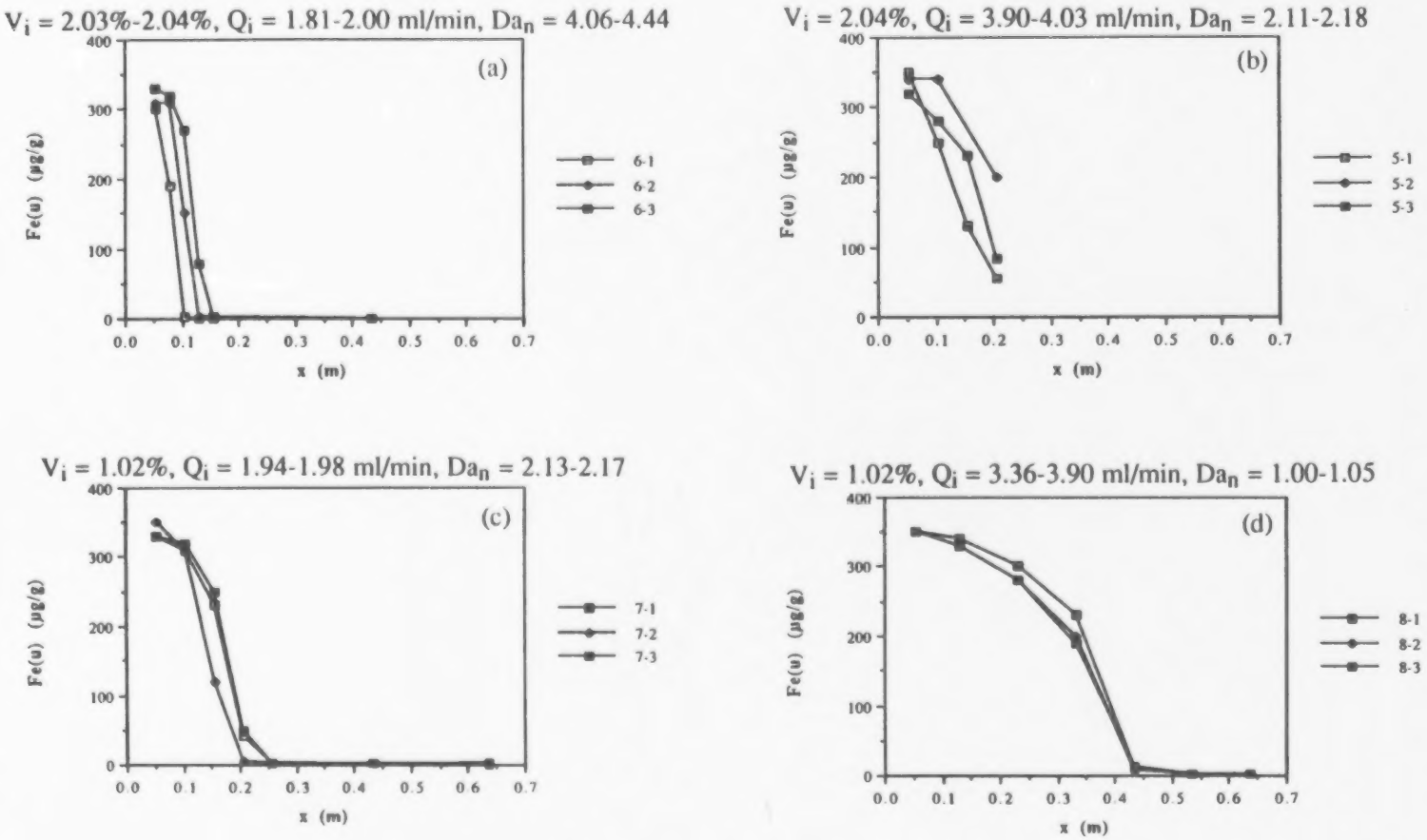

Figure 3.21. Fe trends in unfiltered porewater at the end of
(a) experiment 6, (b) experiment 5, (c) experiment 7, (d) experiment 8.

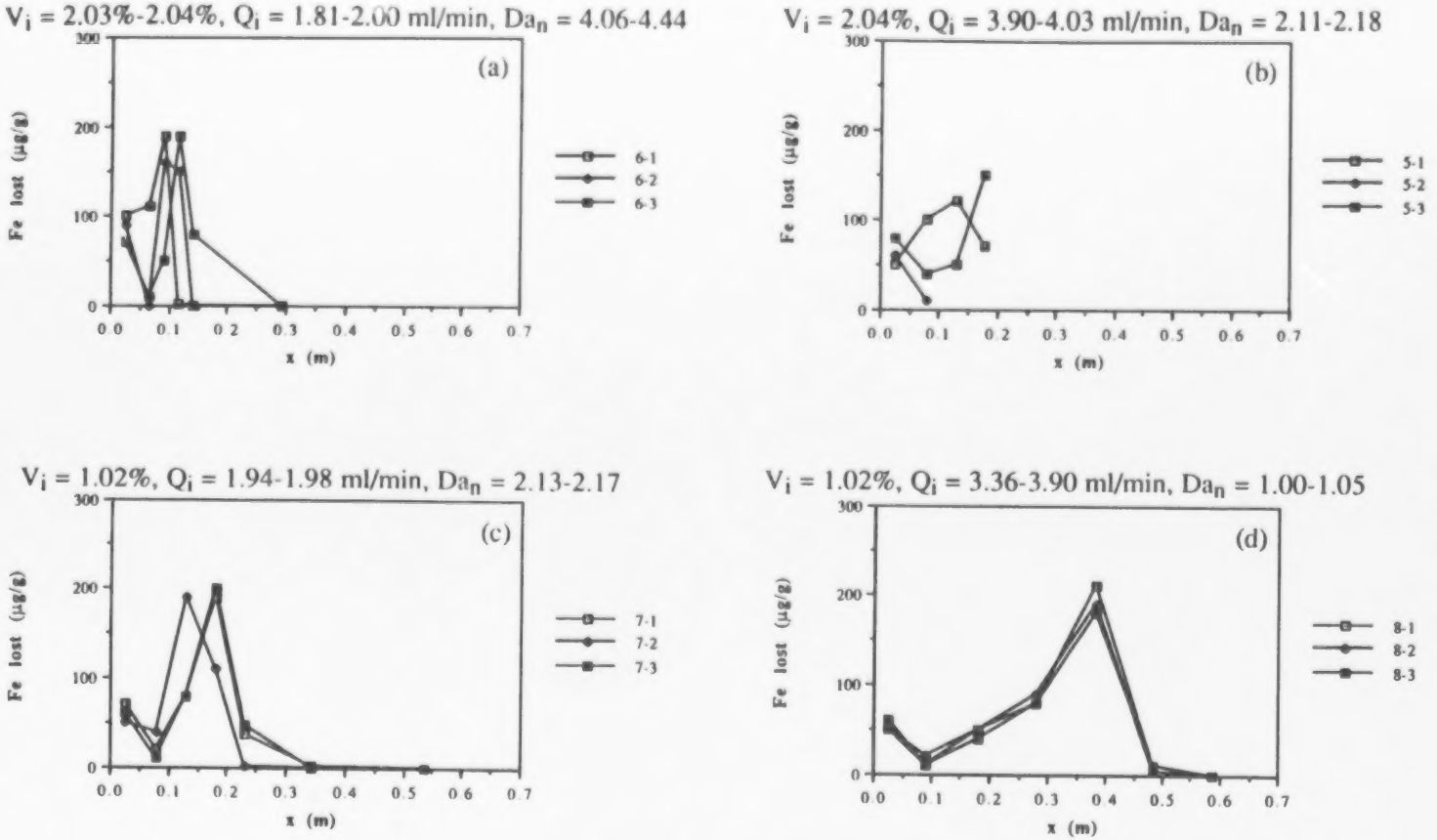

Figure 3.22. Fe deposited between porewater sampling points at the end of (a) experiment 6, (b) experiment 5, (c) experiment 7, (d) experiment 8.

Table 3.10. Concentrations of ferric oxyhydroxide particles larger than 0.05 μm across (μg/g).

x (m)	Fe (u-f) 5-1	Fe (u-f) 5-2	Fe (u-f) 5-3	Fe (u-f) 6-1	Fe (u-f) 6-2	Fe (u-f) 6-3
0.053	40	30	10	20	0	10
0.078				30	30	10
0.103	40	30	30	1.5	40	30
0.129				0.6	1.2	10
0.154	20			0.5	0.4	0.7
0.205	17	40	15			
0.230						
0.256						
0.307						
0.332						
0.434				0.15	0.22	0.12
0.535						
0.637						

x (m)	Fe (u-f) 7-1	Fe (u-f) 7-2	Fe (u-f) 7-3	Fe (u-f) 8-1	Fe (u-f) 8-2	Fe (u-f) 8-3
0.053	0	30	0	0	10	10
0.078						
0.103	10	20	30			
0.129				10	10	10
0.154	40	40	20			
0.205	20.	3.0	17			
0.230				0	10	20
0.256	2.2	1.0	1.7			
0.307						
0.332				.J	50	30
0.434	0.7	0.6	0.8	10.	4.7	11
0.535				0.5	1.5	2.0
0.637	0.7	0.6	0.4	0.4	0.9	1.3

(Figures 3.23a - d) are noted here. In general, the concentration of large aggregates increased with distance down-gradient from the inlet, peaking just behind the maximum in the deposition profile, then declining.

Some of the difference between parameter values in effluent and the nearest porewater values can be attributed to the effluent samples having traveled a longer flowpath and, thereby, having encountered more calcite. The nearest porewater sampling points were approximately 0.13 to 0.33 m up-gradient from the outlet. However, greater agitation occurred during the collection of effluent than during the sampling of porewater, so that effluent samples could also be expected to reflect enhanced degassing. Still, only pH and TIC displayed pronounced differences between down-gradient porewater and effluent. Values of electrical conductivity overlapped between porewater and effluent because ClO_4^-, the predominant electrolyte, was conservative, and because concentrations of Ca^{2+}, the next most prominent, did not change appreciably. Any calcite precipitation, and thus the loss of Ca^{2+}, would have occurred slowly due to kinetic limitations, despite an increase in the saturation index with degassing. Slight differences in cation concentrations probably resulted from the fact that effluent samples were filtered prior to analysis, whereas porewater values have typically been reported for unfiltered samples.

3.3.4. Solid-phase data

Initial information on solid-phase mineralogy was obtained from samples in experiments 1 to 4. X-ray diffraction analysis on a sieved, near-inlet sample yielded a diffractogram with several sharp peaks corresponding to quartz and a shallow, broad peak between 2.47 and 2.53 Å, indicative of ferrihydrite (primary peak at 2.50 Å) (JCPDS, 1984). Although solid-phase digestions were not conducted for these experiments, sections of sediment within the reaction zones were examined, consistently

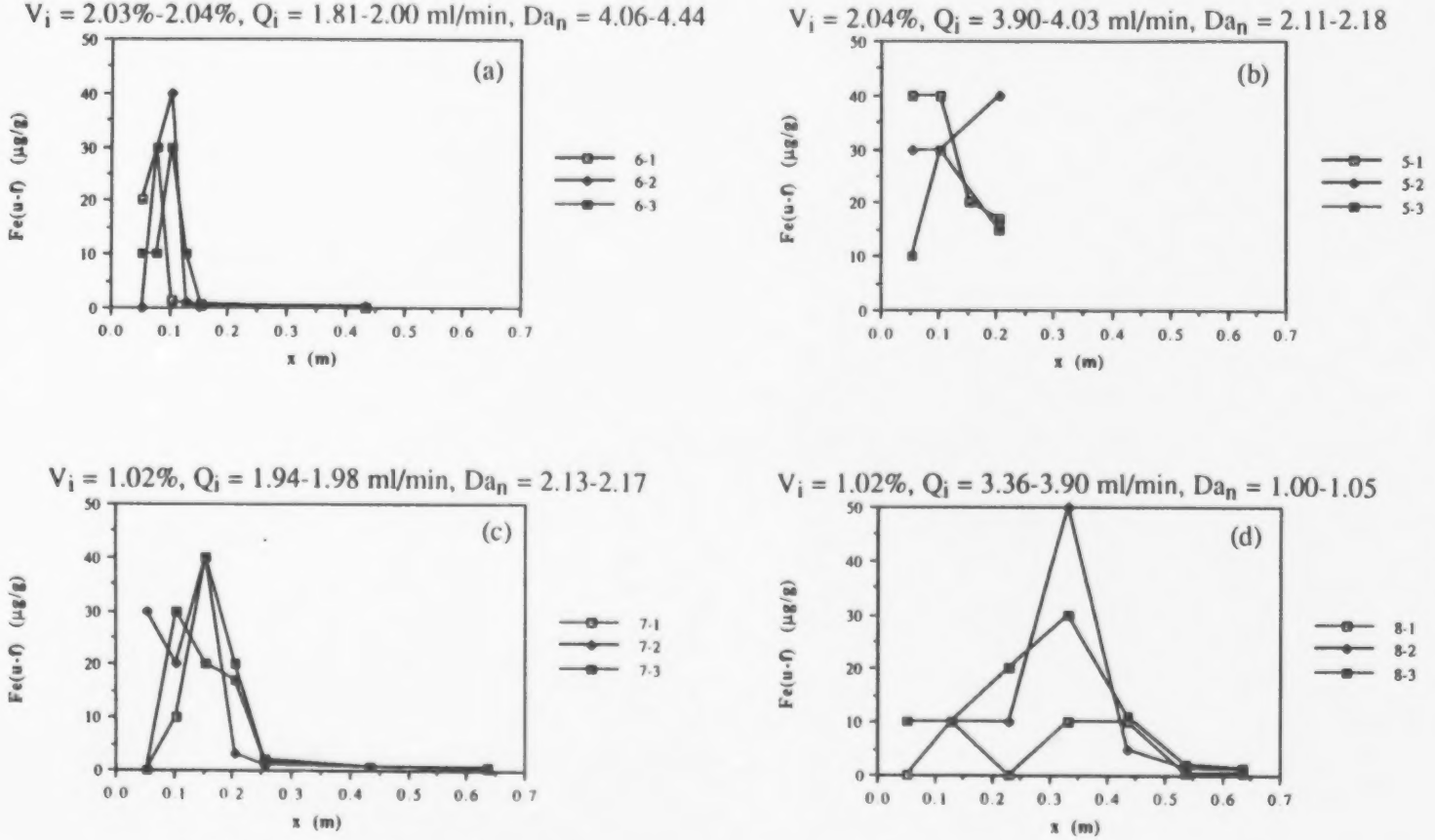

Figure 3.23. Distributions of ferric oxyhydroxide particles >0.05 µm across (as µg Fe/g porewater) along flowpath at the end of (a) experiment 6, (b) experiment 5, (c) experiment 7, (d) experiment 8.

revealing large, uncoated calcite grains, even after 537 hr of reaction in experiment 1. In that experiment, precipitation was sufficiently pervasive to form friable nodules greater than 0.01 m long (Figure 3.24). No calcite grains, which might have acted as nuclei for the accretion of these nodules, were visible at the centers. Figure 3.25a shows an aggregate of several quartz grains from experiment 1 encrusted with precipitated ferric oxyhydroxide. As evident from the close-up in Figure 3.25b, smaller aggregates (typically less than 10 μm) had begun constricting pore throats by bridging, although an open pore diameter of approximately 100 μm was still visible.

Digestion and atomic adsorption analysis on unreacted, triplicate samples of Ottawa sand and crushed calcite provided information on background levels of Ca and Fe in the sediment. For the Ottawa sand, mean concentrations were 9.1 μg Ca per g solid and 11μg Fe per g of solid (μg/g (s)). The Ca may have resulted from trace grains of anorthite or calcite, while red and brown grains occasionally observed in the sand may have been hematite or goethite, which would have provided Fe. The average level of Fe in the calcite was 190 μg/g (s), which may have resulted from inclusions, trace solid-solution with siderite, coatings on the rinds of the original boulders, or cross-contamination from the rock crusher. Background concentrations of Fe in the mixed sediment were 17 μg/g (s) for experiments 5 and 6 and 14 μg/g (s) for 7 and 8.

Analyses of sediment samples taken from frozen columns have provided information on solid-phase concentration distributions at the end of experiments. Values from within the endcap were plotted at 0.026 m, midway between the basal plate and port 1. For solid-phase Ca (Ca_S), the ranges of these values, while overlapping, tended to decrease with Da_n (Table 3.11). On the whole, they indicate little or no calcite remaining adjacent to the inlet, and suggest some dissolution of sources of trace Ca in the sand as well, which generally agrees with the corresponding Ca/TIC ratios in porewater. Unreacted Ca_S values in the sediment were calculated as 13000 μg/g (s) for experiments 5 and 6 and 6600 μg/g (s) for 7 and 8. To facilitate visual comparison,

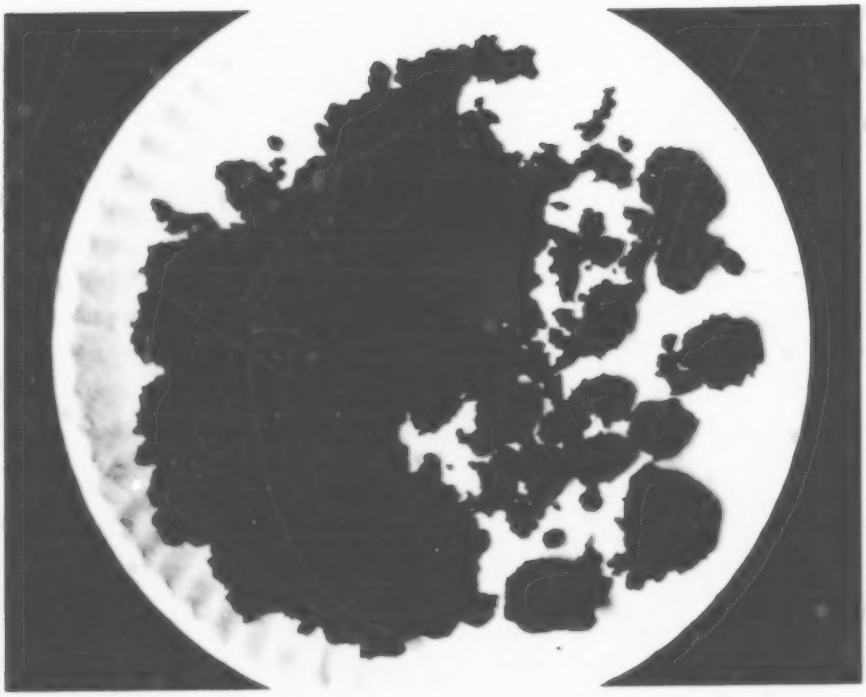

Figure 3.24.
Partly disaggregated sediment from lower endcap; column 1-2. Bright specks are large calcite grains (to approximately 0.005m across) Largest ferrihydrite-aggregated nodule approximately 0.03 m long.

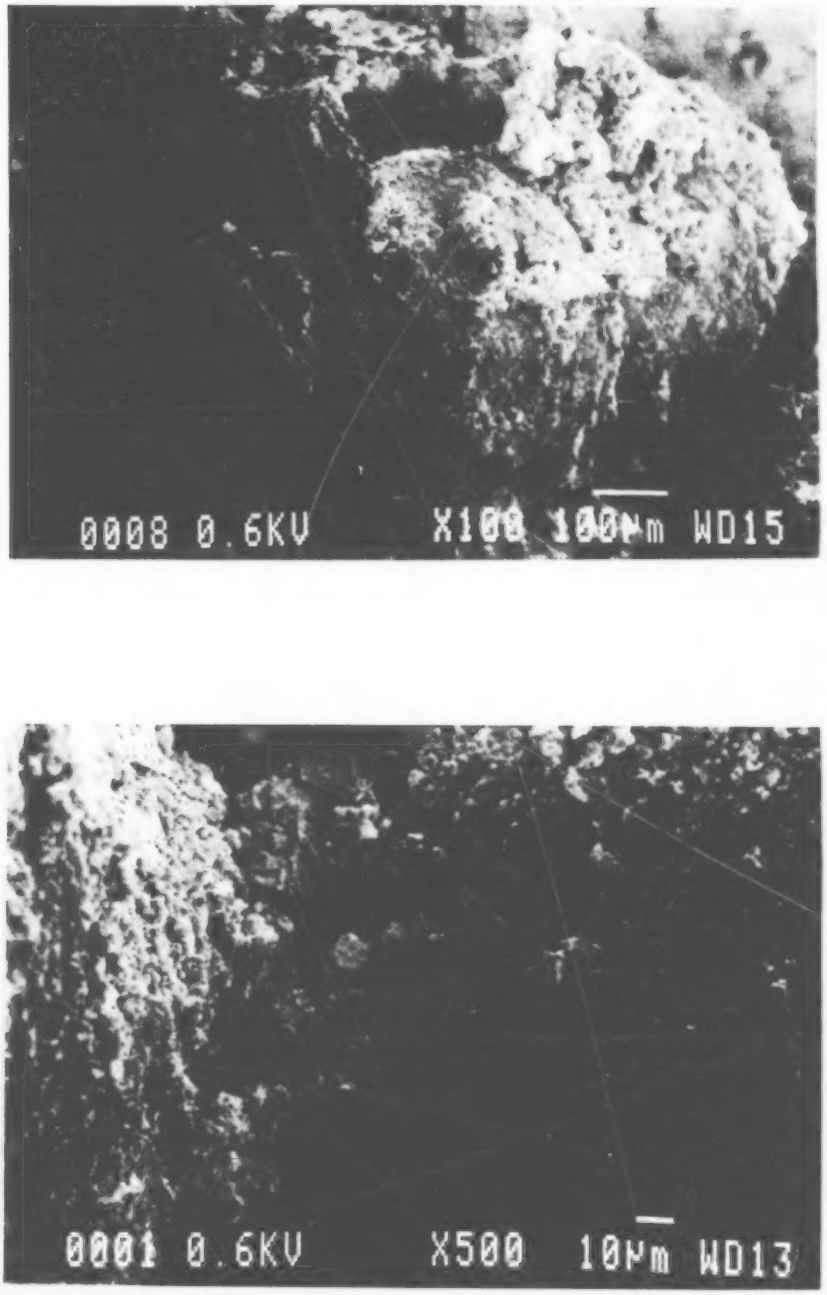

Figure 3.25.
Aggregate of several quartz grains indurated by ferrihydrite, (a) top, 100x, (b) bottom, 500x, scales as shown on photos.

Table 3.11. Solid-phase Ca along flowpath for columns containing sieved calcite (μg/g(s)).

x (m)	Ca (s) 5-1	Ca (s) 5-2	Ca (s) 5-3	Ca (s) 6-1	Ca (s) 6-2	Ca (s) 6-3
0.020	50	0.82	82	3.3	18	160
0.053	10	4.1	300	330	870	1100
0.078				1100	2400	3400
0.104	980	560	1000	10000	7400	9500
0.129	1800			13000	11000	12000
0.154	1800	2300	2300	13000	12000	12000
0.205	5000	4400	4200			
0.230						
0.256	11000	13000	12000			
0.307	13000	13000	12000			
0.332						
0.434				13000	13000	13000
0.535	12000	13000	13000			
0.637						

x (m)	Ca (s) 7-1	Ca (s) 7-2	Ca (s) 7-3	Ca (s) 8-1	Ca (s) 8-2	Ca (s) 8-3
0.020	1.2	2.6	0.90	0.00	0.88	0.00
0.053	7.6	0.39	30	0.00	2.1	0.00
0.078						
0.104	150	97	340			
0.129				280	83	16
0.154	970	1500	1100			
0.205	4000	4600	4200			
0.230				560	600	490
0.256	6300	5800	6500			
0.307						
0.332				1500	1700	1000
0.434	6400	6400	6700	5500	5700	5500
0.535				6700	6800	6600
0.637	6900	6600	6300	6200	6300	6800

measured Ca_s concentrations have been normalized against these unreacted values (Figures 3.26a - d). The resulting profiles display shapes similar to those of pH, TIC, and Ca profiles in porewater. The solid-phase profiles tend to be more uniform than the others, probably because each slice of sediment was mixed prior to analysis. The profiles for experiments 5 and 7 (Figures 3.26b - c), with virtually identical values of Da_n, overlap over approximately the first 0.154 m, and again beyond the reaction front. In the heart of the reaction zone, however, the profile for 7 is displaced slightly up-gradient relative to that of 5, indicating more dissolution of calcite locally for 5. Across experiments 5 to 8, normalized values of approximately 1.0 down-gradient from the reaction front indicate minimal calcite dissolution.

In contrast to Ca_s, solid-phase Fe (Fe_s) values at 0.026 m, where reaction was most pervasive, do not show a dependence on Da_n (Table 3.12). As shown in Figure 3.27, Fe_s at 0.026 m increased with an increase in the initial amount of calcite present, but also increased with an increase in the initial flow rate. Fe_s profiles tend to decrease sharply from 0.026 m to 0.053 m, which coincides with the initial minimum in Fe deposition shown in Figures 3.22a - d. Beyond 0.053 m, the profiles flatten, which corresponds to the increasing loss of Fe from porewater with movement toward the reaction front. Final Fe_s values down-gradient from the reaction front were several μg/g (s) higher than background values, thus supporting porewater data in indicating deposition of trace amounts of Fe ahead of the visible limit.

3.4. Hydraulic Evolution of the System

The effects of reaction upon hydraulics have been evaluated by monitoring flow rates at the outlet of each column and hydraulic heads along each column and calculating corresponding values of hydraulic conductivity at various times. Experiments 1 to 4 were distinguished by reductions in flow rates due to back-pressuring and by failure of

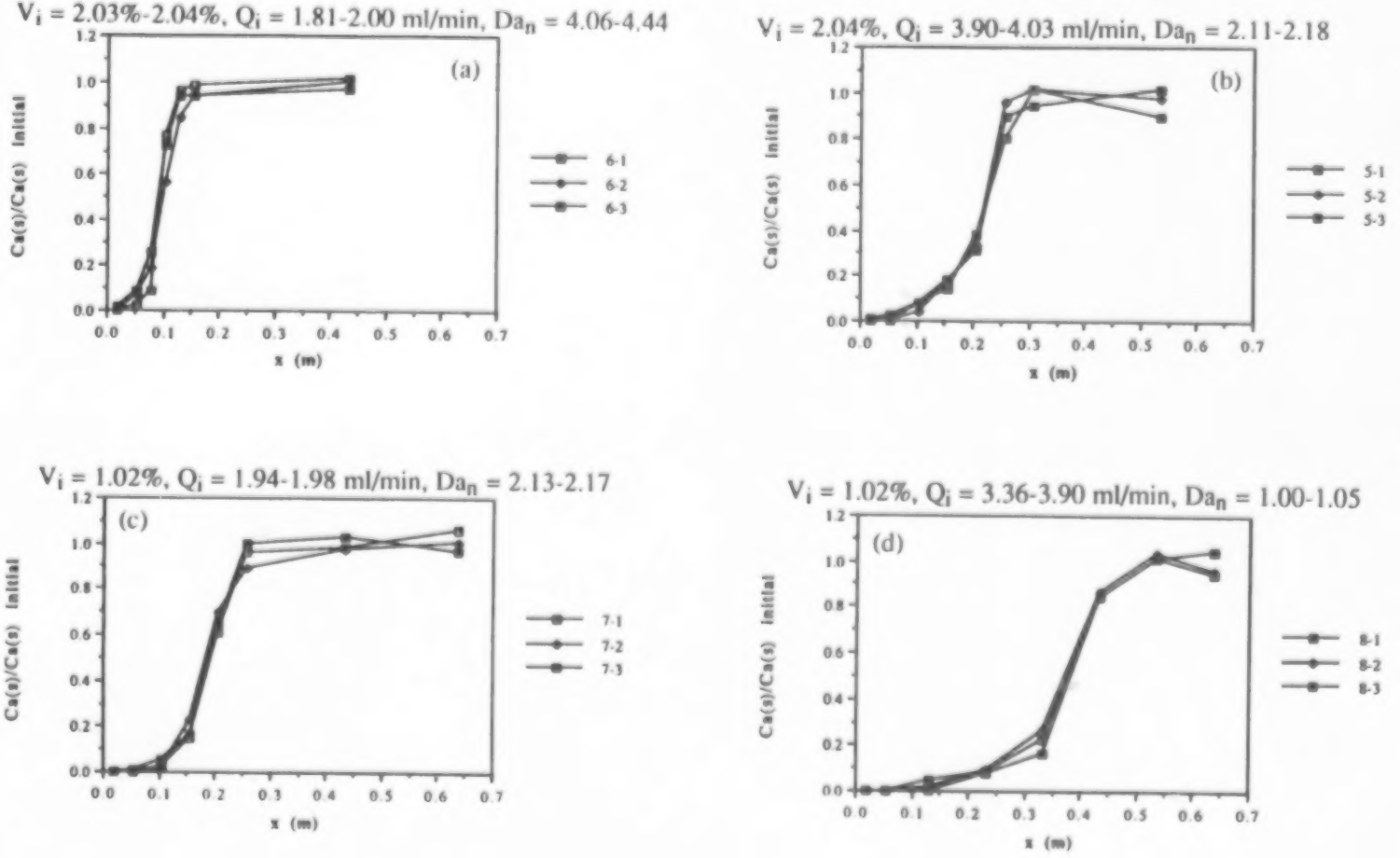

Figure 3.26. Solid-phase Ca, normalized against initial amount present, at the end of (a) experiment 6, (b) experiment 5, (c) experiment 7, (d) experiment 8.

Table 3.12. Solid-phase Fe along flowpath for columns containing sieved calcite (μg/g (s)).

x (m)	Fe (s) 5-1	Fe (s) 5-2	Fe (s) 5-3	Fe (s) 6-1	Fe (s) 6-2	Fe (s) 6-3
0.020	12000	10000	11000	12000	7000	8400
0.053	11000	8000	7700	5400	4400	3600
0.078				4800	4000	3600
0.104	7700	5000	5600	1700	1200	1900
0.129				130	200	440
0.154	6900	4200	5400	36	34	34
0.205	5000	4300	3700			
0.230						
0.256	300	250	370			
0.307	35	28	33			
0.332						
0.434				30	41	30
0.535	33	31	30			
0.637						

x (m)	Fe (s) 7-1	Fe (s) 7-2	Fe (s) 7-3	Fe (s) 8-1	Fe (s) 8-2	Fe (s) 8-3
0.020	4500	5000	4800	6500	5900	6400
0.053	3000	2700	2700	3600	5000	4200
0.078						
0.104	2000	3200	2300			
0.129				2300	2600	2800
0.154	1900	1900	2200			
0.205	1300	1100	990			
0.230				1900	2300	1900
0.256	27	28	27			
0.307						
0.332				1300	1800	1800
0.434	25	23	22	630	430	680
0.535				26	23	30
0.637	23	20	19	27	21	23

V_i = 2.03%-2.04%, Q_i = 1.81-2.00 ml/min, Da_n = 4.06-4.44

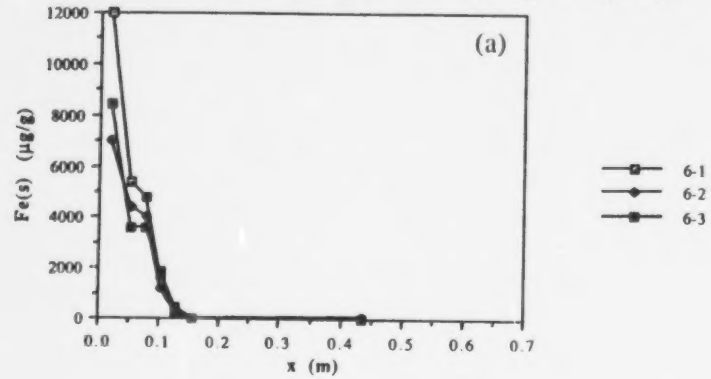

V_i = 2.04%, Q_i = 3.90-4.03 ml/min, Da_n = 2.11-2.18

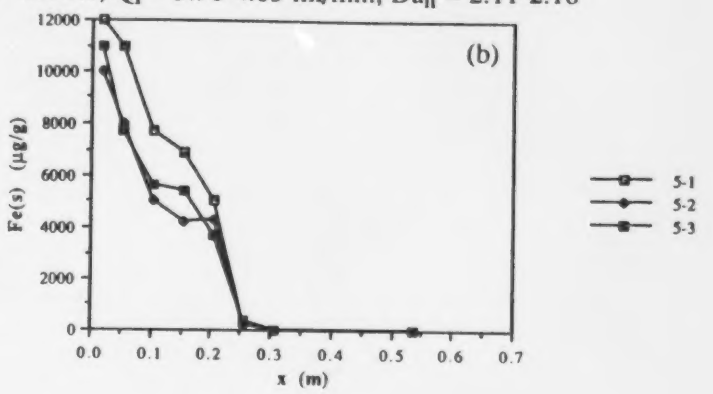

V_i = 1.02%, Q_i = 1.94-1.98 ml/min, Da_n = 2.13-2.17

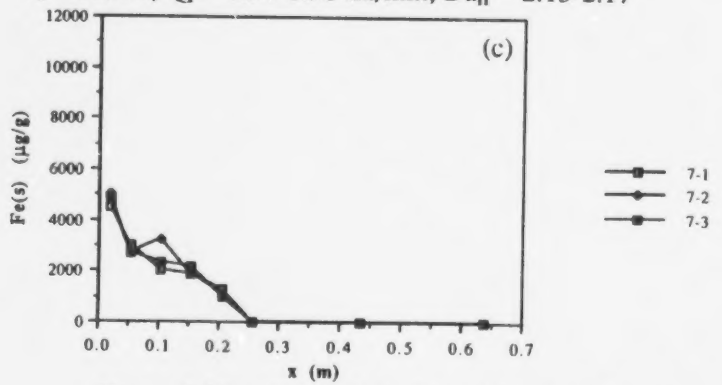

V_i = 1.02%, Q_i = 3.36-3.90 ml/min, Da_n = 1.00-1.05

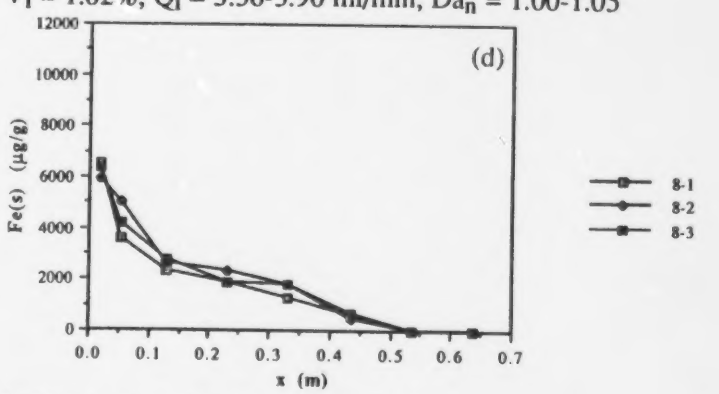

Figure 3.27. Solid-phase Fe at the end of (a) experiment 6, (b) experiment 5, (c) experiment 7, (d) experiment 8.

seals, as noted in Section 3.2.1, as well as by the occasional overflow of the manometer adjacent to the inlet. Therefore, the presentation of hydraulic results is divided between experiments 1 to 4 and 5 to 8. Appendix III contains listings of flow rates, hydraulic heads, and hydraulic conductivities for each experiment.

Though measurements of flow rates were sparse in experiments 1 to 3, the decreases in flow rates for the case of unsieved calcite did not appear to depend on either Da_n, the initial surface area, or the initial flow rate. Experiments 1 and 2 were more prone to failure than to declines in flow rates. Flow rates measured at 529 hr were greater than those measured at 72 hr (2.1 ml/min versus 1.8 ml/min) for column 1-2 (Figure 3.28a). For column 2-3, flow rates were relatively uniform (4.7 to 4.8 ml/min) during the first 73 hr, beyond which monitoring was discontinued (Figure 3.28b).

Reductions in flow were pronounced in experiment 4 (Figure 3.28c) and columns 3-1 and 3-3 (Figure 3.28d). Column 4-3 exhibited the greatest reduction, from a rate of 2.05 ml/min at 1 hr to 0.00326 ml/min at 121 hr, though this latter value may have been affected by evaporation during the 5-hr collection period. The timing of the reductions showed no clear trends. Flow in both 3-1 and 3-3 declined after approximately 120 hr. 4-1 declined from an initial value of 3.21 ml/min to 1.76 ml/min at 24 hr, near which the flow rate hovered until after 125 hr. 4-2 began to decline after 99 hr, whereas 4-3 declined from the start. Near the end of experiment 4, the pump was adjusted to maintain flow in columns 4-1 and 4-3. The fact that flow rates declined in experiments 3 and 4, but columns did not fail as in previous experiments, may simply reflect an improvement in the technique of sealing joints with caulk.

For experiments 5 to 8, which contained sieved calcite and had relatively low values of Da_n, the flow rates did not permanently decline. However, these rates tended to fluctuate more (Figures 3.29a - d) than in experiments 1 to 4, perhaps because of differences in the volume of effluent collected for monitoring. In 5 to 8, point measurements of the flow rate were made by collection of effluent during a one-minute

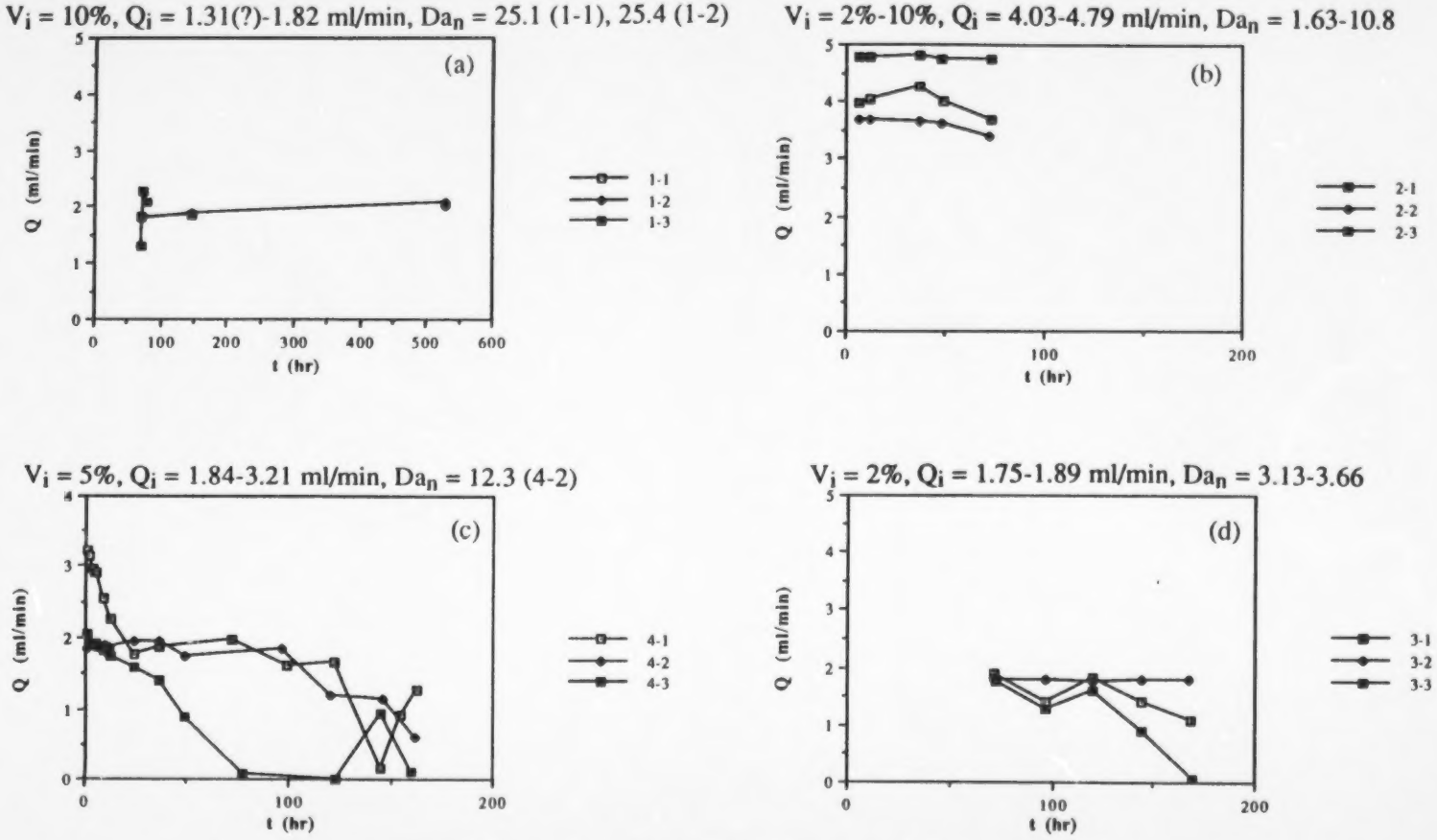

Figure 3.28. Volumetric flow rate trends during (a) experiment 1, (b) experiment 2, (c) experiment 4, (d) experiment 3.

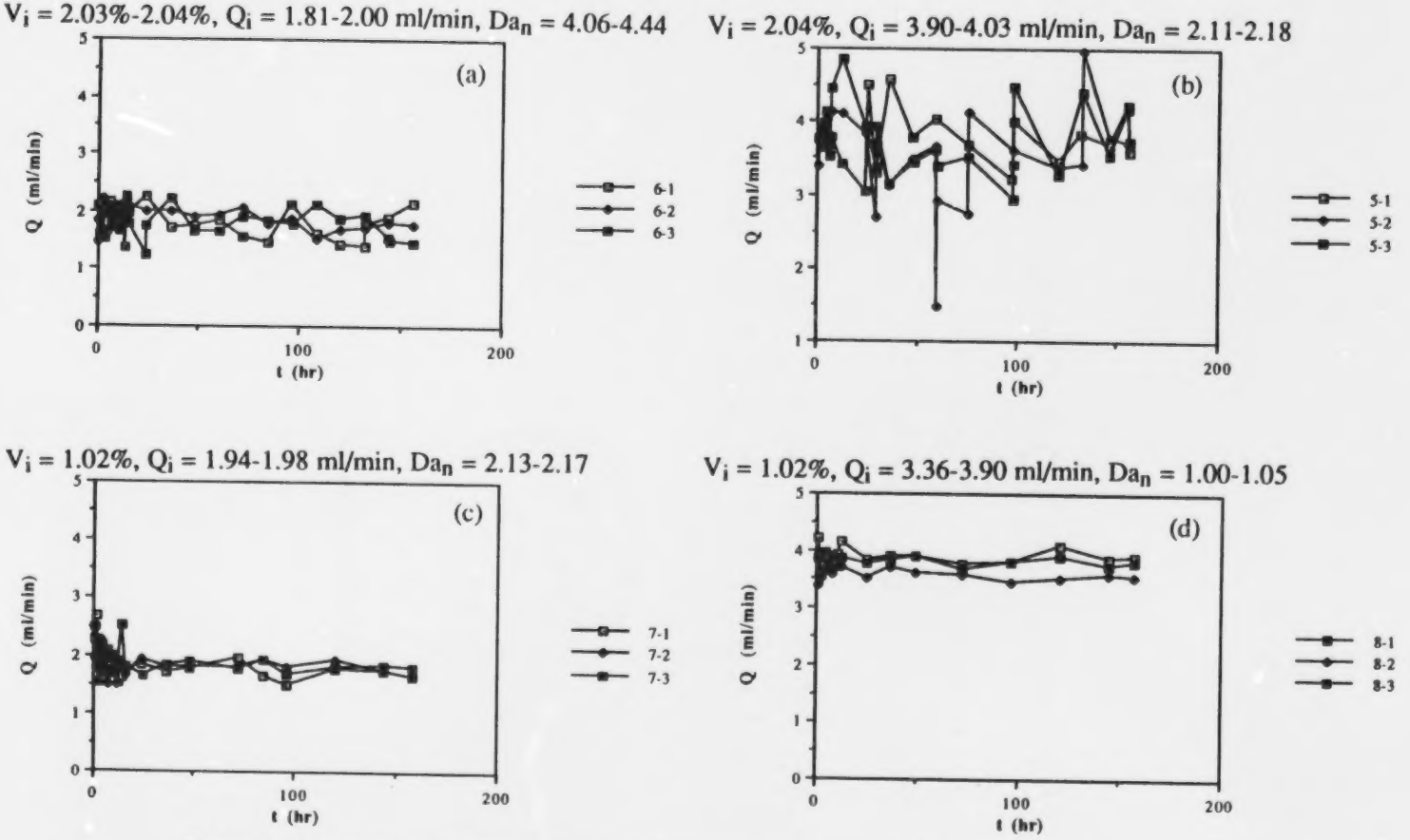

Figure 3.29. Volumetric flow rate trends during (a) experiment 6, (b) experiment 5, (c) experiment 7, (d) experiment 8.

period. Each value in experiments 1 to 4 had been based on collecting effluent over several minutes, so that fluctuations had been averaged over a longer period of time.

In the case of unsieved calcite, the increase in hydraulic heads beyond initial values occurred more quickly at high initial flow rates. Inlet manometers for columns in experiment 2 overflowed between 1 hr (column 2-2) and 12 hr (columns 2-1, 2-3) after the introduction of influent (Figure 3.30b). At low initial flow rates, the time at which the inlet head rose generally lengthened as the initial surface area of calcite decreased between experiments. For columns 1-2 and 1-3, the rise in head at the inlet was gradual, beginning after 24 hr, while 1-1 exhibited a more abrupt rise after 77 hr (Figure 3.30a). The inlet head increased gradually after 24 hr in 4-3 and after 76 hr in 4-2, versus an abrupt rise after 98 hr in 4-1 (Figure 3.30c). The earlier rise for 4-3 probably reflected the continuous decline in its flow rate. For experiment 3, the head at the inlet rose gradually after 37 hr in 3-2 and after 97 hr in 3-3, with 3-1 rising abruptly after 157 hr. The variability in the timing of head increases among replicate columns in these experiments reflects a degree of randomness associated with pore plugging.

Hydraulic head increases in the sieved case were comparatively subtle, as shown for head values adjacent to the inlet in Figure 3.31. The increase occurred sooner, and was larger in magnitude, for experiment 6 versus 7 and for experiment 5 versus 8, indicating a dependence on the surface area. The inlet head increased sooner for experiment 5 versus 6 and experiment 8 versus 7, indicating a dependence on the flow rate. However, as in the unsieved case, the timing of the increase was not a function of Da_n. This lack of dependence is indicated by the fact that experiment 7, with an intermediate value of Da_n, was slowest to respond.

The distance along the column over which the hydraulic gradient had increased by the end of an experiment generally lengthened as Da_n decreased in the case of unsieved calcite. For experiments 1 and 4 and columns 2-1 and 2-2, that distance from the inlet was less than 0.045 m, whereas it was greater than 0.045 m for experiment 3

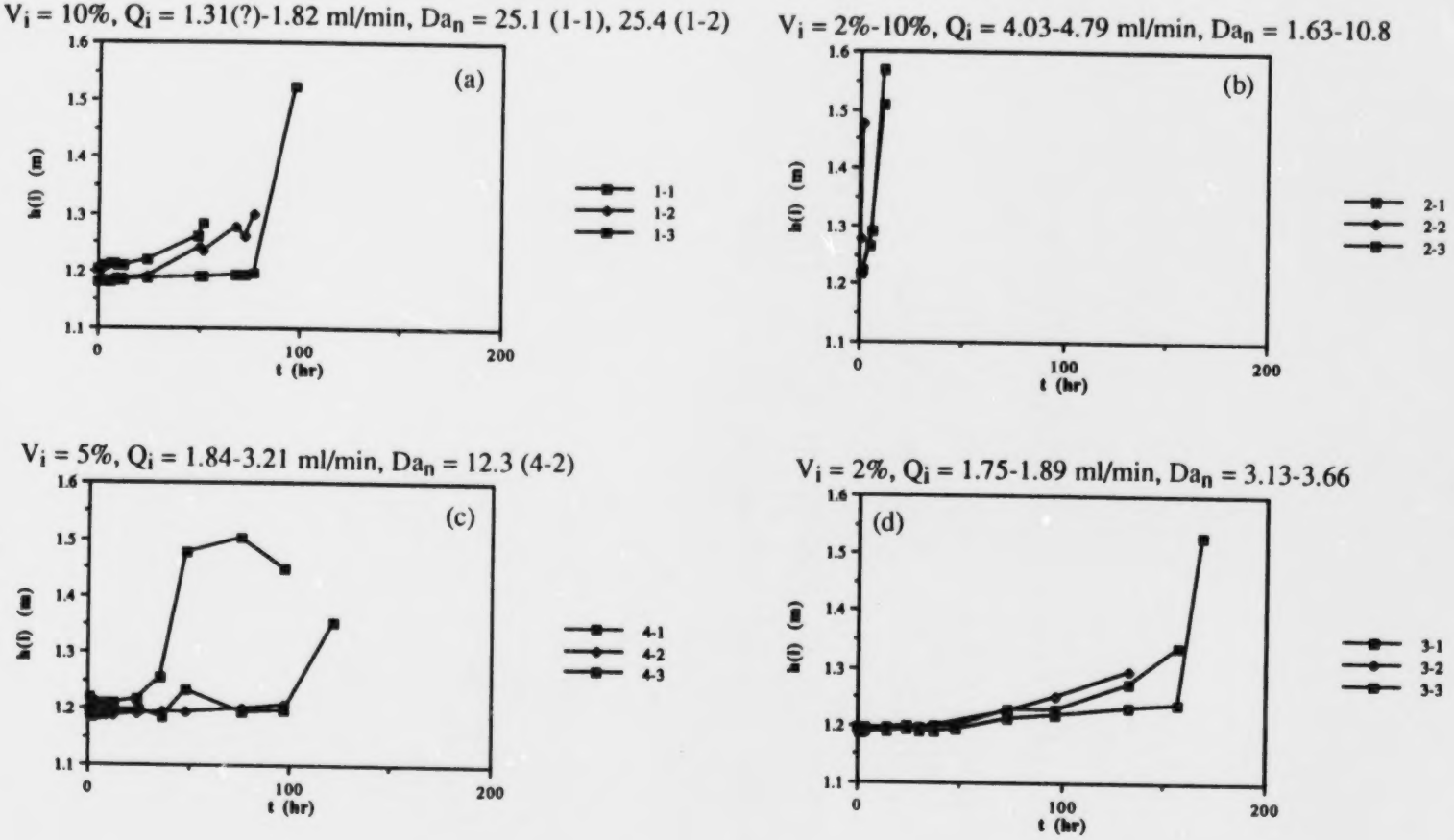

Figure 3.30. Hydraulic head profiles at the inlet manometer during (a) experiment 1, (b) experiment 2, (c) experiment 4, (d) experiment 3.

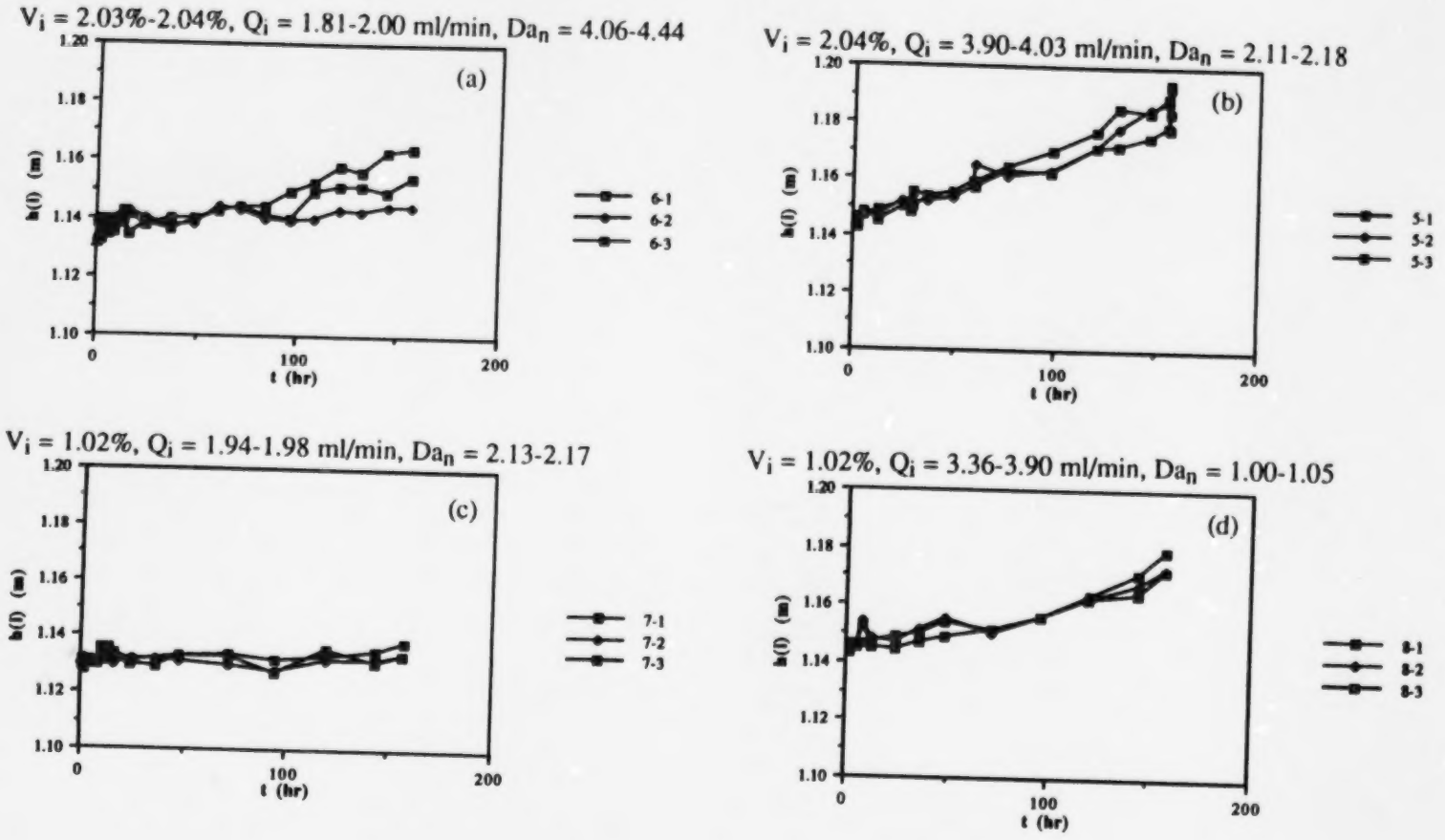

Figure 3.31. Hydraulic head profiles at the inlet manometer during (a) experiment 6, (b) experiment 5, (c) experiment 7, (d) experiment 8. Note that range in h narrower than in previous figure.

and greater than 0.248 m for 2-3. In the sieved experiments, the distances from the inlet were greater than 0.053 m for 6 and 7 and greater than 0.129 m for 5 and 8, which indicates a dependence on the flow rate but not on the calcite surface area. In columns 5-2 and 6-1, an increase in head occurred ahead of the reaction front, probably due to early entrapment of gas.

Values of hydraulic conductivity (K) calculated for the intervals between adjacent manometers have been normalized against background values determined from head profiles preceding experiments 1, 3, 4, and 5. The background hydraulic gradient was taken over virtually the whole length of the column (port 1 to port 7 or 8) in order to dampen small fluctuations in the gradient between adjacent manometers. The replicate background values of hydraulic conductivity were averaged to obtain a single, smoothed value (K_o) representative of each experiment (Table 3.13). Because of a lack of flow rate measurements for column 1-2, and the initial problem with excessive rates of flow for 4-1, the overall background values for experiments 1 and 4 each represent the average of two, rather than three, readings. Hydraulic heads were not measured prior to the starts of experiments 2, 6, 7, and 8. Background hydraulic conductivities from 1, 4, and 3 have thus been assigned to columns 2-1, 2-2, and 2-3, respectively, based on the initial amount of calcite. Similarly, the averaged background value for 5 was extrapolated to 6, 7, and 8, because of the relative uniformity of grain size and low overall percentage of calcite in the sieved experiments.

The pronounced increases in the hydraulic gradient across the inlet and the declines in flow rates indicate greater reductions in normalized hydraulic conductivity for the unsieved experiments. Normalized values adjacent to the inlet, where reductions were greatest, are shown in Figure 3.32. The lowest value observed overall was 4.0×10^{-6} for column 4-3 (Figure 3.32c). However, that value may have been biased downward by evaporation during the collection of effluent to measure the flow rate, as indicated by a parallel decline in K/K_o for down-gradient intervals ahead of the reaction

Table 3.13.
Background values of hydraulic conductivity and averages for experiments 1, 3, 4, and 5; C.V. refers to the coefficient of variation.

Column #	K initial (m/s)	K run (m/s)	C.V.
1-1	0.000437		
1-2	0.000648	0.000543	0.275
3-1	0.00102		
3-2	0.000536		
3-3	0.000632	0.000730	0.353
4-2	0.000571		
4-3	0.000633	0.000602	0.0731
5-1	0.000837		
5-2	0.000675		
5-3	0.000637	0.000716	0.148

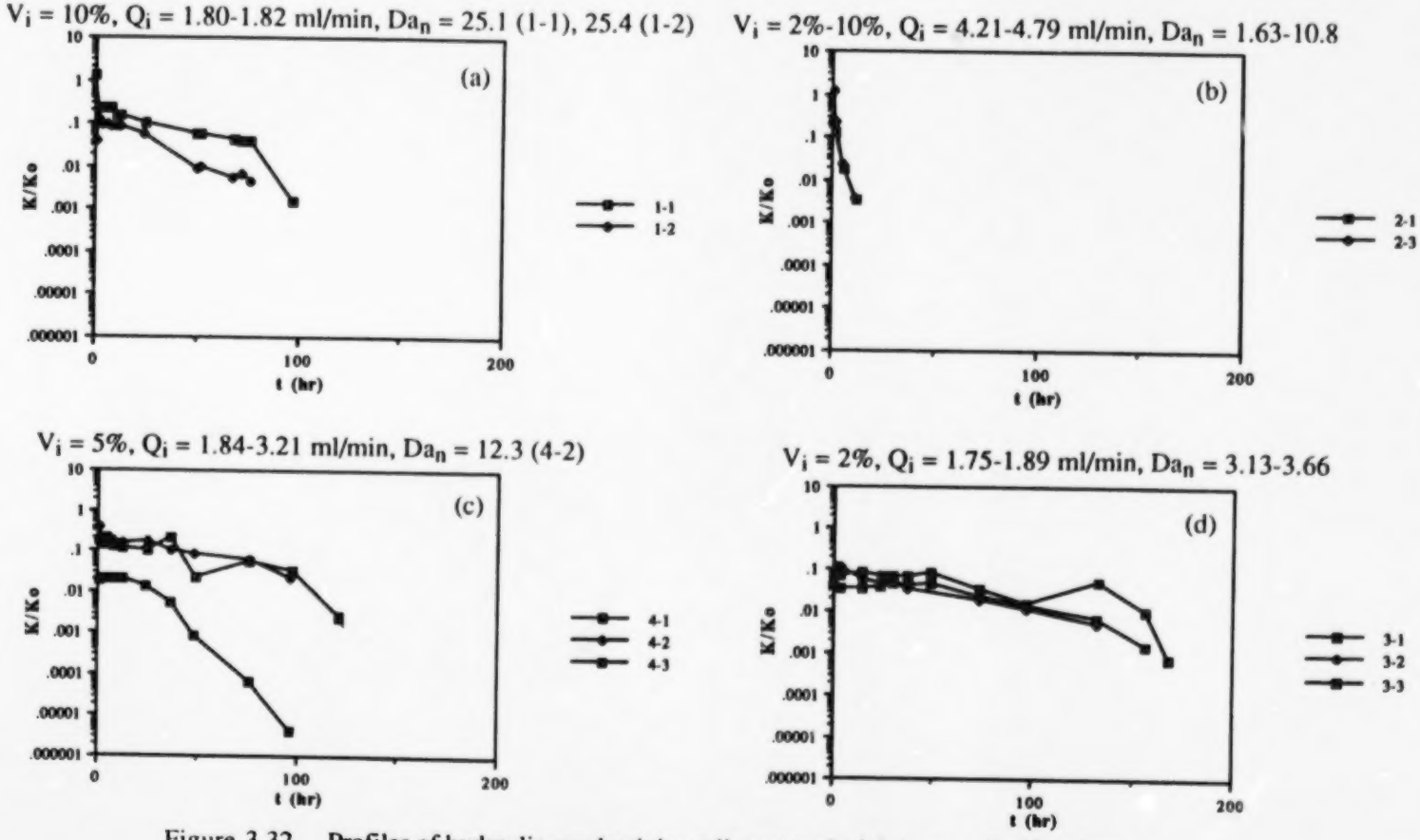

Figure 3.32. Profiles of hydraulic conductivity, adjacent to the inlet, normalized against background values during (a) experiment 1, (b) experiment 2, (c) experiment 4, (d) experiment 3.

front. The final value adjacent to the inlet was less than the next value down-gradient by a factor of 0.0015, which may be a more accurate indication of the decline in K/K_o. In general, initial K/K_o values adjacent to the inlet were less than one, in contrast to initial values down-gradient. The assumption of homogeneity involved in calculating the hydraulic conductivity of the medium apart from the porous metal plate is thus shown to be a simplification. Still, one may consider the decline between initial and final K/K_o values: discounting column 4-3, the maximum decline observed was by a factor of 0.0012 for column 1-1 (Figure 3.32a). The maximum possible decline may be lower, because no profile appeared to attain a limiting value of K/K_o. In keeping with the hydraulic head profiles, declines in hydraulic conductivity were most rapid for experiment 2, followed by 1, 4 (except for 4-3), and 3.

For the sieved case, normalized values of hydraulic conductivity for the interval across the inlet were less prone to decline (Figure 3.33). The lowest value of K/K_o was 0.022 for column 6-1 (Figure 3.33a), while the greatest decline between initial and final normalized values was by a factor of 0.014 for column 8-2 (Figure 3.33d). Generally speaking, hydraulic conductivity values adjacent to the inlet appear to have stabilized by the end of experiments 5 to 7, but not by the end of 8. Still, the maximum possible decline would appear to be less for sieved versus unsieved calcite. For some profiles, particularly in experiments 7 and 8, initial values of K/K_o were greater than one, and data points are sparse because negative values (physically nonsensical) have been excluded. These aberrations resulted when the hydraulic conductivity of the region adjacent to the inlet, including the plate, exceeded the hydraulic conductivity of the plate itself by a critical amount, so that the assumptions of homogeneity of the sand and the plate were overly simple.

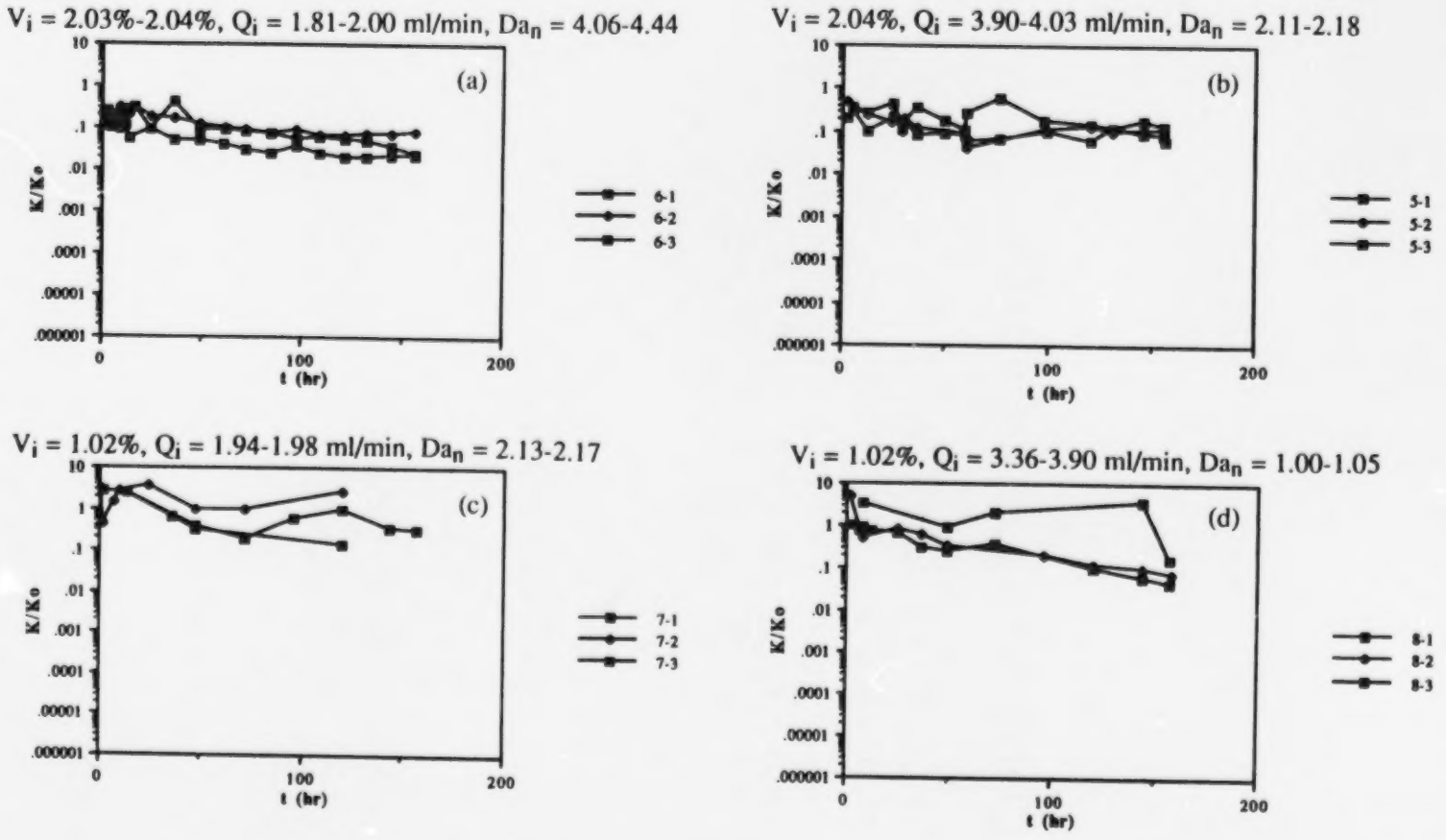

Figure 3.33. Profiles of hydraulic conductivity, adjacent to the inlet, normalized against background values during (a) experiment 6, (b) experiment 5, (c) experiment 7, (d) experiment 8.

4. DISCUSSION

4.1. Mechanisms of Geochemical and Hydraulic Evolution

4.1.1. Geochemical evolution along the flowpath

The infiltration of $Fe(ClO_4)_3$ solution into the porous medium and subsequent reaction can be conceptualized in terms of the migration of a fluid packet, or a discrete elemental volume of porewater, traversing the length of the column (Lichtner, 1988). Although samples for porewater and solid phase analyses were taken at the end of each experiment, it is possible to reconstruct geochemical evolution starting with the first fluid packet. Based on trends in x, beginning where Ca, TIC, and Ca_S concentrations became greater than a few μg/g, pH decreased slightly with the onset of calcite dissolution. The neutralization of initial acidity was thus outpaced by the additional hydrolysis induced. Hsu and Ragone (1972) and Loeppert et al. (1984) observed a similar decline in batch experiments with 0.01 M $Fe(ClO_4)_3$, but after a prior increase of several tenths of a pH unit, which may have occurred in this study but was not measured. The pH minimum corresponded with a maximum in electrical conductivity, beyond which down-gradient the rate of H^+ production was overtaken by that of consumption.

The behavior of CO_2 generated during calcite dissolution was complex, with degassing and immobilization, degassing and flow, and solution-phase transport all being possible. Early entrapment of gas in pores was evident from observations of patches of bubbles and, for experiment 2, of coherent gas fronts. Separate-phase migration and agglomeration of bubbles have been indicated by the occasional displacement of larger pockets of gas from manometers and outlets. However, because (unfiltered) Ca was typically enriched relative to TIC in porewater by a factor of two, a

majority of the CO_2 generated in experiments 5 to 8 was probably transported in solution. The preferential enrichment in Ca was probably not due to degassing during sampling, because atmospheric exposure during sampling for TIC was minimized by the use of syringes connected to the sample ports.

As hydrolysis and pH buffering progressed, polymerization, precipitation, and deposition should have occurred (Flynn, 1984). Deposition profiles indicate that loss of Fe from porewater increased down-gradient between the pH minimum and the reaction front. Observations of initial front propagation and of porewater samples between the inlet and the reaction front (Figure 4.1) show that the influent penetrated the porous medium for some distance before becoming visibly turbid. However, porewater Fe concentrations decreased with increasing turbidity down-gradient, which suggests simply that a greater fraction of the iron remaining in porewater was suspended. This behavior was borne out by a general increase both in the amount of suspended ferric oxyhydroxide particles larger than 0.05 μm across and in the percentage of the > 0.05-μm fraction toward the front. These results suggest that some particles were migrating and aggregating in suspension prior to deposition. However, precipitation could have been promoted by an increase in pH due to CO_2 degassing during sampling for cations, and aggregation was probably enhanced by filtration after sampling (Gschwend and Reynolds, 1987). Therefore, conclusions about the transport of colloids (particles approximately 1 nm to 10 μm in size) in this system are speculative.

Published information provides a basis for a plausible conceptual model describing particle interaction. Particles smaller than a few μm collided with each other and with the framework solids as a result of Brownian motion (Hunt et al., 1987). The point of zero charge (pzc), the pH at which the total net surface charge of a particle is zero, is approximately 8 for synthetic ferrihydrite (Schwertmann and Taylor, 1989). Therefore, at the pH values encountered behind the reaction front, the suspended particles would have been positively charged. Because the concentration of ClO_4^-, the

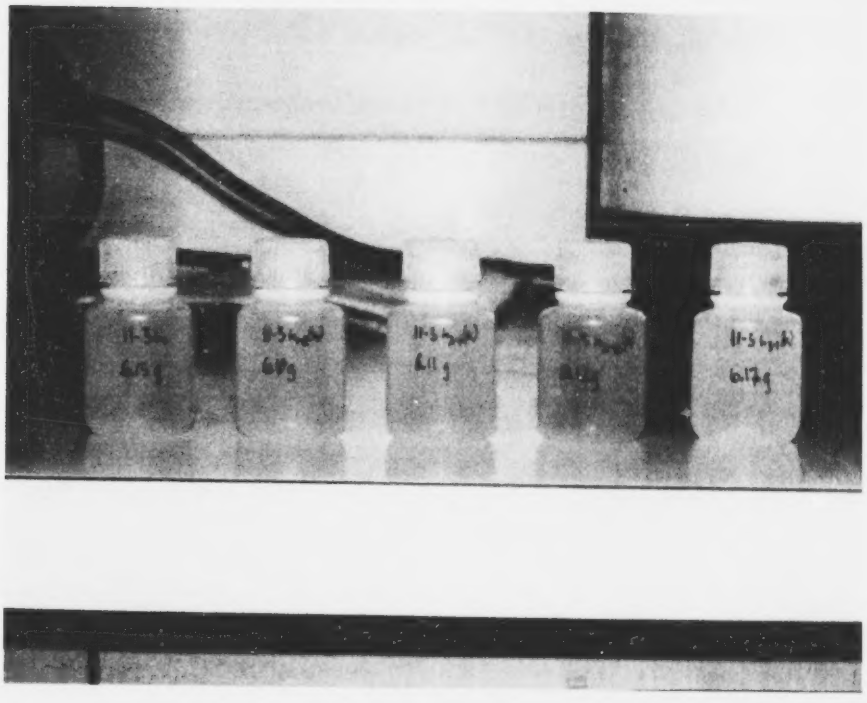

Figure 4.1.
Unfiltered porewater samples after collection from column 7-3. Distance from inlet at which sample was collected and concentrations are (left to right): 0.053 m, 330 μg/g; 0.104 m, 310 μg/g; 0.154 m, 230 μg/g; 0.205 m, 41 μg/g; 0.256 m, 3.8 μg/g. Note that reaction front fell between collection points for fourth and fifth samples.

predominant anion in solution, exceeded 11 +/- 2 mol/m^3, electrostatic repulsion should have been overcome by van der Waals attraction, thus leading to aggregation of ferric oxyhydroxide particles (Sposito, 1989, p. 201). However, the effect of surface charge should still have been sufficient to discourage chemical bonding between particles (Hsu and Ragone, 1972; Schwertmann and Taylor, 1989).

Following collision with the matrix, particle retention may have been promoted where surfaces were oppositely charged. At the values of pH observed in this study, calcite surfaces tended to be positively charged (pzc 10 +/- 1) and surfaces of quartz, which constituted the bulk of the porous medium, negatively charged (pzc 2.0 +/- 0.3) (Sposito, 1984, p. 84). Staining of quartz grains and the lack of staining of calcite grains observed in solid-phase samples provided evidence of the preferential electrostatic attraction of ferric oxyhydroxide to quartz (conceptualized in Figure 4.2b). Even though ferric oxyhydroxide halos appeared to form around calcite grains *in situ* during several experiments, armoring of calcite was not notable in scanning electron micrographs of solid-phase samples collected after experiment 1. These observations concur with those of Loeppert and Hossner (1984), who found that ferrihydrite tended to precipitate from $Fe(ClO_4)_3$-calcite suspensions as a result of reactions involving calcite dissolution products in solution, rather than at grain surfaces. Particle retention by mechanisms other than collision (e.g., straining due to size exclusion and sedimentation due to gravity) was probably minor, given the relatively low concentrations of particles larger than 0.05 μm (Hunt et al., 1987; Sharma and Yortsos, 1987).

At the reaction front, both the dissolution of calcite and the deposition of ferric oxyhydroxide decreased greatly. This change was due to the completion of hydrolysis, so that the visible limit represented a sharp chemical transition, confirming the operational definition of the reaction front. Still, based on Fe concentrations in effluent, porewater, and matrix solids, ferric oxyhydroxide deposition actually extended beyond the visible front, albeit at levels only a few μg/g above background. Calcite dissolution

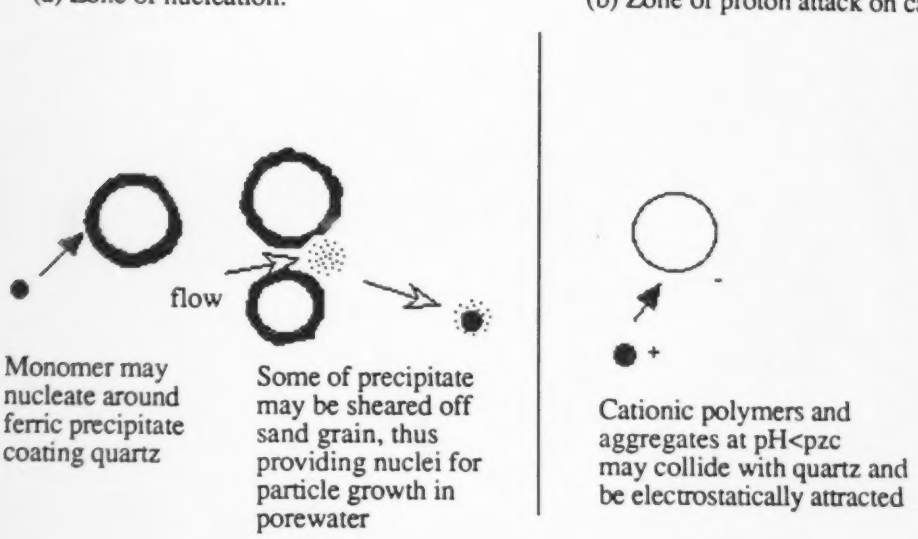
(a) Zone of nucleation:
(b) Zone of proton attack on calcite
flow
Monomer may nucleate around ferric precipitate coating quartz
Some of precipitate may be sheared off sand grain, thus providing nuclei for particle growth in porewater
Cationic polymers and aggregates at pH<pzc may collide with quartz and be electrostatically attracted

Figure 4.2.
Possible mechanisms of ferric particle growth and deposition along flowpath in (a) zone of nucleation and (b) zone of proton attack on calcite.

also continued beyond the front, as indicated by a gradual increase in Ca down-gradient and the fact that maximum Ca concentrations in effluent were consistently higher than concentrations measured at the front. Loeppert et al. (1984) attributed a gradual increase in pH beyond approximately 5 to 6 to the complete neutralization of partially-neutralized polymers, implying attack by H^+ on calcite. However, two lines of evidence suggest that dissolution occurred by a different mechanism. The first is simply the position of the front and the relative lack of Fe down-gradient, which would not have been evident in a batch study. Secondly, electrical conductivity should decline as H^+ is consumed, because the limiting molar conductivity of one H^+ ion is greater than the conductivities of one Ca^{2+} ion and one HCO_3^- ion combined (Castellan, 1983, pp. 778-779). Instead, electrical conductivity rose gradually from the minimum just ahead of the front. It is therefore probable, in keeping with the model of Plummer et al. (1978), that down-gradient dissolution occurred by the reaction of the uncharged species $H_2CO_3^o$ and/or H_2O with calcite.

With the migration of subsequent fluid packets, the mechanisms of reaction were open to change. Fe deposition profiles adjacent to the inlet, where Ca_s concentrations were low, indicate that ferric oxyhydroxide formed by a mechanism other than pH buffering where calcite had been depleted. As noted in Section 3.3.2, auto-polymerization was negligible in experiments 5 to 8, so that the continued accumulation of ferric oxyhydroxide adjacent to the inlet cannot be attributed to the filtration of polymers or particles from the influent solution. In porewater adjacent to the inlet, the decrease in pH and increase in electrical conductivity relative to influent was indicative of additional hydrolysis. The loss of more than 11% of the Fe in influent by a distance of 0.053 m suggests that polymerization was being catalyzed by predeposited ferric oxyhydroxide. Either nucleation around sheared particles and subsequent redeposition or nucleation on matrix surfaces (Figure 4.2a) is plausible. As noted in Section 1.4.2, Hsu (1972) found that the addition of polymer nuclei can induce hydrolysis and

polymerization in fresh $Fe(ClO_4)_3$ solution. However, the clarity of porewater adjacent to the inlet indicates that particle growth in suspension within this zone of nucleation was limited. The spatial relations between this zone, the zone of proton attack, and the zone of lessened calcite dissolution down-gradient from the reaction front are illustrated schematically in Figure 4.3.

4.1.2. Numerical modeling of geochemical speciation

For the influent solution and each sample of porewater, the speciation of Ca, Fe, and TIC was calculated using the program PHREEQE (Parkhurst et al., 1980, with an updated thermodynamic database compiled by J. Ball, U.S. Geological Survey, 1989). PHREEQE calculates solute activities, the formation of complexes and ion pairs, and the saturation state of the solution with respect to minerals of interest. Speciation in the influent solution was determined from the averages of the measured Fe (400 μg/g), pH (2.44), and TIC (0.755 μg/g) values. The molal concentration of ClO_4^-, which was not monitored, was taken as 2100 μg/g, or three times the average molal concentration of Fe in influent solution. The choice of this value for ClO_4^- was supported by the low charge balance error calculated for the influent solution, -0.000079%, which suggests that the impurity in the $Fe(ClO_4)_3$ salt (noted in Section 3.3.1) was simply water and not $HClO_4$. Because of its conservative nature, the concentration of ClO_4^- was considered to be constant throughout each column, and no complexation involving ClO_4^- species was allowed. Concentrations of metals other than Ca and Fe were assumed to be zero, while temperature was assumed to remain constant at 23°C.

The oxidation-reduction potential for input to the program was estimated from the theoretical relation for the pe of pure water in equilibrium with atmospheric oxygen as a function of pH:

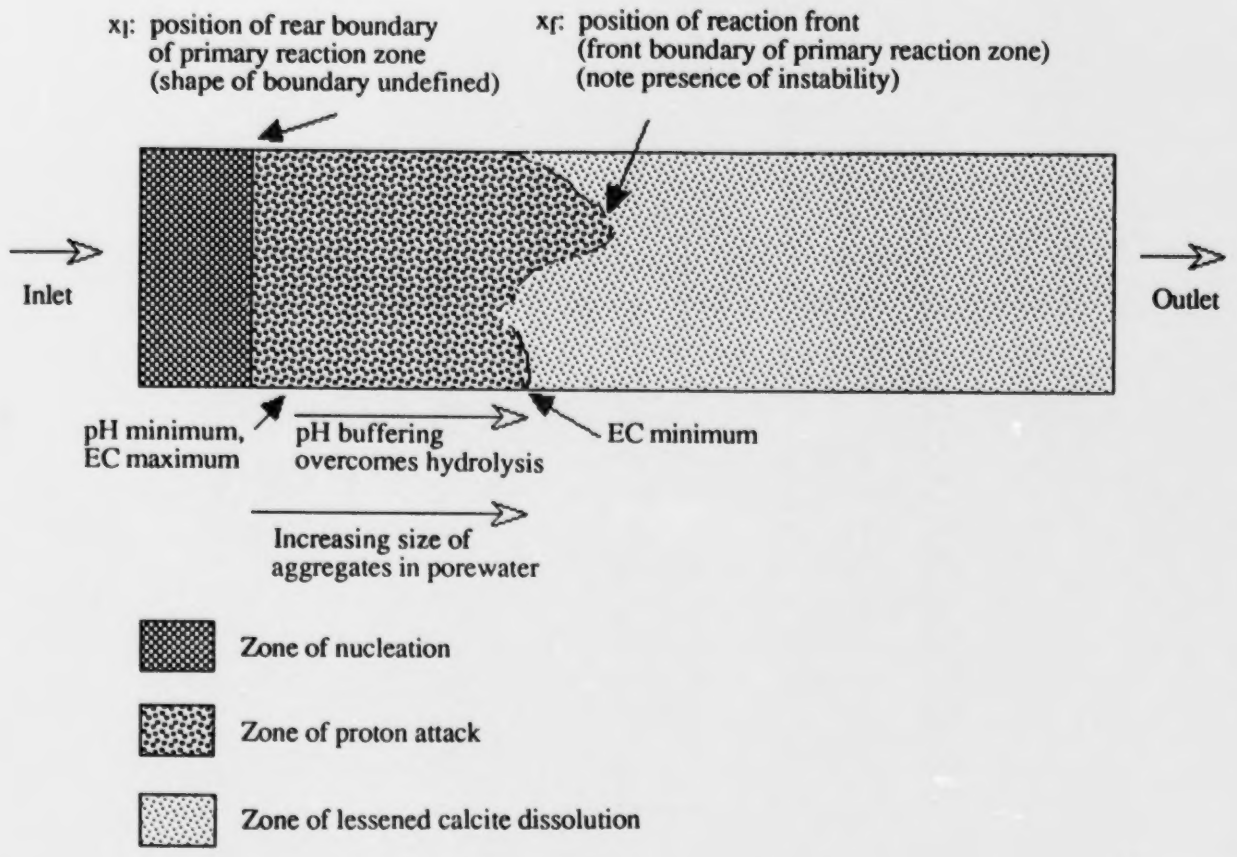

Figure 4.3. Conceptualization of reaction zonation along flowpath.

(4.1) $pe = 0.072 - 0.0035pH$

(after Garrels and Christ, 1965). The relatively short length of the flowpath, and/or the fact that manometers were open to the atmosphere (which could have permitted diffusion of dissolved oxygen into each column), should have helped to maintain oxidizing conditions. This supposition is supported by the mineralogy of the precipitate: ferrihydrite is formed under oxidizing conditions (Schwertmann and Taylor, 1989). Furthermore, Loeppert et al. (1984) observed high values of pe during the reaction of aerated 0.01 M $Fe(ClO_4)_3$ solution with calcite (R.H. Loeppert, Texas A&M University, personal communication).

Initial calculations were based on taking unfiltered concentrations of Fe and Ca in porewater as equivalent to dissolved concentrations and adjusting pH to achieve charge balance. pH was allowed to "float" because measurements had been made on samples exposed to the atmosphere for more than eight minutes, so that exsolution of CO_2 could have altered pH. The resulting saturation indices (defined as log (IAP/K_{sp}), where IAP is the ion activity product and K_{sp} is the solubility product constant for a particular mineral or gas) were greater than zero, indicating that the porewater down-gradient from the reaction front was supersaturated with respect to (that is, unable to dissolve more) calcite. It therefore seems likely that the charge balance errors, rather than being due entirely to errors in pH, results at least partly from errors in measurement of Ca, Fe, or TIC, or from non-zero values of trace constituents (such as Mg or Si) for which analyses were not conducted. Subsequent speciation calculations were therefore left unbalanced, leading to saturation indices less than zero for (or undersaturation with respect to) calcite all along the flowpath (shown for experiment 8 in Table 4.1 and Figure 4.4). The resulting charge imbalances are less than 0.42%, which in turn is less than the value of 5% cited as normally acceptable by Freeze and Cherry (1979, p. 97).

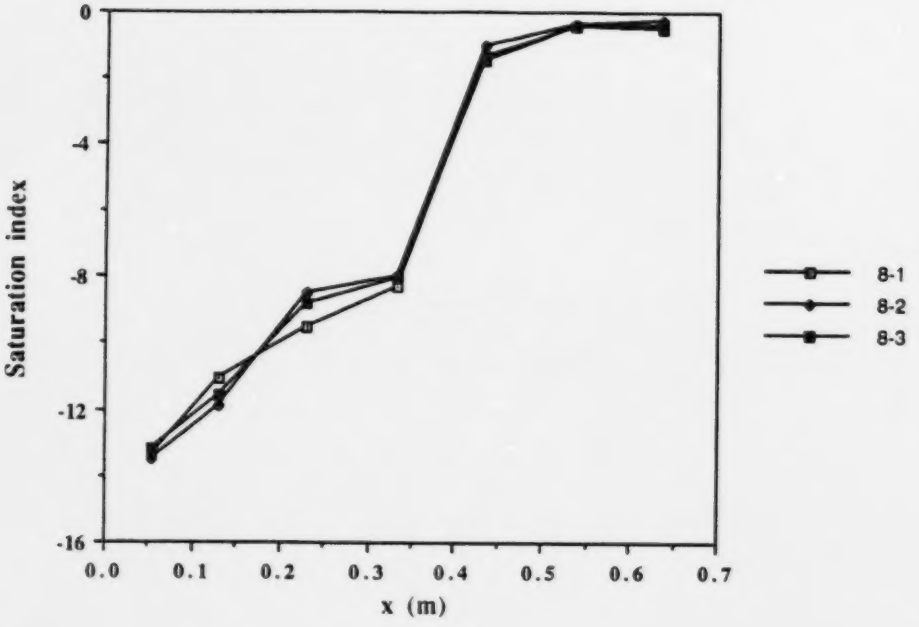

Figure 4.4. Saturation index with respect to calcite along flowpath at the end of experiment 8.

Table 4.1.
Values of saturation index with respect to calcite in porewater at the end of experiment 8.

x (m)	SI calcite, 8-1	SI calcite, 8-2	SI calcite, 8-3
0.053	-13	-13	-13
0.129	-11	-12	-12
0.230	-9.6	-8.5	-8.8
0.332	-8.3	-8.0	-8.0
0.434	-1.3	-1.0	-1.5
0.535	-0.43	-0.39	-0.43
0.637	-0.50	-0.28	-0.36

Speciation calculations indicate that the partial pressure of CO_2 in solution (P_{CO2}) increased with distance along the flowpath, peaking at the reaction front, then declined slightly toward the outlet, as shown for experiment 7 (Figure 4.5). Down-gradient from the reaction front, calcite dissolution probably occurred as a result of reaction with $H_2CO_3^o$, because the partial pressure of CO_2 exceeded 0.1 atm (Plummer et al., 1978). Because of calcite dissolution, calculated values of P_{CO2} in porewater (given for experiment 7 in Table 4.2) were in all cases greater than atmospheric ($10^{-3.5}$ atm). Therefore, at locations open to the atmosphere, a concentration gradient should have driven CO_2 out of solution (Herman and Lorah, 1987). Such degassing was evidenced by the lower concentrations of TIC in effluent relative to porewater. Alternatively, the gas bubbles observed within the columns may have formed when the concentration of CO_2 (aq) at the surface of a dissolving calcite grain exceeded the solubility of CO_2 in water (Compton and Daly, 1984), even though the bulk solution was undersaturated with respect to CO_2 (P_{CO2} of porewater less than 1 atm). Although there are other explanations for the origin of the gas *in situ* (e.g., exsolution of dissolved air, or generation of biogas by microbes, because the sand had not been sterilized (R. Mace, Bureau of Economic Geology, University of Texas, personal communication)), none seems as plausible as the generation of CO_2.

As noted in Sections 1.3.2 and 3.3.1, for the initial concentration of total Fe (0.0071 m) and initial pH of 2.44, the influent solution should have been supersaturated with respect to ferric oxyhydroxide. However, the saturation index for that mineral was -0.68 in influent solution and, as illustrated for experiment 8 (Figure 4.6, Table 4.3), only became greater than zero (indicating supersaturation) down-gradient from the reaction front, despite a systematic decline in Fe concentrations (indicating precipitation) along the flowpath. According to Flynn (1984), log K_{sp} for "amorphous ferric hydroxide" (written as $Fe(OH)_3$ (s)) ranges from -39.0 to -37.1, with the latter value, used in the thermodynamic database for PHREEQE, representing fresh precipitate.

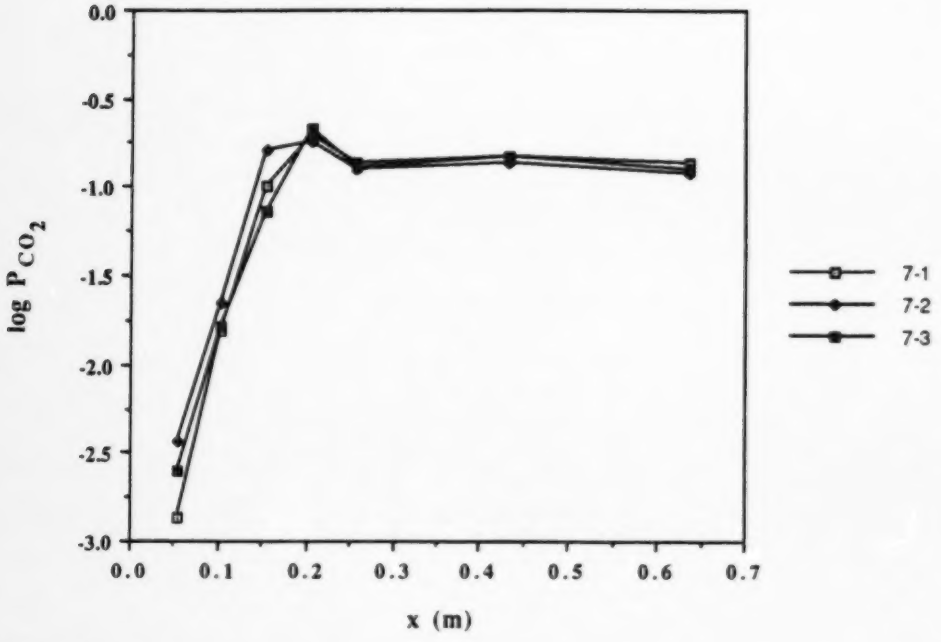

Figure 4.5.
Calculated partial pressure (in atm) of CO_2 in porewater along flowpath at the end of experiment 7.

Table 4.2. Values of log P_{CO_2} in porewater at the end of experiment 7.

x (m)	log PCO2, 7-1	log PCO2, 7-2	log PCO2, 7-3
0.053	-2.9	-2.4	-2.6
0.104	-1.8	-1.7	-1.8
0.154	-1.0	-0.79	-1.1
0.205	-0.70	-0.75	-0.68
0.256	-0.87	-0.90	-0.88
0.434	-0.82	-0.86	-0.83
0.637	-0.86	-0.92	-0.90

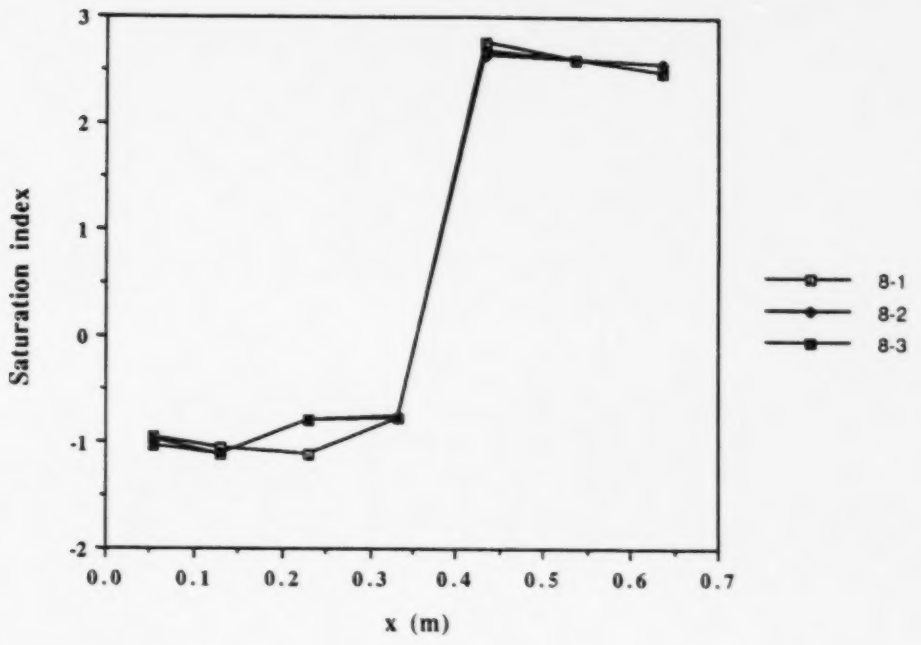

Figure 4.6.
Saturation index with respect to ferric oxyhydroxide along flowpath at the end of experiment 8; log K_{sp} = -37.1.

Table 4.3.
Values of saturation index with respect to ferric oxyhydroxide in porewater at the end of experiment 8; log K_{sp} = -37.1.

x (m)	SI 8-1	SI 8-2	SI 8-3
0.053	-0.95	-0.98	-1.0
0.129	-1.1	-1.1	-1.1
0.230	-1.1	-0.80	-0.80
0.332	-0.78	-0.76	-0.78
0.434	2.8	2.6	2.7
0.535	2.6	2.6	2.6
0.637	2.5	2.5	2.5

Therefore, calculations were subsequently conducted using an intermediate value of log K_{sp}, -38.3, determined by Grundl and Macalady (1989) for 12- to 200-hour-old precipitate. The change in the equilibrium constant, while not affecting calculations of the distribution of aqueous species, resulted in saturation indices greater than zero throughout the system (Figure 4.7, Table 4.4). While the finding that ferric oxyhydroxide can precipitate at pH < 2.3 is not new (e.g., cf. Flynn, 1984; Rege and Fogler, 1989), its potential importance should be emphasized: in field settings, coprecipitation of heavy metals such as Cd and Pb could occur. Minima in the plots of the saturation index coincided with minima in the profiles of pH and of ferric oxyhydroxide deposition, reflecting the fact that as $[H^+]$ increased, the ion activity product $[Fe^{3+}][OH^-]^3$ decreased. The applicability of the more negative value of log K_{sp} may reflect continued crystallization between the time of sample collection and of preservation. Another possible explanation is that the value of log K_{sp} in the PHREEQE database simply reflects poorer crystallinity under different experimental conditions.

Up-gradient from the reaction front, the majority of iron in solution consisted of the species Fe^{3+} and $Fe(OH)^{2+}$, with lesser amounts of $Fe(OH)_2^+$ and $Fe_2(OH)_2^{4+}$ (shown for column 8-1 in Figure 4.8 and Table 4.5). Even though ferric oxyhydroxide was precipitating, the simultaneous occurrence of hydrolysis meant that the relative abundances of different ferric species did not change greatly between the inlet and the reaction front. This continuity of speciation was evident both in the absence and the presence of calcite, notwithstanding the apparent difference in mechanisms of initiating ferric oxyhydroxide precipitation (i.e., nucleation around existing precipitate versus the promotion of polymerization by pH buffering). Across the reaction front, with the completion of hydrolysis, the concentrations of $Fe(OH)_3^o$ and $Fe(OH)_4^-$ increased by several orders of magnitude, while the concentration of $Fe(OH)_2^+$ remained relatively uniform and the concentrations of higher-valence ferric complexes decreased by several orders of magnitude.

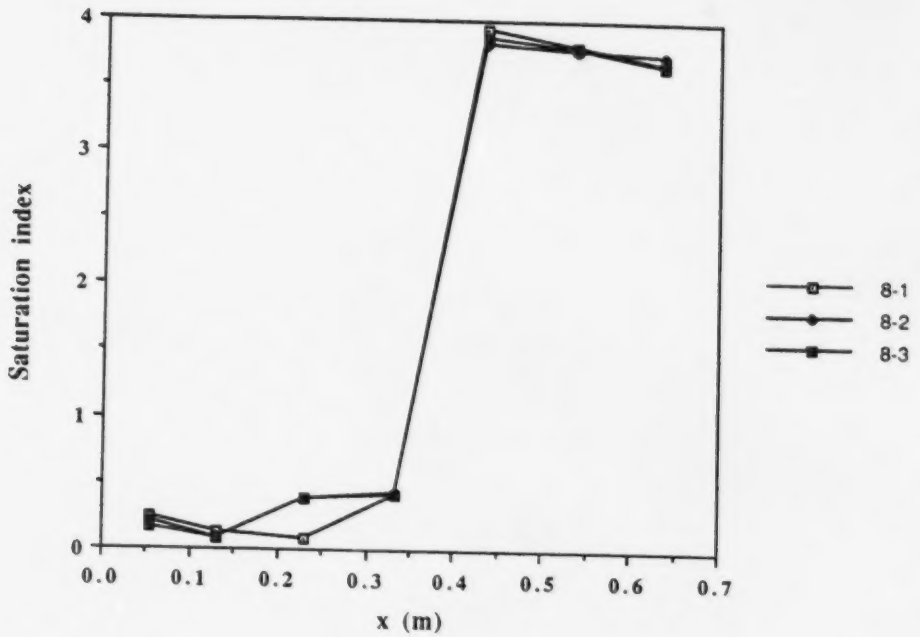

Figure 4.7.
Saturation index with respect to ferric oxyhydroxide along flowpath at the end of experiment 8; log K_{sp} = -38.3.

Table 4.4.
Values of saturation index with respect to ferric oxyhydroxide in porewater at the end of experiment 8; log K_{sp} = -38.3.

x (m)	SI 8-1	SI 8-2	SI 8-3
0.053	0.24	0.21	0.17
0.129	0.13	0.075	0.075
0.230	0.083	0.39	0.39
0.332	0.41	0.43	0.41
0.434	3.9	3.8	3.9
0.535	3.8	3.8	3.8
0.637	3.7	3.7	3.7

Table 4.5.
Speciation of ferric monomers and simple polymers in influent solution and porewater at the end of experiment, column 8-1: (a) Fe^{3+}; (b) $Fe(OH)^{2+}$; (c) $Fe(OH)_2^{+}$; (d) $Fe(OH)_3^{o}$; (e) $Fe(OH)_4^{-}$; (f) $Fe_2(OH)_2^{4+}$; (g) $Fe_3(OH)_4^{5+}$.

x (m)	(a)	(b)	(c)	(d)	(e)	(f)	(g)
0.000	-3.1	-2.9	-4.0	-8.5	-15	-4.4	-5.9
0.053	-3.1	-3.0	-4.2	-8.7	-15	-4.5	-6.2
0.129	-3.1	-3.0	-4.2	-8.9	-16	-4.6	-6.4
0.230	-3.1	-3.1	-4.3	-8.9	-16	-4.7	-6.5
0.332	-3.3	-3.1	-4.1	-8.6	-15	-4.7	-6.4
0.434	-9.2	-5.8	-3.7	-5.0	-8.5	-10	-12
0.535	-11	-7.0	-4.4	-5.2	-8.1	-13	-15
0.637	-11	-7.0	-4.4	-5.3	-8.3	-13	-15

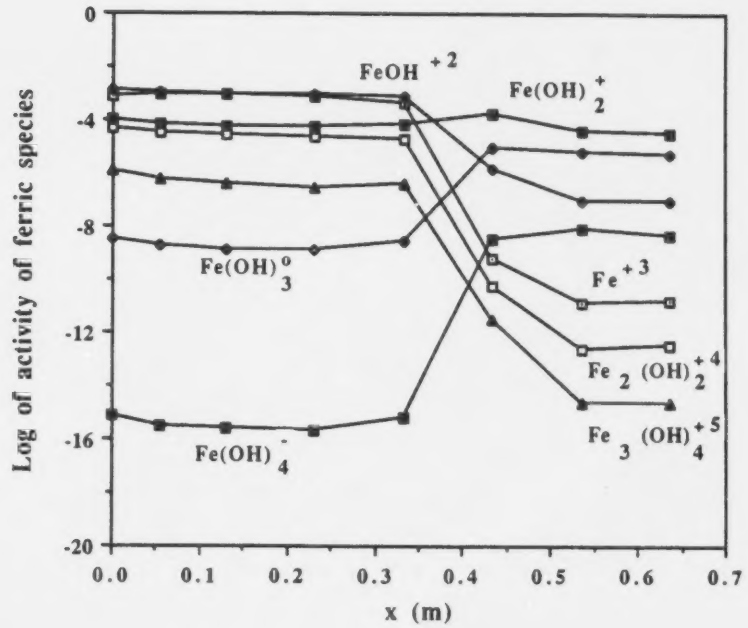

Figure 4.8.
Speciation of ferric monomers and simple polymers in influent solution and in porewater along flowpath at the end of experiment, column 8-1.

The discussion thus far has focused on concentration data from unfiltered porewater samples because of evidence that calcite may have precipitated during sampling (i.e., differences in Ca between unfiltered and filtered samples). However, as noted previously, some ferric oxyhydroxide may have been carried in suspension following precipitation, so additional simulations were conducted using filtered concentrations. As shown for column 7-1 (Figure 4.9, Table 4.6), the resulting trends in saturation indices for CO_2, calcite, and ferric oxyhydroxide are qualitatively similar to the trends obtained using unfiltered data. In particular, porewater down-gradient from the reaction front remained supersaturated with respect to ferric oxyhydroxide even at concentrations approaching the detection limit of iron (approximately 0.09 μg/g in this study). This result suggests that the distance ahead of the reaction front at which Fe became detectable in effluent (less than one meter) does not represent a physical limit on particulate transport, in keeping with the finding of Gschwend and Reynolds (1987) that iron phosphate colloids can be transported hundreds of meters in groundwater. Instead, continued precipitation along the flowpath most likely caused Fe concentrations in porewater to decrease below the detection limit.

4.1.3. Hydraulic changes

Various physical and chemical mechanisms operating in the porous medium were capable of altering permeability or hydraulic conductivity. Calcite dissolution may increase hydraulic conductivity, as indicated by the growth of fingers during the initial penetration of influent. However, values of hydraulic conductivity tended to decline behind the reaction front as experiments progressed. One possible cause was compaction due to settlement of overburden as calcite grains were removed. Stoichiometry indicates that one mole of ferrihydrite forms for every 7.5 moles of calcite consumed. Given a density for ferrihydrite of 3.96 Mg/m^3 (Schwertmann and Taylor,

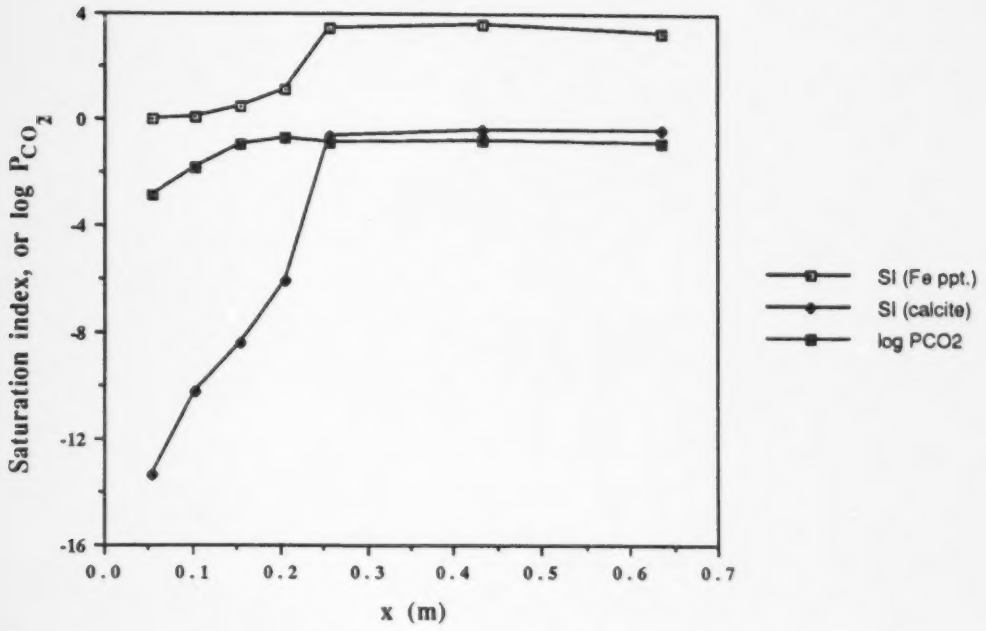

Figure 4.9.
Saturation indices of calcite and ferric oxyhydroxide and partial pressure of CO_2 along flowpath at the end of experiment, column 7-1; calculation based on concentrations of Fe and Ca in filtered porewater.

Table 4.6.
Values of saturation indices for calcite and ferric oxyhydroxide and values of log P_{CO_2} in porewater at the end of experiment, column 7-1.

x (m)	SI (Fe ppt.)	SI (calcite)	log PCO2
0.053	0.0008	-13	-2.9
0.104	0.041	-10	-1.8
0.154	0.52	-8.4	-1.0
0.205	1.1	-6.1	-0.70
0.256	3.4	-0.64	-0.87
0.434	3.6	-0.39	-0.82
0.637	3.3	-0.39	-0.86

1989), the volume of the reactive fraction decreased by 56.1%. However, calcite constituted a relatively small percentage of the total volume of each column, and no shrinkage in height was evident when columns were examined after freezing.

The deposition of solids and entrapment of gas remain as probable mechanisms for reducing hydraulic conductivity. Such reduction may have affected the subsequent migration of fluid packets by diverting flow locally or by forcing a reduction in the volumetric flow rate. The inflection in the frontal advance plots can be explained by diversion away from initial regions of preferred dissolution as ferric oxyhydroxide deposition or gas entrapment commenced (Sherwood, 1987). With flow being redirected across the entire width of the column, the no-flow boundary posed by the column wall should have forced the reactivation of plugged fingers. Although only six columns (1-1, 2-1, 2-3, 3-2, 4-2, and 5-2) appear to have had sustained declines in hydraulic conductivity during the first 14 hr, plugging sufficient to divert flow at the pore scale might not have caused a measurable decrease in K/K_0. As an alternative to diversion, the flow rate may decline, as observed in experiments 3 and 4. These declines may be common in natural systems, which are often driven by a constant hydraulic gradient rather than a constant flow rate (Hunt et al., 1987).

The degree of permeability reduction is a function of both mechanical strength and geometry. Taylor and Jaffe′ (1990a, Figure 7) have shown that permeability declines with biofilm growth in sand columns to a steady-state limit of 5×10^{-4} times the original value. In comparison, for the experiments containing sieved calcite, hydraulic conductivity values adjacent to the inlet appear to have declined with increasing Fe_s toward a limiting value of approximately 0.02 to 0.1 times the original value (Figure 4.10). Concentrations continued to increase beyond the limit at which permeability (or hydraulic conductivity) leveled off for both biofilm and Fe_s. The limiting value probably corresponded to a critical value of velocity at which the width of the pore throat was maintained by shear stresses (Hunt et al., 1987; Taylor and Jaffe′, 1990a). Warner

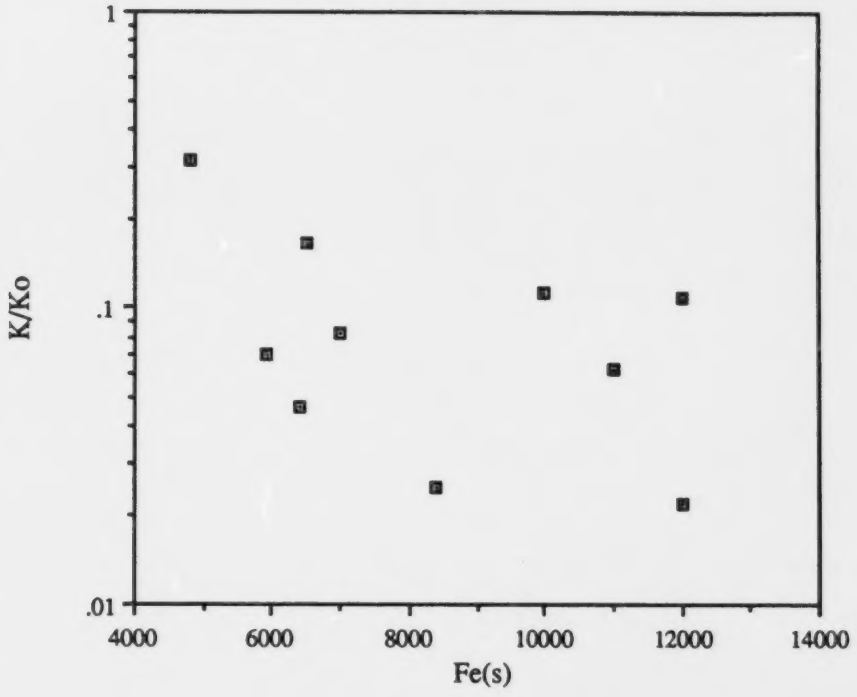

Figure 4.10
Final normalized hydraulic conductivity values adjacent to inlet as a function of solid-phase Fe (μg/g) (s), experiments 5 to 8.

(1966) found that the precipitation of ferric oxyhydroxide which occurred as NaOH solution displaced $FeCl_3$ solution from an Ottawa sand column caused permeability to decline by a factor of only 0.25. The greater effectiveness of biofilm in reducing permeability was probably due to a higher shear strength, since the van der Waals force promoting attraction of ferric oxyhydroxide particles to the framework is relatively weak (Hunt et al., 1987).

For the experiments containing unsieved calcite, the maximum observed reduction in hydraulic conductivity was approximately an order of magnitude beyond that for the unsieved case. Declines in hydraulic conductivity were greater for column 2-3 than for experiment 8 and greater for experiment 3 than for experiment 6, even though the masses of calcite and the flow rates were comparable for each pair of trials. Actually, the amounts of ferric oxyhydroxide which precipitated should have been less for the unsieved experiments, because large calcite grains remained at the end, than for the corresponding sieved experiments, in which calcite was largely removed adjacent to the inlet. Straining of calcite fines in the unsieved experiments would not have accounted for the discrepancy in hydraulic conductivity values, because head measurements were relatively constant prior to the onset of reaction in 1, 3 and 4. By elimination, relatively rapid generation of gas resulting from the dissolution of the fine fraction was probably responsible for the discrepancy. The difference in plugging behavior (conceptualized in Figure 4.11) can be explained on geometric grounds. As CO_2 bubbles are entrapped, they may coalesce so that they effectively occlude pore throats, in contrast to the mere constriction of pore throats by deposited particles. With occlusion, flow should have been diverted more completely and a larger increase in hydraulic head should have resulted.

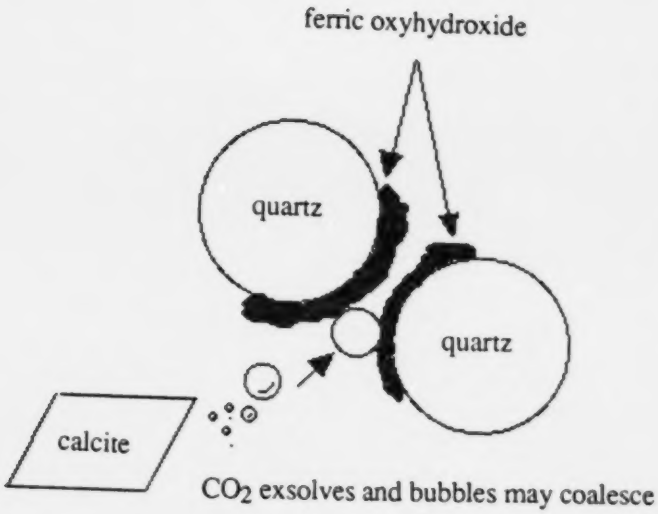

Figure 4.11.
Conceptualization of pore-throat constriction by ferric oxyhydroxide and occlusion by CO_2 (g).

4.2. Behavior of the System under Different Initial Conditions

4.2.1. Trends in frontal or zonal length and velocity

The determination of frontal velocity (v_f) values in this study has been based on various approximations, including one-dimensional flow and a constant rate of frontal advance, which warrant further discussion. One-dimensionality was assumed based on the small diameter of the column relative to its length; the length-to-diameter ratio of 10:1 is approximately the same as that used by Taylor and Jaffe′ (1990a), who also assumed one-dimensionality in studying biofilm growth. Although fingering illustrated the multidimensionality of the flow regime along the front, the general smoothness of porewater concentration profiles, which indicated little variability transverse to flow, supports treating the column as a whole as one-dimensional. The approximation of a constant rate of frontal advance is based on the relative linearity of the frontal advance plots after initial penetration of influent solution (and prior to failure or a reduction in flow rates in experiments 1 to 4).

This study has identified the reaction front as the visible limit of ferric oxyhydroxide deposition, coinciding with the neutralization of acidity generated by hydrolysis. In contrast, for a generic dissolution reaction of first-order rate (akin to calcite dissolution, but with a single component), Lichtner (1988) considered the front as the boundary behind which all of the soluble mineral had been removed. That boundary apparently did not materialize during experiments 1 to 4 because of the persistence of large calcite grains, but it occurred late in experiments 5 to 8 where Ca_s went to zero. Taken together, the forward, visible front and the rear boundary defined by Lichtner (1988) delimited the zone of calcite dissolution by proton attack.

One can visualize the rear boundary as detaching from the inlet when all calcite has been consumed. The time at which this detachment occurs, the delay time, has been defined by Lichtner (1988) as

$$(4.2)\quad \tau_0 = 3V_i/(VkA_r(C_{eq} - C_0)),$$

where V_i is the initial volume of the soluble mineral (M/L^3); V is the molar volume of that mineral (M/L^3); k is the reaction rate constant (L/t); A_r is the reactive surface area (L^2/L^3); and C_{eq} and C_0 are the equilibrium and initial concentrations (M/L^3), respectively, of a solute species reacting with the mineral. The solution is presumed to be sufficiently dilute that solute activities can be taken as concentrations. The factor of three accounts for surface area varying over time with a geometric dependence upon the volume fraction. The delay time should have been approximately constant for experiments 5 to 8, because A_r varied with V_i between experiments and τ_0 is not a function of porewater velocity. However, calculating τ_0 is complicated by the difficulty in quantifying A_r.

There arises the question of whether the rear boundary of the reaction zone migrated at the same rate as observed for the forward boundary. Lund and Fogler (1976) and Lichtner (1988) found that, where advective transport overwhelms diffusive and dispersive transport, the velocity of the rear boundary is a function of the amount of mass capable of being transferred and the porewater velocity (v). These variables are encapsulated in another dimensionless group (besides the Peclet and Damkohler numbers), the constant of proportionality between the porewater velocity and v_l, the boundary velocity after detachment. Lund and Fogler (1976) have defined this group in terms of the acid capacity (Ac), which is the ratio of the concentration of acid present in a unit volume of porous medium to that necessary to dissolve all the soluble mineral in

the volume. Lichtner (1988) has defined the same group in terms of the distribution coefficient (K_d), analogous to an ion-exchange reaction, so that

$$(4.3)\ v_l = v/(1 + K_d) = v(Ac/(1 + Ac))$$

$$(4.4)\ K_d = V_f/(Vn(C_{eq} - C_0)),$$

where n is the porosity (L^3/L^3).

In strict terms, equations 4.3 and 4.4 apply where the reactive surface area and permeability can be considered constant over time (Lichtner, 1988). However, Lichtner found that, for the case of surface area changing over time, the velocity of the boundary declines to the value obtained if surface area were constant. Likewise, where solute mass is transported by advection and dispersion, the boundary velocity declines toward the advective-dominated value. The approximation of an advective-dominated system inherent in Lund and Fogler (1976) is based on the work of Lund et al. (1976), who tracked acid dissolution fronts through sandstone cores. Their porewater velocities (0.12 to 0.16 m/hr) are similar to those in the current study (0.067 to 0.20 m/hr). The apparent lack of tailing for the breakthrough curves here suggests that, at least initially, dispersion was minimal. Furthermore, although Taylor and Jaffe' (1990b) have noted that pore plugging by biofilm can result in dispersive transport overwhelming advective transport in sand columns, the reduction in hydraulic conductivity in the current study was much less severe.

Values of v_l have been calculated by taking (C_{eq} - C_0) as the maximum value of Ca^{2+} measured in effluent during experiments 5 to 8 (600 μg/g, or 0.0150 mol/kg) (Table 4.7). The values of v_l based on Ca^{2+} for experiments 5 to 8 are remarkably similar to the values of v_f obtained by least-squares fits to the frontal advance plots. The greatest deviation occurs for column 7-2, with v_l overesti.nating v_f by 12%. The

Table 4.7.
Values of frontal velocity v_f (determined by least-squares linear fits to observed post-plateau data) and of rear-boundary velocity v_l (calculated on the basis of a distribution coefficient as formulated by Lichtner (1988)).

Column #	vf (m/hr)	vl (Ca2+)	vl (H+)
1-2	0.00016	0.00013	0.0000309
2-2	0.00076	0.00057	0.000138
2-3	0.0028	0.0017	0.000410
3-1	0.0011	0.00067	0.000162
3-2	0.00084	0.00064	0.000155
3-3	0.00079	0.00062	0.000150
5-1	0.0016	0.0014	0.000345
5-2	0.0015	0.0014	0.000334
5-3	0.0013	0.0014	0.000341
6-1	0.00070	0.00072	0.000177
6-2	0.00072	0.00072	0.000176
6-3	0.00074	0.00067	0.000164
7-1	0.0014	0.0014	0.000338
7-2	0.0012	0.0013	0.000331
7-3	0.0013	0.0014	0.000333
8-1	0.0027	0.0029	0.000722
8-2	0.0027	0.0029	0.000714
8-3	0.0029	0.0028	0.000685

similarity may be simply coincidental, though, because values of v_l calculated for experiments prior to 5 underestimate v_f by as much as 39%. More importantly, the dissolution of calcite may not be first-order (as assumed in equation 4.4) with respect to Ca^{2+} (Plummer and Wigley, 1976). Therefore, values of v_l have been recalculated by taking the concentration gradient as the difference between $[H^+]$ in influent solution and in effluent (0.00363), because the first term of the PWP equation for calcite dissolution (equation 1.1) is linear with respect to H^+ (Plummer et al., 1978). These values of v_l (Table 4.7) range from 0.15 to 0.28 times the corresponding values of v_f.

Given that Lichtner (1988) simulated boundary propagation over time scales of 10^7 to 10^9 seconds, the reaction fronts in this study might have gradually decelerated further to velocities less than the fit values of v_f. No such prolonged deceleration, though, was evident over the 22-day (1.9×10^6-second) lifetime of column 1-2. One should note that the pH decline due to hydrolysis associated with nucleation behind the calcite dissolution zone might eventually have caused v_l to decline further than has been calculated. The values of v_l calculated for experiments 1 to 4 are actually projected values, because the complete dissolution of calcite did not occur. Because of the inability to observe detachment, the calculated values of v_l for experiments 5 to 8 could not be corroborated by visual tracking. However, the solid-phase Ca profiles (Figure 3.26) have confirmed that the length of the region from which calcite has been removed increases with the initial ratio of calcite volume to porewater velocity.

The deceleration of the rear boundary toward the limit of v_l appears analogous to the deceleration of the reaction front toward the value of v_f. It is possible, as noted by Lichtner (1988) for the rear boundary, that the reaction front slowed as dispersive transport became overwhelmed by advective transport, or as the surface area of calcite evolved with dissolution. Because the initial grain-size distributions differed in the cases of sieved and unsieved calcite, the corresponding distributions of surface area presumably evolved differently, although changes in surface area were not monitored.

The fact that plots of v_f versus Da_n overlapped for the two cases (Figure 3.5) is consistent with the observation by Lichtner (1988) that v_l is independent of surface-area evolution. It is also possible, as noted above, that the front decelerated due to diversion associated with pore plugging, which was not considered by Lichtner (1988).

The velocity of the reaction front has been defined here as equivalent to the rate of growth of the reaction zone. The dependence of v_f upon Da_n is in keeping with the findings of Lund and Fogler (1976) and Bahr (1990) that the length of the reaction zone depends upon the Damkohler number. Because the surface area was a function of the volume of calcite, varying Da_n (by varying the initial A_r) should have had the same effect on v_f that varying K_d (by varying V_i) had on v_l, though the values of v_f and v_l should not necessarily have been identical. Comparing column 1-2 with column 2-3 (end-members for the unsieved experiments), one observes that a decrease in Da_n by a factor of 15.6 was sufficient to lengthen the reaction zone from very compact to very diffuse. Similarly, porewater and solid-phase concentration profiles became less steep with decreasing Da_n. Local equilibrium was not attained, even at the highest value of Da_n, because a jump discontinuity in concentrations (i.e., a shock wave) was not observed at the column scale. However, in keeping with Steefel and Lasaga (1990), the transition would have been relatively sharp if viewed at a larger scale.

The divergence from local equilibrium and the variability of v_f with changes in surface area indicate that the system was not strictly transport-controlled. Under transport control, the length of instabilities (i.e., fingers) is relatively insensitive to the rate of reaction. The decrease in the number of instabilities and the increase in their spacing with decreasing Da_n was reflective of surface control (after Sherwood, 1987, and Ortoleva et al., 1987). The tendency, though, for finger lengths to increase with decreasing Da_n indicates conditions which were more transport- than surface-controlled (Steefel and Lasaga, 1990, Figure 6). At intermediate values of Da_n, the propagation of multiple fingers is promoted (as noted by Steefel and Lasaga (1990)), although the

persistence of fingers may also be aided by diversion and reactivation associated with pore plugging. Overall, a mixed-control regime was evident for calcite dissolution with ferric oxyhydroxide precipitation in sands. This finding extends the results of Loeppert and Hossner (1984) from batch studies to more realistic conditions of laminar flow through porous media.

The trend in the saturation length for calcite is analogous to the zonal length and porewater concentration trends. As surface control is approached, the distance along the flowpath at which a fluid packet attains equilibrium with calcite is inversely proportional to the Damkohler number. This relationship has been derived by Palciauskas and Domenico (1976) for flow through carbonate rocks, and demonstrated experimentally for the flow of CO_2-charged water through calcareous sand columns by Schulz (1988). Viewed another way, at a fixed distance where not all calcite has been dissolved, the concentration of Ca should increase as Da_n increases. This behavior is confirmed for the current study by Ca trends in porewater.

Concentration profiles in effluent, in contrast to concentration profiles in porewater, were not clearly dependent on Da_n. Profiles for Ca and, to some extent, pH and TIC in effluent appeared to depend upon the flow rate but not the surface area, for reasons which are unclear. However, the differences among the profiles for each of these parameters are slight, reflecting only the differing amounts of calcite dissolved down-gradient from the reaction front in each column. The concentration of Fe in effluent was more indicative of the proximity of the reaction front to the outlet, and thus was more dependent upon Da_n.

4.2.2. Limitations of the Damkohler number

Although the relationship of the initial Damkohler number to frontal and zonal behavior in this system is evident, there were circumstances in which Da_n broke down

as a basis for comparison between experiments. For relatively uniform initial grain size distributions and nearly identical values of Da_n, concentration profiles may not coincide, as shown for Ca_s concentrations in experiments 5 and 7 (Figure 4.12). The greater amount of calcite remaining, and the lesser amount of ferric oxyhydroxide precipitated, in the middle of the reaction zones for experiment 7 can be explained in several different ways by the difference in flow rates. The increased porewater velocity for experiment 5 could have decreased the thickness of the diffusion boundary layer adjacent to each calcite grain. In a system which is at least partly transport-controlled, a thinning of the diffusion boundary layer increases the rate of dissolution. In examining the data of Weyl (1958) for the dissolution of granular calcite packs, Palciauskas and Domenico (1976) concluded that the dependence of the boundary layer thickness on velocity is weak under laminar flow conditions. The difference in solid-phase concentrations may also have resulted from the greater initial penetration of influent at the higher flow rates of experiment 5. The profiles for experiment 5 were displaced down-gradient by approximately 0.020 m, which is similar to the difference in penetration lengths.

The ability of the Damkohler number to characterize hydraulic changes is problematic. Rege and Fogler (1989) have shown that as the initial flow rate increases, or as the initial Damkohler number decreases, ferric oxyhydroxide is less effective in reducing the permeability of limestone. Here, hydraulic conductivity reductions became more severe as the flow rate increased. The difference in flow rate dependence for plugging of limestone versus calcareous sand can be attributed to the occurrence of wormholing. In a rigid, uniformly calcareous matrix, the precipitate should accumulate at the tips of fingers, rather than along pore throats en route, which are prone to widening by dissolution. As fingers are abandoned, flow is channeled into the remaining clear pores at increased velocity, which facilitates dissolution and pore growth and hinders deposition. Soon thereafter, a "wormhole" breaks through to the down-gradient boundary, and the pressure drop decreases.

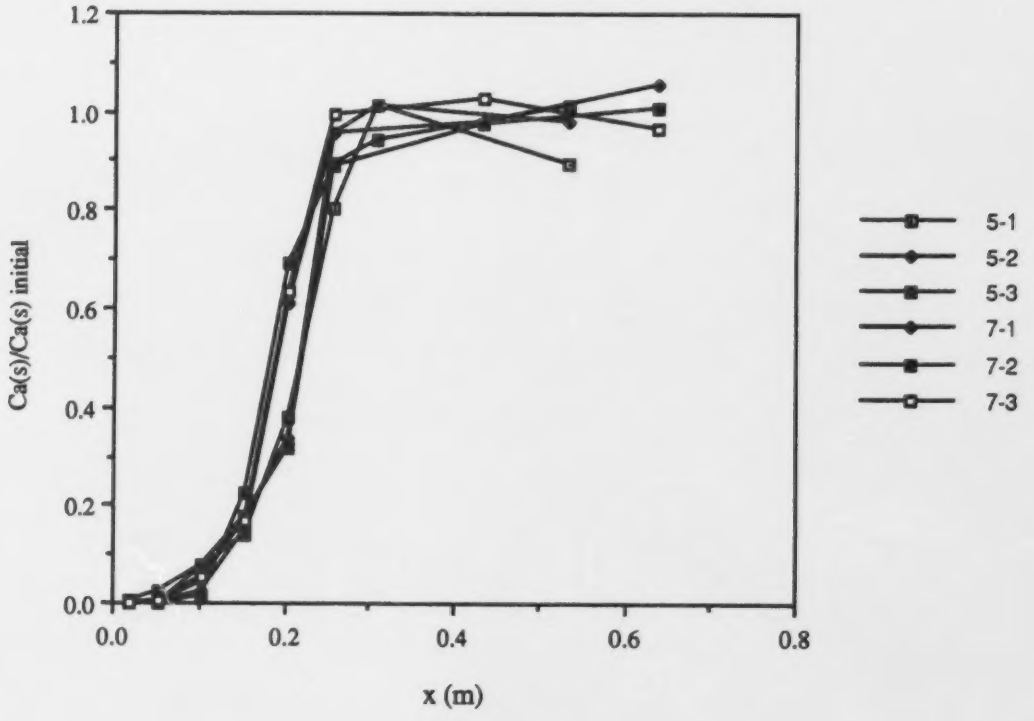

Figure 4.12.
Normalized solid-phase Ca concentration profiles after experiments 5 and 7.

Because of the relatively inert quartzitic matrix, wormholing should not have occurred in the sand (Rege et al., 1991). Rather, the greater number of pore volumes at an increased initial flow rate simply would have hastened the removal of calcite and the deposition of ferric oxyhydroxide along pore throats. Thus, as indicated in Figure 4.13, Fe_s was higher, and the hydraulic conductivity thereby lower, at a given distance along the flowpath as the initial flow rate increased between experiments. In addition, by simulating overburden pressures, Rege and Fogler (1989) did not allow the generation of gas, thus avoiding the sort of plugging seen in sand containing unsieved calcite. The rapidity of plugging in experiment 2 may have resulted from increased dissolution of calcite fines at high flow rates, followed by rapid exsolution of CO_2 (g), as indicated by the presence of coherent gas fronts.

The hydraulic conductivity of the sand was also reduced as the initial amount of calcite increased. The Damkohler number accounts for the resulting change in surface area, but not in the volumetric percentage of calcite, which controls the mass of ferric oxyhydroxide precipitated. To the extent that increasing the surface area, and thereby the rate of reaction, may have increased the solid-phase concentration of Fe or the tendency for degassing, reductions in hydraulic conductivity could have resulted from an increase in the initial Damkohler number as well as a decrease (at high initial flow rate). Regardless of Da_n, in the absence of significant plugging by gas, one would expect a uniform lower bound on hydraulic conductivity as nucleation drives Fe_s toward a maximum value.

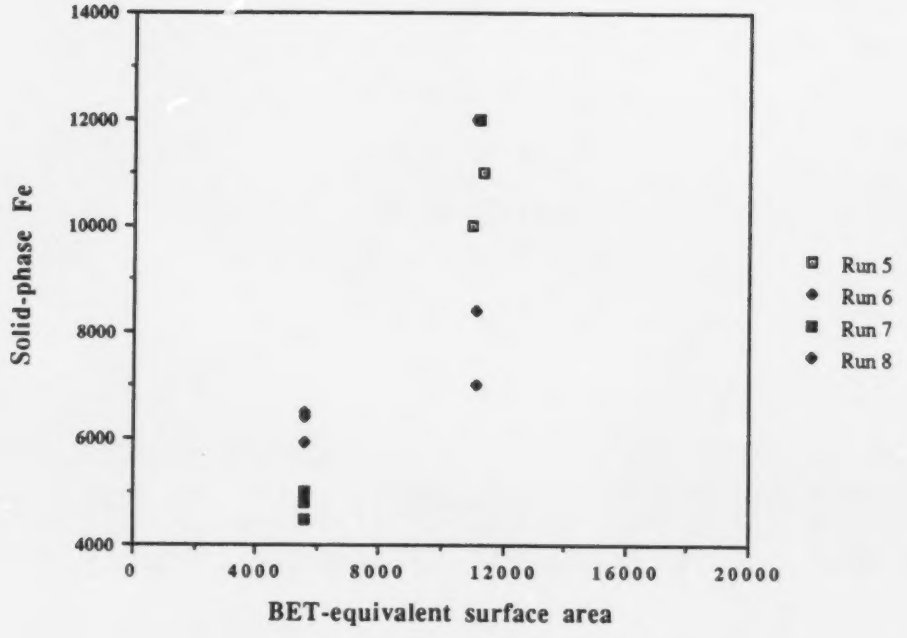

Figure 4.13.
Final solid-phase Fe concentrations (μg/g) (s) adjacent to inlet as a function of BET-equivalent surface area (m^2/m^3), experiments 5 to 8.

5. SUMMARY AND CONCLUSIONS

This work has examined the coupled mechanisms causing geochemical and hydraulic changes in an idealized yet generally relevant sedimentary environment, that of ferric solutions flowing through calcareous sands. These mechanisms include dissolution, precipitation, permeability enhancement and reduction, the generation of gas, and possibly colloidal transport. In particular, the study has addressed how the propagation of the reaction front and the growth of instabilities along the front vary with changes in the initial reaction rate (as expressed through the reactive surface area of calcite) or the initial rate of mass transport (as expressed through the volumetric flow rate). Previous studies of unstable reaction fronts in aquifers and petroleum reservoir rocks (e.g., Steefel and Lasaga, 1990) have been largely numerical and largely focused on the coupling between fluid flow, dissolution, and permeability enhancement. Those studies have indicated that the perturbation of the reaction front can depend upon the balance between reaction and advection, as expressed in the Damkohler number, or between advection and dispersion, expressed in the Peclet number.

The major findings of this study can be summarized as follows:

1. The deposition of ferric oxyhydroxide peaks at, but is not restricted to, the visible reaction front, where the neutralization of acidity generated by hydrolysis of dissolved iron is completed. Simultaneously, the concentration of ferric oxyhydroxide particles > 50 nm in porewater increases toward the front, which suggests (but, due to complications associated with sampling, does not prove) that some of the precipitate aggregates and is transported in suspension. Even beyond the visible front, calcite dissolution and ferric oxyhydroxide precipitation continue gradually.

2. Up-gradient from the front, where all calcite has been removed from the porous medium, ferric oxyhydroxide precipitation continues due to nucleation around older precipitate. Because of associated hydrolysis and lack of buffering capacity,

precipitation occurs at a pH less than the influent pH. Speciation modeling indicates that, regardless of whether precipitation occurs by nucleation or as a result of pH buffering, the relative abundances of different ferric species do not change greatly prior to reaching the front.

3. In the absence of significant gas generation, the value of hydraulic conductivity following ferric oxyhydroxide precipitation may be as low as 0.02 to 0.1 times the initial value prior to reaction. Where gas generation also becomes significant, the resulting combined reduction in hydraulic conductivity may be at least an order of magnitude greater.

4. After propagating at the porewater velocity during an initial period of minutes to hours, the reaction front tends to decelerate. This transition may reflect surface area evolution, dispersive transport being overwhelmed by advective transport, or diversion of flow away from initial regions of preferred dissolution as ferric oxyhydroxide deposition and/or gas entrapment commences. The front subsequently propagates at a relatively uniform velocity less than the original porewater velocity; this final frontal velocity does not appear to be affected by differences in surface area evolution which would result from different initial grain-size distributions.

5. The velocity of the reaction front, or the length of the reaction zone (the zone of hydrolysis and buffering in this system), is inversely proportional to the initial value of the Damkohler number. The observed values of frontal velocity are similar to or greater than velocities calculated for the rear boundary of the reaction zone. Future experiments could compare the frontal velocity, which should depend upon the reactive surface area, with the rear-boundary velocity, which is supposed to depend upon the volumetric percentage of the dissolving mineral, by varying the initial surface area and initial volumetric percentage of calcite separately.

6. The size of instabilities (or fingers) along the reaction front is proportional, and the number of instabilities inversely proportional, to the initial Damkohler number.

Therefore, based on previous studies of fingering, the chemical system can be considered a mixed-control regime, in which reaction progress depends both on the rate of reaction and the rate of fluid flow.

7. The initial Damkohler number is inadequate to describe the timing and magnitude of permeability changes in this system. The normalized concentration of ferric oxyhydroxide increases, and the hydraulic conductivity decreases, both with an increase in the initial surface area of calcite and with an increase in the initial rate of flow. This dependence upon the flow rate is opposite to that reported for the flow of acidic, ferric solution through limestone. In addition, gas generation seems to be promoted as the flow rate increases. Regardless of the initial Damkohler number, nucleation should determine the ultimate concentration of ferric oxyhydroxide and, in the absence of significant plugging by gas, the lower limit of hydraulic conductivity.

8. The recent concern among contaminant hydrogeologists about pre-existing physical (e.g., Sudicky, 1986) and chemical (e.g., Barber, 1987) heterogeneities in porous media should extend to self-organizational heterogeneities resulting from reaction coupled to fluid transport. Future work in this area could examine the role of pre-existing heterogeneities, such as depositional structures, in amplifying or repressing geochemical and hydraulic evolution in sediments. Column and other physical analog studies are well-suited for such work, in comparison with numerical models, which often idealize small-scale physical and chemical processes.

REFERENCES

Bahr, J.M., Kinetically influenced terms for solute transport affected by heterogeneous and homogeneous classical reactions, *Water Resour. Res., 26*, 21-34, 1990.

Barber, L.B., II, Influence of geochemical heterogeneity in a sand and gravel aquifer on the transport of nonionic organic solutes: methods of sediment characterization, in *U.S. Geological Survey Program on Toxic Waste--Ground-Water Contamination: Proceedings of the third technical meeting, Pensacola, Florida, March 23-27, 1987*, edited by B.J. Franks, *U.S. Geol. Surv. Open-File Rep. 87-109*, B-45-B-51, 1987.

Blatt, H., *Sedimentary Petrology*, W.H. Freeman, San Francisco, 1982.

Blowes, D.W., E.J. Reardon, J.L. Jambor, and J.A. Cherry, The formation and potential importance of cemented layers in inactive sulfide mine tailings, *Geochim. Cosmochim. Acta*, 55, 965-978, 1991.

Byrne, R.H., and D.R. Kester, Solubility of hydrous ferric oxide and iron speciation in seawater, *Mar. Chem.*, 4, 255-274, 1976.

Castellan, G.W., *Physical Chemistry*, 3rd ed., Addison-Wesley, Reading, Mass., 1983.

Catto, N.R., and Quaternary Research Group, Univ. of Alberta, *Geology 482 Field and Laboratory Manual*, 1989.

Cherry, J.A., R.W. Gillham, and J.F. Barker, Contaminants in groundwater: Chemical processes, in *Studies in Geophysics, Groundwater Contamination*, edited by the National Research Council Geophysics Committee, pp. 46-64, National Academy Press, Washington, D.C., 1984.

Compton, R.G., and P.J. Daly, The dissolution kinetics of Iceland spar single crystals, *J. Coll. Interf. Sci.*, 101, 159-166, 1984.

Compton, R.G., K.L. Pritchard, and P.R. Unwin, The direct measurement of dissolution kinetics at the calcite/water interface, *J. Chem. Soc., Chem. Commun.*, 4, 249-251, 1989.

Dept. of Soil Science, Univ. of Alberta, *Soil Science 415 Laboratory Manual*, 1987.

Dobrovolsky, E.V., Physico-chemical mechanisms of weathering processes and corresponding models of dynamics of mineral zonality evolution, *Chem. Geol.*, 60, 89-94, 1987.

Domenico, P.A., and F.W. Schwartz, *Physical and Chemical Hydrogeology*, John Wiley & Sons, New York, 1990.

Dreybrodt, W., *Processes in Karst Systems, Physics, Chemistry, and Geology, Springer Series in Physical Environment, 4*, Springer-Verlag, Berlin, 1988.

Ferguson, J., R.V. Burne, and L.A. Chambers, Iron mineralization of peritidal carbonate sediments by continental groundwaters, Fisherman Bay, South

Australia, *Sed. Geol.*, 34, 41-57, 1983.

Ferret, J., R. Gout, Y. Kihn, and J. Sevely, The influence of grinding on the dissolution kinetics of calcite, *Phys. Chem. Min.*, 15, 163-170, 1987.

Flynn, C.M., Jr., Hydrolysis of inorganic iron(III) salts, *Chem. Rev.*, 84, 31-41, 1984.

Freeze, R.A., and J.A. Cherry, *Groundwater*, Prentice-Hall, Englewood Cliffs, N.J., 1979.

Garrels, R.M., and C.L. Christ, *Solutions, Minerals and Equilibria*, Freeman, Cooper & Co., San Francisco, 1965.

Glover, M.C., and J.A. Guin, Dissolution of a homogeneous porous medium by surface reaction, *AIChE J.*, 19, 1190-1195, 1973.

Grundl, T.J., and D.L. Macalady, Electrode measurement of redox potential in anaerobic ferric/ferrous chloride systems, *J. Contam. Hydrol.*, 5, 97-117, 1989.

Gschwend, P.M., and M.D. Reynolds, Monodisperse ferrous phosphate colloids in an anoxic groundwater plume, *J. Contam. Hydrol.*, 1, 309-327, 1987.

Hekim, Y., and H.S. Fogler, On the movement of multiple reaction zones in porous media, *AIChE J.*, 26, 403-411, 1980.

Herman, J.S., and M.M. Lorah, CO_2 outgassing and calcite precipitation in Falling Spring Creek, Virginia, U.S.A., *Chem. Geol.*, 62, 251-262, 1987.

Hoefner, M.L., and H.S. Fogler, Pore evolution and channel formation during flow and reaction in porcus media, *AIChE J.*, 34, 45-54, 1988.

Holdren, G.R., Jr., and P.M. Speyer, Reaction rate-surface area relationships during the early stages of weathering, 1. Initial observations, *Geochim. Cosmochim. Acta*, 49, 675-681, 1985.

Hower, W.F., R.A. Lasater, and R.G. Mihram, Compatibility of injection fluids with reservoir components, in *Underground Waste Management and Environmental Implications*, edited by T.D. Cook, pp. 287-293, Memoir 18, American Association of Petroleum Geologists, Tulsa, Okla., 1972.

Hsu, P.H., Nucleation, polymerization, and precipitation of FeOOH, *J. Soil Sci.*, 23, 409-419, 1972.

Hsu, P.H., Appearance and stability of hydrolyzed $Fe(ClO_4)_3$ solutions, *Clays Clay Min.*, 21, 267-277, 1973.

Hsu, P.H., and S.E. Ragone, Aging of hydrolysed iron (III) solutions, *J. Soil Sci.*, 23, 17-31, 1972.

Hunt, J.R., L. McDowell-Boyer, and N. Sitar, Colloid migration in porous media: An analysis of mechanisms, in *Coupled Processes Associated with Nuclear Waste Repositories*, edited by C.-F. Tsang, pp. 453-472, Academic Press, Orlando,

Fla., 1987.

Joint Committee on Powder Diffraction Standards (JCPDS), Powder diffraction file search manual (Hanawalt method): inorganic, Swarthmore, Penn., 1984.

Konikow, L.F., and S.S. Papadopulos, Scientific problems, in *The Geology of North America, Vol. O-2, Hydrogeology*, edited by W. Back, J.S. Rosenshein, and P.R. Seaber, pp. 503-507, Geological Society of America, Boulder, Colo., 1988.

Leenheer, J.A., R.L. Malcolm, and W.R. White, Physical, chemical, and biological aspects of subsurface organic waste injection near Wilmington, North Carolina, *U.S. Geol. Surv. Prof. Pap. 987*, 1976.

Lichtner, P.C., The quasi-stationary state approximation to coupled mass transport and fluid-rock interaction in a porous medium, *Geochim. Cosmochim. Acta*, 52, 143-165, 1988.

Loeppert, R.H., and L.R. Hossner, Reactions of Fe^{2+} and Fe^{3+} with calcite, *Clays Clay Min.*, 32, 213-222, 1984.

Loeppert, R.H., L.R. Hossner, and P.K. Amin, Formation of ferric oxyhydroxides from ferrous and ferric perchlorate in stirred calcareous systems, *Soil Sci. Soc. Am. J.*, 48, 677-683, 1984.

Lund, K., and H.S. Fogler, Acidization--V. The prediction of the movement of acid and permeability fronts in sandstone, *Chem. Eng. Sci.*, 31, 381-392, 1976.

Lund, K., H.S. Fogler, C.C. McCune, and J.W. Ault, Acidization--IV. Experimental correlations and techniques for the acidization of sandstone cores, *Chem. Eng. Sci.*, 31, 373-380, 1976.

McArthur, J.M., J.V. Turner, W.B. Lyons, A.O. Osborn, and M.F. Thirwall, Hydrochemistry on the Yilgarn Block, Western Australia: Ferrolysis and mineralisation in acidic brines, *Geochim. Cosmochim. Acta*, 55, 1273-1288, 1991.

Melikhov, I.V., E.D. Kozlovskaya, L.B. Berliner, and M.A. Prokofiev, Kinetics of hydroxide Fe(III) solid phase formation, *J. Coll. Interf. Sci.*, 117, 1-9, 1987.

Melkote, R.R., and K.F. Jensen, Models for catalytic pore plugging: Application to hydrodemetallation, *Chem. Eng. Sci.*, 44, 649-663, 1989.

Ortoleva, P., J. Chadam, E. Merino, and A. Sen, Geochemical self-organization II: The reactive-infiltration instability, *Am. J. Sci.*, 287, 979-1007, 1987.

Palciauskas, V.V., and P.A. Domenico, Solution chemistry, mass transfer, and the approach to chemical equilibrium in porous carbonate rocks and sediments, *Geol. Soc. Am. Bull.*, 87, 207-214, 1976.

Parkhurst, D.L., D.C. Thorstenson, and L.N. Plummer, PHREEQE - A computer program for geochemical calculations, *U.S. Geol. Surv. Water-Resour. Invest. 80-96*, 1980.

Plummer, L.N., D.L. Parkhurst, and T.M.L. Wigley, Critical review of the kinetics of calcite dissolution and precipitation, in *Chemical Modeling in Aqueous Systems*, edited by E.A. Jenne, pp. 537-573, American Chemical Society, Washington, D.C., 1979.

Plummer, L.N., and T.M.L. Wigley, The dissolution of calcite in CO_2-saturated solutions at 25°C and 1 atmosphere total pressure, *Geochim. Cosmochim. Acta*, 40, 191-202, 1976.

Plummer, L.N., T.M.L. Wigley, and D.L. Parkhurst, The kinetics of calcite dissolution in CO_2-water systems at 5° to 60°C and 0.0 to 1.0 atm CO_2, *Am. J. Sci.*, 278, 179-216, 1978.

Reardon, E.J., A.A. Mozeto, and P. Fritz, Recharge in northern clime calcareous sandy soils: soil water chemical and carbon-14 evolution, *Geochim. Cosmochim. Acta*, 44, 1723-1735, 1980.

Rege, S.D., and H.S. Fogler, Competition among flow, dissolution, and precipitation in porous media, *AIChE J.*, 35, 1177-1185, 1989.

Rege, S.D., H.S. Fogler, and M.H. Hoefner, Wormholing in underground injection strata, *Eos, Trans. Am. Geophys. Union*, 72(17), 110, 1991.

Rickard, D.T., and E.L. Sjoberg, Mixed kinetic control of calcite dissolution rates, *Am. J. Sci.*, 283, 815-830, 1983.

Schilt, A.A., *Perchloric Acid and Perchlorates*, G. Frederick Smith Chemical Co., Columbus, Ohio, 1979.

Schincariol, R.A., Migration of dense aqueous phase liquids in homogeneous and heterogeneous porous media, M.Sc. thesis, Univ. of Alberta, Edmonton, 1989.

Schott, J., S. Brantley, D. Crerar, C. Guy, M. Borcsik, and C. Willaime, Dissolution kinetics of strained calcite, *Geochim. Cosmochim. Acta*, 53, 373-382, 1989.

Schulz, H.D., Labormessung der Sättigungslänge als Maß für die Lösungskinetik von Karbonaten im Grundwasser, *Geochim. Cosmochim. Acta*, 52, 2651-2657, 1988.

Schwertmann, U., and R.M. Taylor, Iron oxides, in *Minerals in Soil Environments*, 2nd ed., edited by J.B. Dixon and S.B. Weed, pp. 379-438, Soil Science Society of America, Madison, Wis., 1989.

Scrivner, N.C., K.E. Bennett, R. A. Pease, A. Kopatsis, S.J. Sanders, D.M. Clark, and M. Rafal, Chemical fate of injected wastes, *Ground Water Monitor. Rev.*, 6(3), 53-58, 1986.

Sharma, M.M., and Y.C. Yortsos, Transport of particulate suspensions in porous media: Model formulation, *AIChE J.*, 33, 1636-1643, 1987.

Sherwood, J.D., Stability of a plane reaction front in a porous medium, *Chem. Eng. Sci.*, 42, 1823-1829, 1987.

Sinex, W.E., R.S. Schechter, and I.H. Silberberg, Dissolution of a porous matrix by a slowly reacting acid, *Ind. Eng. Chem. Fundam.*, 11, 205-209, 1972.

Sisler, H.H., R.D. Dresdner, and W.T. Mooney, Jr., *Chemistry, A Systematic Approach*, Oxford University Press, New York, 1980.

Sjoberg, E.L., and D.T. Rickard, Calcite dissolution kinetics: Surface speciation and the origin of the variable pH dependence, *Chem. Geol.*, 42, 119-136, 1984.

Sposito, G., *The Surface Chemistry of Soils*, Oxford University Press, New York, 1984.

Sposito, G., *The Chemistry of Soils*, Oxford University Press, New York, 1989.

Steefel, C.I., and A.C. Lasaga, The evolution of dissolution patterns: Permeability change due to coupled flow and reaction, in *Chemical Modeling in Aqueous Systems II*, edited by D.C. Melchior and R.L. Bassett, American Chemical Society, Washington, D.C., 1990.

Stumm, W., and J.J. Morgan, *Aquatic Chemistry, An Introduction Emphasizing Chemical Equilibria in Natural Waters*, Wiley-Interscience, New York, 1970.

Suarez, D.L., and J.D. Wood, Simultaneous determination of calcite surface area and content in soils, *Soil Sci. Soc. Am. J.*, 48, 1232-1235, 1984.

Sudicky, E.A., A natural gradient experiment on solute transport in a sand aquifer: Spatial variability of hydraulic conductivity and its role in the dispersion process, *Water Resour. Res.*, 22, 2069-2082, 1986.

Sudicky, E.A., R.W. Gillham, and E.O. Frind, Experimental investigation of solute transport in porous media, 1. The nonreactive case, *Water Resour. Res.*, 21, 1035-1041, 1985.

Talman, S.J., Calcite dissolution kinetics: Transport vs. surface reaction control, unpublished manuscript, 1991.

Taylor, S.W., and P.R. Jaffe′, Biofilm growth and the related changes in the physical properties of a porous medium, 1. Experimental investigation, *Water Resour. Res.*, 26, 2153-2159, 1990a.

Taylor, S.W., and P.R. Jaffe′, Biofilm growth and the related changes in the physical properties of a porous medium, 3. Dispersivity and model verification, *Water Resour. Res.*, 26, 2171-2180, 1990b.

Wang, M.K., and P.H. Hsu, Effects of temperature and iron(III) concentration on the hydrolytic formation of iron(III) oxyhydroxides and oxides, *Soil Sci. Soc. Am. J.*, 44, 1089-1095, 1980.

Warner, D.L., Deep well waste injection--Reaction with aquifer water, *J. Sanitary Eng. Div., Proc. Am. Soc. Civ. Eng.*, 92, 45-69, 1966.

Weyl, P.K., The solution kinetics of calcite, *J. Geol.*, 66, 163-176, 1958.

White, A.F., and M.L. Peterson, Role of reactive-surface-area characterization in geochemical kinetic models, in *Chemical Modeling in Aqueous Systems II*, edited by D.C. Melchior and R.L. Bassett, pp. 461-475, American Chemical Society, Washington, D.C., 1990.

Wicks, C.M., and C.G. Groves, Chemical evolution of an acid-mine drainage stream in karst terrain, *Eos, Trans. Am. Geophys. Union* , 72(17), 114, 1991.

APPENDIX I. Grain Size and Calcite Surface Area Determinations

Grain-size analyses were conducted on triplicate samples each of Ottawa sand and unsieved, crushed, unwashed calcite. Each Ottawa sand sample was tested on a Ro-Tap mechanical shaker for 15 minutes between #16 and #120 sieves (Table I.1). Prior grading by the distributor meant that the size range for the sand was relatively narrow, with more than 45% of each sample falling between 297 and 600 μm, and more than 94% between 180 and 600 μm (Figure I.1). By comparison, the amount of fines visible in the calcite samples warranted analysis over a wider range of sieve sizes and by hydrometer. Based on the procedures of Catto et al. (1989), each calcite sample was agitated in a glass cylinder containing 0.5% sodium hexametaphosphate solution, then allowed to settle for 24 hr, during which time hydrometer readings were taken. Afterward, each sample was washed with deionized water over a #230 (62.5 μm) sieve, and the fraction greater than that size was subjected to sieve analysis on the Ro-Tap for approximately 30 minutes. The results of the calcite analyses are combined in Table I.2 and Figure I.2. The "analytical break" between the finest sieve and hydrometer data points is typical, and results from the differing behavior of fine particles under sieving and settling (Catto et al., 1989). As shown in Figure I.2, the agreement among the replicates is excellent. The greatest fraction by mass of each sample, 24.9 to 25.2%, fell between 250 and 500 μm, the size interval chosen for the experiments utilizing sieved calcite (Table I.2).

Under circumstances where surface reaction is influential in determining the overall rate of reaction (i.e., surface or mixed control), the reactive surface area A_r becomes important, yet quantifying that parameter is problematic. This study follows common practice in assuming the reactive surface area to be proportional to the physical surface area, which is estimated geometrically from grain-size analyses or measured directly from gas adsorption isotherms (White and Peterson, 1990). Based on

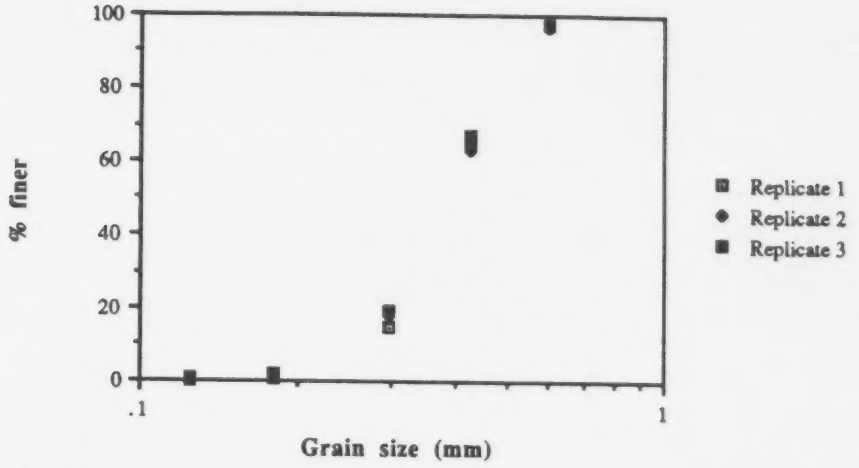

Figure I.1.
Cumulative grain-size curves for Ottawa sand based on sieve analyses.

Table I.1. Grain-size data for Ottawa sand replicates based on sieve analyses (sizes in mm, representing sieve sizes #16 - #120).

Grain size	% finer (1)	% finer (2)	% finer (3)
1.180	100.00	100.00	100.00
0.600	97.18	96.55	97.58
0.425	65.17	63.18	67.01
0.297	14.69	17.88	19.39
0.180	0.91	2.00	2.10
0.125	0.06	0.31	0.49

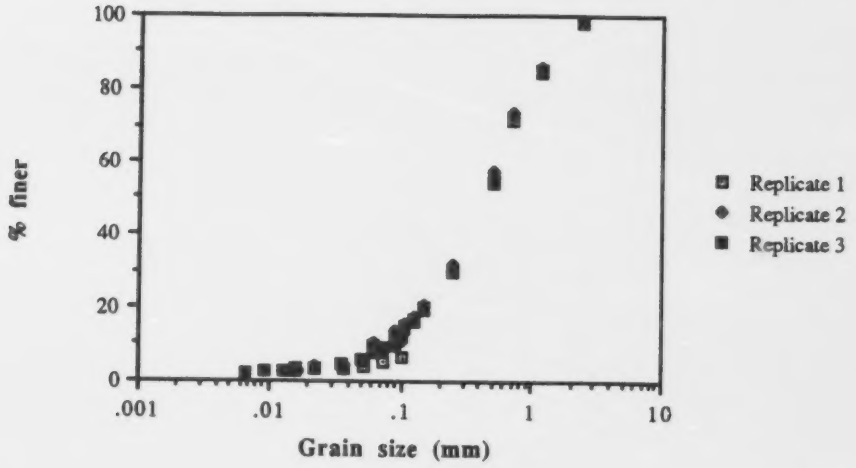

Figure I.2.
Cumulative grain-size curves for crushed calcite based on sieve and hydrometer analyses.

Table I.2. Grain-size data for crushed calcite replicates based on sieve and hydrometer analyses (sizes in mm).

Gr. size 1	% finer (1)	Gr. size 2	% finer (2)	Gr. size 3	% finer (3)
2.360	97.80	2.360	98.00	2.360	98.10
1.180	84.70	1.180	85.90	1.180	84.90
0.710	71.40	0.710	73.30	0.710	71.80
0.500	54.40	0.500	57.10	0.500	55.10
0.250	29.50	0.250	31.90	0.250	30.20
0.150	19.10	0.150	20.70	0.150	19.70
0.125	16.20	0.125	17.50	0.125	16.80
0.106	14.30	0.106	15.40	0.106	14.80
0.102	6.53	0.101	10.80	0.101	13.00
0.090	12.40	0.090	13.40	0.090	9.69
0.073	4.98	0.072	7.74	0.072	9.18
0.062	9.39	0.062	10.20	0.062	7.65
0.052	3.73	0.051	5.88	0.051	5.97
0.037	3.42	0.036	4.33	0.036	4.59
0.023	3.11	0.023	4.03	0.023	3.52
0.016	2.64	0.016	2.79	0.016	3.06
0.013	2.49	0.013	2.32	0.013	2.60
0.009	2.33	0.009	2.32	0.009	2.45
0.007	2.02	0.007	1.70	0.007	1.84

precipitation rates and grain-size data from a travertine-depositing stream observed by Herman and Lorah (1987), White and Peterson (1990) determined the geometric and reactive surface areas of calcite to be approximately equal. Holdren and Speyer (1985) have found that dissolution rates for various feldspars increase linearly with decreasing grain size (or increasing physical surface area) to a limit of approximately 50 to 100 μm, beyond which the dependence is non-linear. The transition was attributed to grain size becoming less than the spacing between crystal defects, which are preferred sites for reaction. Schott et al. (1989) proposed that, below a defect density of 2×10^7 cm^{-2}, the rate of dissolution of calcite should be proportional to the physical surface area. This threshold density is five orders of magnitude greater than that estimated for K-feldspar, so that the critical grain size below which physical and reactive surface areas diverge may be much smaller for calcite than that observed by Holdren and Speyer (1985). However, Ferret et al. (1987) have determined that grinding of calcite causes small particles to microcrystallize, leading to faster dissolution.

Geometric surface areas have been calculated following Suarez and Wood (1984), who assumed the calcite particles to be "equidimensional rhombohedrons passing through square grid openings." The edge lengths x were thus corrected for the 101.92° cleavage angle using the relation $x = 0.910\ d$, where d is the mesh width (L), as shown in Table I.3. The surface area was then determined based on the harmonic mean edge length of each size interval (Ferret et al., 1987) and corrected for the formula weight of calcite. Table I.4 lists both the surface area for each size interval in m^2/g and the corresponding surface area in m^2/m^3 for each of the replicate calcite samples.

Determining the geometric surface area on particles less than 62.5 μm is problematic because of the limiting assumption in hydrometer analysis that particles settle as spheres according to Stokes' law (Catto et al., 1989). In addition, as much as 1.7% by mass of the calcite particles had not settled out by 24 hr; the significance of this seemingly small fraction lies in the fact that the geometric surface area increases

Table I.3.
Edge lengths of calcite particles which underwent sieve analyses.

Sieve #	Mesh (mm)	Edge (mm)
4	4.75	4.32
8	2.36	2.15
16	1.18	1.07
25	0.710	0.646
35	0.500	0.455
60	0.250	0.228
100	0.150	0.137
120	0.125	0.114
140	0.106	0.0965
170	0.090	0.0819
230	0.0625	0.0569

Table I.4.
Geometric surface area for sieve intervals (in m^2/g) (based on the harmonic mean edge length) and the corresponding surface area of those intervals (in m^2/m^3) based on the mass distribution of the crushed calcite replicates.

Sieve interval	Mean edge length (mm)	A (m2/g)	Normalized A1 (m2/m3)	Normalized A2 (m2/m3)	Normalized A3 (m2/m3)
#4 - #8	2.87	7.71x10-4	1.73x10-5	1.55x10-5	1.50x10-5
#8 - #16	1.43	1.55x10-3	2.02x10-4	1.87x10-4	2.04x10-4
#16 - #25	0.807	2.74x10-3	3.64x10-4	3.45x10-4	3.58x10-4
#25 - #35	0.534	4.14x10-3	7.05x10-4	6.70x10-4	6.94x10-4
#35 - #60	0.303	7.29x10-3	1.81x10-3	1.84x10-3	1.82x10-3
#60 - #100	0.171	1.30x10-2	1.35x10-3	1.45x10-3	1.35x10-3
#100 - #120	0.124	1.78x10-2	5.30x10-4	5.86x10-4	5.20x10-4
#120 - #140	0.104	2.12x10-2	3.92x10-4	4.40x10-4	4.35x10-4
#140 - #170	0.0886	2.50x10-2	4.88x10-4	4.91x10-4	4.55x10-4
#170 - #230	0.0672	3.30x10-2	9.84x10-4	1.07x10-3	1.08x10-3
		Total > #230	6.85x10-3	7.09x10-3	6.92x10-3

exponentially with decreasing particle size. The overall average calcite surface area was estimated by assuming a constant proportionality between the calculated geometric surface area and the surface area measured using gas adsorption. White and Peterson (1990) compiled a list of studies where particle size ranges and measurements of gas adsorption (based on a BET isotherm) were both reported for samples of various minerals, including calcite. From a regression analysis of these data, those authors found that BET values of physical surface area exceeded estimates based on geometry by a factor of approximately 7. For 2.3 to 26.4 μm particles of crushed calcite, Ferret et al. (1987) found that BET measurements were greater than geometric estimates by a factor of approximately 3 to 5.

BET measurements were made on two sets of washed, triplicate samples, one comprised of calcite grains 250 to 500 μm across and the other containing the calcite which passed the #230 sieve after hydrometer analysis, with an Omnisorp 360 N_2-sorptometer in the Department of Chemical Engineering at the University of Alberta. The average BET surface area of the 250 to 500 μm fraction was 0.1282 m^2/g, 17.6 times the geometric value for the same interval (Table I.5). This multiplying factor was used in conjunction with Table I.4 to determine the BET-equivalent surface area for the entire portion larger than 62.5 μm of each of the three original, unwashed calcite samples. The resulting number for each sample was added to the corresponding BET value measured on the fraction smaller than 62.5 μm. Finally, this sum for each sample was averaged, yielding an overall value of 0.150 m^2/g. S.E. Wanke (University of Alberta, personal communication) has noted that the values measured by BET analysis are sufficiently low (less than 0.5 m^2/g) that the differences among them may be insignificant. However, the reproducibility of the grain size analyses supports taking the average surface area value to determine the normalized Damkohler number (Chapter 3). The physical surface area of calcite was taken to be 0.150 m^2/g for experiments P1 to 4 and 0.128 m^2/g for 5 to 8.

Table I.5.
BET surface-area measurements on sets of triplicate calcite samples.

Sample #	Size (um)	A (m2/g)
1a	< 62.5	0.2599
1b	< 62.5	0.3279
1c	< 62.5	0.2532
2a	250-500	0.1554
2b	250-500	0.07548
2c	250-500	0.1535

APPENDIX II. Supplementary Geochemical Data

Table II.1.
Reaction front position as a function of time for (a) experiment 1, (b) experiment 2, (c) experiment 3, (d) experiment 4.

(a) t 1-2 (hr)	Front 1-2 (m)
240.00	0.054
267.70	0.059
289.30	0.062
313.53	0.069
337.32	0.077
433.30	0.090
457.23	0.091
480.02	0.094
504.45	0.097
529.15	0.100

(b) t 2-1 (hr)	Front 2-1 (m)	t 2-2 (hr)	Front 2-2 (m)	t 2-3 (hr)	Front 2-3 (m)
70.50	0.040	11.67	0.040	1.25	0.040
96.42	0.058	27.23	0.049	1.65	0.060
108.97	0.062	48.70	0.066	2.38	0.068
		73.17	0.085	4.13	0.075
				12.38	0.127
				24.58	0.161
				36.42	0.183
				48.53	0.213
				85.30	0.305
				96.08	0.330
				108.88	0.368
				120.05	0.414
				132.38	0.440
				143.75	0.461
				156.67	0.483
				167.96	0.507

(c) t 3-1 (hr)	Front 3-1 (m)	t 3-2 (hr)	Front 3-2 (m)	t 3-3 (hr)	Front 3-3 (m)
25.25	0.071	2.73	0.049	2.90	0.047
36.52	0.084	5.82	0.051	6.02	0.054
49.38	0.096	12.07	0.059	12.00	0.058
71.75	0.122	25.00	0.076	25.25	0.077
97.70	0.146	36.25	0.084	36.50	0.085
120.05	0.166	49.15	0.098	49.37	0.093
144.05	0.177	71.88	0.119	72.50	0.123
168.28	0.196	97.57	0.154	97.77	0.132
		119.85	0.158	120.10	0.145
		143.93	0.174		
		167.98	0.184		

(d) t 4-1 (hr)	Front 4-1 (m)	t 4-2 (hr)	Front 4-2 (m)
55.58	0.040	97.57	0.099
97.65	0.091	120.28	0.109
120.50	0.094		

Table II.2.
Reaction front position as a function of time for (a) experiment 5, (b) experiment 6, (c) experiment 7, (d) experiment 8.

(a) t 5-1 (hr)	Front 5-1 (m)	t 5-2 (hr)	Front 5-2 (m)	t 5-3 (hr)	Front 5-3 (m)
1.67	0.067	2.28	0.057	1.50	0.071
3.08	0.070	5.95	0.060	2.05	0.076
5.95	0.074	13.13	0.060	3.08	0.078
8.60	0.074	24.07	0.062	4.00	0.080
13.17	0.077	30.07	0.076	5.95	0.080
24.13	0.077	37.57	0.076	8.52	0.080
30.15	0.085	48.62	0.092	13.10	0.080
36.58	0.092	60.28	0.117	24.03	0.091
48.70	0.108	71.88	0.131	29.98	0.102
60.45	0.130	76.18	0.140	36.53	0.105
71.95	0.147	96.12	0.168	48.53	0.125
76.25	0.158	108.90	0.198	60.20	0.150
96.20	0.184	120.42	0.207	71.82	0.162
108.95	0.202	132.42	0.217	76.12	0.174
120.42	0.221	144.53	0.231	96.03	0.187
132.45	0.241	161.42	0.255	108.87	0.201
144.62	0.260			120.32	0.215
161.48	0.273			132.28	0.228
				144.45	0.241
				161.35	0.268

(b) t 6-1 (hr)	Front 6-1 (m)	t 6-2 (hr)	Front 6-2 (m)	t 6-3 (hr)	Front 6-3 (m)
48.35	0.048	38.30	0.054	28.53	0.059
60.37	0.059	48.32	0.059	48.38	0.070
71.95	0.071	60.47	0.067	60.57	0.081
83.87	0.076	72.18	0.081	72.22	0.089
95.93	0.087	83.92	0.091	83.98	0.097
108.47	0.094	96.10	0.098	96.15	0.108
120.73	0.100	108.52	0.106	108.55	0.114
131.90	0.109	120.77	0.112	120.80	0.126
143.95	0.118	132.00	0.118	132.02	0.133
156.38	0.123	144.06	0.127	144.20	0.140
		156.43	0.136	156.47	0.147

Table II.2 (continued).

(c) t 7-1 (hr)	Front 7-1 (m)	t 7-2 (hr)	Front 7-2 (m)	t 7-3 (hr)	Front 7-3 (m)
15.73	0.044	4.07	0.048	4.08	0.047
24.78	0.051	8.12	0.051	12.32	0.047
36.50	0.062	12.30	0.055	24.88	0.061
48.52	0.075	24.80	0.075	36.85	0.074
72.78	0.116	36.58	0.098	48.68	0.095
95.93	0.151	48.60	0.108	73.00	0.125
120.58	0.184	72.88	0.128	96.00	0.152
144.95	0.212	95.98	0.161	120.87	0.183
156.88	0.221	120.80	0.199	145.07	0.212
		145.00	0.213	156.98	0.221
		156.93	0.219		

(d) t 8-1 (hr)	Front 8-1 (m)	t 8-2 (hr)	Front 8-2 (m)	t 8-3 (hr)	Front 8-3 (m)
0.96	0.054	0.98	0.056	0.98	0.061
1.98	0.080	2.00	0.074	2.07	0.088
3.00	0.086	3.03	0.085	3.05	0.095
11.95	0.095	12.00	0.099	12.02	0.104
24.43	0.132	24.50	0.150	24.58	0.141
35.98	0.168	36.05	0.181	36.07	0.180
48.22	0.207	48.27	0.206	48.33	0.227
71.95	0.251	72.02	0.265	72.12	0.319
96.25	0.305	96.32	0.354	96.35	0.366
120.05	0.380	120.15	0.385	120.20	0.398
143.92	0.436	143.98	0.430	144.07	0.448
157.33	0.467	157.62	0.461	157.65	0.489

Table II.3.
Electrical conductivity of influent solution for (a) experiment 5, (b) experiment 6, (c) experiment 7, (d) experiment 8.

	early, unfiltered	early, filtered	late, unfiltered	late, filtered
(a) EC 5 (µS)				
Batch #				
1			3400	3400
2	3350	3350	3320	3400
3	3300	3350	3080	
4			3300	
5	3370	3070	3300	3220
6	3320	3180	3150	3300
7	3380	3550	3250	
(b) EC 6 (µS)				
Batch #				
1	3500		3450	
2	3450			
3	3610		3500	
4	3420			
(c) EC 7 (µS)				
Batch #				
1		3520		
2		3430		
3		3420		
4		3410		
(d) EC 8 (µS)				
Batch #				
1		3440		
2		3350		
3		3320		
4		3340		
5		3410		
6		3410		
7		3370		

Table II.4.
pH of influent solution for (a) experiment 5, (b) experiment 6, (c) experiment 7, (d) experiment 8.

	early, unfiltered	early, filtered	late, unfiltered	late, filtered
(a) pH 5				
Batch #				
1			2.47	2.47
2	2.42	2.45		
3				
4				
5			2.39	2.44
6	2.44	2.42	2.42	2.42
7	2.44	2.39	2.45	
(b) pH 6				
Batch #				
1	2.43		2.45	
2	2.48		2.45	
3	2.39		2.40	
4	2.40			
(c) pH 7				
Batch #				
1		2.45		
2		2.43		
3		2.45		
4		2.43		
(d) pH 8				
Batch #				
1		2.36		
2		2.46		
3		2.41		
4		2.48		
5		2.46		
6		2.44		
7		2.47		

Table II.5.
Fe concentration of influent solution for (a) experiment 5, (b) experiment 6, (c) experiment 7, (d) experiment 8.

	early, unfiltered	early, filtered	late, unfiltered	late, filtered
(a) Fe 5 (µg/g)				
Batch #				
1			410	390
2	390	420		360
3	400	420		380
4			410	400
5	380	410	410	
6	400		420	410
7	400	420	390	370
(b) Fe 6 (µg/g)				
Batch #				
1	390	400	390	400
2	390	390	400	390
3	390	390	390	390
4	390	400		
(c) Fe 7 (µg/g)				
Batch #				
1		410		420
2		410		410
3		400		400
4		410		410
(d) Fe 8 (µg/g)				
Batch #				
1		400		400
2		390		370
3		410		400
4		420		410
5		400		
6				
7		420		400

Table II.6.
Electrical conductivity of effluent for (a) experiment 1, (b) experiment 2, (c) experiment 3, (d) experiment 4.

(a)

t 1-3 (hr)	EC 1-3 (dS/m)
0.15	0.113
0.58	0.106
1.18	0.098
3.22	0.084
4.30	0.073
5.32	0.064
6.27	0.056
7.15	0.049
8.27	0.041
9.22	0.032
10.18	0.027
11.22	0.024
12.17	0.024
20.65	2.52
21.78	2.24
22.03	2.00
24.13	2.20
49.98	2.49
52.27	2.61
68.23	2.55
76.98	2.56

(b)

t 2-1 (hr)	EC 2-1 (dS/m)	t 2-2 (hr)	EC 2-2 (dS/m)	t 2-3 (hr)	EC 2-3 (dS/m)
1.43	0.044	1.18	0.040	1.02	0.039
2.37	0.052	2.12	0.042	1.95	0.040
3.23	0.053	3.15	0.046	3.13	0.041
6.15	0.703	6.07	0.235	6.02	2.24
12.25	2.73	12.18	2.70	12.15	2.66
25.12	2.69	25.07	2.65	25.13	2.58
36.23	2.67	36.23	2.65	36.23	2.59
48.15	2.67	48.12	2.89		
72.15	2.97				

Table II.6 (continued).

(c) t 3-1 (hr)	EC 3-1 (dS/m)	t 3-2 (hr)	EC 3-2 (dS/m)	t 3-3 (hr)	EC 3-3 (dS/m)
1.47	0.097	1.48	0.096	1.95	0.060
2.25	0.089	2.60	0.072	2.73	0.058
3.28	0.082	3.22	0.082	3.25	0.050
4.45	0.067	4.28	0.077	4.78	0.045
5.42	0.066	5.25	0.064	5.63	0.049
9.33	0.063	9.30	0.052	9.33	0.053
10.48	0.077	10.25	0.052	10.32	0.071
11.48	0.713	11.33	0.058	11.40	1.023
72.13	2.830	71.96	2.840	72.40	2.830
97.05	3.180	96.75	2.870	96.92	2.860
120.18	2.840	119.87	2.810	120.05	2.860
144.25	2.990	143.96	2.820	144.17	2.840
		167.93	2.940		

(d) t 4-1 (hr)	EC 4-1 (dS/m)	t 4-2 (hr)	EC 4-2 (dS/m)	t 4-3 (hr)	EC 4-3 (dS/m)
1.11	0.150	1.20	0.479	2.28	0.487
2.13	0.121	2.23	0.371	3.25	0.388
3.15	0.096	3.22	0.266	4.27	0.286
4.21	0.090	4.21	0.206	5.23	0.232
5.14	0.095	5.22	0.183	6.28	0.177
6.15	0.077	6.21	0.153	9.24	0.115
9.16	2.320	9.25	0.108	10.45	0.113
24.23	3.010	10.22	0.111	11.27	0.110
36.31	2.970	11.25	0.083	12.24	0.250
48.72	2.630	12.23	0.106	24.26	2.990
72.24	2.960	24.21	2.980	36.31	2.950
96.52	2.960	36.21	2.990	48.80	2.930
120.00	2.930	48.67	2.890	77.12	2.940
		72.23	2.860	144.00	3.010
		96.37	2.900		
		120.34	2.880		
		144.07	2.930		

Table II.7.
Electrical conductivity of effluent for (a) experiment 5, (b) experiment 6, (c) experiment 7, (d) experiment 8. Values used for least-squares fitting of breakthrough curves marked by an asterisk.

(a) t 5-1 (hr)	EC (dS/m)	t 5-2 (hr)	EC (dS/m)	t 5-3 (hr)	EC (dS/m)
1.05	0.0433	1.17	0.0423	1.27	0.0420
3.20	0.113	4.38	0.0400	3.43	0.0400
4.27	0.0390	5.53	0.163*	3.58	0.0393
5.45	0.0840*	6.53	1.01*	5.73	0.103*
6.45	0.990*	7.37	2.58*	6.73	1.58*
7.20	2.52*	12.48	2.65	7.48	2.55*
12.37	2.62	24.58	2.64	12.72	2.65
24.45	2.65	36.15	2.60	24.75	2.68
36.08	2.58	48.17	2.55	36.23	2.56
48.08	2.55	75.57	2.48	48.25	2.55
75.65	2.52	97.67	2.55	75.50	2.48
97.53	2.55	120.82	2.42	98.10	2.40
120.77	2.52	144.32	2.40	144.27	2.52
144.20	2.40				

(b) t 6-1 (hr)	EC (dS/m)	t 6-2 (hr)	EC (dS/m)	t 6-3 (hr)	EC (dS/m)
1.23	0.0485	1.27	0.0560	1.35	0.0600
2.45	0.0440	2.50	0.0480	2.55	0.0495
3.77	0.0400	3.57	0.0442	3.42	0.0450
4.52	0.0385	4.60	0.0410	4.62	0.0420
6.37	0.0355	6.42	0.0362	6.45	0.0380
7.23	0.0347	7.28	0.0348	7.33	0.0370
9.45	0.0445	9.52	0.0402	9.62	0.0380
11.32	0.540*	11.38	0.472*	11.43	0.348*
12.42	1.48*	12.48	1.43*	12.62	1.08*
13.58	2.25*	13.63	2.31*	13.68	1.85*
14.58	2.45	14.58	2.53	14.58	2.26*
15.35	2.52	15.60	2.56	15.62	2.42
24.53	2.68	36.63	2.64	24.70	2.71
36.52	2.61	48.52	2.59	36.67	2.68
48.45	2.63	60.68	2.67	48.55	2.69
60.52	2.69	72.40	2.60	60.73	2.69
72.37	2.68	96.77	2.48	72.43	2.69
96.70	2.57	108.60	2.58	96.80	2.68
108.58	2.58	120.53	2.56	108.63	2.48
120.42	2.49	144.67	2.60	120.65	2.59
144.63	2.59			145.05	2.53

Table II.7 (continued).

(c) t 7-1 (hr)	EC (dS/m)	t 7-2 (hr)	EC (dS/m)	t 7-3 (hr)	EC (dS/m)
1.43	0.0395	1.48	0.0395	1.53	0.0385
2.45	0.0385	2.55	0.0385	2.65	0.0380
3.45	0.0380	3.68	0.0383	3.70	0.0380
4.45	0.0378	4.62	0.0382	4.70	0.0372
5.40	0.0372	5.45	0.0372	5.52	0.0371
6.47	0.0370	7.52	0.0369	6.57	0.0365
7.48	0.0369	9.73	0.0502	7.53	0.0361
9.63	0.0385	11.32	0.462*	9.75	0.0520
11.27	0.108*	12.85	1.26*	11.35	0.458*
12.75	0.620*	14.42	2.19*	12.90	1.22*
14.38	1.80*	16.40	2.66	14.45	2.00*
16.38	2.55*	24.72	2.64	16.43	2.56
24.68	2.65	36.70	2.67	24.82	2.54
36.67	2.70	48.38	2.73	36.80	2.68
48.30	2.72	72.55	2.62	48.43	2.71
72.50	2.70	96.57	2.56	72.60	2.62
96.50	2.57	120.67	2.55	96.60	2.52
120.48	2.55	144.65	2.52	120.70	2.52
144.55	2.52			144.68	2.49

(d) t 8-1 (hr)	EC (dS/m)	t 8-2 (hr)	EC (dS/m)	t 8-3 (hr)	EC (dS/m)
1.30	0.0303	1.37	0.0309	1.45	0.0305
2.47	0.0303	2.53	0.0303	2.55	0.0308
3.43	0.0303	3.47	0.0305	3.53	0.0310
4.38	0.0309	4.45	0.0315	4.48	0.0307*
5.25	0.164*	5.30	0.333*	8.27	2.59*
6.33	1.20*	6.37	1.25*	10.58	2.57
8.20	2.52*	8.25	2.50*	12.38	2.55
10.50	2.52	10.53	2.57	25.08	2.61
12.30	2.54	12.35	2.55	36.58	2.51
25.03	2.63	25.07	2.61	49.22	2.51
36.48	2.55	36.52	2.52	72.87	2.51
49.05	2.53	49.12	2.53	96.87	2.42
72.72	2.53	72.83	2.50	120.88	2.51
96.77	2.41	96.82	2.42	144.85	2.41
120.75	2.51	120.82	2.55		
144.67	2.50	144.78	2.50		

Table II.8.
pH of effluent for (a) experiment 5, (b) experiment 6, (c) experiment 7, (d) experiment 8.

(a) t 5-1 (hr)	pH 5-1	t 5-2 (hr)	pH 5-2	t 5-3 (hr)	pH 5-3
		3.28	7.80	3.43	8.32
6.45	7.53	6.53	7.64	6.73	7.39
12.37	7.01	12.48	6.94	12.72	6.92
24.45	6.99	24.58	6.98	24.75	6.92
36.08	6.82	36.15	6.92	36.23	6.74
48.08	6.77	48.17	6.72	48.25	6.74
75.65	6.55	75.57	6.48	75.50	6.46
97.53	6.56	97.67	6.41	98.10	6.55
120.77	6.44	120.82	6.48	120.88	6.43
144.20	6.36	144.32	6.51	144.27	6.32

(b) t 6-1 (hr)	pH 6-1	t 6-2 (hr)	pH 6-2	t 6-3 (hr)	pH 6-3
3.77	8.15	3.57	8.12	3.42	7.71
6.37	8.78	6.42	8.54	6.45	8.56
12.42	7.30	12.48	7.16	12.62	7.40
24.53	7.06	24.63	6.99	24.70	6.94
36.52	6.87	36.63	6.72	36.67	6.79
48.45	6.82	48.52	6.85	48.55	6.82
60.52	6.82	60.68	6.75	60.73	6.75
72.37	6.70	72.40	6.75	72.43	6.79
96.70	6.75	96.77	6.78	96.80	6.70
120.42	6.70	120.53	6.65	120.65	6.62
144.63	6.72	144.67	6.79	145.05	6.63

(c) t 7-1 (hr)	pH 7-1	t 7-2 (hr)	pH 7-2	t 7-3 (hr)	pH 7-3
3.45	7.23	3.68	7.48	3.70	7.67
6.47	7.78	12.85	7.23	6.57	8.19
12.75	7.46	24.72	6.81	12.90	7.34
24.68	6.86	36.70	6.81	24.82	6.96
36.67	6.83	48.38	6.84	36.80	6.87
48.30	6.81	72.55	6.74	48.43	6.93
72.50	6.74	96.57	6.75	72.60	6.77
96.50	6.67	120.67	6.60	96.60	6.69
120.48	6.60	144.65	6.53	120.70	6.67
144.55	6.65			144.68	6.70

(d) t 8-1 (hr)	pH 8-1	t 8-2 (hr)	pH 8-2	t 8-3 (hr)	pH 8-3
3.43	7.90	3.47	8.36	3.53	8.32
6.33	6.98	6.37	6.99	6.42	7.13
12.30	6.86	12.35	6.79	12.38	6.91
25.03	6.72	25.07	6.67	25.08	6.94
36.48	6.34	36.52	6.43	36.58	6.58
49.05	6.50	49.12	6.52	49.22	6.62
72.72	6.50	72.83	6.60	72.87	6.58
96.77	6.47	96.82	6.49	96.87	6.50
120.75	6.42	120.82	6.42	120.88	6.54
144.67	6.35	144.78	6.43	144.85	6.55

Table II.9.
TIC of effluent for (a) experiment 5, (b) experiment 6, (c) experiment 7, (d) experiment 8.

(a) t 5-1 (hr)	TIC 5-1 (µg/g)	t 5-2 (hr)	TIC 5-2 (µg/g)	t 5-3 (hr)	TIC 5-3 (µg/g)
6.45	32.1	6.53	34.7	6.73	47.7
12.37	86.2	12.48	82.8	12.72	80.2
24.45	81.5	24.58	89.0	24.75	82.3
36.08	75.1	36.15	79.9	36.23	79.4
48.08	78.6	48.17	66.5	48.25	75.2
75.65	66.3	75.57	65.1	75.50	69.4
97.53	56.1	97.67	62.7	98.10	57.9
120.77	66.6	120.82	52.0	120.88	63.5
144.20	54.6	144.32	52.9	144.27	65.0

(b) t 6-1 (hr)	TIC 6-1 (µg/g)	t 6-2 (hr)	TIC 6-2 (µg/g)	t 6-3 (hr)	TIC 6-3 (µg/g)
3.77	3.61	3.57	4.33	3.42	4.35
6.37	3.31	6.42	3.23	6.45	4.15
12.42	48.7	12.48	44.8	12.62	38.2
24.53	85.3	24.63	85.9	24.70	86.1
36.52	83.8	36.63	89.3	36.67	83.6
48.45	82.2	48.52	85.1	48.55	88.7
60.52	87.3	60.68	89.4	60.73	88.2
72.37	85.3	72.40	88.3	96.80	86.3
96.70	79.9	96.77	82.8	120.65	82.3
120.42	73.1	120.53	81.7	145.05	74.8
144.63	67.8	144.67	71.4		

(c) t 7-1 (hr)	TIC 7-1 (µg/g)	t 7-2 (hr)	TIC 7-2 (µg/g)	t 7-3 (hr)	TIC 7-3 (µg/g)
3.45	3.62	3.68	3.78	3.70	3.97
6.47	3.64	6.52	3.64	6.57	3.67
12.75	21.2	12.85	41.8	12.90	40.1
24.68	79.7	24.72	82.9	24.82	84.6
36.67	82.9	36.70	80.3	36.80	80.7
48.30	82.2	48.38	84.6	48.43	77.5
72.50	80.6	72.55	75.9	72.60	76.2
96.50	72.1	96.57	65.3	96.60	68.0
120.48	66.6	120.67	63.7	120.70	66.1
144.55	64.7	144.65	65.0	144.68	63.6

(d) t 8-1 (hr)	TIC 8-1 (µg/g)	t 8-2 (hr)	TIC 8-2 (µg/g)	t 8-3 (hr)	TIC 8-3 (µg/g)
3.43	2.7	3.47	2.7	3.53	2.7
6.33	38	6.37	42	6.42	40
12.30	81	12.35	92	12.38	82
25.03	83	25.07	82	25.08	80
36.48	74	36.52	82	36.58	69
49.05	67	49.12	76	49.22	70
72.72	63	72.83	63	72.87	67
96.77	66	96.82	64	96.87	62
120.75	71	120.82	72	120.88	62
144.67	73	144.78	74	144.85	68

Table II.10.
Ca concentrations in effluent for (a) experiment 5, (b) experiment 6, (c) experiment 7, (d) experiment 8.

(a) t 5-1 (hr)	Ca 5-1 (µg/g)	t 5-2 (hr)	Ca 5-2 (µg/g)	t 5-3 (hr)	Ca 5-3 (µg/g)
3.20	7.6	3.28	7.8	3.43	7.2
6.45	180	6.53	250	6.73	290
12.37	480	12.48	510	12.72	510
24.45	510	24.58	490	24.75	490
36.08	580	36.15	560	36.23	550
48.08	540	48.17	550	48.25	540
75.65	550	75.57	610	75.50	540
97.53	470	97.67	520	98.10	510
120.77	520	120.82	530	120.88	520
144.20	450	144.32	440	144.27	420

(b) t 6-1 (hr)	Ca 6-1 (µg/g)	t 6-2 (hr)	Ca 6-2 (µg/g)	t 6-3 (hr)	Ca 6-3 (µg/g)
3.77	7.6	3.57	8.6	3.42	8.6
6.37	12	6.42	7.3	6.45	7.9
12.42	310	12.48	310	12.62	230
24.53	540	24.63	590	24.70	600
36.52	580	36.63	580	36.67	590
48.45	580	48.52	590	48.55	580
60.52	570	60.68	580	60.73	570
72.37	560	72.40	580	72.43	550
96.70	560	96.77	570	96.80	570
120.42	510	120.53	590	120.65	560
144.63	550	144.67	550	145.05	560

(c) t 7-1 (hr)	Ca 7-1 (µg/g)	t 7-2 (hr)	Ca 7-2 (µg/g)	t 7-3 (hr)	Ca 7-3 (µg/g)
3.45	7.5	3.68	7.5	3.70	7.3
6.47	6.6	6.52	6.8	6.57	6.5
12.75	110	12.85	270	12.90	250
24.68	590	24.72	590	24.82	580
36.67	560	36.70	580	36.80	580
48.30	560	48.38	580	48.43	580
72.50	560	72.55	550	72.60	570
96.50	570	96.57	560	96.60	560
120.48	550	120.67	550	120.70	550
144.55	540	144.65	550	144.68	540

(d) t 8-1 (hr)	Ca 8-1 (µg/g)	t 8-2 (hr)	Ca 8-2 (µg/g)	t 8-3 (hr)	Ca 8-3 (µg/g)
3.43	5.2	3.47	5.3	3.53	5.5
6.33	240	6.37	250	6.42	270
12.30	580	12.35	560	12.38	560
25.03	550	25.07	560	25.08	560
36.48	550	36.52	540	36.58	540
49.05	540	49.12	540	49.22	540
72.72	530	72.83	540	72.87	520
96.77	520	96.82	520	96.87	520
120.75	520	120.82	530	120.88	520
144.67	520	144.78	530	144.85	520

Table II.11.
Fe concentrations in effluent for (a) experiment 5, (b) experiment 6, (c) experiment 7, (d) experiment 8.

(a) t 5-1 (hr)	Fe 5-1 (µg/g)	t 5-2 (hr)	Fe 5-2 (µg/g)	t 5-3 (hr)	Fe 5-3 (µg/g)
6.12	0.08	6.53	0.04	3.10	0.004
12.37	0.000	12.48	0.08	6.73	0.000
24.45	0.05	24.58	0.05	12.72	0.07
36.08	0.05	36.15	0.09	24.75	0.08
48.08	0.10	48.17	0.09	36.23	0.05
75.65	0.10	75.57	0.08	48.25	0.05
97.53	0.20	97.67	0.35	75.50	0.10
120.77	0.45	120.82	0.16	98.10	0.20
144.20	0.64	144.32	0.27	120.88	0.27
				144.27	0.23

(b) t 6-1 (hr)	Fe 6-1 (µg/g)	t 6-2 (hr)	Fe 6-2 (µg/g)	t 6-3 (hr)	Fe 6-3 (µg/g)
3.77	0.000	3.57	0.000	3.42	0.000
6.37	0.000	6.42	0.000	6.45	0.02
12.42	0.000	12.48	0.03	12.62	0.009
24.53	0.03	24.63	0.000	24.70	0.009
36.52	0.000	36.63	0.000	36.67	0.03
48.45	0.000	48.52	0.000	48.55	0.000
60.52	0.000	60.68	0.08	60.73	0.000
72.37	0.04	72.40	0.007	72.43	0.000
96.70	0.000	96.77	0.000	96.80	0.000
120.42	0.22	120.53	0.04	120.65	0.000
144.63	0.08	144.67	0.03	145.05	0.07

(c) t 7-1 (hr)	Fe 7-1 (µg/g)	t 7-2 (hr)	Fe 7-2 (µg/g)	t 7-3 (hr)	Fe 7-3 (µg/g)
3.45	0.02	3.68	0.000	3.70	0.000
6.47	0.000	6.52	0.000	6.57	0.05
12.75	0.009	12.85	0.000	12.90	0.000
24.68	0.000	24.72	0.002	24.82	0.05
36.67	0.004	36.70	0.002	36.80	0.002
48.30	0.002	48.38	0.004	48.43	0.05
72.50	0.004	72.55	0.02	72.60	0.04
96.50	0.02	96.57	0.09	96.60	0.05
120.48	0.10	120.67	0.09	120.70	0.000
144.55	0.31	144.65	0.28	144.68	0.05

(d) t 8-1 (hr)	Fe 8-1 (µg/g)	t 8-2 (hr)	Fe 8-2 (µg/g)	t 8-3 (hr)	Fe 8-3 (µg/g)
3.43	0.04	3.47	0.04	3.53	0.04
6.33	0.04	6.37	0.08	6.42	0.07
12.30	0.03	12.35	0.000	12.38	0.07
25.03	0.07	25.07	0.07	25.08	0.03
36.48	0.10	36.52	0.10	36.58	0.06
49.05	0.10	49.12	0.20	49.22	0.20
72.72	0.24	72.83	0.20	72.87	0.24
96.77	0.80	96.82	0.48	96.87	0.30
120.75	0.98	120.82	0.47	120.88	0.23
144.67	1.7	144.78	0.54	144.85	0.71

Table II.12. Filtered Ca values for columns containing sieved calcite.

x (m)	Ca 5-1 (µg/g)	Ca 5-2 (µg/g)	Ca 5-3 (µg/g)	Ca 6-1 (µg/g)	Ca 6-2 (µg/g)	Ca 6-3 (µg/g)
0.053	36	0	39	71	26	6.3
0.078				230	82	28
0.104	140	15	140	490	260	110
0.129				530	520	390
0.154	250	81	190	520	530	530
0.205	400	220	350			
0.230						
0.256	530	500	510			
0.307	490	490	500			
0.332						
0.434				540	540	540
0.535	470	490	510			
0.637						

x (m)	Ca 7-1 (µg/g)	Ca 7-2 (µg/g)	Ca 7-3 (µg/g)	Ca 8-1 (µg/g)	Ca 8-2 (µg/g)	Ca 8-3 (µg/g)
0.053	0.33	4.8	2.2	0.33	0.32	0.54
0.078						
0.104	38	51	39			
0.129				10	3.2	4.5
0.154	180	340	170			
0.205	430	490	450			
0.230				66	120	110
0.256	520	520	520			
0.307						
0.332				180	240	240
0.434	530	530	510	460	480	470
0.535				510	520	510
0.637	510	510	510	520	530	520

Table II.13. Filtered Fe values for columns containing sieved calcite.

x (m)	Fe 5-1 (µg/g)	Fe 5-2 (µg/g)	Fe 5-3 (µg/g)	Fe 6-1 (µg/g)	Fe 6-2 (µg/g)	Fe 6-3 (µg/g)
0.053	310	320	310	280	310	310
0.078				160	280	310
0.104	200	310	250	0.84	110	240
0.129				0.48	0.38	67
0.154	110	240		0.52	0.95	0.62
0.205	31	170	67			
0.230						
0.256	1.5	1.0	1.1			
0.307	1.1	0.80	1.1			
0.332						
0.434				0.20	0.40	0.34
0.535	0.73	0.49	0.66			
0.637						

x (m)	Fe 7-1 (µg/g)	Fe 7-2 (µg/g)	Fe 7-3 (µg/g)	Fe 8-1 (µg/g)	Fe 8-2 (µg/g)	Fe 8-3 (µg/g)
0.053	330	320	330	360	350	340
0.078						
0.104	300	290	290			
0.129				330	330	320
0.154	200	78	230			
0.205	20	1.9	33			
0.230				300	270	260
0.256	1.6	1.8	1.2			
0.307						
0.332				210	150	160
0.434	1.8	1.6	1.1	3.1	1.9	2.1
0.535				2.6	1.4	1.1
0.637	0.89	0.77	0.65	2.3	1.5	0.98

APPENDIX III. Supplementary Hydraulic Data

Table III.1.
Volumetric flow rates for (a) experiment 1, (b) experiment 2, (c) experiment 3, (d) experiment 4. Rates marked with an asterisk where adjusted to maintain flow.

(a) t 1-1 (hr)	Q (ml/min)	t 1-2 (hr)	Q (ml/min)	t 1-3 (hr)	Q (ml/min)
71.60	1.82	71.84	1.80	72.06	1.31
146.67	1.85	146.87	1.89	72.68	2.27*
		529.13	2.07	79.87	2.07*
		529.13	2.02		

(b) t 2-1 (hr)	Q (ml/min)	t 2-2 (hr)	Q (ml/min)	t 2-3 (hr)	Q (ml/min)
6.23	3.99	6.16	3.70	6.28	4.79
12.33	4.03	12.27	3.69	12.41	4.78
36.60	4.26	36.94	3.66	36.90	4.82
48.42	4.01	47.88	3.61	48.28	4.75
72.77	3.70	71.77	3.41	72.48	4.73

(c) t 3-1 (hr)	Q (ml/min)	t 3-2 (hr)	Q (ml/min)	t 3-3 (hr)	Q (ml/min)
72.13	1.89	71.96	1.81	72.40	1.75
97.05	1.41	96.75	1.78	96.92	1.27
120.18	1.83	119.87	1.77	120.05	1.60
144.25	1.41	143.96	1.79	144.17	0.897
168.41	1.09	167.93	1.81	169.18	0.0649

(d) t 4-1 (hr)	Q (ml/min)	t 4-2 (hr)	Q (ml/min)	t 4-3 (hr)	Q (ml/min)
1.11	3.21	1.20	1.84	1.22	2.05
2.13	3.14	4.21	1.86	2.28	1.93
3.15	2.96	5.22	1.87	3.25	1.90
4.21	2.92	6.21	1.89	5.23	1.92
5.14	2.91	9.25	1.88	6.28	1.88
9.16	2.54	10.22	1.89	9.24	1.83
12.21	2.27	11.25	1.88	10.45	1.81
24.23	1.76	24.21	1.96	11.27	1.79
36.31	1.87	36.21	1.96	12.24	1.75
72.24	1.98	48.67	1.75	24.26	1.59
98.31	1.61	96.37	1.84	36.31	1.39
121.66	1.67	120.34	1.19	48.80	0.887
144.72	0.144	145.46	1.14	77.12	0.0851
155.07	0.911*	161.88	0.585	122.69	0.00326
162.47	1.28*			144.59	0.924*
				159.67	0.106*

Table III.2.
Volumetric flow rates for (a) experiment 5, (b) experiment 6, (c) experiment 7, (d) experiment 8.

(a) t 5-1 (hr)	Q (ml/min)	t 5-2 (hr)	Q (ml/min)	t 5-3 (hr)	Q (ml/min)
1.05	3.76	1.17	3.38	1.27	3.77
3.20	3.98	1.38	3.89	3.43	3.63
4.27	3.69	4.38	4.00	4.58	4.13
5.45	3.65	5.53	3.82	5.73	3.71
6.12	3.65	6.25	3.79	6.35	3.52
7.20	3.78	7.37	4.14	7.48	4.45
12.37	3.41	12.48	4.11	12.72	4.84
24.45	3.04	24.58	3.82	24.75	3.93
24.90	4.50	29.37	2.68	29.47	3.37
29.28	3.29	29.42	3.71	29.87	3.94
29.77	3.37	29.82	3.69	36.23	3.13
36.08	4.59	36.15	3.12	48.25	3.43
48.08	3.78	48.17	3.48	59.33	3.62
59.90	4.03	59.30	3.67	60.07	3.39
75.65	3.69	59.93	1.47	75.50	3.50
97.72	3.22	60.00	2.92	98.13	2.93
97.77	3.42	75.57	2.74	98.17	4.47
97.78	4.01	75.60	4.14	120.88	3.25
120.77	3.46	97.88	3.60	132.15	4.41
131.98	3.83	120.82	3.35	146.32	3.53
146.20	3.69	132.03	3.42	155.28	4.18
155.15	4.23	132.10	4.97	156.10	3.74
156.00	3.58	146.27	3.78		
		155.22	3.70		
		156.05	3.73		

(b) t 6-1 (hr)	Q (ml/min)	t 6-2 (hr)	Q (ml/min)	t 6-3 (hr)	Q (ml/min)
0.30	2.09	0.35	1.44	1.17	1.59
1.03	2.05	0.40	1.82	2.25	1.93
2.13	2.00	1.12	1.88	3.13	1.52
3.02	2.00	2.18	1.55	4.23	1.64
4.13	1.93	3.08	2.22	7.12	1.95
6.03	2.15	4.18	2.09	9.30	1.80
6.97	2.02	6.07	1.81	11.10	1.66
9.15	1.70	7.03	1.84	12.22	1.85
10.98	1.99	9.22	2.09	13.42	1.99
12.12	2.03	11.05	2.08	14.45	2.24
13.32	1.35	12.17	2.13	15.50	1.78
14.27	2.06	13.37	1.85	24.33	1.24
15.35	1.97	14.33	1.93	24.38	1.73
24.20	2.24	15.47	2.09	36.30	2.20
36.22	1.70	24.28	2.00	48.22	1.65
48.15	1.74	36.27	1.98	60.28	1.66
60.18	1.82	48.17	1.89	72.12	1.89
72.03	1.55	60.23	1.94	84.27	1.83
84.17	1.46	72.07	2.06	96.47	1.78
96.30	2.13	84.22	1.78	108.38	2.11
108.23	1.61	96.40	1.86	120.12	1.86
120.03	1.43	108.33	1.51	132.18	1.93
132.07	1.38	120.08	1.67	144.38	1.54
132.10	1.77	132.10	1.70	144.52	1.49
144.27	1.90	144.35	1.80	156.20	1.45
156.12	2.15	156.17	1.76		

Table III.2 (continued).

(c) t 7-1 (hr)	Q (ml/min)	t 7-2 (hr)	Q (ml/min)	t 7-3 (hr)	Q (ml/min)
1.12	2.27	1.22	1.92	1.33	2.50
2.22	2.67	2.28	1.92	2.37	1.53
3.08	1.83	3.13	2.27	3.27	2.02
4.17	2.18	4.20	1.82	4.22	1.72
5.13	1.72	5.18	1.87	5.28	1.66
6.05	1.63	6.13	1.92	6.18	1.74
7.18	1.82	7.23	1.48	7.32	2.09
9.42	1.67	9.52	1.91	9.60	1.98
11.08	1.67	11.15	1.48	11.18	1.80
12.40	1.52	12.45	1.90	12.50	1.90
14.13	1.61	14.18	1.80	14.27	2.53
16.25	1.73	16.28	1.65	16.32	1.79
24.32	1.83	24.42	1.93	24.48	1.64
36.28	1.70	36.33	1.81	36.38	1.84
47.98	1.78	48.05	1.80	48.10	1.88
72.18	1.97	72.23	1.80	72.28	1.78
84.43	1.66	84.52	1.94	84.57	1.91
96.15	1.48	96.23	1.79	96.30	1.67
120.10	1.78	120.30	1.91	120.37	1.80
144.22	1.73	144.28	1.73	144.35	1.84
158.02	1.64	158.07	1.66	158.12	1.79

(d) t 8-1 (hr)	Q (ml/min)	t 8-2 (hr)	Q (ml/min)	t 8-3 (hr)	Q (ml/min)
1.03	4.20	1.12	3.37	1.15	3.87
2.32	3.71	2.37	3.50	2.42	3.85
3.22	3.74	3.30	3.60	3.35	3.86
4.17	3.91	4.23	3.65	4.28	3.94
5.05	3.90	5.13	3.74	5.20	3.85
6.08	3.67	6.17	3.63	6.22	3.82
8.02	3.85	8.08	3.58	8.13	3.90
10.33	3.93	10.42	3.69	10.45	3.86
12.10	4.16	12.17	3.71	12.22	3.85
24.78	3.83	24.85	3.52	24.90	3.77
36.27	3.90	36.33	3.70	36.40	3.84
48.85	3.90	48.90	3.61	48.97	3.90
72.55	3.78	72.62	3.56	72.68	3.67
96.60	3.79	96.65	3.45	96.70	3.79
120.50	4.07	120.58	3.50	120.65	3.89
144.50	3.86	144.55	3.57	144.62	3.72
157.25	3.89	157.33	3.53	157.42	3.80

Table III.3. Hydraulic head values at distances x along columns (a) 1-1, (b) 1-2, (c) 1-3.

	x(i) (m)	x(1) (m)	x(2) (m)	x(3) (m)	x(4) (m)	x(5) (m)	x(6) (m)	x(7) (m)	x(8) (m)
	-0.0032	0.045	0.147	0.248	0.350	0.451	0.553	0.655	0.756
(a) t (hr)	h(i) 1-1 (m)	h(1) 1-1 (m)	h(2) 1-1 (m)	h(3) 1-1 (m)	h(4) 1-1 (m)	h(5) 1-1 (m)	h(6) 1-1 (m)	h(7) 1-1 (m)	h(8) 1-1 (m)
0.20	1.179	1.174	1.172	1.173	1.174	1.174	1.172	1.168	1.166
1.62	1.181	1.174	1.172	1.173	1.173	1.174	1.172	1.169	1.166
3.26	1.181	1.174	1.172	1.173	1.174	1.174	1.172	1.168	1.166
6.28	1.181	1.174	1.172	1.173	1.173	1.173	1.171	1.168	1.166
8.23	1.182	1.175	1.173	1.174	1.175	1.174	1.172	1.169	1.166
10.28	1.183	1.175	1.173	1.174	1.174	1.174	1.172	1.169	1.166
12.27	1.183	1.175	1.173	1.174	1.173	1.174	1.171	1.169	1.166
24.23	1.185	1.175	1.173	1.174	1.174	1.175	1.173	1.169	1.167
50.08	1.189	1.175	1.173	1.174	1.175	1.175	1.173	1.169	1.167
52.08	1.190	1.176	1.174	1.175	1.176	1.176	1.174	1.169	1.166
68.33	1.194	1.177	1.175	1.175	1.177	1.177	1.175	1.169	1.167
72.58	1.194	1.176	1.174	1.175	1.177	1.177	1.175	1.169	1.167
77.08	1.195	1.177	1.175	1.175	1.177	1.177	1.175	1.169	1.167
97.65	1.523	1.171	1.170	1.170	1.172	1.171	1.168	1.164	1.162
104.75		1.172	1.170	1.170	1.173	1.172	1.169	1.165	1.162
105.48		1.169	1.168	1.167	1.170	1.168	1.166	1.162	1.160
120.27		1.167	1.165	1.165	1.168	1.167	1.165	1.161	1.159
145.08		1.175	1.174	1.174	1.176	1.176	1.173	1.169	1.168
151.82		1.178	1.177	1.177	1.179	1.178	1.176	1.172	1.171
175.45		1.186	1.185	1.184	1.187	1.186	1.184	1.179	1.176
193.18		1.180	1.178	1.177	1.180	1.179	1.178	1.173	1.172

Table III. 3 (continued).

	x(i) (m)	x(1) (m)	x(2) (m)	x(4) (m)	x(5) (m)	x(6) (m)	x(7) (m)	x(8) (m)
	-0.0032	0.045	0.147	0.350	0.451	0.553	0.655	0.756

(b) t (hr)	h(i) 1-2 (m)	h(1) 1-2 (m)	h(2) 1-2 (m)	h(4) 1-2 (m)	h(5) 1-2 (m)	h(6) 1-2 (m)	h(7) 1-2 (m)	h(8) 1-2 (m)
0.47	1.198	1.180	1.179	1.181	1.178	1.177	1.171	1.167
1.63	1.183	1.174	1.173	1.171	1.169	1.169	1.169	1.167
3.26	1.184	1.174	1.173	1.176	1.174	1.174	1.169	1.167
6.23	1.184	1.174	1.173	1.176	1.174	1.173	1.169	1.167
8.18	1.185	1.174	1.173	1.176	1.174	1.173	1.169	1.167
10.23	1.185	1.174	1.173	1.176	1.174	1.174	1.169	1.167
12.22	1.185	1.174	1.173	1.176	1.174	1.174	1.169	1.167
24.18	1.189	1.175	1.174	1.177	1.174	1.174	1.169	1.167
50.03	1.240	1.175	1.174	1.176	1.174	1.174	1.169	1.167
52.23	1.234	1.174	1.173	1.176	1.174	1.174	1.171	1.169
68.28	1.275	1.174	1.173	1.176	1.174	1.174	1.172	1.169
72.53	1.259	1.174	1.173	1.176	1.174	1.174	1.172	1.169
77.03	1.299	1.174	1.173	1.176	1.174	1.174	1.172	1.169
97.60		1.174	1.173	1.176	1.174	1.174	1.172	1.170
104.70		1.173	1.172	1.176	1.174	1.173	1.172	1.170
105.43		1.174	1.173	1.176	1.174	1.173	1.170	1.168
120.22		1.174	1.173	1.176	1.174	1.173	1.169	1.168

(c) t (hr)	h(i) 1-3 (m)	h(1) 1-3 (m)	h(2) 1-3 (m)	h(3) 1-3 (m)	h(4) 1-3 (m)	h(5) 1-3 (m)	h(7) 1-3 (m)	h(8) 1-3 (m)
0.45	1.204	1.195	1.195	1.193	1.191	1.192	1.190	1.187
1.63	1.206	1.196	1.196	1.194	1.192	1.193	1.191	1.189
3.22	1.208	1.198	1.198	1.195	1.193	1.193	1.192	1.190
6.18	1.211	1.199	1.198	1.197	1.195	1.196	1.194	1.191
8.13	1.212	1.201	1.200	1.198	1.196	1.196	1.195	1.192
10.18	1.210	1.200	1.199	1.196	1.195	1.194	1.192	1.190
12.17	1.210	1.199	1.198	1.195	1.194	1.193	1.191	1.188
24.13	1.218	1.201	1.200	1.198	1.196	1.196	1.194	1.191
49.98	1.260	1.201	1.200	1.198	1.196	1.196	1.194	1.191
52.18	1.284	1.198	1.197	1.196	1.192	1.191	1.190	1.187
68.23		1.190	1.189	1.188	1.185	1.184	1.183	1.181
72.48		1.210	1.208	1.206	1.202	1.201	1.199	1.196
76.98		1.211	1.210	1.208	1.205	1.204	1.207	1.198

Table III.4. Hydraulic head values at distances x along columns (a) 2-1, (b) 2-2, (c) 2-3.

	x(i) (m)	x(1) (m)	x(2) (m)	x(3) (m)	x(4) (m)	x(5) (m)	x(6) (m)	x(7) (m)	x(8) (m)
	-0.0032	0.045	0.147	0.248	0.350	0.451	0.553	0.655	0.756
(a) t (hr)	h(i) 2-1 (m)	h(1) 2-1 (m)	h(2) 2-1 (m)	h(3) 2-1 (m)	h(4) 2-1 (m)	h(5) 2-1 (m)	h(6) 2-1 (m)	h(7) 2-1 (m)	h(8) 2-1 (m)
0.75	1.217	1.201	1.200	1.197	1.195	1.192	1.190	1.190	1.185
1.85	1.222	1.202	1.202	1.199	1.196	1.193	1.192	1.190	1.186
6.03	1.290	1.212	1.212	1.208	1.205	1.202	1.201	1.199	1.195
12.08	1.568	1.212	1.210	1.207	1.204	1.201	1.199	1.198	1.193
27.78		1.209	1.207	1.203	1.199	1.196	1.194	1.192	1.189
37.18		1.209	1.208	1.204	1.202	1.199	1.199	1.198	1.194
48.10		1.216	1.215	1.212	1.209	1.205	1.203	1.202	1.197
71.97		1.208	1.206	1.202	1.199	1.196	1.195	1.193	1.189
96.83		1.212	1.211	1.207	1.203	1.259	1.199	1.197	1.193
(b) t (hr)	h(i) 2-2 (m)	h(1) 2-2 (m)	h(2) 2-2 (m)	h(3) 2-2 (m)	h(4) 2-2 (m)	h(5) 2-2 (m)	h(6) 2-2 (m)	h(7) 2-2 (m)	h(8) 2-2 (m)
0.55	1.276	1.202	1.199	1.198	1.196	1.193	1.190	1.188	1.184
1.42	1.478								
1.63		1.208	1.205	1.203	1.201	1.199	1.195	1.193	1.191
5.82		1.215	1.212	1.211	1.208	1.205	1.201	1.199	1.195
11.92		1.211	1.207	1.206	1.204	1.202	1.197	1.195	1.191
27.58		1.211	1.207	1.209	1.207	1.205	1.200	1.199	1.194
37.05		1.213	1.210	1.198	1.196	1.193	1.188	1.186	1.182
48.26		1.206	1.202	1.201	1.199	1.196	1.192	1.190	1.185
71.78		1.210	1.204	1.203	1.201	1.198	1.194	1.192	1.188

Table III.4 (continued).

	x(i) (m)	x(1) (m)	x(2) (m)	x(3) (m)	x(4) (m)	x(5) (m)	x(6) (m)	x(7) (m)	x(8) (m)
	-0.0032	0.045	0.147	0.248	0.350	0.451	0.553	0.655	0.756
(c) t (hr)	h(i) 2-3 (m)	h(1) 2-3 (m)	h(2) 2-3 (m)	h(3) 2-3 (m)	h(4) 2-3 (m)	h(5) 2-3 (m)	h(6) 2-3 (m)	h(7) 2-3 (m)	h(8) 2-3 (m)
0.800	1.217	1.204	1.201	1.200	1.197	1.193	1.194	1.192	1.188
1.520	1.222	1.205	1.202	1.201	1.197	1.193	1.193	1.195	1.188
5.680	1.266	1.211	1.208	1.206	1.203	1.199	1.199	1.197	1.192
11.780	1.509	1.214	1.209	1.208	1.204	1.200	1.200	1.198	1.194
27.500		1.214	1.209	1.208	1.204	1.199	1.199	1.198	1.193
36.920		1.213	1.207	1.206	1.203	1.197	1.198	1.196	1.192
48.130		1.229	1.222	1.221	1.217	1.213	1.213	1.211	1.207
72.120		1.225	1.211	1.207	1.204	1.199	1.199	1.197	1.193
96.470		1.230	1.219	1.209	1.206	1.200	1.201	1.198	1.195
120.850		1.255	1.226	1.211	1.206	1.201	1.201	1.198	1.194
144.430		1.252	1.244	1.229	1.217	1.210	1.211	1.207	1.204
168.350		1.266	1.257	1.242	1.222	1.206	1.205	1.202	1.198

Table III.5. Hydraulic head values at distances x along columns (a) 3-1, (b) 3-2, (c) 3-3.

	x(i) (m)	x(1) (m)	x(2) (m)	x(3) (m)	x(4) (m)	x(5) (m)	x(6) (m)	x(7) (m)	x(8) (m)
	-0.0032	0.045	0.147	0.248	0.350	0.451	0.553	0.655	0.756
(a) t (hr)	h(i) 3-1 (m)	h(1) 3-1 (m)	h(2) 3-1 (m)	h(3) 3-1 (m)	h(4) 3-1 (m)	h(5) 3-1 (m)	h(6) 3-1 (m)	h(7) 3-1 (m)	h(8) 3-1 (m)
0.53	1.188	1.177	1.178	1.178	1.177	1.176	1.175	1.174	1.172
2.03	1.189	1.178	1.178	1.178	1.177	1.176	1.176	1.175	1.172
3.73	1.189	1.178	1.178	1.178	1.177	1.176	1.175	1.174	1.172
14.47	1.190	1.180	1.180	1.179	1.178	1.177	1.177	1.175	1.174
24.12	1.194	1.183	1.182	1.181	1.180	1.179	1.178	1.177	1.175
30.23	1.190	1.179	1.177	1.177	1.176	1.175	1.175	1.173	1.172
37.53	1.191	1.180	1.176	1.176	1.175	1.174	1.174	1.173	1.171
48.73	1.193	1.183	1.198	1.176	1.175	1.174	1.174	1.173	1.172
73.35	1.212	1.195	1.197	1.178	1.176	1.175	1.175	1.173	1.172
97.08	1.219	1.195	1.196	1.175	1.174	1.173	1.173	1.172	1.171
132.73	1.232	1.219	1.195	1.178	1.177	1.176	1.176	1.174	1.173
156.68	1.239	1.204	1.206	1.179	1.179	1.178	1.178	1.177	1.175
168.70	1.529	1.193	1.207	1.174	1.173	1.177	1.178	1.177	1.176
(b) t (hr)	h(i) 3-2 (m)	h(1) 3-2 (m)	h(2) 3-2 (m)	h(3) 3-2 (m)	h(4) 3-2 (m)	h(5) 3-2 (m)	h(6) 3-2 (m)	h(7) 3-2 (m)	h(8) 3-2 (m)
0.20	1.186	1.188	1.177	1.177	1.176	1.173	1.173	1.172	1.171
1.70	1.186	1.178	1.177	1.177	1.177	1.174	1.173	1.172	1.171
3.40	1.186	1.178	1.177	1.177	1.177	1.173	1.173	1.172	1.171
14.13	1.191	1.179	1.178	1.178	1.178	1.174	1.173	1.172	1.171
23.78	1.194	1.181	1.179	1.178	1.178	1.174	1.174	1.172	1.171
29.90	1.196	1.183	1.179	1.180	1.179	1.175	1.174	1.173	1.172
37.20	1.199	1.183	1.179	1.179	1.179	1.175	1.174	1.173	1.172
73.02	1.225	1.199	1.180	1.180	1.180	1.176	1.175	1.174	1.173
96.75	1.252	1.212	1.181	1.180	1.180	1.176	1.176	1.174	1.173
132.40	1.296	1.216	1.186	1.180	1.180	1.176	1.175	1.174	1.173
156.35		1.227	1.184	1.183	1.182	1.179	1.178	1.176	1.175
168.37		1.228	1.185	1.183	1.182	1.179	1.178	1.177	1.176

Table III.5 (continued).

	x(i) (m)	x(1) (m)	x(2) (m)	x(3) (m)	x(4) (m)	x(5) (m)	x(6) (m)	x(7) (m)	x(8) (m)
	-0.0032	0.045	0.147	0.248	0.350	0.451	0.553	0.655	0.756
(c) t (hr)	h(i) 3-3 (m)	h(1) 3-3 (m)	h(2) 3-3 (m)	h(3) 3-3 (m)	h(4) 3-3 (m)	h(5) 3-3 (m)	h(6) 3-3 (m)	h(7) 3-3 (m)	h(8) 3-3 (m)
0.37	1.196	1.181	1.180	1.179	1.179	1.178	1.177	1.176	1.175
1.87	1.197	1.181	1.180	1.179	1.179	1.178	1.177	1.176	1.174
3.57	1.197	1.181	1.180	1.179	1.179	1.177	1.177	1.176	1.174
14.30	1.197	1.181	1.180	1.179	1.179	1.177	1.177	1.176	1.174
23.95	1.198	1.183	1.179	1.178	1.178	1.177	1.176	1.175	1.173
30.07	1.197	1.184	1.179	1.177	1.177	1.176	1.176	1.175	1.173
37.37	1.198	1.184	1.178	1.177	1.176	1.175	1.175	1.174	1.173
48.57	1.200	1.187	1.177	1.176	1.176	1.175	1.175	1.174	1.172
73.18	1.228	1.206	1.182	1.181	1.180	1.179	1.179	1.178	1.176
96.92	1.228	1.205	1.179	1.178	1.177	1.176	1.177	1.176	1.174
132.57	1.273	1.219	1.180	1.179	1.178	1.177		1.177	1.175
156.52	1.337	1.201	1.177	1.176		1.175		1.175	1.174
168.53		1.174	1.172	1.182	1.181	1.181	1.171	1.171	1.170

Table III.6. Hydraulic head values at distances x along columns (a) 4-1, (b) 4-2, (c) 4-3.

	x(i) (m)	x(1) (m)	x(2) (m)	x(3) (m)	x(4) (m)	x(5) (m)	x(6) (m)	x(7) (m)	x(8) (m)
	-0.0032	0.045	0.147	0.248	0.350	0.451	0.553	0.655	0.756
(a) t (hr)	h(i) 4-1 (m)	h(1) 4-1 (m)	h(2) 4-1 (m)	h(3) 4-1 (m)	h(4) 4-1 (m)	h(5) 4-1 (m)	h(6) 4-1 (m)	h(7) 4-1 (m)	h(8) 4-1 (m)
0.88	1.199	1.186	1.185	1.183	1.182	1.179	1.181	1.180	1.177
2.33	1.199	1.186	1.185	1.183	1.181	1.179	1.181	1.179	1.177
3.48	1.199	1.186	1.185	1.183	1.181	1.178	1.181	1.179	1.177
4.47	1.199	1.186	1.185	1.183	1.182	1.178	1.181	1.179	1.177
5.43	1.199	1.186	1.185	1.183	1.182	1.178	1.181	1.179	1.177
6.47	1.198	1.186	1.185	1.183	1.182	1.178	1.181	1.179	1.177
9.48	1.198	1.186	1.185	1.184	1.182	1.180	1.182	1.180	1.178
12.53	1.197	1.186	1.185	1.184	1.182	1.179	1.182	1.180	1.178
24.82	1.196	1.187	1.187	1.185	1.184	1.182	1.184	1.183	1.182
36.53	1.186	1.179	1.178	1.177	1.176	1.174	1.177	1.176	1.175
48.95	1.233	1.206	1.204	1.201	1.198	1.184	1.196	1.193	1.190
76.40	1.195	1.180	1.179	1.178	1.177	1.175	1.176	1.175	1.173
97.48	1.196	1.179	1.178	1.176	1.176	1.174	1.176	1.174	1.173
121.33	1.353	1.180	1.179	1.178	1.177	1.175	1.176	1.175	1.174
145.25		1.186	1.187	1.187	1.187	1.185	1.189	1.188	1.187

Table III.6 (continued).

	x(i) (m)	x(1) (m)	x(2) (m)	x(3) (m)	x(4) (m)	x(5) (m)	x(6) (m)	x(7) (m)	x(8) (m)
	0 0032	0 045	0 147	0 248	0 350	0 451	0 553	0 655	0 756
(b) t (hr)	h(i) 4-2 (m)	h(1) 4-2 (m)	h(2) 4 2 (m)	h(3) 4-2 (m)	h(4) 4 2 (m)	h(5) 4-2 (m)	h(6) 4-2 (m)	h(7) 4-2 (m)	h(8) 4-2 (m)
0 67	1 186	1 180	1 180	1 179	1 179	1 178	1 175	1.175	1 174
2 12	1 186	1 179	1 179	1 179	1 178	1 177	1 174	1 172	1 173
3 27	1 186	1 179	1 179	1 179	1 178	1 177	1 174	1 172	1 173
4 25	1 191	1 184	1 183	1 182	1 181	1 180	1 176	1.174	1 174
5 22	1 187	1 180	1 180	1 179	1 178	1 177	1 174	1.173	1 173
6 25	1 188	1 180	1 180	1 179	1 178	1 177	1 174	1.173	1 173
9 27	1 188	1 180	1 180	1 180	1 179	1 177	1 174	1 173	1 174
12 32	1 189	1 181	1 181	1 181	1 180	1 177	1 174	1.173	1 174
24 73	1 191	1 183	1 182	1 180	1 180	1 178	1 175	1.173	1 173
36 52	1 194	1 184	1 184	1 183	1 183	1 181	1 178	1.176	1.176
48 73	1 193	1 183	1 183	1 182	1 181	1 180	1 177	1.175	1 175
76 18	1 200	1 187	1 186	1 184	1 183	1 181	1 178	1.176	1.175
97 27	1 208	1 182	1 182	1 181	1 180	1 178	1.175	1.174	1.173
121 18		1 182	1 182	1 182	1 181	1 180	1 177	1.175	1.175
145 03		1 180	1 180	1.179	1 178	1.178	1 175	1.174	1.173

(c) t (hr)	h(i) 4-3 (m)	h(1) 4-3 (m)	h(2) 4-3 (m)	h(3) 4-3 (m)	h(4) 4-3 (m)	h(5) 4-3 (m)	h(6) 4-3 (m)	h(7) 4-3 (m)	h(8) 4-3 (m)
0 52	1.219	1 182	1.181	1.180	1 179	1.178	1 175	1.175	1.174
1 97	1.213	1 181	1.180	1.179	1 178	1.177	1 175	1.175	1.174
3 12	1.211	1 181	1 180	1.179	1 178	1.177	1 175	1.175	1.174
4 10	1.212	1.181	1 180	1.179	1 178	1.176	1.175	1.175	1.173
5 07	1.211	1.181	1.180	1.179	1 178	1.176	1.174	1.174	1.173
6 10	1.211	1.181	1 180	1.179	1 178	1.176	1.174	1.174	1.173
9 12	1.210	1 181	1 180	1.179	1 178	1.176	1.173	1.174	1.173
12 17	1.211	1.182	1 181	1.180	1 179	1.177	1.174	1.175	1.174
24 65	1.217	1 182	1 181	1.180	1 179	1.178	1.175	1.176	1.178
36 42	1.256	1 180	1 179	1.178	1.177	1.176	1.173	1.174	1.177
48 58	1.476	1.183	1 182	1.181	1.180	1.179	1.177	1.178	1.178
76 03	1.503	1.172	1 172	1.172	1.171	1.170	1.178	1.179	1.179
97 12	1.449	1.171	1 171	1.170	1 170	1 169	1.167	1.168	1.168
121 05		1.170	1.170	1.170	1.170	1.169	1.167	1.168	1.168

Table III.7. Hydraulic head values at distances x along columns (a) 5-1, (b) 5-2, (c) 5-3.

	x(i) (m)	x(1) (m)	x(2) (m)	x(3) (m)	x(4) (m)	x(5) (m)	x(6) (m)	x(7) (m)
	-0.0032	0.053	0.129	0.231	0.332	0.434	0.536	0.637
(a) t (hr)	h(i) 5-1 (m)	h(1) 5-1 (m)	h(2) 5-1 (m)	h(3) 5-1 (m)	h(4) 5-1 (m)	h(5) 5-1 (m)	h(6) 5-1 (m)	h(7) 5-1 (m)
2.42	1.142	1.132	1.131	1.125	1.124	1.124	1.122	1.121
4.95	1.148	1.136	1.135	1.129	1.127	1.127	1.126	1.125
12.22	1.145	1.133	1.131	1.127	1.124	1.124	1.122	1.121
25.10	1.150	1.136	1.134	1.129	1.126	1.126	1.124	1.123
28.95	1.148	1.134	1.132	1.127	1.125	1.124	1.123	1.122
29.90	1.150	1.136	1.135	1.130	1.127	1.127	1.125	1.124
36.42	1.153	1.138	1.136	1.131	1.129	1.128	1.126	1.125
49.45	1.155	1.140	1.137	1.132	1.129	1.128	1.129	1.128
58.90	1.159	1.141	1.137	1.133	1.131	1.131	1.128	1.126
60.13	1.157	1.139	1.135	1.132	1.129	1.128	1.126	1.125
76.06	1.163	1.152	1.139	1.132	1.128	1.127	1.125	1.123
97.63	1.162	1.148	1.135	1.129	1.126	1.124	1.123	1.121
120.20	1.171	1.156	1.146	1.132	1.128	1.126	1.125	1.123
130.75	1.172	1.154	1.142	1.129	1.126	1.126	1.123	1.122
146.02	1.175	1.160	1.152	1.129	1.126	1.124	1.123	1.121
155.33	1.179	1.160	1.147	1.129	1.125	1.124	1.123	1.121
155.93	1.184	1.165	1.159	1.134	1.128	1.126	1.123	1.122
156.17	1.178	1.160	1.147	1.128	1.125	1.123	1.122	1.120

Table III.7 (continued).

	x(i) (m)	x(1) (m)	x(2) (m)	x(3) (m)	x(4) (m)	x(5) (m)	x(6) (m)	x(7) (m)
	-0.0032	0.053	0.129	0.231	0.332	0.434	0.536	0.637
(b) t (hr)	h(i) 5-2 (m)	h(1) 5-2 (m)	h(2) 5-2 (m)	h(3) 5-2 (m)	h(4) 5-2 (m)	h(5) 5-2 (m)	h(6) 5-2 (m)	h(7) 5-2 (m)
2.45	1.144	1.132	1.132	1.130	1.128	1.127	1.121	1.120
4.98	1.147	1.134	1.134	1.131	1.129	1.128	1.119	1.119
12.25	1.147	1.132	1.132	1.129	1.127	1.126	1.118	1.118
24.27	1.152	1.136	1.135	1.131	1.129	1.128	1.120	1.121
25.13	1.150	1.136	1.135	1.131	1.129	1.128	1.120	1.120
29.00	1.151	1.135	1.134	1.131	1.129	1.127	1.119	1.119
29.93	1.151	1.137	1.134	1.131	1.129	1.127	1.119	1.119
36.45	1.152	1.137	1.134	1.131	1.129	1.127	1.120	1.119
49.48	1.153	1.140	1.133	1.130	1.128	1.126	1.118	1.119
58.93	1.157	1.137	1.134	1.131	1.128	1.127	1.118	1.118
60.18	1.165	1.142	1.140	1.136	1.128	1.126	1.119	1.119
76.08	1.161	1.145	1.138	1.132	1.130	1.128	1.120	1.120
97.65	1.163	1.145	1.141	1.131	1.128	1.126	1.119	1.119
120.25	1.171	1.156	1.151	1.130	1.128	1.126	1.119	1.118
130.77	1.178	1.157	1.153	1.130	1.128	1.127	1.119	1.118
146.07	1.185	1.166	1.162	1.133	1.130	1.129	1.121	1.120
155.35	1.187	1.172	1.171	1.131	1.128	1.126	1.119	1.118
156.18	1.192	1.174	1.169	1.134	1.131	1.129	1.121	1.121

Table III.7 (continued).

	x(i) (m)	x(1) (m)	x(2) (m)	x(3) (m)	x(4) (m)	x(5) (m)	x(6) (m)	x(7) (m)
	-0.0032	0.053	0.129	0.231	0.332	0.434	0.536	0.637
(c) t (hr)	h(i) 5-3 (m)	h(1) 5-3 (m)	h(2) 5-3 (m)	h(3) 5-3 (m)	h(4) 5-3 (m)	h(5) 5-3 (m)	h(6) 5-3 (m)	h(7) 5-3 (m)
2.47	1.146	1.132	1.132	1.129	1.127	1.128	1.121	1.121
5.02	1.147	1.133	1.133	1.132	1.129	1.128	1.122	1.121
12.28	1.149	1.134	1.133	1.131	1.129	1.128	1.122	1.121
25.15	1.151	1.136	1.135	1.133	1.131	1.130	1.123	1.122
29.03	1.151	1.134	1.134	1.132	1.130	1.129	1.122	1.121
29.95	1.155	1.139	1.138	1.136	1.134	1.133	1.126	1.124
36.45	1.154	1.136	1.135	1.134	1.132	1.130	1.123	1.122
49.50	1.155	1.136	1.135	1.133	1.130	1.129	1.123	1.122
58.98	1.159	1.138	1.135	1.133	1.130	1.129	1.123	1.122
60.20	1.159	1.145	1.137	1.132	1.134	1.133	1.126	1.124
76.13	1.164	1.142	1.136	1.134	1.132	1.130	1.124	1.122
98.82	1.170	1.151	1.139	1.135	1.133	1.131	1.125	1.123
120.27	1.177	1.155	1.185	1.133	1.131	1.129	1.123	1.122
130.78	1.185	1.164	1.154	1.138	1.136	1.134	1.128	1.125
146.08	1.184	1.165	1.159	1.134	1.132	1.130	1.124	1.122
155.42	1.189	1.165	1.157	1.134	1.131	1.129	1.124	1.122
156.20	1.194	1.169	1.164	1.137	1.134	1.132	1.125	1.122

Table III.8. Hydraulic head values at distances x along columns (a) 6-1, (b) 6-2, (c) 6-3.

	x(i) (m)	x(1) (m)	x(2) (m)	x(3) (m)	x(4) (m)	x(5) (m)	x(6) (m)	x(7) (m)
	-0.0032	0.053	0.129	0.231	0.332	0.434	0.536	0.637
(a) t (hr)	h(i) 6-1 (m)	h(1) 6-1 (m)	h(2) 6-1 (m)	h(3) 6-1 (m)	h(4) 6-1 (m)	h(5) 6-1 (m)	h(6) 6-1 (m)	h(7) 6-1 (m)
0.57	1.138	1.128	1.128	1.125	1.124	1.125	1.125	1.124
2.33	1.139	1.129	1.129	1.125	1.124	1.126	1.125	1.124
4.42	1.139	1.129	1.129	1.125	1.124	1.125	1.125	1.124
6.27	1.139	1.130	1.129	1.125	1.124	1.125	1.126	1.125
9.35	1.139	1.130	1.129	1.125	1.124	1.125	1.125	1.124
11.65	1.140	1.130	1.129	1.125	1.124	1.125	1.125	1.124
13.48	1.139	1.129	1.128	1.125	1.124	1.124	1.124	1.123
16.02	1.141	1.140	1.139	1.126	1.125	1.126	1.125	1.123
24.45	1.137	1.125	1.125	1.121	1.120	1.121	1.120	1.119
36.43	1.140	1.127	1.126	1.123	1.122	1.122	1.122	1.121
48.58	1.140	1.126	1.125	1.122	1.121	1.121	1.122	1.121
61.07	1.142	1.126	1.125	1.122	1.121	1.121	1.121	1.160
71.72	1.144	1.126	1.125	1.122	1.121	1.120	1.120	1.153
84.32	1.144	1.125	1.123	1.119	1.118	1.118	1.118	
96.53	1.149	1.128	1.125	1.122	1.121	1.122	1.122	
108.73	1.152	1.130	1.126	1.123	1.122	1.122	1.121	
120.65	1.158	1.135	1.130	1.126	1.125	1.126	1.126	1.149
131.83	1.156	1.131	1.126	1.122	1.121	1.122	1.122	1.142
144.82	1.163	1.136	1.130	1.126	1.124	1.125	1.125	1.140
156.55	1.164	1.133	1.126	1.122	1.121	1.121	1.121	1.139

Table III.8 (continued).

	x(i) (m)	x(1) (m)	x(2) (m)	x(3) (m)	x(4) (m)	x(5) (m)	x(6) (m)
	-0.0032	0.053	0.129	0.231	0.332	0.434	0.536
(b) t (hr)	h(i) 6-2 (m)	h(1) 6-2 (m)	h(2) 6-2 (m)	h(3) 6-2 (m)	h(4) 6-2 (m)	h(5) 6-2 (m)	h(6) 6-2 (m)
0.62	1.133	1.127	1.126	1.125	1.124	1.123	1.118
2.37	1.139	1.131	1.130	1.129	1.128	1.127	1.122
4.43	1.136	1.128	1.127	1.126	1.125	1.125	1.119
6.28	1.136	1.129	1.128	1.127	1.126	1.125	1.120
9.37	1.138	1.131	1.130	1.129	1.128	1.127	1.121
11.68	1.140	1.132	1.131	1.130	1.129	1.128	1.122
13.50	1.139	1.132	1.131	1.130	1.129	1.128	1.122
16.03	1.142	1.135	1.134	1.133	1.132	1.131	1.124
24.48	1.140	1.132	1.131	1.130	1.129	1.128	1.122
36.47	1.137	1.129	1.128	1.127	1.126	1.125	1.119
48.60	1.138	1.129	1.128	1.127	1.126	1.125	1.119
61.13	1.144	1.134	1.133	1.131	1.130	1.129	1.123
71.80	1.143	1.132	1.131	1.130	1.128	1.127	1.121
84.35	1.140	1.129	1.127	1.126	1.124	1.123	1.118
96.57	1.139	1.129	1.127	1.125	1.124	1.123	1.117
108.75	1.140	1.130	1.126	1.125	1.123	1.122	1.117
120.86	1.143	1.132	1.128	1.127	1.125	1.125	1.119
131.87	1.142	1.132	1.127	1.126	1.124	1.123	1.118
144.85	1.144	1.133	1.127	1.126	1.124	1.123	1.118
156.58	1.144	1.134	1.127	1.125	1.124	1.123	1.117

Table III.8 (continued).

	x(i) (m)	x(1) (m)	x(2) (m)	x(3) (m)	x(4) (m)	x(5) (m)	x(6) (m)	x(7) (m)
	-0.0032	0.053	0.129	0.231	0.332	0.434	0.536	0.637
(c) t (hr)	h(i) 6-3 (m)	h(1) 6-3 (m)	h(2) 6-3 (m)	h(3) 6-3 (m)	h(4) 6-3 (m)	h(5) 6-3 (m)	h(6) 6-3 (m)	h(7) 6-3 (m)
0.65	1.131	1.125	1.124	1.124	1.121	1.121	1.117	1.117
2.38	1.132	1.125	1.124	1.124	1.120	1.121	1.117	1.117
4.45	1.134	1.127	1.126	1.125	1.123	1.123	1.119	1.119
6.47	1.134	1.127	1.126	1.125	1.123	1.123	1.119	1.119
9.38	1.135	1.128	1.127	1.126	1.124	1.124	1.119	1.119
11.70	1.138	1.131	1.130	1.129	1.127	1.127	1.123	1.122
13.52	1.142	1.135	1.133	1.133	1.131	1.130	1.127	1.126
16.05	1.134	1.128	1.127	1.126	1.122	1.123	1.119	1.119
24.55	1.138	1.130	1.129	1.128	1.125	1.125	1.122	1.121
36.53	1.136	1.129	1.128	1.127	1.124	1.125	1.121	1.120
48.63	1.139	1.130	1.129	1.128	1.126	1.126	1.122	1.121
61.15	1.142	1.133	1.132	1.131	1.129	1.129	1.124	1.124
71.82	1.144	1.133	1.132	1.131	1.129	1.129	1.124	1.124
84.37	1.141	1.130	1.128	1.127	1.124	1.125	1.121	1.120
96.58	1.140	1.127	1.125	1.124	1.121	1.122	1.118	1.117
108.78	1.149	1.135	1.132	1.131	1.130	1.129	1.126	1.125
120.90	1.151	1.137	1.134	1.133	1.131	1.130	1.126	1.125
131.88	1.151	1.136	1.132	1.132	1.129	1.129	1.125	1.124
144.47	1.149	1.134	1.133	1.128	1.125	1.125	1.121	1.120
156.60	1.154	1.135	1.130	1.130	1.128	1.128	1.124	1.123

Table III.9. Hydraulic head values at distances x along columns (a) 7-1, (b) 7-2, (c) 7-3.

	x(i) (m)	x(1) (m)	x(2) (m)	x(3) (m)	x(4) (m)	x(5) (m)	x(6) (m)	x(7) (m)
	-0.0032	0.053	0.129	0.231	0.332	0.434	0.536	0.637
(a) t (hr)	h(i) 7-1 (m)	h(1) 7-1 (m)	h(2) 7-1 (m)	h(3) 7-1 (m)	h(4) 7-1 (m)	h(5) 7-1 (m)	h(6) 7-1 (m)	h(7) 7-1 (m)
0.98	1.129	1.126	1.127	1.125	1.125	1.124	1.125	1.123
2.02	1.128	1.125	1.125	1.125	1.124	1.123	1.123	1.121
4.83	1.131	1.128	1.128	1.127	1.126	1.126	1.125	1.124
7.62	1.130	1.127	1.127	1.126	1.125	1.124	1.124	1.123
9.85	1.133	1.129	1.130	1.129	1.128	1.127	1.127	1.125
13.05	1.131	1.127	1.128	1.127	1.126	1.125	1.124	1.123
15.62	1.131	1.127	1.128	1.126	1.125	1.124	1.124	1.122
24.22	1.130	1.126	1.127	1.125	1.124	1.123	1.124	1.121
36.15	1.129	1.124	1.125	1.124	1.123	1.122	1.123	1.120
47.82	1.133	1.127	1.129	1.128	1.127	1.126	1.126	1.124
72.05	1.133	1.129	1.128	1.127	1.126	1.125	1.125	1.123
95.48	1.127	1.124	1.122	1.121	1.120	1.119	1.118	1.117
119.97	1.136	1.128	1.127	1.120	1.119	1.118	1.123	1.121
143.45	1.131	1.128	1.127	1.124	1.123	1.122	1.121	1.120
157.25	1.134	1.131	1.130	1.127	1.126	1.125	1.124	1.123

Table III.9 (continued).

	x(i) (m)	x(1) (m)	x(2) (m)	x(3) (m)	x(4) (m)	x(5) (m)	x(6) (m)	x(7) (m)
	-0.0032	0.053	0.129	0.231	0.332	0.434	0.536	0.637

(b) t (hr)	h(i) 7-2 (m)	h(1) 7-2 (m)	h(2) 7-2 (m)	h(3) 7-2 (m)	h(4) 7-2 (m)	h(5) 7-2 (m)	h(6) 7-2 (m)	h(7) 7-2 (m)
0.98	1.131	1.126	1.127	1.127	1.125	1.125	1.124	1.122
2.00	1.132	1.126	1.127	1.127	1.124	1.125	1.124	1.122
4.83	1.130	1.126	1.125	1.125	1.123	1.123	1.122	1.119
7.62	1.130	1.126	1.125	1.125	1.123	1.122	1.121	1.118
9.85	1.131	1.126	1.125	1.125	1.123	1.122	1.121	1.119
13.05	1.134	1.130	1.129	1.128	1.127	1.126	1.124	1.122
15.62	1.130	1.127	1.125	1.125	1.123	1.122	1.121	1.118
24.23	1.132	1.127	1.126	1.126	1.125	1.124	1.122	1.120
36.15	1.132	1.128	1.198	1.126	1.125	1.124	1.123	1.120
47.83	1.131	1.126	1.133	1.149	1.123	1.122	1.121	1.118
72.05	1.130	1.125	1.123	1.187	1.122	1.121	1.120	1.117
95.50	1.128	1.124	1.121	1.193	1.120	1.119	1.118	1.115
119.98	1.132	1.127	1.124	1.191	1.123	1.122	1.121	1.118
143.63	1.132	1.128	1.125	1.200	1.122	1.121	1.120	1.117
157.25	1.134	1.130	1.127		1.123	1.122	1.121	1.118

(c) t (hr)	h(i) 7-3 (m)	h(1) 7-3 (m)	h(2) 7-3 (m)	h(3) 7-3 (m)	h(4) 7-3 (m)	h(5) 7-3 (m)	h(6) 7-3 (m)	h(7) 7-3 (m)
0.98	1.131	1.129	1.128	1.127	1.125	1.124	1.126	1.125
2.02	1.131	1.127	1.126	1.125	1.123	1.122	1.124	1.123
4.83	1.130	1.127	1.126	1.123	1.122	1.121	1.123	1.122
7.62	1.130	1.126	1.125	1.123	1.121	1.121	1.123	1.122
9.90	1.136	1.132	1.131	1.130	1.127	1.127	1.128	1.127
13.05	1.136	1.131	1.130	1.128	1.126	1.125	1.127	1.125
15.63	1.134	1.130	1.129	1.127	1.125	1.125	1.126	1.125
24.23	1.131	1.127	1.126	1.124	1.122	1.121	1.123	1.121
47.85	1.133	1.127	1.171	1.124	1.122	1.121	1.123	1.122
72.03	1.134	1.127	1.172	1.125	1.123	1.122	1.124	1.122
95.52	1.132	1.127	1.177	1.123	1.121	1.120	1.122	1.121
119.98	1.133	1.128	1.177	1.123	1.121	1.120	1.122	1.121
143.63	1.135	1.129	1.178	1.135	1.122	1.130	1.123	1.121
157.37	1.138	1.132	1.129	1.126	1.125	1.123	1.125	1.124

Table III.10. Hydraulic head values at distances x along columns (a) 8-1, (b) 8-2, (c) 8-3.

	x(i) (m)	x(1) (m)	x(2) (m)	x(3) (m)	x(4) (m)	x(5) (m)	x(6) (m)	x(7) (m)
	-0.0032	0.053	0.129	0.231	0.332	0.434	0.536	0.637
(a) t (hr)	h(i) 8-1 (m)	h(1) 8-1 (m)	h(2) 8-1 (m)	h(3) 8-1 (m)	h(4) 8-1 (m)	h(5) 8-1 (m)	h(6) 8-1 (m)	h(7) 8-1 (m)
1.88	1.144	1.135	1.134	1.132	1.131	1.130	1.128	1.126
3.88	1.145	1.136	1.134	1.133	1.131	1.130	1.128	1.127
5.82	1.145	1.136	1.134	1.133	1.131	1.129	1.127	1.125
8.33	1.152	1.142	1.139	1.138	1.136	1.135	1.127	1.126
12.68	1.147	1.139	1.136	1.134	1.132	1.131	1.129	1.127
24.65	1.149	1.140	1.137	1.135	1.133	1.132	1.130	1.128
36.12	1.150	1.141	1.138	1.141	1.134	1.133	1.130	1.129
48.70	1.154	1.143	1.140	1.172	1.136	1.133	1.133	1.132
72.43	1.151	1.141	1.138	1.192	1.131	1.129	1.127	1.176
96.12	1.156	1.148	1.139	1.194	1.133	1.131	1.128	1.172
120.25	1.162	1.153	1.144	1.196	1.135	1.133	1.130	1.175
144.13	1.164	1.154	1.145	1.212	1.135	1.130	1.128	1.174
157.70	1.172	1.156	1.154	1.192	1.139	1.157	1.130	1.179
(b) t (hr)	h(i) 8-2 (m)	h(1) 8-2 (m)	h(2) 8-2 (m)	h(3) 8-2 (m)	h(4) 8-2 (m)	h(5) 8-2 (m)	h(6) 8-2 (m)	h(7) 8-2 (m)
1.90	1.144	1.135	1.134	1.131	1.129	1.127	1.126	1.123
3.93	1.146	1.137	1.134	1.131	1.129	1.128	1.126	1.123
5.83	1.146	1.138	1.135	1.132	1.130	1.128	1.126	1.123
8.35	1.154	1.143	1.141	1.139	1.137	1.135	1.133	1.131
12.70	1.148	1.139	1.136	1.133	1.131	1.129	1.127	1.124
24.67	1.147	1.137	1.134	1.132	1.130	1.128	1.126	1.127
36.15	1.151	1.140	1.137	1.135	1.133	1.131	1.124	1.132
48.73	1.155	1.143	1.150	1.136	1.140	1.155	1.133	1.141
72.37	1.150	1.142	1.182	1.131	1.161	1.185	1.126	1.146
96.13	1.156	1.143	1.140	1.134	1.149	1.203	1.159	1.143
120.27	1.162	1.146	1.142	1.137	1.148	1.198	1.159	1.147
144.17	1.167	1.149	1.145	1.139	1.148	1.211	1.161	1.156
157.78	1.173	1.151	1.149					

Table III.10 (continued).

	x(i) (m)	x(1) (m)	x(2) (m)	x(3) (m)	x(4) (m)	x(5) (m)	x(6) (m)	x(7) (m)
	-0.0032	0.053	0.129	0.231	0.332	0.434	0.536	0.637
(c) t (hr)	h(i) 8-3 (m)	h(1) 8-3 (m)	h(2) 8-3 (m)	h(3) 8-3 (m)	h(4) 8-3 (m)	h(5) 8-3 (m)	h(6) 8-3 (m)	h(7) 8-3 (m)
1.91	1.143	1.134	1.133	1.130	1.128	1.127	1.124	1.123
3.95	1.146	1.135	1.133	1.131	1.128	1.127	1.126	1.125
5.85	1.145	1.134	1.132	1.129	1.127	1.125	1.124	1.122
8.37	1.146	1.135	1.133	1.130	1.128	1.126	1.124	1.123
12.75	1.145	1.134	1.132	1.130	1.127	1.126	1.124	1.123
24.68	1.144	1.133	1.130	1.128	1.126	1.124	1.122	1.121
36.17	1.147	1.134	1.132	1.135	1.127	1.126	1.124	1.122
48.77	1.149	1.135	1.132	1.177	1.128	1.126	1.124	1.123
72.40	1.151	1.139	1.134	1.177	1.127	1.126	1.124	1.123
96.15	1.156	1.149	1.136	1.209	1.127	1.125	1.123	1.122
120.28	1.163	1.143	1.140	1.206	1.128	1.125	1.124	1.144
144.18	1.171	1.145	1.142	1.202	1.134	1.127	1.125	1.180
157.75	1.179	1.148	1.145	1.204	1.133	1.127	1.137	1.189

Table III.11.
Hydraulic conductivity values, normalized with respect to the calculated mean initial value for experiment 1, for selected intervals along columns (a) 1-1, (b) 1-2.

	x = 0-0.045 m	x = 0.045 - 0.147 m
(a) t 1-1 (hr)	K(i-1)/Ko	K(1-2)/Ko
0.20	1.3	0.60
1.62	0.22	0.60
3.26	0.22	0.60
6.28	0.22	0.60
8.23	0.22	0.60
10.28	0.16	0.60
12.27	0.098	0.60
24.23	0.098	0.60
50.08	0.057	0.60
52.08	0.057	0.60
68.33	0.043	0.60
72.58	0.040	0.60
77.08	0.040	0.60
97.65	0.0015	1.2
104.75		0.60
105.48		1.2
120.27		0.62
145.08		1.2
151.82		1.2
175.45		1.2
193.18		0.62

(b) t 1-2 (hr)	K(i-1)/Ko	K(1-2)/Ko
0.47	0.039	1.2
1.63	0.12	1.2
3.26	0.096	1.2
6.23	0.096	1.2
8.18	0.082	1.2
10.23	0.082	1.2
12.22	0.082	1.2
24.18	0.056	1.2
50.03	0.0087	1.2
52.23	0.0095	1.2
68.28	0.0055	1.2
72.53	0.0065	1.2
77.03	0.0044	1.2
97.60		1.2
104.70		1.2
105.43		1.2
120.22		1.3

Table III.12.
Hydraulic conductivity values, normalized with respect to the calculated mean initial value for experiment 2, for selected intervals along columns (a) 2-1, (b) 2-2, (c) 2-3

	x = 0-0.045 m	x = 0.045 - 0.147 m	x = 0.147 - 0.248 m	x = 0.248 - 0.350 m	x = 0.350 - 0.451 m
(a) t 2-1 (hr)	K(i-1)/Ko	K(1-2)/Ko			
0.75	0.20	2.7			
1.85	0.12				
6.03	0.017				
12.08	0.0034	1.3			
27.78		1.4			
37.18		2.8			
48.10		2.7			
71.97		1.2			
96.83		2.5			
(b) t 2-2 (hr)	K(i-1)/Ko	K(1-2)/Ko			
0.55	0.015	0.74			
1.63		0.74			
5.82		0.74			
11.92		0.55			
27.58		0.55			
37.05		0.73			
48.26		0.54			
71.78		0.34			
(c) t 2-3 (hr)	K(i-1)/Ko	K(1-2)/Ko			
0.80	1.1	0.70	2.1	0.70	0.53
1.52	0.21	0.79	2.4	0.59	0.59
5.68	0.024	0.79	1.2	0.79	0.59
11.78	0.0037	0.47	2.4	0.59	0.59
27.50		0.48	2.4	0.60	0.48
36.92		0.40	2.4	0.80	0.40
48.13		0.34	2.3	0.59	0.59
72.12		0.17	0.59	0.78	0.47
96.47		0.21	0.23	0.78	0.39
120.85		0.081	0.16	0.47	0.47
144.43		0.29	0.16	0.19	0.33
168.35		0.26	0.16	0.12	0.15

Table III.13.
Hydraulic conductivity values, normalized with respect to the calculated mean initial value for experiment 3, for selected intervals along columns (a) 3-1, (b) 3-2, (c) 3-3.

	x = 0-0.045 m	x = 0.045 - 0.147 m	x = 0.147 - 0.248 m	x = 0.248 - 0.350 m
(a) t 3-1 (hr)	K(i-1)/Ko	K(1-2)/Ko	K(2-3)/Ko	K(3-4)/Ko
0.53	0.066			0.94
2.03	0.066			0.94
3.73	0.066			0.94
14.47	0.078		0.94	0.94
24.12	0.066	0.94	0.94	0.94
30.23	0.066	0.47		0.94
37.53	0.066	0.23		0.94
48.73	0.078			0.94
73.35	0.034			0.47
97.08	0.015			0.70
132.73	0.048			0.90
156.68	0.0098			
168.70	0.00071			0.54
(b) t 3-2 (hr)	K(i-1)/Ko	K(1-2)/Ko	K(2-3)/Ko	K(3-4)/Ko
0.20				0.89
1.70	0.11	0.89		
3.40	0.11	0.89		
14.13	0.053	0.89		
23.78	0.047	0.45	0.89	
29.90	0.047	0.22		0.89
37.20	0.035	0.22		
73.02	0.018	0.047		
96.75	0.011	0.028	0.88	
132.40	0.0051	0.029	0.15	
156.35		0.021	0.89	0.89
168.37		0.021	0.45	0.90
(c) t 3-3 (hr)	K(i-1)/Ko	K(1-2)/Ko	K(2-3)/Ko	K(3-4)/Ko
0.37	0.036	0.87	0.87	
1.87	0.033	0.87	0.87	
3.57	0.033	0.87	0.87	
14.30	0.033	0.87	0.87	
23.95	0.036	0.22	0.87	
30.07	0.044	0.17	0.43	
37.37	0.040	0.14	0.87	0.87
48.57	0.045	0.087	0.87	
73.18	0.022	0.036	0.87	0.87
96.92	0.014	0.024	0.63	0.63
132.57	0.0070	0.020	0.79	0.79
156.52	0.0015	0.018	0.44	
168.53		0.016		0.032

Table III.14.
Hydraulic conductivity values, normalized with respect to the calculated mean initial value for experiment 4, for selected intervals along columns (a) 4-1, (b) 4-2, (c) 4-3.

	x = 0-0.045 m	x = 0.045 - 0.147 m	x = 0.147 - 0.248 m
(a) t 4-1 (hr)	K(i-1)/Ko	K(1-2)/Ko	K(2-3)/Ko
0.88	0.17	1.9	0.96
2.33	0.16	1.9	0.94
3.48	0.14	1.8	0.89
4.47	0.14	1.8	0.88
5.43	0.14	1.8	0.87
6.47	0.17	1.7	0.87
8.48	0.12	1.5	1.5
12.53	0.11	1.4	1.4
24.82	0.10		0.53
36.37	0.22	1.1	1.1
48.95	0.022	0.56	0.37
76.40	0.052	1.1	1.2
97.48	0.033	0.97	0.48
121.33	0.0026	1.0	1.0
145.25	0.000098		
(b) t 4-2 (hr)	K(i-1)/Ko	K(1-2)/Ko	K(2-3)/Ko
0.67	0.37		1.1
2.12	0.21		
3.27	0.21		
4.25	0.21	1.1	1.1
5.22	0.22		1.1
6.25	0.15		1.1
9.27	0.15		
12.32	0.15		
24.73	0.17	1.2	0.59
36.42	0.10		1.2
48.73	0.084		1.1
76.18	0.058	1.1	0.55
97.27	0.023		1.1
145.03			0.68
(c) t 4-3 (hr)	K(i-1)/Ko	K(1-2)/Ko	K(2-3)/Ko
0.52	0.017	1.2	1.2
1.97	0.019	1.2	1.2
3.12	0.020	1.1	1.1
4.10	0.019	1.1	1.1
5.07	0.020	1.2	1.2
6.10	0.020	1.1	1.1
9.12	0.020	1.1	1.1
12.17	0.019	1.0	1.0
24.65	0.014	0.95	0.95
36.42	0.0051	0.84	0.84
48.58	0.00081	0.53	0.53
76.03	0.000068		
97.12	0.0000040		0.0026
121.05	0.0000021		

Table III.15.
Hydraulic conductivity values, normalized with respect to the calculated mean initial value for experiment 5, for selected intervals along columns (a) 5-1, (b) 5-2, (c) 5-3.

	x = 0-0.053 m	x = 0.053 - 0.129 m	x = 0.129 - 0.231 m	x = 0.231 - 0.332 m
(a) t 5-1 (hr)	K(i-1)/Ko	K(1-2)/Ko	K(2-3)/Ko	K(3-4)/Ko
2.42		2.01	0.335	2.01
4.95	0.34	1.84	0.307	0.92
12.22	0.26	0.86	0.430	0.57
25.10	0.44	1.14	0.454	0.76
28.95	0.15	0.83	0.332	0.83
29.90	0.16	1.70	0.339	0.57
36.42	0.35	1.16	0.464	1.16
49.45	0.18	0.64	0.381	0.64
58.90	0.10	0.45	0.450	0.90
60.20	0.275	0.25	0.339	0.68
76.06	0.569	0.14	0.265	0.47
97.63	0.182	0.14	0.297	0.59
120.20	0.144	0.17	0.125	0.44
130.75	0.121	0.16	0.148	0.64
146.02	0.170	0.23	0.081	0.62
155.33	0.133	0.16	0.119	0.53
155.93	0.094	0.30	0.072	0.30
156.17	0.108	0.14	0.095	0.60

(b) t 5-2 (hr)	K(i-1)/Ko	K(1-2)/Ko	K(2-3)/Ko	K(3-4)/Ko
2.45	0.462		0.980	0.99
4.98	0.326		0.658	0.99
12.25	0.231		0.691	1.04
24.27	0.157	1.93	0.482	0.96
25.13	0.229	1.93	0.482	0.96
29.00	0.102	1.59	0.531	0.80
29.93	0.206	0.62	0.620	0.93
36.45	0.115	0.53	0.525	0.79
58.93	0.089	0.62	0.617	0.62
60.13	0.042	0.26	0.261	0.35
97.65	0.106	0.45		0.60
120.25	0.134	0.34	0.080	0.84
130.77	0.102	0.52	0.090	1.04
146.07	0.105	0.48	0.066	0.64
156.18	0.113	0.38	0.054	0.63

Table III.15 (continued).

	x = 0-0.053 m	x = 0.053 - 0.129 m	x = 0.129 - 0.231 m	x = 0.231 - 0.332 m
(c) t 5-3 (hr)	K(i-1)/Ko	K(1-2)/Ko	K(2-3)/Ko	K(3-4)/Ko
2.47	0.20		0.61	0.91
5.02	0.30		2.1	0.69
12.28	0.097	1.5	0.72	0.72
25.15	0.20	2.0	0.99	0.99
29.03	0.10		0.85	0.85
29.95	0.17	2.0	0.99	0.99
36.45	0.081	1.6	1.6	0.79
49.50	0.087	1.7	0.86	0.58
58.98	0.080	0.61	0.91	0.61
60.18	0.061	0.85	0.85	0.57
76.13	0.070	0.29	0.88	0.88
98.82	0.096	0.15	0.46	0.91
120.27	0.062			0.82
130.78	0.12	0.22	0.14	1.1
146.08	0.092	0.30	0.071	0.89
155.42	0.081	0.26	0.092	0.70
156.20	0.063	0.38	0.070	0.63

Table III.16.
Hydraulic conductivity values, normalized with respect to the calculated mean initial value for experiment 6, for selected intervals along columns (a) 6-1, (b) 6-2, (c) 6-3.

	x = 0-0.053 m	x = 0.053 - 0.129 m	x = 0.129 - 0.231 m
(a) t 6-1 (hr)	K(i-1)/Ko	K(1-2)/Ko	K(2-3)/Ko
0.57	0.12		0.081
2.33	0.11		0.25
4.42	0.098		0.24
6.27	0.16	1.1	0.27
9.35	0.094	0.86	0.21
11.65	0.11	1.0	0.26
13.48	0.054	0.68	0.23
16.02		0.99	0.076
24.45	0.093		0.28
36.43	0.051	0.86	0.29
48.58	0.047	0.88	0.29
61.07	0.042	0.92	0.31
71.72	0.029	0.78	0.26
84.32	0.025	0.37	0.18
96.53	0.036	0.36	0.36
108.73	0.024	0.20	0.27
120.85	0.019	0.14	0.18
131.83	0.019	0.16	0.20
144.82	0.022	0.16	0.24
156.55	0.022	0.16	0.27
(b) t 6-2 (hr)	K(i-1)/Ko	K(1-2)/Ko	K(2-3)/Ko
0.62	0.22	0.82	0.82
2.37	0.099	0.78	0.78
4.43	0.20	1.1	1.1
6.28	0.19	0.91	0.91
9.37	0.32	1.1	1.1
11.68	0.21	1.1	1.1
13.50	0.21	0.93	0.93
16.03	0.32	1.1	1.1
24.48	0.18	1.0	1.0
36.47	0.17	1.0	1.0
48.60	0.12	0.95	0.95
61.13	0.099	0.98	0.49
71.80	0.093	1.0	1.0
84.35	0.072	0.45	0.90
96.57	0.092	0.47	0.47
108.75	0.064	0.19	0.76
120.86	0.064	0.21	0.84
131.87	0.078	0.17	0.86
144.85	0.073	0.15	0.91
156.58	0.083	0.13	0.44

Table III.16 (continued).

	x = 0-0.053 m	x = 0.053 - 0.129 m	x = 0.129 - 0.231 m	x = 0.231 - 0.332 m
(c) t 6-3 (hr)	K(i-1)/Ko	K(1-2)/Ko	K(2-3)/Ko	K(3-4)/Ko
0.65	0.21	0.80		0.27
2.38	0.24	0.97		0.24
4.45	0.15	0.83	0.83	0.41
6.47	0.14	0.81	0.81	0.41
9.38	0.19	0.91	0.91	0.45
11.70	0.21	0.93	0.93	0.47
13.52	0.26	0.50		0.50
16.05	0.31	0.90	0.90	0.22
24.55	0.089	0.74	0.74	0.25
36.53	0.40	1.1	1.1	0.37
48.63	0.089	0.83	0.83	0.42
61.15	0.090	0.84	0.84	0.42
71.82	0.079	0.95	0.95	0.48
84.37	0.075	0.46	0.92	0.31
96.58	0.055	0.45	0.90	0.30
108.78	0.064	0.35	1.1	1.1
120.90	0.052	0.31	0.94	0.47
131.88	0.050	0.24		0.32
144.47	0.036	0.76	0.15	0.25
156.60	0.025	0.15		0.37

Table III.17.
Hydraulic conductivity values, normalized with respect to the calculated mean initial value for experiment 7, for selected intervals along columns (a) 7-1, (b) 7-2, (c) 7-3.

	x = 0-0.053 m	x = 0.053 - 0.129 m	x = 0.129 - 0.231 m	x = 0.231 - 0.332 m
(a) t 7-1 (hr)	K(i-1)/Ko	K(1-2)/Ko	K(2-3)/Ko	K(3-4)/Ko
0.98			0.57	
2.02				1.3
4.83			0.87	0.87
7.62			0.92	0.92
9.85			0.84	0.84
13.05	2.3		0.77	0.77
15.62			0.44	0.87
24.22			0.46	0.92
36.15	0.62		0.86	0.86
47.82	0.31		0.90	0.90
72.05		0.99	0.99	0.99
95.48		0.37	0.75	0.75
119.97	0.13	0.90	0.13	0.90
143.45		0.87	0.29	0.87
157.25		0.83	0.28	0.83
(b) t 7-2 (hr)	K(i-1)/Ko	K(1-2)/Ko	K(2-3)/Ko	K(3-4)/Ko
0.98	3.0			0.48
2.00	0.43			0.32
4.83		0.94		0.47
7.62	1.4	0.75		0.37
9.85	2.6	0.96		0.48
13.05		0.96	0.96	0.96
15.62		0.42		0.42
24.23	3.6	0.97		0.97
36.15				0.91
47.83	1.0			
72.05	1.0	0.45		
95.50		0.33		
119.98	2.6	0.32		
143.63		0.29		
157.25		0.28		
(c) t 7-3 (hr)	K(i-1)/Ko	K(1-2)/Ko	K(2-3)/Ko	K(3-4)/Ko
0.98		1.3	1.3	0.63
2.02	2.7	0.77	0.77	0.39
4.83		0.84	0.28	0.84
7.62		1.1	0.53	0.53
9.90		1.0	1.0	0.33
13.05	2.3	0.96	0.48	0.48
15.63		0.90	0.45	0.45
24.23		0.83	0.41	0.41
47.85	0.39			0.47
72.03	0.19			0.45
95.52	0.55			0.42
119.98	1.0			0.45
143.63	0.35			
157.37	0.31	0.30	0.30	0.90

Table III.18.
Hydraulic conductivity values, normalized with respect to the calculated mean initial value for experiment 8, for selected intervals along columns (a) 8-1, (b) 8-2, (c) 8-3.

	x = 0-0.053 m	x = 0.053 - 0.129 m	x = 0.129 - 0.231 m
(a) t 8-1 (hr)	K(i-1)/Ko	K(1-2)/Ko	K(2-3)/Ko
1.88		1.9	0.94
3.88		0.99	2.0
5.82		0.93	1.9
8.33	3.3	0.65	1.9
12.68		0.70	1.0
24.65		0.64	0.97
36.12		0.65	
48.70	0.87	0.65	
72.43	2.0	0.64	
96.12		0.21	
120.25		0.23	
144.13	3.6	0.22	
157.70	0.16	0.98	
(b) t 8-2 (hr)	K(i-1)/Ko	K(1-2)/Ko	K(2-3)/Ko
1.90	5.0	1.8	0.59
3.93		0.61	0.61
5.83		0.61	0.61
8.35	0.47	0.90	0.90
12.70		0.62	0.62
24.67	0.82	0.59	0.89
36.15	0.58	0.62	0.93
48.73	0.33		
72.37			
96.13	0.21	0.58	0.29
120.27	0.13	0.44	0.35
144.17	0.10	0.45	0.30
157.78	0.070	0.89	
(c) t 8-3 (hr)	K(i-1)/Ko	K(1-2)/Ko	K(2-3)/Ko
1.91		1.9	0.65
3.95	0.96	0.99	0.99
5.85	0.73	0.96	0.64
8.37	0.87	0.98	0.98
12.75	0.78	0.97	0.97
24.68	0.66	0.63	0.95
36.17	0.30	0.97	
48.77	0.24	0.65	
72.40	0.35	0.37	
96.15		0.15	
120.28	0.10	0.65	
144.18	0.059	0.63	
157.75	0.046	0.64	